ACTA UNIVERSITATIS SZEGEDIENSIS

ACTA MINERALOGICA-PETROGRAPHICA

Tomus XL.

SZEGED, HUNGARIA
1999

NOTE TO CONTRIBUTORS

General

The Acta Mineralogica–Petrographica publishes original studies on the field of geochemistry mineralogy and petrology, first of all studies Hungarian researches, papers resulted in by cooperation of Hungarian researches and those of other countries and, in a limited volume, papers from abroad on topics of global interest.

Manuscripts should be written in English and submitted to the Editor-in-chief, Institute of Mineralogy, Geochemistry and Petrography, Attila József University, H–6701 Szeged, Pf. 651 Hungary.

The authors are responsible for the accuracy of their data, references and quotations from other sources.

Manuscript

Manuscript should be typewritten with double spacing, 25 lines on a page and space for 50 letter in a line. Each new paragraph should begin with an indented line. Underline only words that should be typed in italics.

Manuscript should be generally be organized in the following order:

Title
Name(s) of author(s) and their affiliations, in foot-note the address of the author to whom the correspondence should be sent
Abstract
Introduction
Methods, techniques, material studied, description of the area investigated, etc.
Results
Discussion or conclusions
Acknowledgement
Explanation of plates (if any)
Tables
Captions of figures (drawings, photomicrographs, etc.)

Abstract

The abstract cannot be longer than 500 words.

Tables

The tables should be typewritten on separate sheets and numbered according to their sequence in the text, which refers to all tables.

The title of the table as well as the column headings must be brief, but sufficiently explanatory.

The tables generally should not exceed the type-area of the journal, i.e. 12,5x18,5 cm. Foldouts can only exceptionally be accepted.

(continuation on the inner side of verso)

ACTA UNIVERSITATIS SZEGEDIENSIS

ACTA MINERALOGICA-PETROGRAPHICA

Tomus XL.

SZEGED, HUNGARIA
1999

HU ISSN 0365–8006
HU ISSN 0324–6523

SERIES NOSTRA AB INSTITUTIS MINERALOGICS, GEOCHEMICIS PETROGRAPHICS UNIVERSITATUM HUNGARICUM ADIUVATUR

Adjuvantibus

IMRE KUBOVICS
GYÖRGY BUDA
FRIGYES EGERER
PÁL GYARMATI
BÉLA KLEB

Regidit

TIBOR SZEDERKÉNYI

Editor

Institut Mineralogicum, Geochemicum et Petrographicum
Universitatis Szegediensis de Attila József nominatae

Nota

Acta Miner. Petr., Szeged

Szerkeszti

SZEDERKÉNYI TIBOR

a szerkesztőbizottság tagjai

KUBOVICS IMRE
BUDA GYÖRGY
EGERER FRIGYES
GYARMATI PÁL
KLEB BÉLA

Kiadja

a József Attila Tudományegyetem Ásványtani, Geokémiai és Kőzettani Tanszéke
H-6722 Szeged, Egyetem u. 2–6.

Kiadványunk címének rövidítése
Acta Miner. Petr., Szeged

SOROZATUNK A MAGYARORSZÁGI EGYETEMEK ROKON TANSZÉKEINEK TÁMOGATÁSÁVAL JELENIK MEG

Printed in JUHÁSZ NYOMDA KFT., Szeged

Acta Mineralogica-Petrographica, Szeged, XL, 3–10, 1999

STRUCTURAL DISORDER IN NATURAL CUBIC HGS

V. KOVÁCS KIS[1] and I. DÓDONY

Department of Mineralogy, L. Eötvös University

ABSTRACT

Cubic HgS crystals (loc.: Róka-hegy, Budapest, Hungary) were examined from the crystallographic point of view. The SAED patterns revealed structural disorder. The measure of the disorder, namely the ratio of the hexagonal close packed lamellae in the cubic close packed host was determined by using the Pandey-Lele method (1986). The sample examined can be characterised by low fault concentrations and relatively high growth probability by the calculations. The ratios of the hexagonal layers vary between 30-50%. The traces of structural deformation were observed on etched surfaces.

INTRODUCTION

The sphalerite-wurtzite system has the best-known structural properties among the sulphide compounds of II.B elements (MARDIX, 1986; FLEET, 1976, 1983; AKIZUKI, 1983; PÓSFAI et. al., 1988). The representatives of the close packed structure types are the common forms of ZnS, sphalerite (fcc) and wurtzite (hcp). The different stacking orders in the polytype modifications imply different physical properties too.

Other II.B sulphides are less investigated. There is one mentioned polytypic form of cubic CdS without description of its symmetry, and there were no traces of structural disorder found in the case of HgS (RAI et al., 1972). The structural disparities can be deduced from the different electron configurations. While the stable form of ZnS is the tetrahedrally co-ordinated sphalerite, the cubic HgS because of the presence of the 4f electrons results metastable. The cinnabar has distorted NaCl structure that is common in the nature.

In this paper we report the structural disorder of the cubic HgS and the calculated hexagonality of the sample.

THE SAMPLE AND THE EXPERIMENTAL METHODS

The sample is from a hydrothermal ore bearing carbonate vein, from Róka-hegy, Budapest, Hungary. The specimen was obtained by acidic solution, it was ground and mounted in suspension onto a Cu grid covered with graphite film. The SAED patterns were obtained by using a JEOL JEM 100U microscope at 100 kV and 120 mA. High rate of damaging caused by the electron beam was characteristic.

The X-ray data were obtained on a Siemens D5000 powder diffractometer (Bragg-Brentano geometry, scan mode: 4.8 sec/0.02°).

[1] Budapest, 1088 Múzeum krt. 4/A Hungary, vis@ludens.elte.hu

The etched surface (30% c. aqua regia, 1 min) was observed with ore microscope and a Hitachi S-2300N scanning electron microscope operating at 20 kV, 100 mA.

For the calculation of the diffracted intensity with known input parameters a C program was used.

RESULTS AND DISCUSSION

Disorder in face-centered cubic HgS

The orientation of the crystals on the electron diffraction patterns (Fig. 1.) is the same: the electron beam is parallel to the zone axis [110]. This is the adequate orientation for examining the sequence of the layers of the fcc structure perpendicular to [111] direction (Fig. 2.). The electron diffraction patterns reveal through the presence of cinnabar, metacinnabar also the disordered metacinnabar phase as it can be seen on Fig. 1.

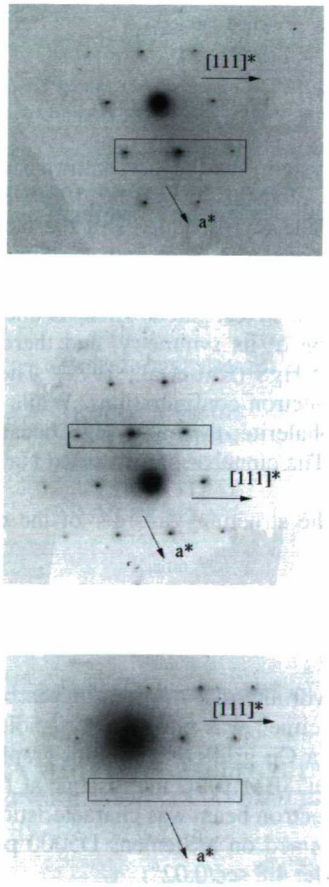

Fig 1a-c. SAED patterns of disordered metacinnabar. Intensifying diffuse streak in direction a → b → c along the 111* axis. Satellite reflections appear on the third pattern.

On the SAED patterns a diffuse streak is observable parallel to the 111* axis. It's intensity increases in the direction a → b → c. On Fig. 1c. nor yet separate satellite reflections arise in the vicinity of the 11$\bar{1}$ 220 113 and 002 reflections. That is indicative of the disruption of the fcc's characteristic stacking sequence ABCABC.... , and at the same time the condensation of hexagonal close packed lamellae (Fig. 3.).

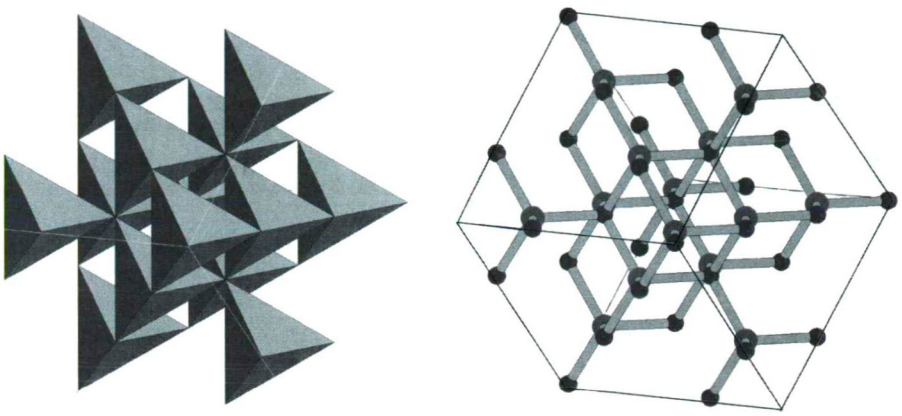

Fig. 2. Crystal structure of metacinnabar, face centered cubic structure viewing from the [111] direction.

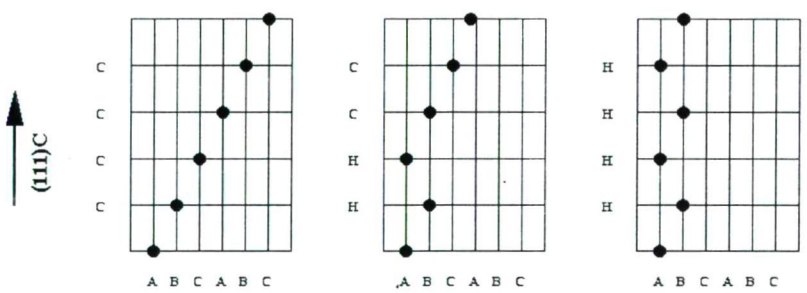

Fig. 3. Relationship between the fcc and hcp structures, appearance of the stacking fault. After Bollmann (1970.), modified.

Method for characterising the disorder

The PANDEY and LELE's (1986.a, 1986.b) model applied to determine the observed disorder's degree of cinnabar-metacinnabar crystals. Although the hcp modification of HgS is unknown in the nature, several aspects account for it's use: the structural analogy between the sphalerite and metacinnabar, the observed phenomena on the diffraction pattern and the reference to a natural γ-modification of HgS (hypercinnabar), with hexagonal symmetry, but without the exact space group determination (POTTER and BARNES, 1978.).

The model describes the different transition stages between the two close packed structures with two probability variants: the fault concentration (α) and the fault's growth probability (β). These two parameters can be calculated by measuring the diffracted

intensity along a given direction. The measurement was made along the direction 111* in the surroundings of the marked reflections on Fig. 1. The measured intensity is shown on Fig. 4.

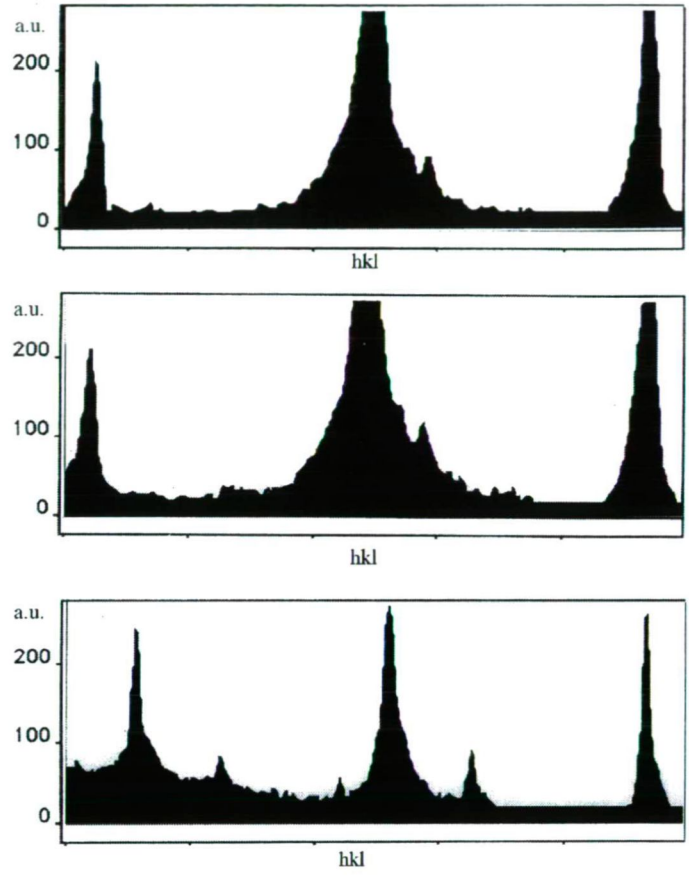

Fig. 4a-c. Measured diffracted intensity in the surroundings of the marked reflections of Fig. 1.

On the first intensity profile (Fig.4.a) a moderate asymmetric broadening of the reflections can be seen, which intensifies in the next profile (Fig. 4.b) where a small additional shoulder appears too in the vicinity of the reflection 113. Fig. 4.c shows a completely separated satellite near the main reflection 113 (or 1$\bar{1}$1) and both of them are considerably sharper than the profiles of the same reflections on Figs. 4.a and 4.b. With the appearance of the well defined satellite there is also observable the tendency of a slight shifting of the reflection maximum 113 (or 11$\bar{1}$) and 002 (or 220).

Degree of the disorder

Supposing different default conditions characterised with known fault concentration and growth probability data, a set of calculated intensity curves was traced. The best fitting curves and the corresponding input data are shown in Fig. 5.

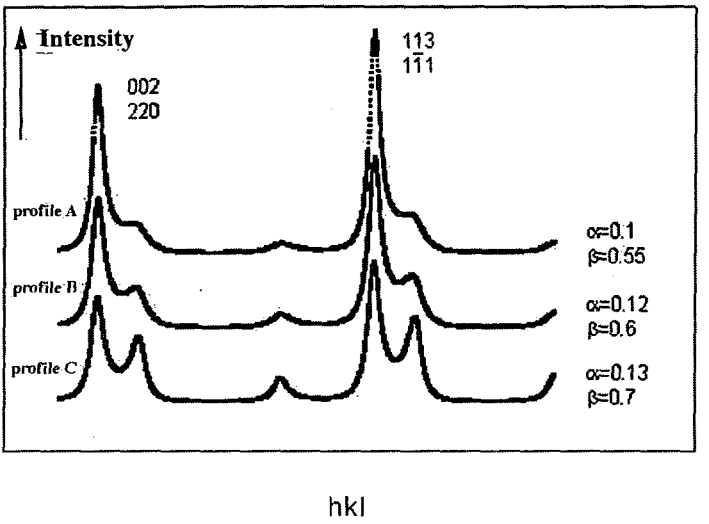

Fig. 5. Calculated diffracted intensity best fitting to the measured one. Parameters are given for all the curves.

All the examined samples are characterised typically with low fault concentration and relatively high growth probability. In the direction profile a.→profile b.→profile c. parallel with the observed intensifying reflection broadening and satellite separating both of the parameters are growing, although the growth rate is different. In spite of the growth the fault probability α in all cases it remains low, it's value varies between 0.1 and 0.13, that means the nucleation rate is moderated. The growth probability's β value is considerably higher, it is between 0.55 and 0.7.

The probability of the appearance of one stacking fault in the cubic structure of the HgS is not significant, but once the fault appeared the growth of the faulted region begins with an elevated probability in average 60-65 %. Basing on this we can deduce that the microstructure of the sample shows thick alternating lamellae of hexagonal and cubic close packing.

The Pandey-Lele's model with known α and β values allows the calculation of the ratio of hexagonal and cubic close packed lamellae using the following equations (PANDEY and LELE, 1986.a):

$$f_C = \frac{1-\beta}{1+2\alpha-\beta},$$

$$f_H = \frac{2\alpha}{1+2\alpha-\beta}$$

where f_C stands for the ratio of the cubic, and f_H for the ratio of the hexagonal layers. Considering the calculated α and β values the resulting data are the following:

f_C (a) = 0.6923	f_H (a) = 0.3077
f_C (b) = 0.6250	f_H (b) = 0.3750
f_C (c) = 0.5357	f_H (c) = 0.4643

The evidency of increasing hexagonality — which means the formation of stacking fault in the cubic host — with increasing fault concentration and growths probability is clearly seen.

The stacking fault arises with the decomposition of partial dislocations. The partials bordering the faulted region repel each other. The shove between them depends on the stacking fault energy. The appearance of the stacking faults is indicative of the enough low stacking fault energy during the crystallisation that allowed the formation of stable partials.

The anomalous profile-distortion on X-ray powder diffraction patterns caused by the structural disorder, because of the close intergrowth of the two HgS phases – the cubic and the trigonal (see Fig. 6.), – doesn't provide facilities in the identifying of hexagonality.

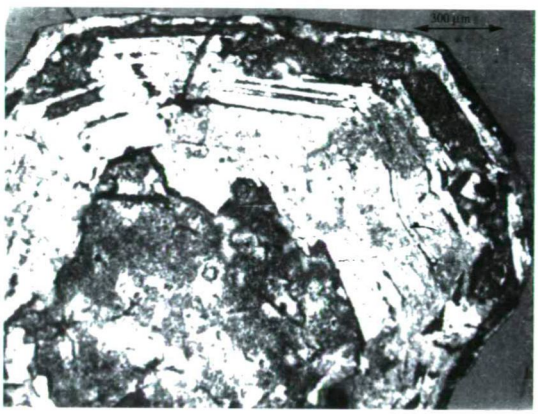

Fig 6. Etched surface of a strongly zoned grain. The core of the grain is homogeneous metacinnabar with resorbed margin. The core is surrounded by thick inclusion-hole rich cinnabar bands and thin inclusion-hole free metacinnabar stripes. Traces of structural inhomogenity are observable in the isotropic core. Ore-microscope photograph || N.

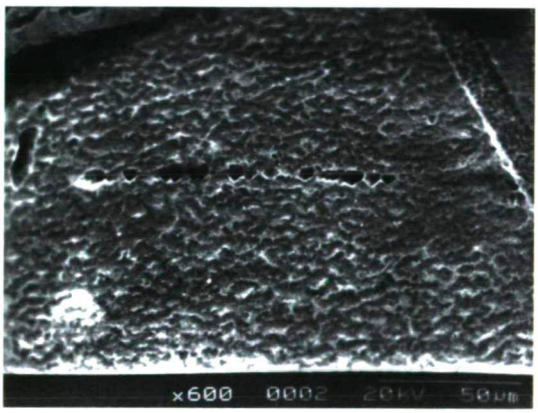

Fig. 7. Traces of structural inhomogenity: narrow stark point-lines and wider shallow bands in the core of the grain in *Fig.6.* SEM photograph.

Etched surface examination

Because of the etching first dissolves the unstable part of the crystal, different structural deformations and partial dislocations which boarder the stacking faults become more conspicuous on etched surfaces. For etching it was used 30% concentration aqua regia during 1 minute. The observed etching traces which origin sometimes is doubtful are shown on Figs. 6. and 7.

SUMMARY

Cubic HgS crystals (loc.: Róka-hegy, Budapest, Hungary) were examined from the crystallographic point of view. The main aim of the work was to observe structural disorder, stacking faults, and/or polytypic stacking. Our results can be summarised in the followings.

The SAED (Selected Area Electron Diffraction) method proved to be the most adequate method for the observation of the structural feature. By the diffraction patterns the sample examined consists of cinnabar, metacinnabar, and disordered metacinnabar. Disorder was not observable with X-ray powder diffraction method.

The disorder revealed to be hexagonal close packed lamellae in cubic close packed host. The stacking faults are supposed to be traces of dislocation reactions. By the calculations the sample can be characterised by low fault concentration and relatively high growth probability. The ratios of hexagonal layers vary between 30-50%. By increasing of the two probabilities variable increase the density of the hexagonal close packed layers.

Scanning electron microscopy and ore microscopy was applied to observe partial dislocations at the vicinity of the faulted regions.

REFERENCES

AKIZUKI, M. (1983.): Investigation of phase transition of natural ZnS minerals by high resolution electron microscoy: reply. American Mineralogist 68, 847-848.

BOLLMANN, W. (1970.): Crystal defects and crystalline interfaces. Springer Verlag Berlin, 1970.

FLEET, E. (1976.): Stacking disorder in natural 2H wurtzite. J. Appl. Cryst. 9, 190-192.

FLEET, M. E. (1983.): Investigation of phase transition of natural ZnS minerals by high resolution electron microscoy: discussion. American Mineralogist 68, 845-846.

MARDIX, S., ALEXANDER, E., BRAFMAN, O., STEINBERGER, I. T. (1967.): Polytype families in zinc sulphide crystals. Acta Crystalligraphica 22, 808-812.

PANDEY, D., LELE, S. (1986.a): On the study of the fcc-hcp martensitic transformation using a diffraction approach I. Fcc→hcp transformation. Acta Metall. 34-3, 405-413.

PANDEY, D., LELE, S. (1986.b): On the study of the fcc-hcp martensitic transformation using a diffraction approach II. Hcp→fcc transformation. Acta Metall. 34-3. 415-424.

PÓSFAI, M., DÓDONY, I., SOÓS, M. (1988.): Stacking disorder in the ZnS from Gyöngyösoroszi, Hungary. N. Jb. Miner. Mh. 10, 438-445.

POTTER, R., BARNES, H. L. (1978.): Phase relations in the binary Hg-S. Am. Min. 63. 1143-1152.

RAI, K. N., SRIVASTAVA, O. N. (1972.): Electon microscopic study of ZnS, CdS and HgS crystals in relation to their polytypic growth. Indian Journal of Pure and Appl. Phys. 10, 108-110.

Manuscript received: 2. Sep. 1999.

Acta Mineralogica-Petrographica, Szeged, XL, 11–20, 1999

CLAY MINERALS IN PALEOSOLS AT VISONTA, HUNGARY

NÉMETH TIBOR[1], BERÉNYI-ÜVEGES JUDIT[2], MICHÉLI ERIKA[2], TÓTH MÁRIA[1]

[1]Hung. Acad. Sci. Laboratory for Geochemical Research*
[2]University of Agricultural Sci. Dept. of Soil Sci. and Agric. Chem.**

ABSTRACT

Clay mineral associations of a paleosol sequence in the roof strata of the lignite mine at Visonta were studied by means of XRD, TEM, FTIR, DTA. Investigations show that several clay mineral phases (smectite, kaolinite, illite, vermiculite) are present together in all the strata. High charge montmorillonite oocurs in the present day soil, high charge beidellite is characteristic of the red paleosol and montmorillonite and beidellite are present together in the grey clays. This various clay mineralogy indicate complex genesis of the strata.

Key words: XRD, TEM, layer charge, smectite, beidellite, paleosol, Visonta

INTRODUCTION

Mineralogical composition, clay mineral association and the characteristics of the clay mineral species were studied in a paleosol sequence in order to reconstruct the environment in which the paleosols were formed. The studied paleosol sequence is situated in the wall of the opencast lignite mine at Visonta (pediment of the Mátra mountains, Hungary). The Mátra mountains consist of Miocene neutral volcanic rocks. On the pediment, Pannonian sediments overly the volcanic rocks on which loess and colluvial sediments were deposited in the Pleistocene. These sediments contain the paleosols.

The area of the opencast mine at Visonta has already been studied by some authors. The geologic and hydrogeologic conditions were studied by MIKLÓS (1967). Complex investigation including geomorphology, paleontology and paleomagnetic measurements was carried out by a working group of KRETZOI, MÁRTON, PÉCSI, SCHWEITZER, VÖRÖS and HAHN (1985). They studied the Eastern II. pit of the „Thorez Mine" where alluvial sediments with paleontological evidence of Pleistocene age were observed. Below the Pleistocene strata, a red clay layer considered to be formed in the Pliocene was found.

Investigations on mineralogy has not been carried out yet. This study on mineralogy is connected to a new research project focusing on soil development, paleopedology and paleoenvironmental reconstruction that was started in 1996. The work was so far concentrated on the Small South pit of the mine. Our results differ from the published data (MICHÉLI et al, 1999, HORVÁTH, 1999).

THE STUDIED SITE

General soil profile description and sampling of the selected layers were carried out using Munsell colour notations. The studied profile (*Fig. 1.*) consists of a Chernozem

* H-1112 Budapest Budaörsi út 45., Hungary
** Gödöllő, Péter K u. 1.

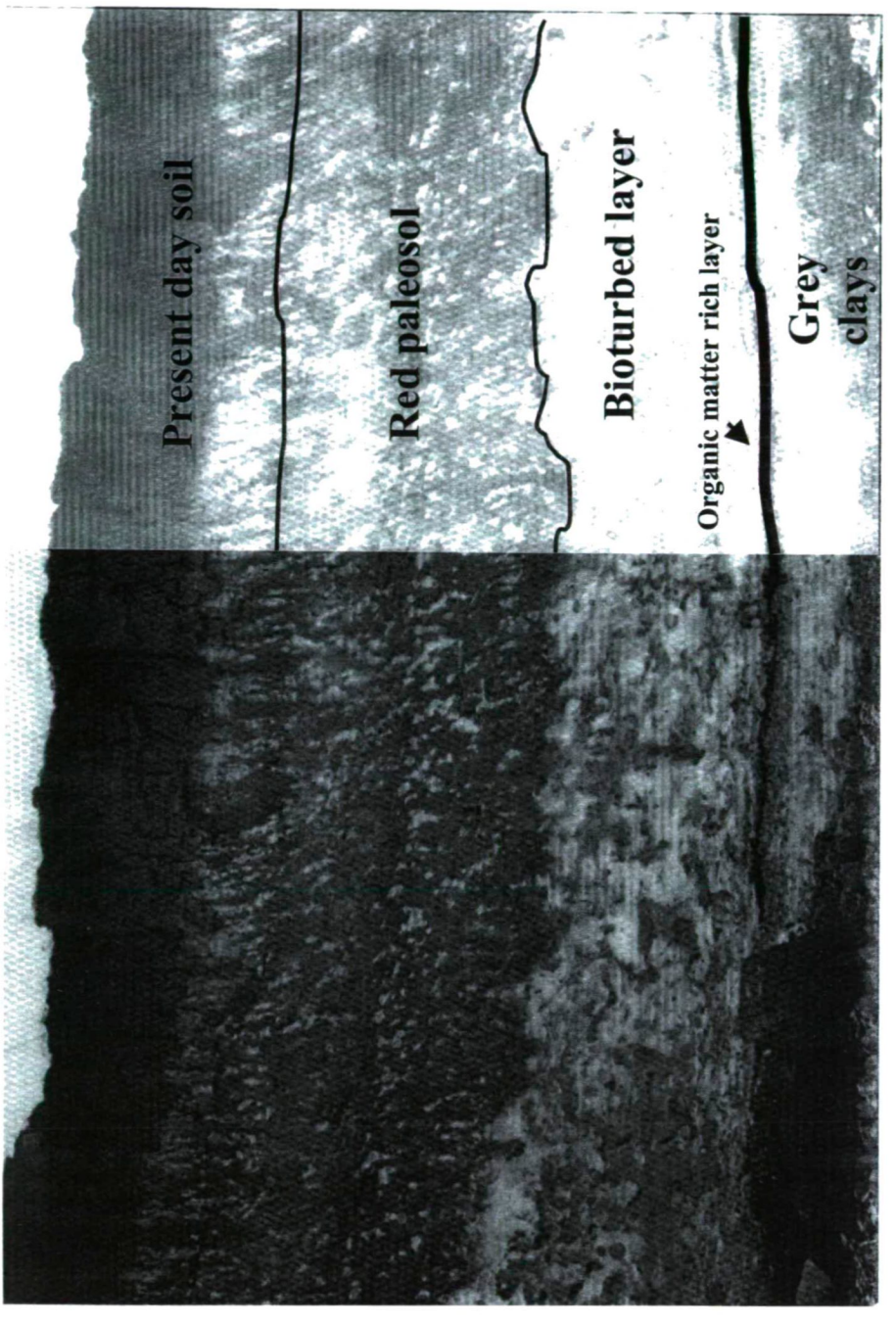

Fig. 1. The studied sequence in the lignite mine at Visonta

brown forest soil (Argic Chernozem) on the top with a black „A" (10YR 3/2) horizon and a brown „B" (10YR 6/3) horizon that has prismatic structure, and clay films on ped surfaces. The border between the two horizons is gradual. Below it a $CaCO_3$ accumulation horizon (5YR 4/6) was identified that has a sharp boundary to the „B" horizon.

Under it a red paleosol (5YR 5/8) was found that has prismatic structure with slickensides, stress surfaces and black and yellowish mottles basically on ped surfaces. The red paleosol has sharp boundary to the underlying layer. Based on colour and texture this layer consist of different materials. In the upper part a pink silt (5YR 7/4), in the lower part a yellowish fine sand (2.5Y 7/8) is the predominant material. In the matrix greenish grey clay clasts (5Y 5/6) which gradually decreasing in size and abundance towards the top of the layer, large $CaCO_3$ accumulations in the bottom part, biogalleries filled with the red material from the overlying layer were found.

It the bottom part of the profile two greyish layers are located. The darker grey (5Y 5/2) one has a black organic matter accumulation horizon that gradually transits into the dark grey clay. The part rich in organic matter was identified as a thin lignite layer (2.5Y 2/0). The lower one has a clay texture and greenish grey colour (5Y 6/4) and is separated by a sharp boundary from the other layer.

METHODS

The mineral composition of the studied layers and horizons was determined by semi-quantitative X-ray diffraction, differential thermal analysis, Fourier Transform Infrared Spectroscopy and Transmission Electronmicroscopy. Random powder samples were analysed by a Philips PW-1730 diffractometer equipped with a graphite monochromator using Cu-Kα radiation at 45 kV and 35 mA with 1° divergence slit and 1° receiving slit. Scanning rate was 0,05° 2Θ per minute from 3° to 70°. The total mineral composition was determined by semi-quantitative phase analysis on the random powder samples (NÁRAY-SZABÓ and PÉTERNÉ, 1964). Clay minerals were identified on the Mg-, Ca- K- and Li-saturated, ethylene-glycol and glycerol solvated and heated samples from the clay fraction (less than 2 μm) which was obtained by sedimentation.

FTIR spectra were obtained from the clay fraction of the samples with the self-supporting clay film technique. Measurements were made by a BIO-RAD FTS 165 FTIR spectrometer. The clay fraction was also analyzed with DTA (MOM derivatograph) . The clay fractions of the red and grey clays were investigated by Transmission Electron Microscopy (Phillips CM 20, acceleration voltage: 200kV)

MINERAL COMPOSITION OF THE STRATA

In all samples quartz is the predominating mineral, its amount vary between 50 and 80%. The clay mineral content varies between 4 and 40%. The K-feldspar content is negligible (less than 5%). The amount of plagioclase generally decreases from the top to the bottom of the profile: 10-15% in the topsoil horizons, 4-8% in the red paleosol layers, about 2-3% in the bioturbed layer and 3-7% in the greyish clay layers except the lignite bearing layer (13%). The decreasing tendency of feldspar content is related to the higher weathering state of the red paleosol.

From the group of carbonate minerals calcite and dolomite were identified. The amount of calcite ranges between 0 and 60% and it increases from the top to the bottom of the profile. It reaches maximum in the bioturbed layer. Dolomite was identified in some samples, it has the highest value in the greenish grey clay layer (7%). It is detrital in the topsoil and in the red paleosol. Based on ^{13}C stable isotope data, the calcite is of pedogenic origin, and the dolomite was precipitated in lacustrine environment in the grey clay layer (DEMÉNY and EMBEY-ISZTIN, 1997). Hematite was identified in trace amount in the „B" horizon of the present day soil and in the red paleosol.

CLAY MINERALS IN THE LAYERS

All the XRD diagrams exhibited 14-, 10-, 7 Å basal reflections on the untreated samples. An example of the changes due to different treatments is shown in *Fig. 2*. The 14 Å peak on the Ca- and Mg-saturated, ethylene glycol treated samples is shifted to 17 Å. It indicates the presence of smectites or vermiculite. After glycerol solvation this peak

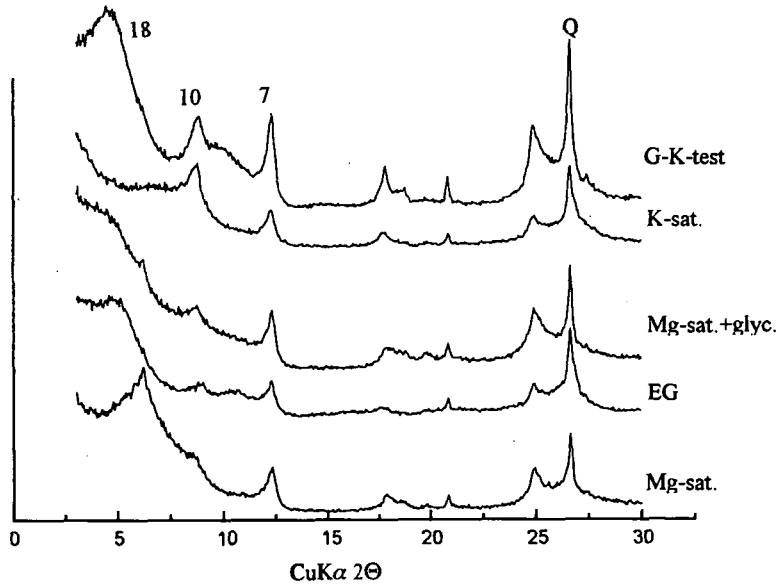

Fig. 2. The XRD patterns of the red paleosol after the different treatments

splits up: the smaller part remains at 14 Å, the major part has shifted to 18 Å. The former represents vermiculite, the later stands for smectite. The peak at 4.72 Å supports the presence of vermiculite. The position of (060) reflection at 1.5 Å shows that the smectite is dioctahedral. The peak at 10 Å belongs to illite and illite/smectite and the 7 Å peak with the 3.58 Å peak is kaolinite. After heat treatment (550°C) the 7 Å peak disappeared, this also indicates the presence of kaolinite (BRINDLEY and BROWN, 1980). Due to potassium saturation, the 14 Å peak of the samples from the topsoil and from the red paleosol collapsed to 10 Å. In case of grey clays a broad peak at around 12 Å appears

besides the 10 Å reflection. After this treatment high layer charge swelling structures collapse to 10.4 Å, low layer charge swelling structures collapses to 12.4 Å. (*Fig. 3.*) The Green-Kelly test was used to differentiate between montmorillonite and beidellite (THOREZ, 1976). Beidellite is an aluminous smectite having a layer charge mainly due to substitution in the tetrahedral sheet while montmorillonite is mainly substituted in the octahedral sheet. Montmorillonite was identified in the topsoil and in the grey clays and beidellite is present in the red paleosol and in the grey clays (*Fig. 4.*).

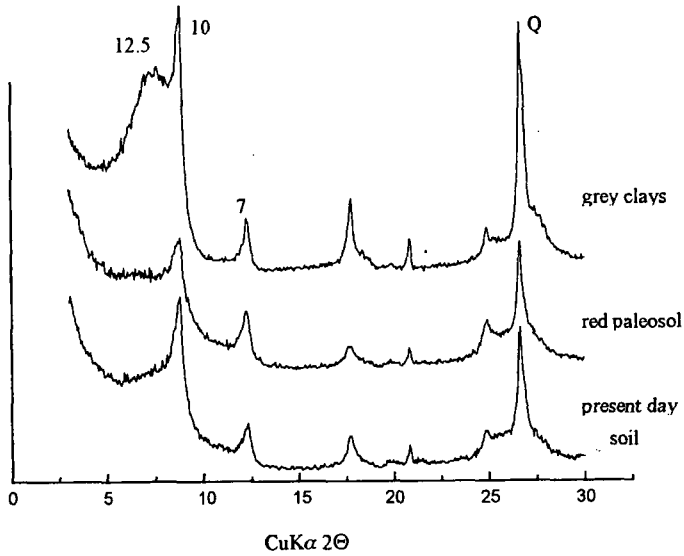

Fig. 3. The XRD patterns of the K-saturated samples of the different layers.

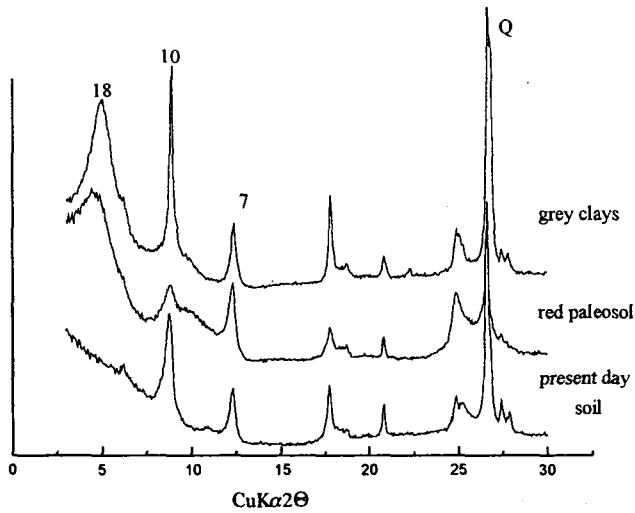

Fig. 4. The XRD patterns of samples after the Green-Kelly test

The determination of smectite crystallinity is calculated from the peak and valley intensity ratio of the (001) and the from presence of (002) reflection of EG solvated samples (THOREZ, 1976). The crystallinity of the smectite increases downward. In the topsoil it is poorly crystalline, in the red paleosol it is moderately crystalline, in the grey clay layers it is well crystalline. This also indicates the different origin of the clay minerals in the grey clays, in red paleosol and in the topsoil.

The FTIR spectra of the clay fraction of all layers are very similar. The aluminous character of the smectites is indicated by a peak at 916 cm^{-1} that is characteristic of AlOHAl band (RIGHI et al., 1995).

Data obtained by differential thermal analysis present an endothermal peak at 100°C that indicates the loss of adsorbed water, and an endothermal dehydroxylation peak around 500°C, with an endothermal-exothermal peak system at 830-900°C that shows the phase transformation. The dehydroxylation peak at 500°C is characteristic of soil smectites. The dehidroxylation peak of other smectites occurs at 700°C (MACKENZIE, 1970).

The purpose of TEM investigation was to gain information on the morphology, structure and stacking order. This feature is characteristic of the species within the smectite group. Nontronite and montmorillonite are characterised by turbostratic structure (MERING, 1975) which is indicated by ring-like diffraction pattern. Saponite and beidellite has high stacking order that is indicated by the spot-like diffraction pattern (ZVYAGIN, 1967). The unusually small size of the smectite particles can be observed both in the red paleosol and in the grey clay. The size of the irregular shaped or platy pseudohedral smectite crystallites is only 0.0x μm in the clay aggregates of 0.x μm size. A somewhat larger (0.05-0.1 μm) elongated fibrous lath-shaped smectite crystallites also occur (*Fig. 5.*). The pseudohedral 0.5-1 μm sized crystallites of kaolinite are the most characteristic in the grey clay.

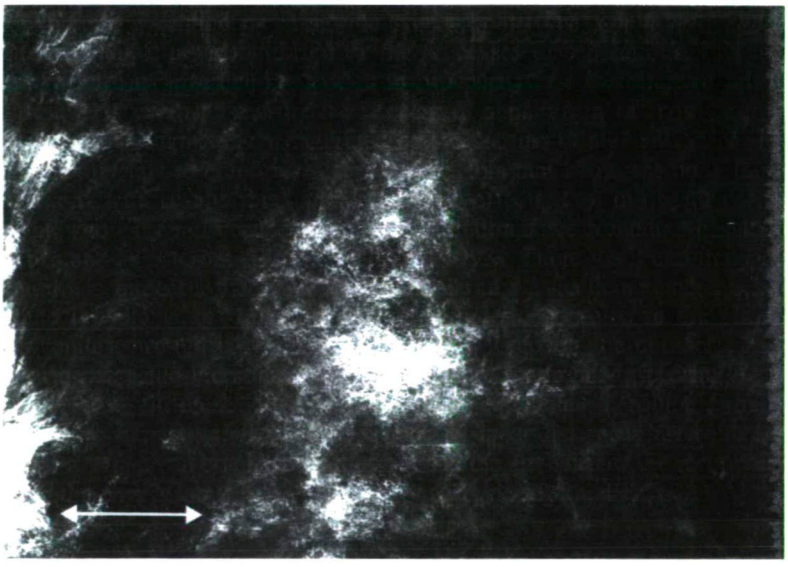

Fig. 5. Electron micrograph of the smectite from the red paleosol showing very fine irregular shaped and elongated lath shaped crystals. Scale bar: 0.25 μm

The ring like diffraction pattern indicates turbostratic structure. This kind of pattern may also be the result of polycrystalline diffraction due to small crystal size. In this case the turbostratic structure is more probable because the single crystal diffraction of relatively larger crystals also shows ring like pattern. The heterogeneity of the material in the grey clay can be observed in *Fig 6.* in which both ring-like and spot-like patterns are present. Ring-like pattern is caused by the presence of smectite and the spot-like pattern is characteristic of a well ordered clay mineral (mica, illite, vermiculite or well ordered beidellite). Based on intensity ratio this ordered phase consists of two politypes. Preliminary EDS investigation shows the ferous beidellitic nature of smectite. When comparing to data in literature, the beidellitic smectite in the red paleosol is not as ordered as it can be expected (SUQUET and PEZERAT, 1987).

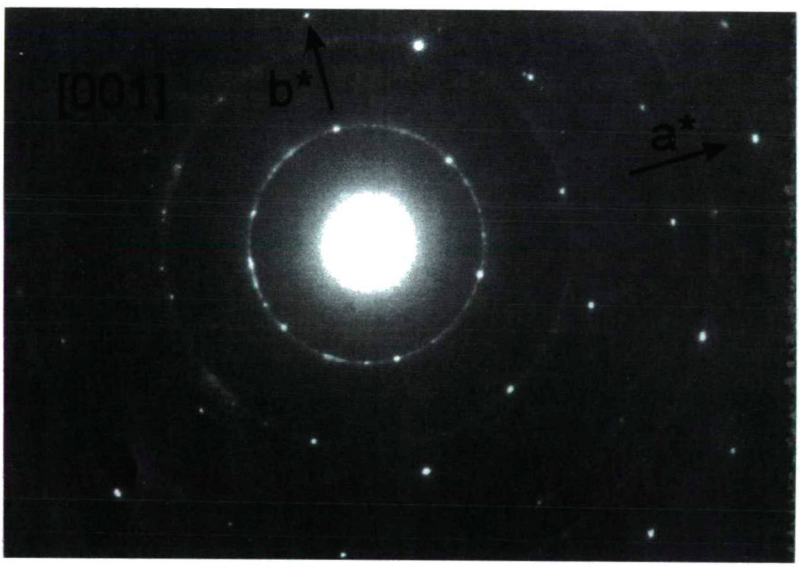

Fig. 6. SAED pattern of a clay particle from the grey clay layer

High layer charge smectites are abundant in soils (ARAGONESES and GARCIA-GONZALEZ, 1991). The low layer charge smectites have authigenic or hydrothermal origin or are formed by weathering of volcanic glass, pyroxenes, amphiboles and feldspars. Low layer charge smectites transformed into high layer charge ones in vertisols having high pH and low organic matter content (RIGHI et al., 1998). We think that high layer charge smectites were transformed from low layer charge ones and also formed by the weathering of intermixed micas and illite in the red paleosol during pedogenesis. Smectites formed from 2:1 phyllosilicates have their charges mostly in the tetrahedral sheet (DIXON and WEED, 1986). The identified high layer charge smectites belong to this type.

The origin of kaolinite cannot be identified with the method used. It can be a weathering product indicating warm humid climate with high leaching rate (SINGER, 1980). According to the fact that it is not the predominant mineral and its quantity is the same in all layers, it is more probably that kaolinite here is not the result of in situ weathering, but it was rather transported within the sediment providing parent material of the topsoil and paleosols. Illite

is originated from the dust mixed to the material at the time of transportation. Illite is a common 2:1 layer silicate in loess (PÉCSI-DONÁTH, 1987).

CONCLUSIONS

Considering complexity and heterogeneity, the clay mineralogy of the layers in the studied sequence is similar. The small differences between the mineral species and their relative amount supported by other results can answer the questions raised in the introduction. The source of the difference is the amount of the layer charge and from where (i. e. the tetrahedral or octahedral sheet) it derives. Kaolinite can be considered the only stable phase in all the layers though it is not predominating and it is probably detrital in this case. Illite in discrete and in illite/smectite interstratified form is also common. The swelling clays predominate and vary from each other according to layers and genesis. The presence of different types of smectites (beidellite, montmorillonite and vermiculite) indicates heterogeneous origin. The high-charge beidellite in the red paleosol was formed due to pedogenesis probably from a red clay having smectite as a predominating mineral. The layer stacking of this beidellite is poorly ordered and the crystallinity is also poor that suggests pedogenic origin. The high charge montmorillonite and vermiculite are also the result of pedogenesis but in different environment.

ACKNOWLEDGEMENTS

The authors are grateful to KOVÁCS ISTVÁN and RADNÓCZI GYÖRGY (Research Institute for Technical Physics and Materials Science) for their help in TEM analysis and to Dódony István for discussion during TEM data evaluation and HORVÁTH ZOLTÁN for the contribution during the field work, RUDNYÁNSZKY LIVIA for the photos. The authors thank the Soros Foundation and the OMFB for the financial support.

REFERENCES

ARAGONESES, F. J., GARCIA-GONZALEZ, M. T. (1991): High-charge smectites in Spanish "Rana" soils. Clays and Clay Minerals, 39, 2, 211-219.

BRINDLEY, G. W., BROWN, G. (1980):Crystal structures of clay minerals and their X-ray identification. London Miner. Soc. 322-360.

DEMÉNY, A., EMBEY-ISZTIN, A. (1997): A stable isotope study on the origin of carbonate in peridotite xenoliths in the Transdanubian range, Hungary, Földtani Közlöny. 127/3-4, Budapest, 371-383. (in Hungarian)

DIXON, J. B., WEED, S. B. (1989): Minerals in soil environments. SSSA Inc. Madison USA.

FODOR L., VÖRÖS, I. (1990): Pleisztocén ösemlösmaradványok Visontáról. Agria 24, 5-20.

HORVÁTH Z. (1999): Plio-Pleisztocén felszínfejlödési rekonstrukció pontosítása a Mátra DK-i előterében, Visonta. Ms thesis, Eötvös Loránd Tudományegyetem Alkalmazott- és Környezetföldtani Tanszék, Budapest. (Manuscript)

KRETZOI, M., MÁRTON, P., SCHWEITZER, F., VÖRÖS L. (1982): Pliocene-Pleistocene piedmont correlative sediments in Hungary. Quaternary Studies in Hungary 43-73., Akadémiai Kiadó, Budapest.

MACKENZIE, R. C. (1970): Differential Thermal Analysis. Academic Press, London-New York, 1970.

MERING, J. (1975): Smectites. In: Soil Componets. ed: GIESEKING, J. 97-119. Springer-Verlag, New York.

MICHÉLI, E., W. W. MCFEE, BERÉNYI-ÜVEGES, J., DOBOS, E. (1999): Evidence of environmental change in paleosols of north central Hungary. (manuscript)

MIKLÓS M. (1967): A visontai kutatási terület és vízföldtani viszonyai. Bányászati Kutatási Intézet Közleményei 11, 95-111.
NÁRAY-SZABÓ, I., PÉTER T.-NÉ (1964): Agyagok és talajok ásványi elelgyrészeinek mennyiségi meghatározása diffraktométerrel. Földtani Közlöny 94, 444-451.
PÉCSI-DONÁTH, É. (1987): Mineralogical and granulometric analyses of the "old loess sequences " of Hungary. In: Loess and Periglacial Phenomena, 47-50. Akadémiai Kiadó Budapest.
RIGHI, D., TERRIBILE, F., PETIT, S. (1995): Low-charge to high-charge beidellite conversion in a vertisol from South Italy. Clays and Clay Minerals. 43, 4, 495-503.
RIGHI, D., TERRIBILE, F., PETIT, S. (1998): Pedogenic formation of high-charge beidellite in a Vertisol of Sardinia (Italy). Clays and Clay Minerals. 46, 2, 167-178.
SINGER, A. (1980): The paleoclimatic interpretation of clay minerals in soils and weathering profiles. Earth Science Reviews, 15 (1979/1980), 303-326. Elsevier, Amsterdam
SUQUET, H., PEZERAT, H. (1987): Parameters influencing layer stacking types in saponite and vermiculite: a review. Clays and Clay Minerals. 35, 5, 353-363.
THOREZ, J.(1976): Practical identification of clay minerals. Editions G. Lelotte, Dison (Belgique)
ZVYAGIN, B. B. (1967): Electron diffraction analysis of clay mineral structures. Plenum Press, New York

Manuscript received: 30. Sep. 1999.

Acta Mineralogica-Petrographica, Szeged, XL, 21–44, 1999

TYPOLOGY AND MICROPROBE ANALYSIS OF ZIRCONS AS AN INDICATOR TO EVOLUTION AND GENESIS OF ABU EL-HASAN GRANITOIDS, NORTHERN EASTERN DESERT, EGYPT

M. L. KABESH[1], M. S. ATIA[2], M. DAWOUD[2]

[1] Dept. of Geological and Geophysical Sciences / National Research Center
[2] Geology Dept., Faculty of Science, Manoufia University

ABSTRACT

Zircons from the older and the younger granitoids of Abu El-Hasan granitic complex are typologically and geochemically characterized. Zircon populations of the older granitoids contain a wide variety of crystal shapes and do not show any overgrowths, outgrowths or corrosion. Zircons of the younger granitoids show much more regularity in distribution. Typological evolutionary trends of the studied zircons are suggested with decreasing age which may indicate some evolution. Microprobe analyses were carried out for different zircons from the granitic rocks to clarify the magmatic evolution, the crystal building and the crystallization of this accessory mineral. Back Scatter Electron (BSE) images of zircons are utilized to reveal zonal growth, crystal effect of the aggressive hydrothermal solutions and inclusions.

Chemical analyses were carried out from the core to the rim of the grains to deduce the variations through crystal growth and the magmatic evolution. Zr/Hf ratio is often between 40 and 30, but lower and higher values are also recorded. Generally, Zr/Hf ratio does not show clear trends from the core to the rim in the studied zircon. However, this ratio shows decreasing trend with differentiation for all the granitoids.

INTRODUCTION

Zircon is one of the most important accessorie in the rocks (if it is not the senior) because of many reasons. It shows a wide distribution in the different rocks, persistence in various environments, high resistance for erosion and stability against renewed high temperatures, pressures and anatexis. SPEER (1982) stated if for no other reason, zircon is a remarkable mineral because of its ubiquitous occurrence in the igneous, metamorphic and sedimentary rocks, meteorites and tektites. Importance of zircon, basically stems from two viewpoints:

1. The morphology and relative developing of its faces in prism(s) and pyramid(s) are tightly genetically related.

2. The ability of zircon to capture some radioactive elements gives it high prestige in age dating for the different types of rocks in different environments along the geological history; moreover a single crystal can tell us the historical geology, dating and geochemical variations through billions of years. Morphology of zircon as a petrogenetic indicator was discussed in some details by SPEER (1982).

The present study encompasses the morphological characters, microprobe analyses and BSE images of zircons with the aim to ascertain the origin and the evolution of the host granitoids of Abu El-Hasan, Northern part of the Eastern Desert, Egypt, (*Fig. 1*).

---

[1] Cairo, Egypt
[2] Manoufia, Egypt

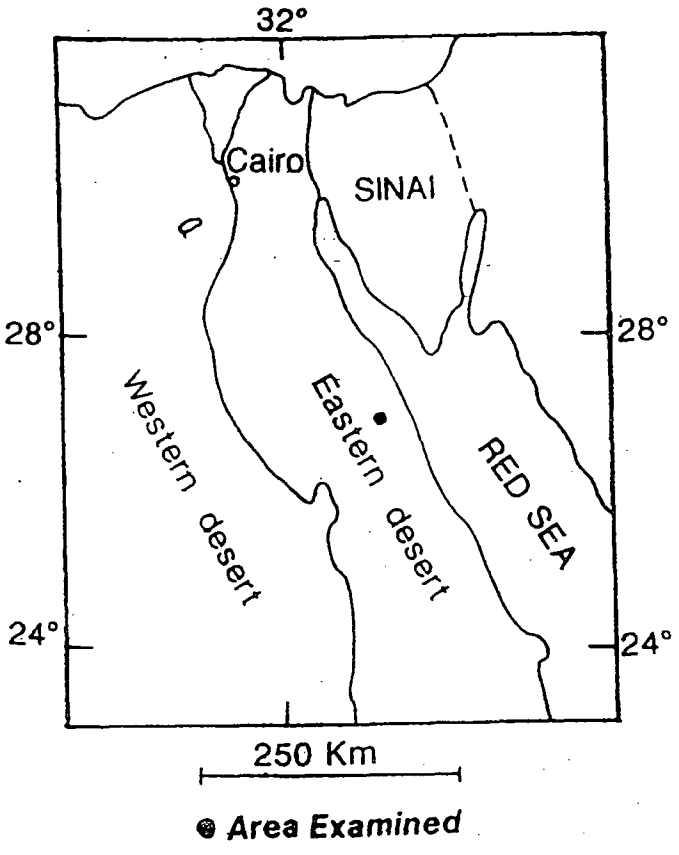

Fig. 1. Location Map

Broadly, the granitoids of Abu El-Hasan comprise older and younger types. However, details of field relations, petrography, tectonic setting and geochemistry of the granitoids of Abu El-Hasan are given by ATIA et al. 1998).

On the basis of typology of zircon population from granitic rocks PUPIN (1980) proposed a genetic classification with three main divisions: 1. granite of crustal or mainly crustal origin ('sub' autochtonous and aluminous granite); 2. granite of crustal + mantle origin, hybrid granites (calc-alkaline and sub-alkaline series granite); 3. granites of mantle or mainly mantle origin (alkaline and tholeiitic series granites). He also presented the spectacular theory that the relative size relations of two common zircon prisms {100} and {110} are controlled by temperature and can be taken as a direct measure for magmatic formation temperatures of granitic rocks, while the relative growth of zircon pyramids is connected with the characteristics of the crystallization medium. Subsequent works of PUPIN (1985, 1988) pointed out the relation between the genesis of the granitoid rocks and zircon morphology. PUPIN (op. Cit) constructed a typological classification „zircon habit chart" (*Fig. 4*) which has been used succesfully by several workers in the study of zircon in granitoids, such as RAJNDAR and HRABEAK (1989), CERGUNENKOF (1991), TONDER et al. (1990) and HUDUCH and LOESCHKE (1993).

REVIEW OF THE EGYPTIAN ZIRCONS

Several trials for studying of zircons from some Egyptian granitoid rocks were carried. Works of KHAFFAGY (1964), ZAGHLOUL and KHAFFAGY (1965), REFAAT (1970), RAGAB (1971), HEIKAL (1973), ABU EL-ELA (1973), ZAGHLOUL et al. (1981 a, b), ABD EL-MAKSOUD (1974) and ABD EL-GHAFFAR (1975) are such examples. Most of these studies are based on the description of the varietal features and the use of the Reduced Major Axis (RMA) as described by LARSEN and POLDERVAART (1957), to interpret the obtained data.

KABESH et al. (1976) clarified the significance of zircons as a guide to the petrogenesis of granites from Ras Barud area, Eastern Desert, and argued the formation of elbow twin to the crystallization from a melt which shows a sudden variation in the rate of crystallization. The presence of parallel growth to the high proportion of zircons crystallized early from a weakly viscous melt which permitted the movement and collision of growing zircon crystals. They noted also some necked zircons and attributed this to dissolution through a late stage of chemical corrosion. The examined zircons were characterized by sharply bounded crystals, uniformity of crystal, morphology and the elongation ratios mainly above two, all these led these authors (op cit.) to conclude a magmatic origin of the host granites.

ZAGHLOUL et al. (1981 a, b) recognized the value and efficiency of zircon study on subdivision of granitoid rocks of Gabal El-Shayib area into two genetically different groups: 1. Synorogenic group of metasomatic or granitization affiliation. 2. An intrusive magmatic group. They (op. cit.) also studied the distribution and abundance of zircons within these rocks and within the rock forming minerals and concluded that zircon was not entirely crystallized at an early stage but it appears to have a range of crystallization partly extending to the late stage.

HEIKAL et al. (1985) differentiated between the older and younger granitoids on the basis of dimensional parameters of zircons of Wadi El-Sheikh, southwestern Sinai. They also observed colour changes in the zircons of younger granitoid and this is attributed to progressively higher uranium and thorium contents, which could be correlated with the stage of differentiation of the younger granitoids. Zircon populations in the older granitoids contain a wide variety of crystal shapes, while those of the younger granitic rocks, become progressively more uniform in morphology rendering the magmatic origin for both.

EL-NASHAR (1992) presented a distinction between the two cycles of Samadai granitoid rocks, Eastern Desert, on the basis of HfO_2 enrichment in zircon. He also noted a change in Fe_2O_3 and Ce_2O_3 from the older to the younger granites, and he attributed this feature to the possibility of presence of two parental magmas.

Recently, EL-NASHAR (1998) studied the typological and geochemical characterization of zircons separated from some granitoids around Gebel Risasa, southeastern Sinai. According to this author, morphometric analyses of zircons proved useful in characterizing magmatic differentiation of the granitoid rocks and to distinguish calc-alkaline and alkaline granitic varieties. Moreover, the Zr/Hf ratios besides Y_2O_3 contents are useful in recognizing the major granitic series in the studied area.

BUDA et al. (1998) studied zircon grains from three different phases of the Precambrian granitoids of South Sinai in terms of complexity of crystal morphology, variability of forms and colour. According to these authors (op cit.) scanning electron microscope confirmed petrogenetic relation particularly those relating changes in zircon

morphology to progressive differentiation of co-magmatic series. BUDA et al. (op cit.) further stated that zircon grains are broadly affected by post-magmatic equilibrations.

Concerning the zircon of Abu El-Hasan, HILMY et al. (1994-1995) described the abundance, distribution, some morphological characters, length and beradth, evolution trends and the reduced major axes for the studied two phases (phase II and phase III) of the younger granitoids. They (op cit.) revealed the physicochemical conditions during zircon crystallization in the two phases, although uniform conditions prevailed in all parts of the pluton.

SAMPLE PREPARATION

Zircons are separated from samples representing the older granitoids and the various three phases of the younger granitoids in a trial to study similarities, differences and relation between their zircons and to give some lights on the evolution and genesis of the host rocks. About 100 gms of each sample were crushed in jaw crusher and then in oscillating disc till materials passed through 250 μm grid sieve. This relatively coarse size was chosen because some zircons in thin sections are coarse (about 0.3 mm). The crushed samples were washed by a jet of water dried at 105 °C. The sieved materials were further separated by settling in tetrabrommethane heavy liquid (D = 2.96), which were washed perfectly by isopropanal alkohol, dried, and then electromagnetically separated by Franz isodynamic separator. About 50-100 zircon crystals were picked and mounted in canada balsam on microscope glass slides beneath a cover glass. Although picking of the zircons takes much time otherwise it facilities the study because the samples have some quartz and feldspar grains.

The studied zircons show variation and gradation in colour, usually it is colorless to pale yellow in the older granitoids and the oldest phase of the younger granitoids. Their similarity in colour and also in morphology could reflect the consanguinity between these rocks, although the zircon of the older granitoids shows wider morphological forms and some crystals are believed to be xenocrysts. The colour of zircons of the leucocratic granites are usually yellow to reddish grey. The red colour increased in the red granites and the fine grained granites (i. e. the red color increases from phase II to phase III). FIELDING (1970) argued the red color to result from color centers of Nb_4^+ ions produced by the radiation-induced reduction of Nb_5^+ substituting for Zr_4^+. In the studied zircon the red color is more or less related to the colour of the rock and increases with increasing of the relative age. It is suggested that this color is directly connected with a late flood of red hematitic iron oxide fluid. This coloration is seen more along the cracks and not only in zircon, but also thorugh all the rock-forming minerals. It should be remembered that the red colour is nearly absent in zircons of the older (grey) granitoids and phase I of the younger granitoids (buff and white). This rule of coloration-causing fluid should be regional in all the Egyptian granitoids and responsible for the field coloration of the younger granitoids which may be buff, pink or red. Occasionally the zircon of the older granitoids shows some red pigments, this may be argued to adhesion of some percolating hematitic drops to the surface of zircon crystals, and is obvious in some samples from the bottom of the wadi. The hematitic material sometimes coats the grains and in some others acts as glue between zircons and the other rock-forming minerals which makes it difficult or impossible to identify the faces of the crystals. Some opaque zircons (malacon or metamict) are occasionally found especially in the red granite and the leucocratic granite. Metamictization is generally attributed to the radiation damage produced by radioactive decay of thorium and uranium (MITCHELL 1973), but in the studied zircons it is believed to be due to the attack of zircon by hematitic solutions.

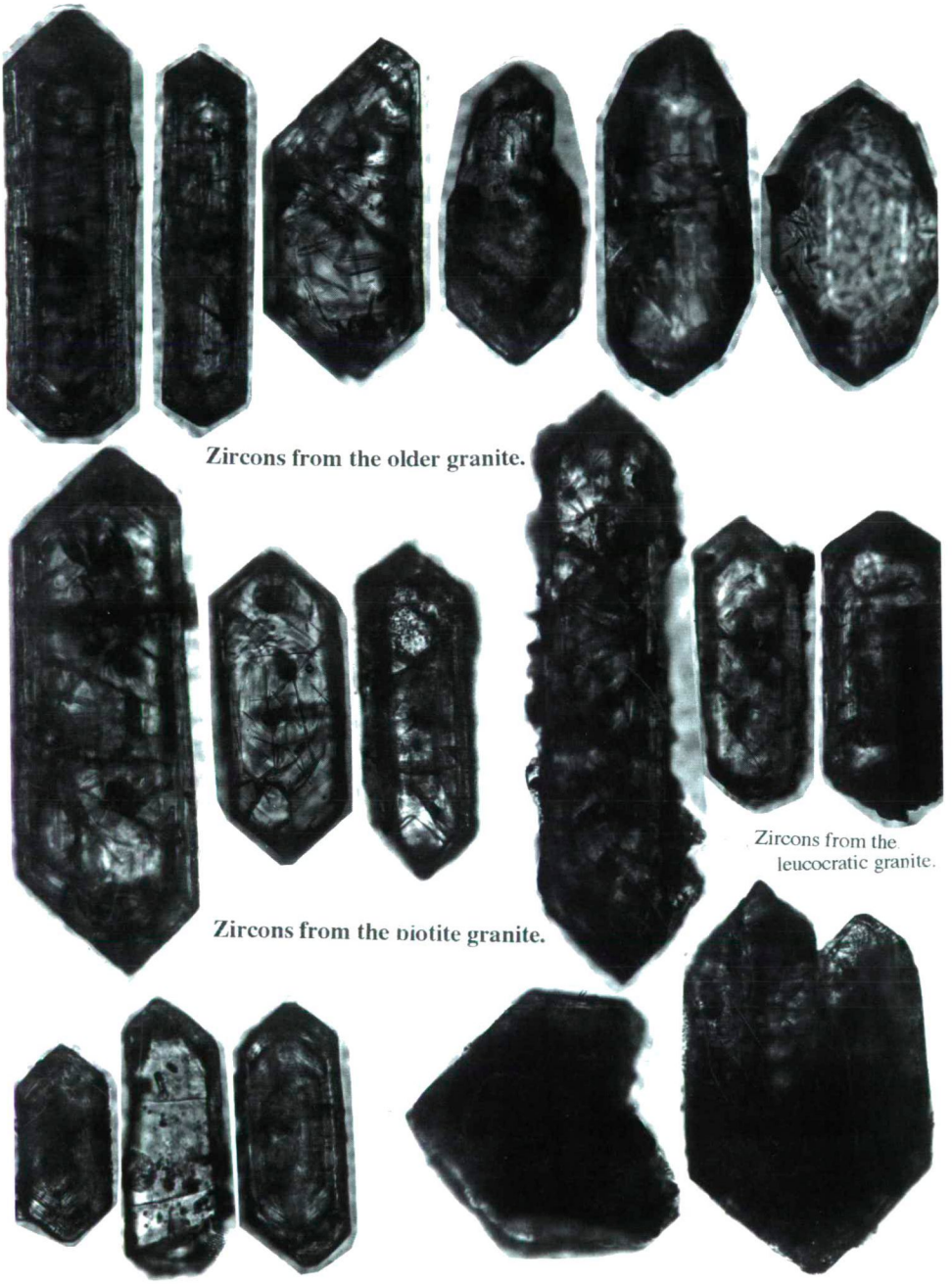

Fig. 2. Photomicrographs showing different varieties of zircons

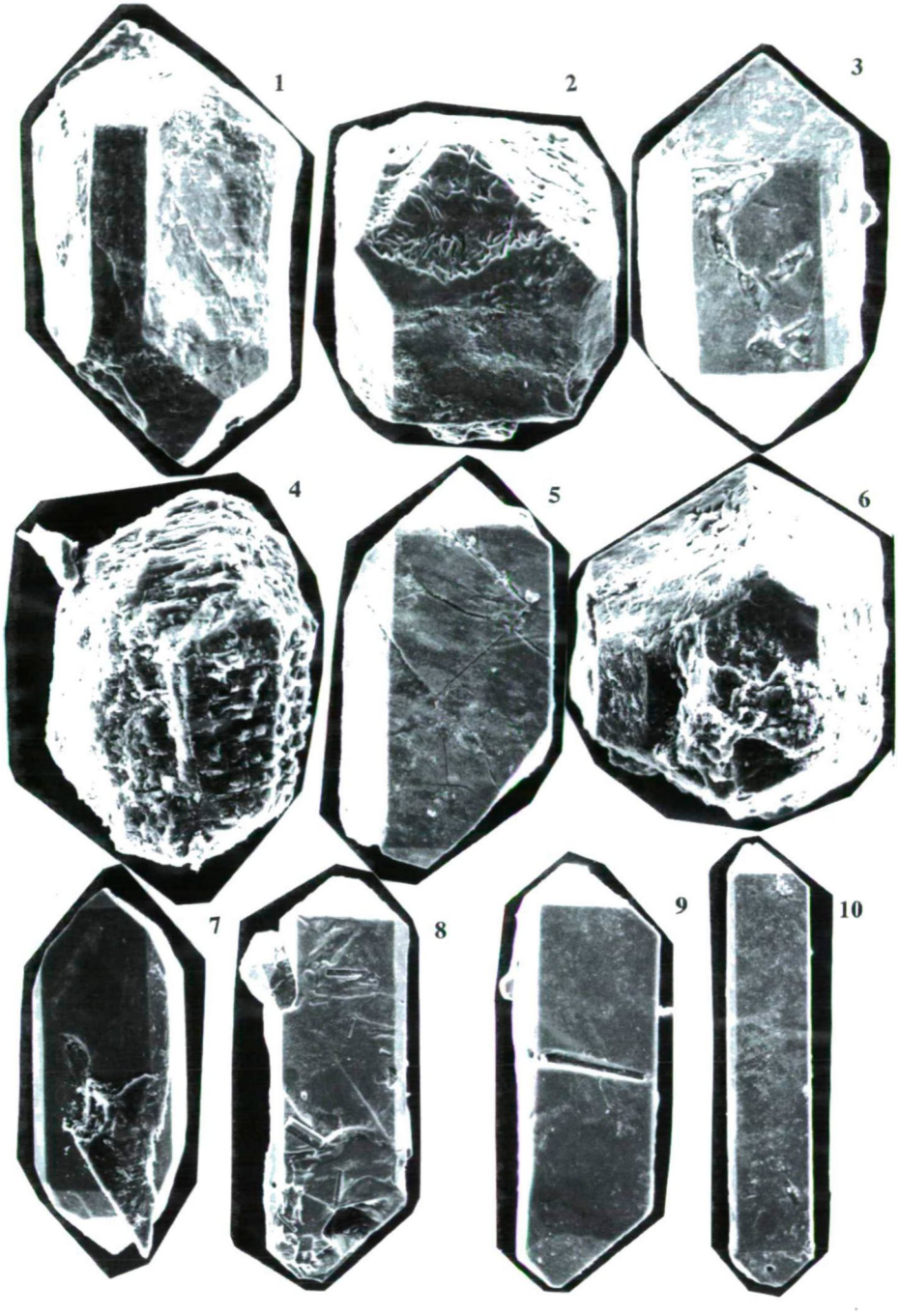

Fig. 2. Continued. SEM images for different varieties of Abu El Hasan zircon.

The abundance of zircon is varied in the studied granitoids and reaches its maximum in the biotite granite (phase I of the younger granites) which contains a fair amount. The older granitoids contain a bit lower. Zircons of both groups are more or less similar in many characters. Leucocratic granite (phase II), red granite and fine grained granite (phase III) have rather low abundance with more or less similar zircons. Some of the zircons of phase II and phase III are attacked by iron oxides or even completely replaced, so fragments and corroded zircons can be seen. Zircons are found as inclusions in the early formed minerals as hornblende, biotite and plagioclase, as well as in the later ones as orthoclase and quartz which supposes early to late crystallization of zircon, also water-rich magma (PUPIN et al., 1979). The zircons of the older granitoids and phase I of the younger granitoids are long prismatic to moderately prismatic in habit with length range from 150 to 300 μm and length / breadth 4 to 2, while those of phase II and III are moderately prismatic to stubby with length range between 250 and 60 μm and length / / breadth about 3 to 1.5. Nearly all the studied crystals are euhedral, but some are attacked and show corrosion canals.

The studied zircons have some inclusions which are mainly apatite, zircon, opaques and dust. These inclusions are haphazardly oriented and more abundant in zircons of the older granitoids. Some zircon crystals are free of inclusions especially those in phase II and III of the younger granitoids. Some of the inclusions are partly enclosed as minute biotite flakes and opaques. It should be mentioned that zircons of the older granitoids and phase I of the younger granitoids have much less cracks than those of phases II and III of the younger granitoids (their zircons are usually brittle and highly cracked).

Overgrowths are rarely seen but they are represented in considerable amount. Both the parallel and elbow twinning are relatively common in the fine grained rather than the other units which is attributed to sudden cooling. Some crystals are massive without any zoning, while zoned crystals are more common. Some of them show unzoned internal area with zoned periphery while others show rhythmic zoning throughout. *Fig. (2)* shows different varieties of the studied zircons.

ZIRCON TYPOLOGY OF ABU EL-HASAN GRANITOIDS

In this context a method which is based on the careful study of the morphology of zircons is used, plotting of the main subtypes, calculation of typological parameters (mean points A-, T-, T.E.T) were carried out according to PUPIN and TURCO (1972a) and results were interpreted principally according to PUPIN (1980).

Fig. (3) shows the typologic frequency distribution of the populations of Abu Al-Hasan zircon, it is clear that the older granitoids occupies larger area with various forms which support the belief that some of those are xenocrystals (with frequency less than 2 %) and could be inherited from more older rocks or digested xenofragments. Although these crystals are very clear and do not show any overgrowths, outgrowths, or corrosion as compared with the original crystals. Otherwise the younger granitoids show much more regularity in the distribution. It can be seen that only the pyramid {101} is the dominant in the older granitoids and the sole in the younger granitoids, while most of the zircons have the two prisms {100} and {110} with larger {100} prisms. It can be noted also that the zircon population moves down on the diagram with decreasing age of the rock units. According to PUPIN (1976) all the studied rocks either older or younger types plot in the fields of alkaline and hyperalkaline syenites and granites, while according to the genetic classification of PUPIN (1980) these rocks plot in the field of mantle or

mainly mantle origin (alkaline and tholeiitic series granites). *Fig. (4)* shows the mean points and typological evolutionary trends of the studied zircons, there is a non-regular movement of the points down with decreasing age which may indicate some evolution or differentiation from the older to the younger rocks. Otherwise if we consider the approximate temperature scale proposed by PUPIN and TURCO (1972b) we will get non-plausible data whereby the older granitoids were formed during a wide range of temperature (600-900 °C) which increase gradually in the younger granitoids being in contradiction with the well known rules.

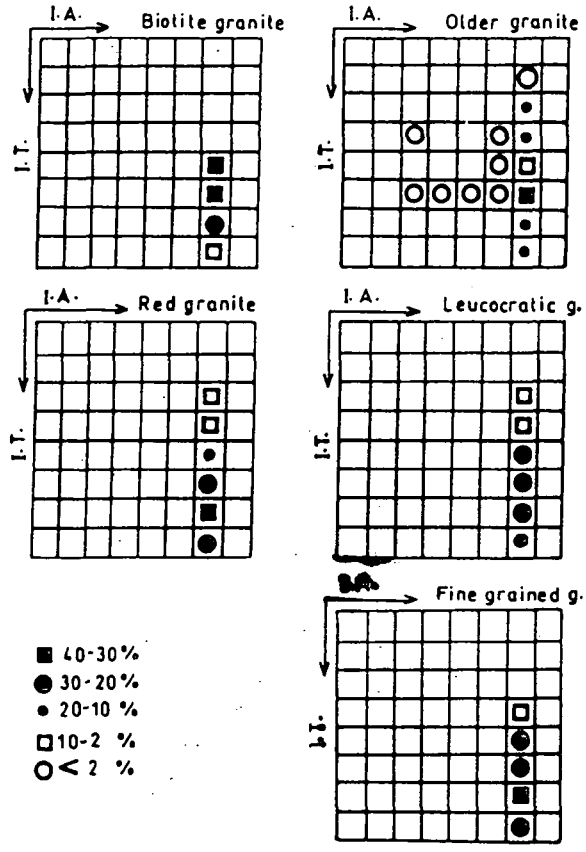

Fig. 3. Typological frequency distribution of the populations of zircons

MICROPROBE STUDY OF ABU EL-HASAN ZIRCON

Extensive microprobe analyses were carried out for different zircons from all the rock units in a trial to identify and study the magmatic evolution and the crystal building during the crystallization of this mineral. This can be done by studying cautiously the chemical variations in the different zones. Because it is believed that the zircon could be an early mineral, it also can tell about the parent magma and the preliminary stages of the magma evolution and composition.

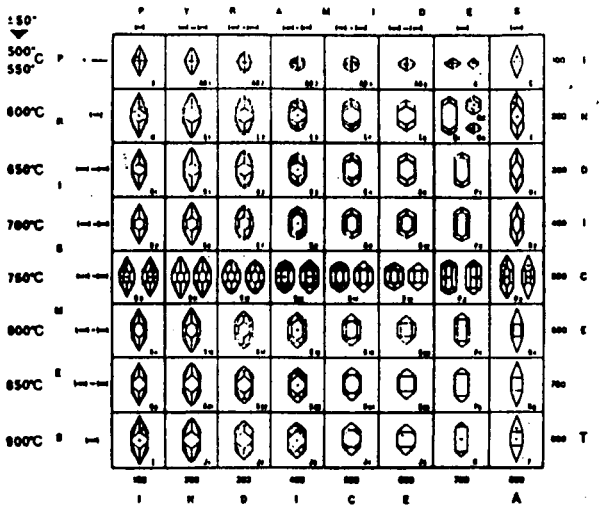

Main types and subtypes of the typological classification, PUPIN (1980)

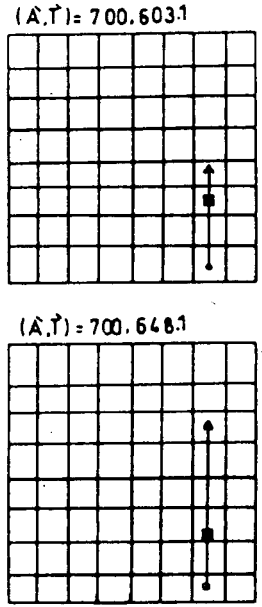

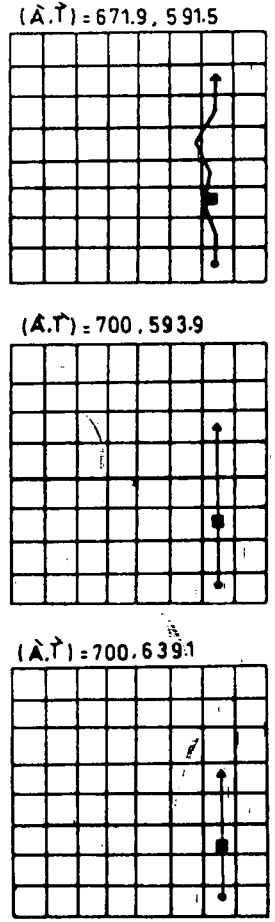

Fig. 4. Mean points (A', T') and typological evolutionary trends (T. E. T.) of zircons

Preparation of the samples and the analytical conditions

For better and accurate understanding of zoning we prepared oriented sections perpendicular to the C axis and others parallel to it, some details about the preparation of such sections were described by BENISEK and FINGER (1993). Briefly the zircons were aligned on a glass slide with glue perpendicular (or parallel) to arbitrary line and then cut cautiously till the middle using fine powder (1200) in the final stages (then the parallel sections were polished), then this slide was fixed perpendicular to another and cut till the zircon thickness reached 20-50 μm. The crystallographic orientation was noted and registered before the treatment, *Fig. 5* shows a sketch after BENISEK and FINGER (op cit.). Afterwards the sections were perfectly polished with 3 and 1 μm diamond.

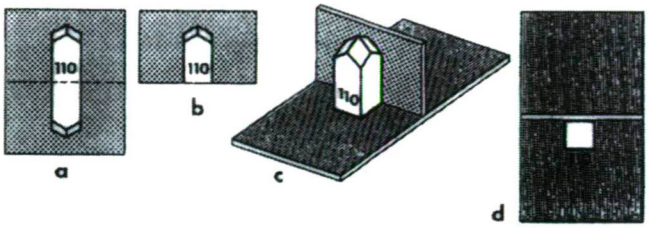

Fig. 5. Sketches showing how zircons were prepared for microprobe work, after BENISEK & FINGER

Microprobe work was carried out on the JEOL probe JXA-800 of Salzburg University. Spot analyses were made with a beam diameter about 1 μm using an accelerating voltage of 20 KV and a beam current of 40 NA. Elements Si, Zr, Hf, U, Th, Y, P, Ca, Al and Fe were routinely determined. Counting between 10-20 seconds per element were chosen. The detection limits reached with these conditions between 0.05 wt % (Y_2O_3) and 0.01 wt % Al_2O_3. Ca, Al and Fe can be detected in some spots and anomalously high values were recorded in the altered spots (up to 3 % CaO, 1.5 % Al_2O_3 and 2.5 % FeO). HREE, LREE, Y, Th and U were detected in some spots. Natural zircon, apatite and synthetic HfO_2, UO_2, ThO_2, $Y_3Al_5O_{12}$, YbF_3, $LuSi_2$, Fe_2O_3 served as standards for microprobe analyses. Raw concentrations were recalculated by applying normal ZAF corrections. Relative δ errors resulting from counting statistics are typically 3-5 % for the 1 wt % level and about 20% for the 0.1 wt % level. Back scatter electron (BSE) images were recorded with constant 20 KV accelerating voltage, but with different beam current and different gain of the photomultiplier to optimize the resolution for each grain. This means that zircon growth zones of similar chemical composition may have the same grey tone in the different BSE picture.

Description of the BSE images

Because these images are based on the differentiation between the mean atomic numbers (bright when they are high and black when they are low) these are very effective in revealing three main features in our zircons: 1. zoning and crystal growth. 2. effect of the aggressive hydrothermal solutions and 3. inclusions. The discrimination between the zircons of the different rock units is rather clear using these images. Zircons from the older granites often show central weakly (narrow-spaced) zoned or unzoned cores (about several tens of micrometers) and more obvious narrow – spaced rim (about 10-30 μm). The crystals have a lot of vugs (very difficult to get good polished surface) and cleavage can be seen. Mineral inclusions are nearly absent, some crystals show

hydrothermal alteration which is thought to be of exogenic origin due to percolating aggressive surfacial or rain water. Zircons from the biotite granites often show nice large-spaced zoning (one zone ranges from few micrometers to few tens of micrometers), many apatite crystals and some vugs are included. It was noted that the cracks are concentrated in the dark zones rather than the bright ones, this can be attributed to the expansion of the bright zones because of the high radiation causing pressure leading to cracking in the dark zones. Zircons from the leucocratic granites show some similarity to those of the older granitoids having inner unzoned cores, and outer highly ragged rims because of hydrothermal alteration. These solutions draw very fascinating pictures which look like the carpets or brain structure. Cleavages and cracks are not uncommon in the altered parts where the solutions were flowing.

Zircons from the red granites show regular spaced zoning throughout the grain from the center to the rim (about 2 μm). The corrosion canals run parallel to the zoning causing low topography (usually dark) corroded zones alternating with high topography brighter zones. Such variation in surface topography makes it impossible to get good polishing. Large scale zoning is represented in some cases. Inclusions are nearly absent. Zircons from the fine grained granites are very fascinating because of the drawing caused by the hydrothermal alteration and they show variation in the structure in contrast to the zircons from other rock units. Some grains have unzoned core and narrow-spaced zoned rim, some others are totally unzoned or show large-spaced regular zoning. In many times alteration obliterated the original zoning and only relics can be seen. Some grains show very clearly the corrosion canals of the solutions. Cracks are common and cleavages are sometimes seen. Inclusions are rare or nearly absent while some vugs are present. *Fig. 6.* shows some BSE images for the different rock types.

It is noted that the effect of the hydrothermal solutions reaches its climax in the case of the leucocratic and fine grained granites, while it is less or absent in the older and biotite granites. These alterations are somehow correlated with the color of the rocks. What is interesting is that zircons of the red granites (the most reddish rocks) have not such apparent alterations but effect of these solutions can be interfered from the analyses and the surface texture of the grains, the infected spots by such solutions have much higher amounts in Fe, Ca and Mn and this is the case for all the spots of the red granites, while the corrosion canals can be detected in the low topography zones. Broadly two different processes can be invoked to explain the origin of these solutions:

1. Exogenic processes in which the source is surfacial or rain solutions. This happened in the case of the older and biotite granites where the rocks as whole are grey or whitish respectively and only some samples (and also some zircons) were infected by the solutions.
2. Endogenic processes which can be classified into secondary (or late magmatic) and primary (or syn-crystallization). The former is invoked for the solutions affecting the leucocratic and fine grained granties where a clear secondary solution effect. The primary or syn-crystallization solutions are thought to be homogenized with the magma which leads to the red granites crystallization where no clear secondary effect but only inferred.

CHEMICAL ANALYSES

Chemical analyses were carried out in spots from the core to the rim of the grains to deduce the variations through crystal growth and the magmatic evolution. Some spots are taken from the altered parts to see the effect of these solutions on the chemistry of the zircon (Table 1). All the studied zircons are typical zircon (CORRERIA NEVES et al.,

TABLE 1

Representative chemical analyses of the studied zircon (Grain LG 1)

No.	1	2	3	4	5	6	7	15	Aver. Fresh	8	9	10	11	12	13	14	Aver Alt.
SiO_2	30.08	30.57	30.78	30.56	30.60	29.72	32.15	30.51	30.62	29.81	29.39	28.54	28.61	28.23	27.96	28.95	28.78
HfO_2	1.74	1.88	2.07	2.08	1.87	1.77	1.99	1.97	1.92	1.74	1.72	1.61	1.69	1.71	1.60	1.61	1.67
Yb_2O_3	0.19	0.49	0.38	0.15	0.09	0.26	0.33	0.00	0.24	0.31	0.28	0.38	0.42	0.52	0.65	0.72	0.47
Al_2O_3	0.00	0.00	0.00	0.00	0.03	0.00	0.01	0.02	0.01	0.09	0.08	0.00	0.00	0.30	0.29	0.42	0.17
Er_2O_3	0.24	0.10	0.00	0.11	0.00	0.20	0.33	0.00	0.12	0.14	0.00	0.11	0.27	0.27	0.60	0.30	0.24
MgO	0.00	0.00	0.00	0.01	0.01	0.00	0.00	0.00	0.00	0.02	0.05	0.01	0.02	0.02	0.00	0.02	0.02
CaO	0.03	0.00	0.02	0.00	0.08	0.04	0.03	0.04	0.03	1.77	1.79	2.06	1.58	1.43	1.22	1.45	1.61
FeO	0.00	0.00	0.00	0.07	0.06	0.00	0.00	0.04	0.02	1.99	1.95	2.32	1.05	1.40	1.22	1.12	1.58
Gd_2O_3	0.00	0.00	0.00	0.13	0.00	0.00	0.00	0.10	0.03	0.10	0.00	0.16	0.14	0.00	0.15	0.11	0.09
MnO	0.00	0.00	0.00	0.00	0.00	0.00	0.00	0.00	0.00	0.38	0.42	0.47	0.28	0.16	0.27	0.26	0.32
Eu_2O_3	0.00	0.00	0.00	0.13	0.00	0.00	0.00	0.00	0.02	0.00	0.00	0.00	0.00	0.00	0.00	0.00	0.00
Sm_2O_3	0.00	0.00	0.00	0.00	0.00	0.00	0.09	0.00	0.01	0.00	0.00	0.00	0.11	0.21	0.12	0.10	0.08
Pr_2O_3	0.18	0.00	0.00	0.00	0.15	0.00	0.00	0.00	0.04	0.20	0.00	0.00	0.00	0.00	0.00	0.00	0.03
Nd_2O_3	0.00	0.00	0.00	0.00	0.00	0.00	0.07	0.00	0.01	0.00	0.00	0.00	0.00	0.18	0.15	0.32	0.09
TiO_2	0.00	0.00	0.08	0.00	0.00	0.00	0.00	0.06	0.02	0.00	0.00	0.00	0.00	0.00	0.00	0.00	0.00
Sc_2O_3	0.06	0.00	0.11	0.00	0.00	0.00	0.06	0.00	0.03	0.00	0.00	0.00	0.00	0.00	0.07	0.00	0.01
P_2O_5	0.14	0.07	0.04	0.00	0.06	0.14	0.12	0.00	0.07	0.09	0.13	0.07	0.11	0.10	0.20	0.15	0.12
Ce_2O_3	0.00	0.08	0.06	0.00	0.06	0.06	0.09	0.06	0.05	0.07	0.08	0.06	0.00	0.27	0.17	0.33	0.14
La_2O_3	0.05	0.00	0.10	0.00	0.07	0.00	0.00	0.00	0.03	0.00	0.00	0.00	0.00	0.00	0.00	0.07	0.01
UO_2	0.62	0.70	0.30	0.20	0.00	0.82	0.40	0.11	0.39	0.71	0.64	0.68	0.69	0.42	0.46	0.37	0.57
ThO_2	0.46	0.45	0.23	0.00	0.08	0.62	0.20	0.00	0.26	0.32	0.36	0.46	0.40	0.26	0.48	0.30	0.37
Nb_2O_3	0.00	0.00	0.00	0.11	0.00	0.13	0.00	0.00	0.03	0.19	0.00	0.00	0.00	0.00	0.00	0.00	0.03
ZrO_2	65.08	64.31	63.29	63.89	64.72	62.39	62.74	64.27	63.84	58.45	59.01	57.51	58.23	57.19	56.07	56.80	57.61
Y_2O_3	1.23	1.20	0.89	0.15	0.30	1.07	0.90	0.36	0.76	0.95	0.98	1.09	0.78	1.74	2.55	0.84	1.28
Total	100.1	99.85	98.35	97.59	98.18	97.22	99.51	97.54	98.54	97.33	96.88	95.53	94.38	94.41	94.23	94.24	95.29

TABLE 1 continued

Representative chemical analyses of the studied zircon (Grain LG 2)

No.	1	2	3	4	5	6	7	8	9	Aver. Fresh
SiO_2	31.33	31.29	31.97	31.88	32.12	32.44	32.29	32.53	32.76	32.07
HfO_2	2.15	2.04	2.19	1.96	1.77	1.94	2.05	5.57	6.03	2.86
Yb_2O_3	0.19	0.22	0.23	0.08	0.11	0.00	0.12	0.07	0.10	0.12
Al_2O_3	0.00	0.00	0.00	0.00	0.00	0.00	0.00	0.00	0.00	0.00
Er_2O_3	0.11	0.13	0.08	0.15	0.11	0.13	0.00	0.00	0.00	0.08
MgO	0.00	0.01	0.00	0.01	0.00	0.01	0.00	0.00	0.00	0.00
CaO	0.03	0.00	0.00	0.00	0.00	0.04	0.00	0.03	0.03	0.01
FeO	0.00	0.00	0.00	0.04	0.00	0.04	0.04	0.06	0.11	0.03
Gd_2O_3	0.00	0.00	0.00	0.00	0.00	0.28	0.00	0.00	0.15	0.05
MnO	0.00	0.00	0.00	0.00	0.00	0.00	0.00	0.00	0.05	0.01
Eu_2O_3	0.09	0.00	0.00	0.13	0.00	0.06	0.00	0.00	0.00	0.02
Sm_2O_3	0.00	0.00	0.00	0.00	0.00	0.00	0.00	0.15	0.00	0.02
Pr_2O_3	0.00	0.00	0.00	0.00	0.00	0.00	0.00	0.00	0.00	0.00
Nd_2O_3	0.00	0.00	0.00	0.00	0.00	0.00	0.00	0.00	0.00	0.00
TiO_2	0.00	0.08	0.00	0.05	0.00	0.00	0.08	0.06	0.00	0.03
Sc_2O_3	0.00	0.00	0.00	0.00	0.00	0.06	0.00	0.00	0.00	0.01
P_2O_5	0.11	0.08	0.06	0.00	0.04	0.00	0.05	0.04	0.00	0.04
Ce_2O_3	0.06	0.13	0.08	0.00	0.00	0.10	0.10	0.00	0.00	0.05
La_2O_3	0.00	0.00	0.08	0.00	0.00	0.09	0.00	0.00	0.00	0.02
UO_2	0.48	0.41	0.25	0.00	0.11	0.00	0.09	0.25	0.19	0.20
ThO_2	0.19	0.33	0.13	0.10	0.12	0.00	0.07	0.13	0.00	0.12
Nb_2O_3	0.00	0.00	0.00	0.00	0.00	0.00	0.00	0.00	0.00	0.00
ZrO_2	62.56	63.26	63.88	64.71	65.43	64.31	63.87	63.63	60.09	63.53
Y_2O_3	0.63	0.66	0.37	0.00	0.39	0.25	0.22	0.00	0.00	0.28
Total	97.93	98.64	99.32	98.98	100.2	99.75	98.99	102.5	99.51	99.54

TABLE 1 continued

Representative chemical analyses of the studied zircon (Grain FG 1)

No.	23	24	25	31	Aver. Fresh	26	27	28	29	30	31	32	33	34	35	36	Aver Alt.
SiO_2	33.00	32.18	31.68	31.55	32.10	29.39	26.67	25.09	28.88	25.74	31.55	28.45	27.36	23.57	25.30	30.62	27.51
HfO_2	1.66	1.34	1.65	2.67	1.83	1.50	1.67	1.73	1.78	2.34	2.67	1.41	1.34	3.66	1.83	2.13	2.01
Yb_2O_3	0.16	0.09	0.00	0.19	0.11	0.74	0.49	0.51	0.47	0.29	0.19	0.48	0.47	0.31	0.43	0.43	0.44
Al_2O_3	0.00	0.00	0.02	0.00	0.01	0.02	1021	1043	0.00	1.26	0.00	0.08	0.34	1.33	1.46	0.00	0.65
Er_2O_3	0.00	0.00	0.00	0.14	0.04	0.52	0.30	0.32	0.34	0.16	0.14	0.29	0.37	0.12	0.37	0.13	0.28
MgO	0.00	0.00	0.00	0.00	0.00	0.01	0.02	0.05	0.00	0.05	0.00	0.01	0.03	0.06	0.06	0.00	0.03
CaO	0.05	0.03	0.03	0.05	0.04	0.45	1.25	1.43	0.98	1.67	0.05	0.64	1.52	1.55	1.58	0.66	1.07
FeO	0.15	0.10	0.06	0.13	0.11	1.21	2.45	2.20	0.61	2.26	0.13	1.19	2.46	2.50	2.10	1.55	1.70
Gd_2O_3	0.00	0.00	0.00	0.00	0.00	0.00	0.00	0.34	0.25	0.00	0.00	0.00	0.11	0.20	0.00	0.00	0.08
MnO	0.00	0.00	0.00	0.00	0.00	0.15	0.20	0.13	0.19	0.15	0.00	0.16	0.14	0.15	0.13	0.22	0.15
Eu_2O_3	0.00	0.00	0.11	0.00	0.03	0.00	0.00	0.00	0.00	0.00	0.00	0.00	0.00	0.00	0.00	0.06	0.01
Sm_2O_3	0.00	0.00	0.08	0.00	0.02	0.00	0.00	0.11	0.00	0.00	0.00	0.13	0.16	0.12	0.00	0.00	0.05
Pr_2O_3	0.25	0.00	0.00	0.00	0.06	0.26	0.00	0.00	0.00	0.00	0.00	0.00	0.00	0.00	0.00	0.00	0.02
Nd_2O_3	0.00	0.00	0.00	0.00	0.00	0.00	0.00	0.00	0.00	0.00	0.00	0.00	0.00	0.00	0.16	0.00	0.01
TiO_2	0.00	0.00	0.09	0.00	0.02	0.00	0.00	0.11	0.10	0.00	0.00	0.00	0.00	0.06	0.00	0.00	0.02
Sc_2O_3	0.00	0.00	0.00	0.00	0.00	0.00	0.06	0.00	0.00	0.00	0.00	0.06	0.05	0.00	0.05	0.00	0.02
P_2O_5	0.06	0.04	0.08	0.12	0.08	0.33	0.49	0.61	0.28	0.62	0.12	0.56	0.29	0.64	0.62	0.22	0.43
Ce_2O_3	0.17	0.05	0.00	0.11	0.08	0.05	0.14	0.18	0.00	0.18	0.11	0.08	0.06	0.15	0.16	0.00	0.10
La_2O_3	0.00	0.00	0.00	0.00	0.00	0.00	0.08	0.07	0.00	0.00	0.00	0.00	0.00	0.00	0.00	0.00	0.01
UO_2	0.00	0.09	0.07	0.37	0.13	0.94	0.89	0.88	0.77	0.62	0.37	0.89	0.83	1.04	0.64	0.70	0.78
ThO_2	0.00	0.09	0.00	0.00	0.02	0.32	0.28	0.38	0.41	0.39	0.00	0.58	0.25	0.14	0.28	0.29	0.30
Nb_2O_3	0.00	0.00	0.00	0.00	0.00	0.00	0.00	0.00	0.00	0.00	0.00	0.00	0.00	0.00	0.00	0.00	0.00
ZrO_2	65.73	63.85	64.70	63.04	64.33	58.47	50.47	56.69	57.93	55.96	63.04	57.87	56.20	58.72	59.29	59.32	58.54
Y_2O_3	0.19	0.18	0.11	0.32	0.21	1.67	1.06	1.27	1.17	0.96	0.34	1.50	1.51	0.68	1.29	1.13	1.14
Total	101.4	98.04	98.66	98.71	99.21	96.03	97.73	93.53	94.16	92.65	98.71	94.38	93.49	95.00	95.75	97.46	95.35

TABLE 1 continued

Representative chemical analyses of the studied zircon (Grain FG 2)

No.	1	2	3	4	5	6	7	Aver. Fresh	8	9	10	Aver. Fresh
SiO_2	31.14	30.86	31.09	31.50	31.96	31.98	31.94	31.50	28.39	26.10	25.38	26.62
HfO_2	2.12	2.18	2.09	2.17	2.00	2.05	2.16	2.11	1.86	1.89	1.67	1.81
Yb_2O_3	0.23	0.36	0.28	0.27	0.13	0.13	0.16	0.22	0.32	0.65	0.96	0.64
Al_2O_3	0.00	0.00	0.00	0.00	0.00	0.00	0.00	0.00	0.02	0.68	1.10	0.60
Er_2O_3	0.17	0.22	0.09	0.09	0.00	0.00	0.00	0.08	0.14	0.46	0.67	0.42
MgO	0.00	0.00	0.00	0.00	0.00	0.00	0.00	0.00	0.03	0.00	0.02	0.02
CaO	0.00	0.05	0.05	0.03	0.03	0.05	0.06	0.04	1.18	0.79	0.92	0.96
FeO	0.00	0.00	0.04	0.00	0.09	0.08	0.03	0.03	0.46	1.07	1.23	0.93
Gd_2O_3	0.00	0.12	0.00	0.00	0.00	0.15	0.00	0.04	0.13	0.34	0.14	0.17
MnO	0.00	0.00	0.00	0.00	0.00	0.00	0.00	0.00	0.21	0.15	0.14	0.17
Eu_2O_3	0.00	0.00	0.12	0.06	0.11	0.00	0.00	0.04	0.00	0.00	0.00	0.00
Sm_2O_3	0.00	0.00	0.00	0.00	0.00	0.00	0.00	0.00	0.16	0.20	0.42	0.26
Pr_2O_3	0.22	0.00	0.00	0.00	0.00	0.25	0.00	0.07	0.17	0.00	0.16	0.11
Nd_2O_3	0.00	0.00	0.00	0.00	0.00	0.00	0.10	0.01	0.00	0.10	0.44	0.18
TiO_2	0.05	0.00	0.12	0.12	0.00	0.05	0.00	0.05	0.00	0.00	0.06	0.02
Sc_2O_3	0.00	0.00	0.00	0.00	0.00	0.00	0.00	0.00	0.00	0.00	0.06	0.02
P_2O_5	0.09	0.01	0.08	0.03	0.00	0.05	0.09	0.05	0300	0.76	0.85	0.54
Ce_2O_3	0.00	0.13	0.06	0.00	0.00	0.10	0.11	0.06	0.09	0.17	0.40	0.22
La_2O_3	0.00	0.00	0.00	0.00	0.00	0.08	0.00	0.01	0.00	0.00	0.00	0.00
UO_2	0.47	0.57	0.49	0.10	0.00	0.08	0.00	0.24	0.54	0.67	0.69	0.63
ThO_2	0.31	0.00	0.00	0.10	0.00	0.18	0.10	0.10	0.32	0.39	0.30	0.34
Nb_2O_3	0.00	0.00	0.00	0.00	0.00	0.00	0.18	0.03	0.00	0.00	0.00	0.00
ZrO_2	63.41	62.69	64.14	64.59	65.03	65.49	64.15	64.36	59.27	56.68	53.09	56.35
Y_2O_3	0.88	0.84	0.84	0.60	0.25	0.39	0.14	0.56	0.90	2.06	3.42	2.13
Total	99.09	98.03	100.5	99.66	99.6	101.1	99.22	99.6	94.22	93.16	92.49	93.29

TABLE 1continued

Representative chemical analyses of the studied zircon (Grain RG 1 and RG2)

No.	1	3	4	5	6	7	8	9	10	Aver. Fresh	16	17	18	19	20	21	22	Aver Alt.
SiO_2	27.51	27.85	27.78	29.59	28.15	27.13	30.08	29.69	28.12	28.43	30.29	26.47	28.68	30.23	32.59	30.90	27.25	29.49
HfO_2	1.97	1.70	1.64	1.78	1.87	1.92	2.22	1.98	2.39	1.94	1.88	1.75	1.65	1.73	2.08	1.90	1.59	1.79
Yb_2O_3	0.55	1.14	0.35	0.56	0.62	1.01	0.18	0.06	0.13	0.51	0.24	0.18	0.50	0.36	0.09	0.12	0.82	0.33
Al_2O_3	0.88	1.11	0.54	0.86	1.12	1.22	0.01	0.00	0.19	0.66	0.37	0.70	0.75	0.93	0.04	0.30	1.00	0.58
Er_2O_3	0.39	0.66	0.14	0.53	0.45	0.91	0.00	0.09	0.18	0.37	0.11	0.52	0.38	0.17	0.14	0.00	0.61	0.28
MgO	0.02	0.04	0.02	0.04	0.03	0.03	0.01	0.00	0.00	0.02	0.01	0.00	0.03	0.02	0.00	0.03	0.03	0.02
CaO	0.91	1.25	1.17	0.77	1.09	1.24	0.04	0.05	0.39	0.77	0.58	0.98	0.28	0.58	0.14	0.76	1.21	0.65
FeO	1.27	1.10	1.42	0.77	0.83	0.81	0.06	0.12	0.30	0.74	0.39	0.44	0.08	0.23	0.00	0.30	0.49	0.28
Gd_2O_3	0.35	0.37	0.11	0.00	0.10	0.29	0.00	0.00	0.00	0.14	0.18	0.24	0.00	0.00	0.00	0.00	0.22	0.09
MnO	0.00	0.05	0.12	0.00	0.11	0.07	0.00	0.00	0.12	0.05	0.00	0.10	0.00	0.07	0.00	0.00	0.13	0.04
Eu_2O_3	0.00	0.07	0.06	0.00	0.07	0.00	0.10	0.00	0.00	0.03	0.00	0.00	0.00	0.00	0.00	0.00	0.00	0.00
Sm_2O_3	0.00	0.17	0.00	0.00	0.00	0.00	0.00	0.15	0.00	0.04	0.00	0.00	0.22	0.00	0.00	0.00	0.00	0.03
Pr_2O_3	0.43	0.00	0.00	0.00	0.17	0.19	0.00	0.16	0.00	0.11	0.00	0.15	0.00	0.00	0.00	0.00	0.00	0.02
Nd_2O_3	0.13	0.00	0.14	0.00	0.11	0.00	0.00	0.00	0.00	0.04	0.00	0.00	0.14	0.00	0.00	0.136	0.17	0.06
TiO_2	0.06	0.00	0.00	0.06	0.07	0.17	0.00	0.00	0.05	0.05	0.12	0.08	0.00	0.00	0.00	0.00	0.140	0.04
Sc_2O_3	0.06	0.12	0.00	0.00	0.00	0.00	0.00	0.00	0.00	0.02	0.11	0.00	0.00	0.05	0.00	0.00	0.00	0.02
P_2O_5	0.59	1.04	0.25	0.47	0.85	1.05	0.04	0.05	0.22	0.51	0.46	0.77	0.60	0.36	0.07	0.47	0.90	0.52
Ce_2O_3	0.13	0.19	0.06	0.05	0.00	0.13	0.00	0.00	0.00	0.06	0.00	0.12	0.11	0.00	0.15	0.00	0.13	0.07
La_2O_3	0.00	0.05	0.00	0.00	0.00	0.00	0.00	0.00	0.00	0.01	0.00	0.00	0.00	0.06	0.00	0.16	0.00	0.03
UO_2	0.55	0.47	0.36	0.27	0.46	0.51	0.08	0.15	0.13	0.33	0.32	0.10	0.23	0.17	0.00	0.07	0.24	0.16
ThO_2	0.34	0.22	0.14	0.00	0.00	0.14	0.00	0.00	0.00	0.09	0.12	0.08	0.00	0.06	0.00	0.00	0.09	0.05
Nb_2O_3	0.00	0.00	0.00	0.13	0.39	0.70	0.00	0.00	0.00	0.14	0.00	0.14	0.26	0.00	0.10	0.00	0.38	0.12
ZrO_2	59.54	55.81	59.51	61.56	58.70	55.11	66.10	66.02	63.75	60.68	61.62	64.97	60.77	60.98	63.01	63.30	59.70	62.05
Y_2O_3	2.69	4.37	1.29	1.12	2.78	4.52	0.11	0.10	0.52	1.94	2.08	0.55	2.88	1.13	0.14	1.13	3.55	1.64
Total	**98.37**	**97.78**	**95.1**	**98.56**	**97.97**	**97.15**	**99.03**	**98.62**	**96.49**	**97.67**	**98.88**	**98.34**	**97.52**	**97.13**	**98.55**	**99.57**	**98.61**	**98.37**

TABLE 1 continued

Representative chemical analyses of the studied zircon (Grain BG 1 and BG2)

No.	1	2	3	4	5	6	7	8	9	Aver. Fresh	1	2	3	4	5	Aver. Fresh	6	7	8	Aver Alt.
SiO_2	32.02	32.16	32.55	32.66	32.62	32.87	32.42	32.11	32.50	32.45	32.51	32.68	32.73	32.46	32.77	32.63	30.11	30.45	29.63	30.06
HfO_2	1.47	1.52	1.75	1.71	1.81	1.76	2.25	1.96	2.28	1.83	1.82	1.81	1.77	2.16	2.85	2.08	2.94	2.77	2.66	2.79
Yb_2O_3	0.24	0.10	0.18	0.07	0.00	0.00	0.314	0.15	0.21	0.12	0.00	0.13	0.00	0.369	0.33	0.17	0.46	0.25	0.22	0.31
Al_2O_3	0.00	0.00	0.00	0.00	0.00	0.00	0.00	0.00	0.00	0.00	0.00	0.00	0.00	0.01	0.02	0.01	0.07	0.20	0.34	0.20
Er_2O_3	0.11	0.00	0.14	0.00	0.00	0.12	0.13	0.00	0.09	0.07	0.00	0.10	0.00	0.30	0.35	0.15	0.28	0.12	0.18	0.19
MgO	0.00	0.00	0.00	0.00	0.00	0.00	0.00	0.00	0.00	0.00	0.00	0.00	0.01	0.00	0.02	0.01	0.00	0.04	0.03	0.02
CaO	0.00	0.00	0.02	0.05	0.03	0.05	0.00	0.00	0.04	0.02	0.00	0.03	0.00	0.00	0.00	0.01	1.98	2.34	2.04	2.12
FeO	0.00	0.04	0.00	0.00	0.00	0.00	0.00	0.00	0.00	0.00	0.00	0.00	0.03	0.00	0.00	0.01	0.28	1.34	2.72	1.45
Gd_2O_3	0.00	0.00	0.19	0.00	0.00	0.11	0.00	0.00	0.00	0.03	0.12	0.14	0.00	0.00	0.14	0.08	0.19	0.00	0.19	0.13
MnO	0.00	0.07	0.00	0.00	0.00	0.00	0.00	0.00	0.00	0.01	0.00	0.00	0.00	0.00	0.00	0.00	0.00	0.18	0.11	0.10
Eu_2O_3	0.00	0.00	0.00	0.00	0.00	0.00	0.00	0.00	0.00	0.00	0.00	0.07	0.00	0.00	0.00	0.01	0.00	0.17	0.00	0.06
Sm_2O_3	0.00	0.00	0.00	0.00	0.00	0.00	0.00	0.00	0.00	0.00	0.00	0.00	0.00	0.00	0.00	0.00	0.00	0.00	0.00	0.00
Pr_2O_3	0.21	0.00	0.30	0.00	0.00	0.00	0.22	0.00	0.00	0.08	0.00	0.00	0.00	0.00	0.00	0.00	0.21	0.20	0.00	0.14
Nd_2O_3	0.00	0.00	0.00	0.00	0.00	0.00	0.00	0.00	0.00	0.00	0.00	0.00	0.00	0.00	0.00	0.00	0.00	0.00	0.10	0.03
TiO_2	0.00	0.00	0.00	0.00	0.06	0.00	0.00	0.00	0.00	0.01	0.00	0.00	0.00	0.00	0.12	0.02	0.00	0.05	0.00	0.02
Sc_2O_3	0.00	0.00	0.00	0.00	0.06	0.00	0.00	0.00	0.00	0.01	0.08	0.00	0.00	0.00	0.00	0.02	0.10	0.00	0.00	0.03
P_2O_5	0.11	0.00	0.07	0.06	0.07	0.09	0.07	0.09	0.04	0.07	0.06	0.00	0.03	0.15	0.16	0.08	0.15	0.12	0.11	0.13
Ce_2O_3	0.00	0.00	0.00	0.09	0.07	0.00	0.11	0.00	0.00	0.03	0.00	0.00	0.08	0.14	0.00	0.04	0.06	0.05	0.16	0.09
La_2O_3	0.00	0.00	0.00	0.00	0.00	0.00	0.00	0.00	0.00	0.00	0.00	0.00	0.00	0.00	0.00	0.00	0.00	0.00	0.00	0.00
UO_2	0.00	0.00	0.17	0.00	0.07	0.19	0.18	0.39	0.18	0.13	0.09	0.00	0.00	0.58	0.74	0.28	0.96	0.68	0.59	0.74
ThO_2	0.07	0.00	0.00	0.00	0.09	0.08	0.16	0.08	0.10	0.06	0.00	0.00	0.00	0.26	0.08	0.07	0.28	0.23	0.00	0.17
Nb_2O_3	0.00	0.00	0.00	0.00	0.00	0.00	0.00	0.00	0.00	0.00	0.00	0.00	0.00	0.10	0.00	0.02	0.09	0.00	0.00	0.03
ZrO_2	64.75	65.36	65.89	66.53	65.98	65.08	64.96	63.73	65.44	65.30	65.20	64.87	66.77	64.47	63.34	64.93	58.70	57.90	56.71	57.77
Y_2O_3	0.79	0.46	0.27	0.23	0.24	0.14	0.66	0.52	0.42	0.41	0.10	0.25	0.15	0.78	0.63	0.38	0.93	0.63	0.59	0.72
Total	**99.77**	**99.71**	**101.5**	**101.4**	**101.3**	**100.5**	**101.3**	**99.03**	**101.3**	**100.6**	**99.98**	**100.1**	**101.6**	**101.8**	**101.6**	**101**	**97.79**	**97.72**	**96.38**	**97.30**

TABLE 1 continued

Representative chemical analyses of the studied zircon (Grain OG 1 and OG2)

No.	1	2	3	4	5	6	7	8	Aver Fresh	1	2	3	4	5	Aver. Fresh	6	7	8	Aver Alt.
SiO_2	32.56	32.84	32.74	33.13	32.88	32.76	32.13	31.23	32.53	31.38	31.52	31.17	31.96	32.54	31.71	28.27	28.45	29.30	28.67
HfO_2	1.67	1.73	1.71	1.69	1.47	1.88	2.36	2.10	1.83	3.10	3.14	3.13	3.29	2.87	3.11	2.71	2.80	2.73	2.75
Yb_2O_3	0.00	0.00	0.14	0.00	0.07	0.24	0.12	0.26	0.10	0.19	0.28	0.27	0.10	0.11	0.19	0.22	0.31	0.28	0.27
Al_2O_3	0.00	0.01	0.00	0.00	0.00	0.00	0.00	0.00	0.00	0.00	0.00	0.00	0.00	0.00	0.00	0.09	0.03	0.09	0.07
Er_2O_3	0.00	0.18	0.09	0.00	0.00	0.19	0.011	0.09	0.08	0.21	0.10	0.24	0.00	0.00	0.11	0.22	0.18	0.00	0.13
MgO	0.00	0.01	0.00	0.01	0.01	0.00	0.00	0.00	0.00	0.00	0.00	0.00	0.00	0.00	0.00	0.01	0.00	0.00	0.00
CaO	0.03	0.05	0.14	0.00	0.07	0.02	0.07	0.07	0.06	0.04	0.03	0.05	0.03	0.04	0.04	3.10	3.18	3.03	3.10
FeO	0.00	0.00	0.00	0.00	0.00	0.00	0.03	0.00	0.00	0.00	0.00	0.00	0.00	0.00	0.00	0.97	0.79	0.75	0.84
Gd_2O_3	0.00	0.11	0.16	0.00	0.10	0.00	0.00	0.00	0.05	0.00	0.00	0.00	0.02	0.00	0.00	0.12	0.00	0.00	0.04
MnO	0.00	0.04	0.00	0.00	0.00	0.00	0.00	0.00	0.01	0.00	0.00	0.00	0.00	0.00	0.00	0.00	0.00	0.11	0.04
Eu_2O_3	0.00	0.00	0.07	0.10	0.00	0.10	0.00	0.11	0.05	0.12	0.00	0.16	0.00	0.00	0.06	0.00	0.00	0.00	0.00
Sm_2O_3	0.00	0.00	0.00	0.00	0.00	0.00	0.00	0.00	0.00	0.00	0.00	0.00	0.00	0.00	0.00	0.00	0.00	0.00	0.00
Pr_2O_3	0.00	0.00	0.00	0.00	0.00	0.28	0.00	0.00	0.04	0.18	0.00	0.00	0.00	0.00	0.04	0.00	0.00	0.00	0.00
Nd_2O_3	0.00	0.10	0.00	0.00	0.00	0.00	0.00	0.00	0.10	0.00	0.00	0.00	0.00	0.12	0.02	0.00	0.00	0.00	0.00
TiO_2	0.06	0.09	0.00	0.00	0.00	0.00	0.13	0.00	0.04	0.00	0.00	0.00	0.13	0.07	0.04	0.05	0.08	0.09	0.07
Sc_2O_3	0.00	0.00	0.00	0.00	0.00	0.07	0.00	0.00	0.01	0.00	0.00	0.00	0.00	0.00	0.00	0.00	0.00	0.06	0.02
P_2O_5	0.04	0.11	0.00	0.04	0.00	0.15	0.03	0.08	0.06	0.07	0.10	0.10	0.07	0.04	0.08	0.10	0.10	0.07	0.09
Ce_2O_3	0.00	0.06	0.07	0.00	0.00	0.07	0.00	0.00	0.03	0.09	0.00	0.09	0.00	0.08	0.05	0.15	0.06	0.10	0.10
La_2O_3	0.00	0.08	0.00	0.00	0.00	0.00	0.08	0.00	0.02	0.00	0.00	0.00	0.00	0.06	0.01	0.00	0.00	0.00	0.00
UO_2	0.00	0.00	0.00	0.08	0.00	0.44	0.37	0.47	0.17	0.50	0.52	0.90	0.31	0.09	0.46	0.57	0.68	0.38	0.54
ThO_2	0.00	0.00	0.00	0.08	0.00	0.09	0.08	0.15	0.05	0.15	0.26	0.24	0.00	0.10	0.15	0.36	0.28	0.00	0.21
Nb_2O_3	0.10	0.00	0.00	0.00	0.00	0.00	0.00	0.00	0.01	0.15	0.00	0.00	0.00	0.00	0.03	0.00	0.00	0.00	0.00
ZrO_2	64.88	66.23	63.87	65.65	63.66	63.55	63.36	63.15	64.29	63.74	63.09	61.73	61.19	62.23	62.40	54.93	55.96	57.41	56.10
Y_2O_3	0.00	0.08	0.08	0.00	0.00	0.68	0.27	0.59	0.21	0.33	0.27	0.65	0.23	0.18	0.33	0.60	0.49	0.43	0.51
Total	**99.34**	**101.7**	**99.07**	**100.8**	**98.26**	**100.5**	**99.14**	**98.3**	**99.64**	**100.3**	**99.31**	**98.73**	**97.33**	**98.53**	**98.83**	**92.47**	**93.39**	**94.83**	**93.56**

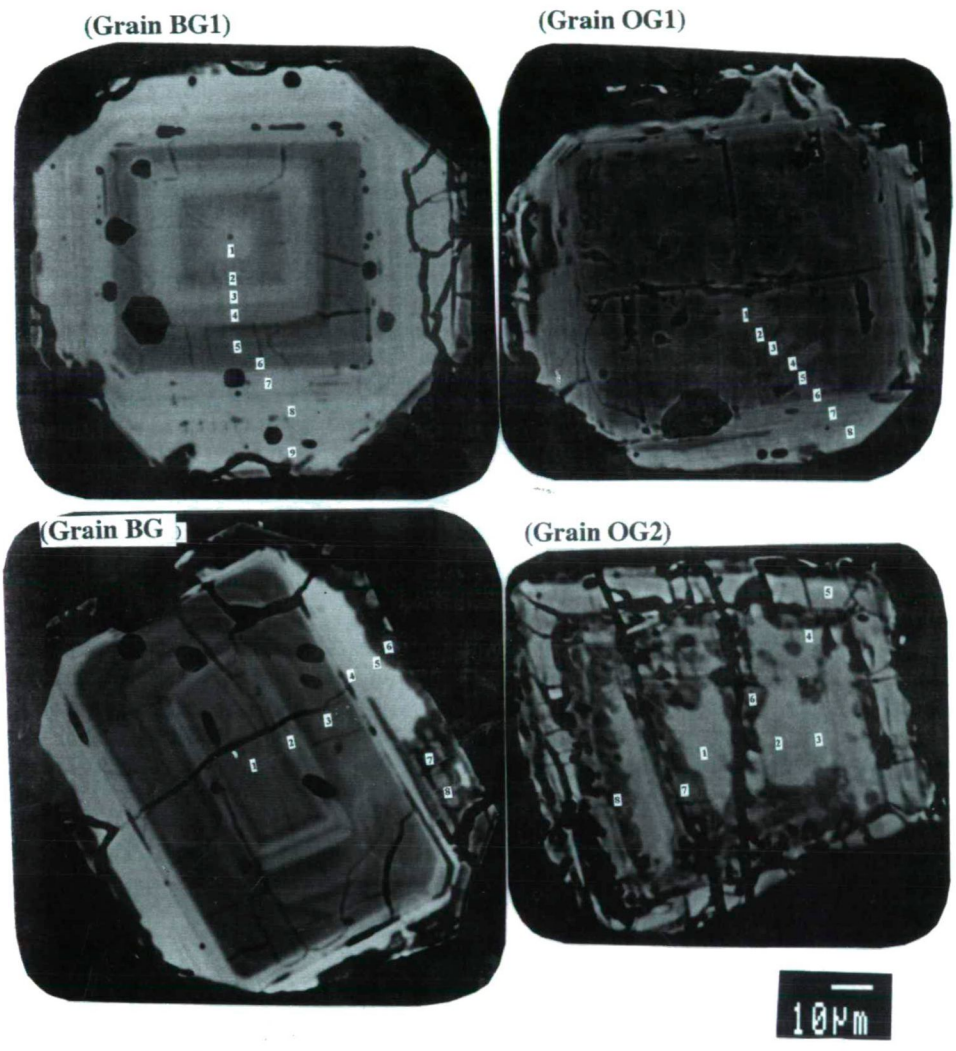

Fig. 6. Representative back scatter electron images (BSEI) for some zircon grains

1974), with HfO_2 ranging mostly between 1 and 2 % but sometimes a bit more than 3 % in a grain from the older granitoids. Moreover the rim of one grain from the leucocratic granites has HfO2 up to 5 or 6 % (hafnian SiO_4 zircon) which is traditionally interpreted as solid solution between ZrSiO4 and HfSiO4. Zr/Hf ratio is often between 40 and 30 but lower and higher values are also recorded. The grain from the older granites which has a high Hf content shows lower Zr/Hf ratio, about 20, while the spots from the rim of grain of the leucocratic granite have Zr/Hf ratio around 10. Zr / Hf ratio generally does not show clear trends from the core tho the rim in the studied zircons, except for those from the biotite granite where it roughly increases towards the rim. Although this ratio shows decreasing trends with differentiation for all the rock groups in the whole rock analyses it is not clear why such trend is not obvious in all zircons. Y and some REE are found in

Fig. 6. Continuation

detectable amounts in many spots. The most common are Y and Yb which show a cognate relation and reach the maxima in zircons from the red granite. Their relation with Hf is not clear. Y is mostly below 1 % but reaches more than 4 % in some spots from the red granites in which Yb reaches more than 1 %, although it is often lower than 0.3 %. Th and U are detected in many spots but are under detection limit in others, U/Th ratio is mostly between 2 and 4 although in the whole rock it usually ranges between 0.33 and 0.25. In the older granites it reaches 0.12, SPEER (1982) attributed such phenomenon either to preferential inclusion of U (r = 1.00 A°) or cocrystallization with Th-enriched phases such as allanite, monazite and thorite or both. In our case the second possibility is not well supported because the biotite granites which are the most enriched in allanite show the same ratio as the other units, so may be the first probability is more realistic. Other elements as Al, Mg, Ca, Fe, Mn, Ti, Sc, P and Nb stayed often below or around the detection limits, but they are detected in more amounts in the altered spots and this is an advantage for analyzing such uncommon elements.

On chemical bases, the variation in zircon compostion (within the same grain) is less in the older granites and biotite granites than the other groups, which could reflect more stable conditions during the crystallization. Zircons from the older granites are somewhat strange while one gratin had high Hf averages 3.11 oxide percent, another one has low Y averages 0.21 oxide percent indicating a very different chemistry of the melt and in turn could also indicate a different span of time for crystallization of zircons in the older granitoids. This is also clear from the widespread zircon typology on Pupin diagram. One grain out of five from the biotite granites show decrease in Y from the center to the end of its core and increases in the outher rim which could be explained by cocrystallization of Y incorporating minerals (only local effect) as hornblende or sphene. The same effect is also seen in grains from the leucocratic granites and fine grained granites. Zircons from the red granites show strong oscillatory zoning although this is not clear in Hf. They are also enriched in Al, Ca, Fe, P, Mn and Y, low in Si, and Zr and look like the altered spots from the other zircons. *Fig. 7.* shows the variations of some elements through chemical traverses in zircons.

The effect of aggressive hydrothermal solutions is very clear in the back scatter electron images (BSEI). These solutions caused dissolution of the zircon and changed its chemistry. They led to decrease in Si and Zr and enhanced all the other elements. The solutions affecting the older granitoids were more rich in Ca (spot analysis of zircon for CaO = 3.1 %) than in the biotite granites (CaO = 2.12) in the leucocratic granites (CaO = 1.61 %) and that of the fine grained granites (CaO = 1.07 %). The reverse is shown in iron where the solutions affecting the older granitoids are less (FeO = 0.84 %) than the others (FeO = 1.45) in biotite granites, 1.58 in the leococratic granites and 1.70 in the fine grained granites, while in the red granites the effect of such solutions is not apparent as mentioned before. It seems that the composition of these solutions is rather compatible with the bulk chemistry of the rock. Two possibilities could be invoked for the explanation of the origin of these solutions: 1. They are residual from the same magma after consolidation, and then can carry the chemical imprints of their original magma. They started to react with the rock in the pneumatolytic stage. If this assumption is correct it requires that the reaction is widespread all over the rock and grains and this is not achieved in the case of the older granites and biotite granites, but could be correct in the other cases. 2. These solutions are exotic and acquired the chemical characteristics of the rocks through the penetration and dissolution of some parts of the rocks. This case could be realistic for the older and biotite granites where the effect is limited to some zircon grains. In the case of the red granites these solutions could be syn-crystallization.

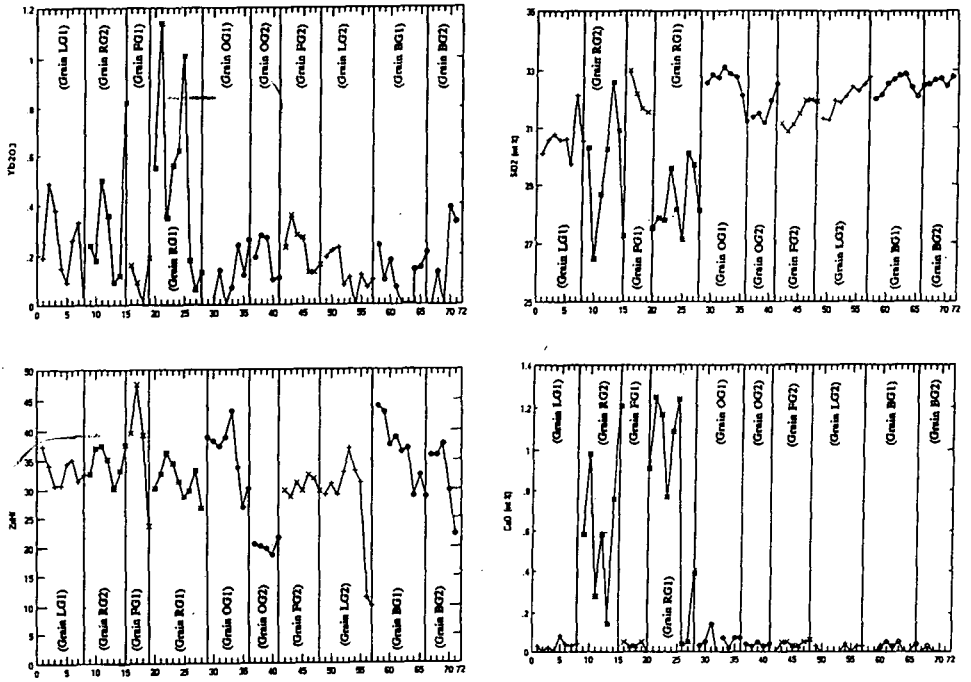

Fig. 7. Variation of some elements during zircon growth from core to rim

CONCLUSIONS

Zircons of the older granitoids of Abu El-Hasan, Northern Eastern Desert, Egypt, exhibit wide variations in crystal shapes. They do not show any overgrowths, outgrowths or corrosion, whereas those of the studied younger granitoids show much more regularity. BSE images of zircons reveal zonal growth, inclusions and different crystal effects due to hydrothermal solutions.

Zr/Hf ratios for zircons range from 40 to 30 with some anomalies. These ratios do not show clear trends from the core to the rim of the zircon grains, whereas they decrease with differentiation for all the studied granitoids.

ACKNOWLEDGEMENT

The authors wish to express their thanks to Prof. F. FINGER, Salzburg University for revising the manuscript for useful suggestions and for facilities offered during the microprobe analyses.

REFERENCES

ABD EL-GHAFFAR, M. M. (1975): Study on the accessry zircon of the granitic rocks in Fawakhir area, Eastern Desert, Egypt. M. Sc. thesis, Ain Shams Univ., Cairo, Egypt.

ABD EL-MAKSOUD, M. A. (1974): Geology of Abu Diab area with special emphasis on the petrogenesis of the granitic rocks. Ph.D. thesis, Cairo Univ., Egypt.

ABU EL ELA, M. S. (1973): A study on the accessory minerals of the crystalline rocks of Aswan area and its petrologic significance. M. Sc. thesis, Ain Shams Univ., Cairo, Egypt.

ATIA, M. S., KABESH, M. L. and DAWOUD, M. (1998): Geochemistry, tectonic setting and classification of some granitoids, Gebel Abu El-Hasan, North East Desert, Egypt. Acta Mineral. Petrog. Szeged, Vol. XXXIX.

BENISEK, A. and FINGER, F. (1993): Factors controlling the development of prism faces in granite zircons: A microprobe study. Cont. Min. Petrol. 114, 441-451.

BUDA, G., HASSAN, I. and DABBOUR, G. (1998): Typological studies on zircon grains from the Precambrian granitoids of Southern Sinai, Egypt. Abs. Fifth Conference on Geology of Sinai for Development. Saint Catherine, South Sinai.

CERGENENKOF, B. B. (1991): On the possibilities of using accessory zircon in the correlation of the granitoids. Zapisk VSSGO N3, 14-30.

CORREIRA NEVES, J. M., LOPES NUES, J. E. and SAHAMA, TH. G. (1974): High hafnium members of the zircon hafniun series from the granite pegmatites of Zambia, Mozambique, Cont, Min. Pet., 48, 73-80.

EL NASHAR, E. R. (1992): Geochemistry of hornblende and zircon from Samadai granitic complex. Eastern Desert, Egypt. Delta Jour. Sci. Tanta Univ., 16 (2), 138-158.

EL NASHAR, E. R. (1998): Chemistry and typology of zircons as a guide to the petrogenesis of granitoid rocks fo the area around Gebel Risasa, Southeastern Sinai, Egypt. Bull. N.R.C., Egypt, 23, No. 4, 483-497.

FIELDING, P. E. (1970): The distribution of uranium, rare earths and colour centres in a crystal of natural zircon. Am. Mineral., 55, 428-440.

HEIKAL, M. A. (1973): Petrographical and petrochemical studies of G. El Ineigi granitic rocks, Eastern Desert, Egypt. Ph. D. thesis, Cairo Univ., Egypt.

HEIKAL, M. A., SALEM, A. A. and EL-SHESHTAWI, Y. A. (1985): Zircon in granitoids from Sinai, Egypt and its genetic significance. Acta Min. Petr. Szeged XXXII, 117-130.

HILMY, M. E., ABDEL MAKSOUD, M. A. and AZER, H. W. (1994-1995): Close Examination of Two Phases of The Anorogenic Granite, Abu El-Hasan Area, Northern Eastern Desert, Egypt, Annals Geol. Surv. v. XX, 143-162.

HUBUCH, V. D. and LOESCHKE, J. (1993): The *comelicoporphyroid* of Western Carnic Alp, Austria / Italy; stratigraphy, petrography, geochemistry and zircon morphology. Jb Geol. B.A.B. and 136 – H2 351-374.

KABESH, M. L., REFAAT, A. M. and ABDALLA, Z. M. (1976): The significance of zircon as a guide to the petrogenesis of granites from Ras Barud area, Eastern Desert, Egypt. J. Univ. Kuwait (Sci) 3, 207-214.

KHAFAGY, M. B. (1964): The granites of Aswan and their accessory zircons. M. Sc. thesis, Assuit Univ., 192 p.

LARSEN, L. H. and POLDERVAART, A. (1957): Measurement and distribution of zircons in some granitic rocks of magmatic origin. Miner. Mag., 31, 544-564.

MITCHELL, R. S. (1973): Metamict minerals: A review, Parts I and II. Mineral. Record, 4, 177-182, 214-223.

PUPIN, J. P. (1976): Signification des characters morphologiques du zircon commun des roches en petrologies. Base de la methode typologie, Applications. These Doct. Etat., Univ. Nice, France.

PUPIN, J. P. (1980): Zircon and granity typology. Contr. Min. Petrol., 73, 207-220.

PUPIN, J. P. (1985): Magmatic zoning of Hercynian granitoids in France based on zircon typology. Schweizer Mineralogisch Petro. Mitt., 65, 29-56.

PUPIN, J. P. (1988): Granites as indicators in paleogeodynamics. Rend. Soc. Ital. Min. Petro., 43-2, 237-262.

PUPIN, J. P., BONIN, B., TESSLER, M. and TURCO, G. (1979): Role de lïeav sur les characters morphologiques et al cristallisation du zircon dans les granites. Bull. Soc. Geol. Fr., 20, 5, 721-725.

PUPIN, J. P. and TURCO, G. (1972a): Une tupologie originale du zircon accessorire. Bull. Soc. Fr. Mineral. Cristallogr., 95, 348-358.

PUPIN, J. P. and TURCO (1972b): Le zircon acessoire en geothermometrie. R. Acad. Sci., Paris, D, 274, 2121-2124.

RAGAB, A. I. (1971): Geology of Gebel El Atawi area, Eastern Desert, Egypt Ph. D. Thesis, Ain Shams Univ., Cairo.

RAJONAHA, J. HRBCAK, M. (1989): Contribution to the research of zircon from granitoids of the Stiavnicke Vrchy Mrs Area (Czechoslovakia), Geologicky Zbornik 6, V. 40 665-768.

REFAAT, A. M., (1970): Geology of Gebel Umm Naggat area, Eastern Desert, U.A.R. Ph. D. Thesis, Cairo Univ.

SPEER, J. A. (1982): Zircon. In P. H. RIBBE (ed.): Reviews in Mineralogy, V. 5, Orthosilicates. Min. Soc. Am., Washington D. C. 67-112.

TONDAR, V. P., NEUMASN, A. and TROLL, G. (1990): Die Petrogenetische Deutung der Zirkon morphologie einiger porphyritisher gesteine der Ostlischen Zentral Alpen. Jb. Geol. B. A. Band 33 Heft 2. S 365-384.

ZAGHLOUL, Z. M. and KHAFFAGY, M. B. (1965): Zircon in the granites of Aswan, Upper Egypt. Bull. Sci. Tech., Assiut Univ., 8, 129-141.

ZAGHLOUL, Z. M., KHAFFAGY, M. B. and ABU EL ELA, M. S. (1973): The growth trends and distribution of the zircons from the basement rocks of Aswan, Egypt. 7th Arab Sc. Cong., Cairo, IV, 399-404.

ZAGHLOUL, Z. M., ZALATA, A. A. and MASHAAL, S. E. (1981a): Zircon distribution and petrogenesis of the granitoid rocks of Gebel El-Shayib area, Eastern Desert, Egypt. Mansoura Bull. Sci., 8, 381-404.

ZAGHLOUL, Z. M., ZALATA, A. A. and MASHAAL, S. E. (1981b): The varietal features and growth trends of zircons in the granitoid rocks of Gabal El-Shayib area, Eastern Desert, Egypt. Mansoura Bull. Sci., 8, 405-443.

Manuscript received: 17. March 1999.

Acta Mineralogica-Petrographica, Szeged, XL, 45–54, 1999

ZIRCON TYPOLOGY IN GRANITOID ROCKS OF THE DITRÓ MASSIF, TRANSYLVANIA, ROMANIA

G. KOVÁCS, T. M TÓTH*

Department of Mineralogy, Geochemistry and Petrology, Attila József University, Szeged

ABSTRACT

The complex magmatic body of the Ditró Massif (Transylvania, Romania) was formed between the Middle Triassic and Lower Cretaceous times. Granitoid rocks can be found in a large area in the NE part of the massif. They were formed either by differentiation of an upper mantle ultramafic intrusion or by assimilation of crustal material.

By the zircon morphological study it was stated that the most frequent zircon types in the granitoid rocks are P_4,P_5, P_3, P_{19}, P_{24} and D. This suggests that the zircon crystals could be formed in hyperalkaline or hypoaluminous environment at high (800-850 °C) temperature. On the basis of the calculated I.A. and I.T. values the studied granite belongs to the alkaline field, close to the alkaline-subalkaline boundary. This indicates an upper mantle origin in the Pupin's system, therefore, granites are supposed to be differentiation products of an upper mantle ultramafic body.

Keywords: zircon, granite, Ditró Massif

INTRODUCTION

Structure and development of the Ditró Syenite Massif (Transylvania, Romania) has been discussed for more than 150 years, and several hypotheses have been suggested (PÁL MOLNÁR, 1994). Here those are mentioned that deal also with the formation of the granitoid rocks.

According to STRECKEISEN (1935, 1938) a mafic intrusion assimilated the limestones of the Eastern Carpathians forming an alkaline gabbro melt in shallow depth which differentiated through the alkaline diorite (orotvite) - alkaline syenite - nepheline syenite path. The ascendent alkaline syenite and nepheline syenite melts assimilated the quartz-rich schists close to the surface producing granitoid rocks as well as all the intermediate members between granite and syenite. On the basis of field observations, in 1952 he stated the chronological order of the rocks (STRECKEISEN, 1952). He regards the ultramafic rocks (and the ditroessexite) to be the oldest ones, supposes the alkaline syenite and alkaline granite to be of the same age, and the nepheline syenite to be a little bit younger.

According to ANASTASIU and CONSTANTINESCU (1977, 1981) the massif is an autochtonous body which formed in several phases, and rooted in the upper crust. They supposed two independent magmatic intrusions. The first has an upper mantle origin and is mafic, while the second one is an intrusion that assimilated Si-poor rock assemblages in the crust.

* H-6701 Szeged, P.O. Box 651, Hungary

JAKAB (1982) separated three magmatic intrusions from each other. The first is a mafic-ultramafic one of upper mantle origin, calk-alkaline, slightly alkaline in character. The second one is a syenite intrusion that formed alkaline syenite, monzonite and, in the margins, also granitoid rocks. The third one is also a syenitic intrusion forming the rocks of the central part of the massif.

Using K/Ar geochronological data on mineral fractions of some rock types PÁL MOLNÁR and ÁRVA-SOÓS proved the existence of two intrusions (PÁL MOLNÁR, ÁRVA-SOÓS, 1995; PÁL MOLNÁR, 1998). The first one is Middle Triassic - Lower Jurassic in age, when ultramafic rocks, nepheline syenite and granite were formed. The second intrusion is Middle Jurassic - Lower Cretaceous and resulted in syenite and alkaline plagioclase syenite.

According to the above mentioned hypotheses there are two possibilities concerning the origin of the granite: it is either a differentiation product of mantle ultramafic melts or it was formed by ACF processes of the intrusion.

A possible way to determine the origin of a granite intrusion is the study of the morphological characteristics of its zircon crystals (PUPIN, 1980, 1985, 1988). He found a tight relationship between the development of pyramid faces of zircons and the alkalinity of the magma as well as between prism faces and the crystallization temperature. The increasing alkalinity is indicated by the increase of the (101) and (301) faces to the detriment of the (211) faces. As the temperature increases, the (100) faces become to be increasingly dominant to the detriment of the (100) faces.

The purpose of this paper is to study the formation of the main granitoid rock types in the Ditró Massif using the zircon morphology method.

PETROGRAPHY OF THE GRANITOID ROCKS OF THE DITRÓ MASSIF

Geographical situation and geological sketch of the Ditró Massif, as well as petrography and geological relationship of its granitoid rocks were discussed by KOVÁCS and PÁL MOLNÁR (1998) in details. The mafic rock-forming minerals are important markers in the granite classification. On the basis of mafic minerals we can subdivide the granitoid rocks of Ditró Massif into two groups. The first group consists of biotite and/or hornblende whereas the second one contains aegirine (overgrown by alkali amphibole) and/or biotite. According to Shand (1947) the biotite-hornblende bearing rocks are metaluminous while the others are peralkaline. In the cases when hornblende and biotite coexist, hornblende is surrounded by biotite. In some metaluminous rocks, however, biotite is the only mafic phase present. In the peralkaline rocks aegirine forms relic core in the alkali amphiboles. Based on optical features these alkali amphiboles may be riebeckite or arfvedsonite, their identification is, however, not exact enough. In several cases alkali amphibole occurs also independently. The mafic minerals are altered significantly, e.g. biotite is replaced by chlorite and alkali amphiboles forms limonite and siderite.

Here, only the samples chosen for zircon morphological studies are characterized petrographically. On the basis of the petrographic features, three handspecimens (ÁGK-6836, ÁGK-6839, ÁGK-6853) were chosen for the studies; those which characterize the granitoid rock types of the massif well enough.

– The first sample (ÁGK-6839) is a hypidiomorphic monzogranite of granular texture. It is the main type of the granitoids occurring along the Török and Laposbükk

brooks. Felsic components (quartz, microcline, oligoclase) represent 92% of the rock. The dominant mafic phase is biotite which is chloritized and contains rutile inclusions. The accessory minerals are apatite, zircon, magnetite and orthite.

– The second sample (ÁGK-6853) is a syenogranite with hypidiomorphic texture representing the biotite and amphibole bearing granitoids that are frequent in the massif. Quartz, microcline and sodic plagioclase give 97% of the rock. The main mafic constituent is biotite (with zircon and apatite inclusions) which at places occurs in contact with hornblende. The accessory phases are zircon, titanite and epidote.

– The third sample (ÁGK-6836) is a liebneritized foidic monzosyenite. Because it occurs in direct contact with the granite, we intended to study their genetic relationship by the zircon analyses.

METHOD OF THE ZIRCON SEPARATION

Density (4.7 g/cm^3) and diamagnetic property of zircon was used for separating them from rock-forming minerals of the granitoids.

About 800-1000 g of each sample was ground, and then strained through wet sieves of 0.25 and 0.063 mm, subsequently. Afterwards, fraction of 0.25-0.063 mm was sedimented in bromoform, since most of zircons in granite are of 0.16 0.05 mm size (PUPIN, 1980). The third step was to separate the heavy minerals by a Frantz Isodynamic magnetic separator at 15° transverse and 10° longitudinal slopes. Part which did not proved to be magnetic at 2 A current intensity was sedimented in methylene iodide; this way, a more than 90 % pure zircon fraction was obtained. The inclusion-rich grains were separated at lower current intensity (1.6-1.7 A).

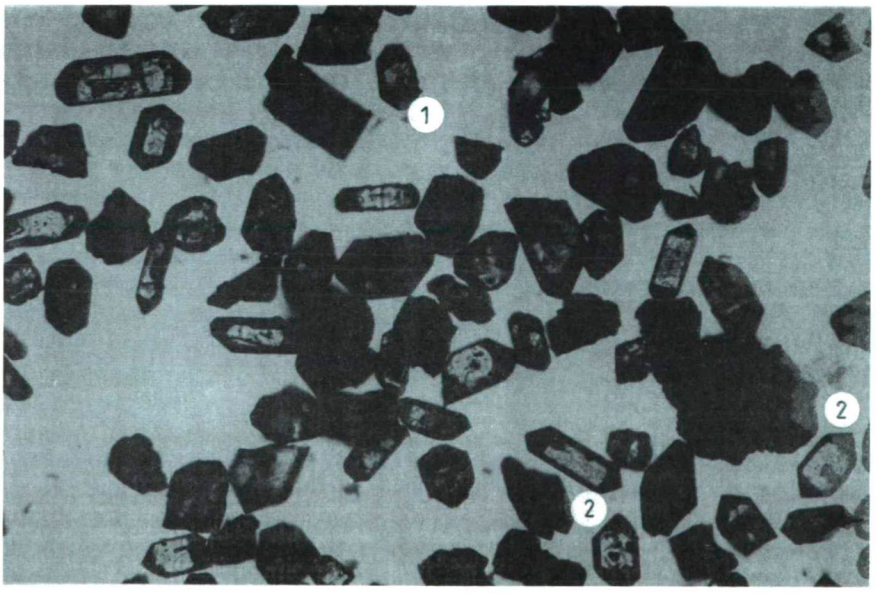

Fig. 1: Zircons from ÁGK-6839 sample under microscope 10x, |N; 1. zircon with inclusion of earlier stage, 2. magnetite inclusion in zircon.

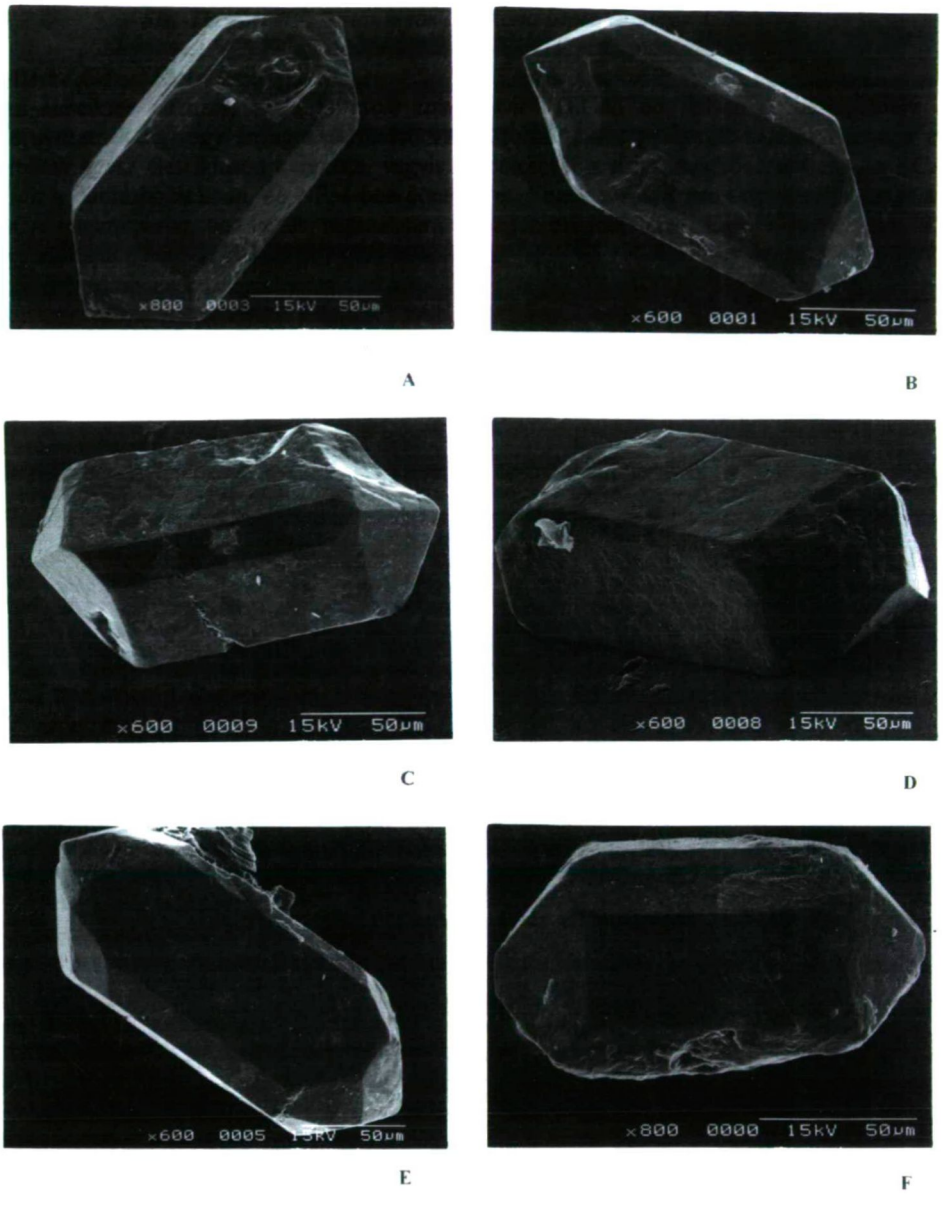

Fig. 2: SEM images of typological zircon types from the Ditró granites; P_4 type (A), P_4 type (B), P_2 type (C), P_5 type (D), S_{19} type (E), S_{20} type (F).

The samples ÁGK-6836, 6839 and 6853 were using for separation. The quantity necessary for typological study, 100-150 possible fresh grains (PUPIN, 1980, 1988), was able to be collected only in the case of the sample ÁGK-6839. Only some tens of grains were separated from the sample ÁGK-6853; this quantity is not enough for a statistical

evaluation. The sample ÁGK-6836 did not contain zircon crystals. The separated fraction was studied by binocular microscope in reflected light at sixtyfold magnifying.

RESULTS

Based on the basic optical features (color, shape, contour, structure (zoning, inclusions) the two zircon-bearing samples (ÁGK-6839 and 6853) are similar. The crystals are mainly transparent, colorless, pale yellow or pale brown in color. Rarely also reddish brown and opaque grains occur. The darker grains contain more magnetite inclusions (*fig.*1.) which changed their magnetic character making the separation at lower current intensity possible. The zircon grains are idiomorphic, they were only mechanically damaged. Most crystals are zoned with a core representing previous crystallization phases. Zonality in several cases makes the recognition of the pyramid faces difficult.

Based on the present typological study, P_4, P_5, P_3, P_{19}, P_{24} and D are the most frequent subtypes of the zircon crystals in both granitoid rock samples of the Ditró Massif (*fig.* 2.).

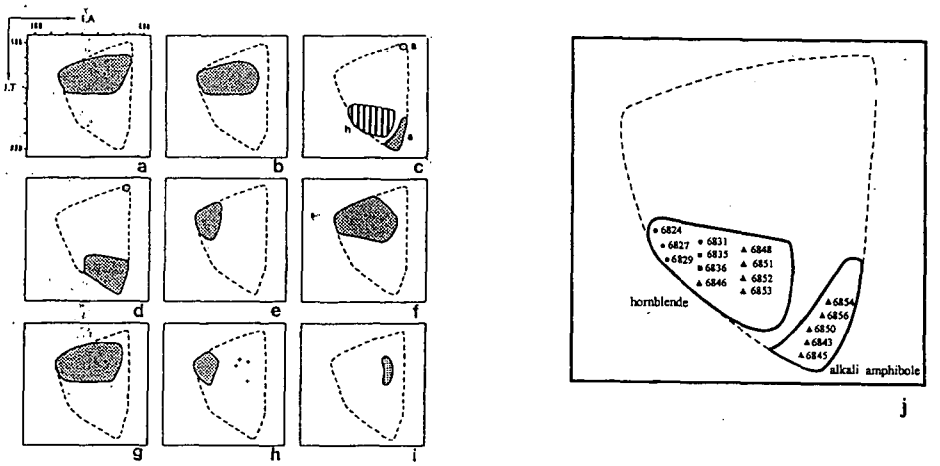

Fig. 3: (a-i.) Distribution of mineral associations in granitic rocks (Pupin, 1980): muscovite (a), anatase and brookite (b), amphiboles (c), pyroxenes and olivines (d), cordierite (e), garnet (f), tourmaline (g), monazite (h), xenotime (i), granitoid samples of Ditró Massif /e.g. ●ÁGK-6827/ (j)

DISCUSSION

Of the investigated granitoid types, only the interpretation of zircon population of the sample ÁGK-6839 is correct statistically. However, having a homogeneous granitoid body, study of even one sample may be enough to obtain correct data about the origin of the intrusion (PUPIN, 1985). Since the sample studied represents the most characteristic rock type of the area (monzogranite), the results were regarded to be representative.

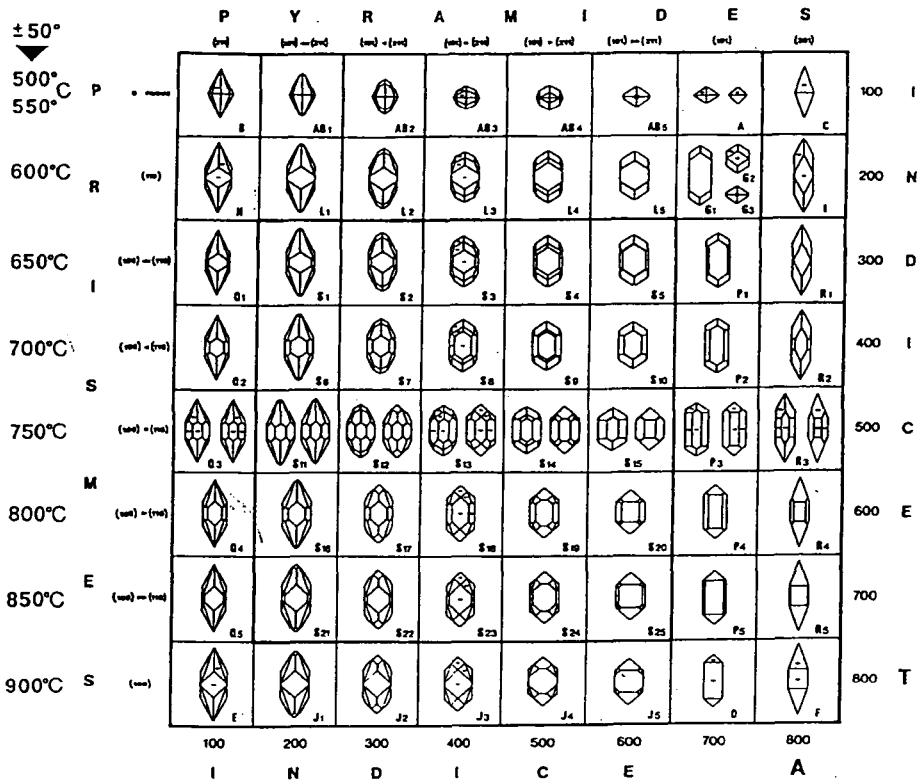

Fig. 4: Main types and subtypes of the typological classification and the corresponding geothermometric scale (PUPIN, 1980)

By the study of zircon crystals from the samples ÁGK-6839 and 6853, it could be stated that they are often zoned, and contain magnetite inclusions as well as older zircon grains representing probably earlier crystallization phases (*fig.* 1.). Interpretation of zoning of the zircon crystals is, however, not obvious. Growing of zircon in granitoids may take a long time and continues through the whole crystallization process of the magma. At present, no data is available to decide weather the core and rim regions of the zircon grains formed during the same event or represent significantly different intrusions. Detailed U/Pb and Pb/Pb radiometric dating would help to trace the successive magmatic events (KLÖTZLI, PARRISH, 1996).

On the basis of the characteristic mineral association of the granitoid rocks, common subtypes of the zircon population can be predicted (PUPIN, 1980). By the hornblende and/or alkali amphibole occurring in the studied granitoids the zircon crystals developed at high temperature and low Al/alkaline ratio (*fig.* 3.). The most frequent zircon types are P_4, P_5, P_3, P_{19}, P_{24}, and D which suggest that the zircon grains were formed in hyperalkaline or hypoaluminous environment at about 800-850 °C (*fig.* 4.).

On the basis of the calculated I.A. and I.T. values, the studied sample belongs to the boundary of the subalkaline and the alkaline fields (*fig.* 5.). According to PUPIN's classi-

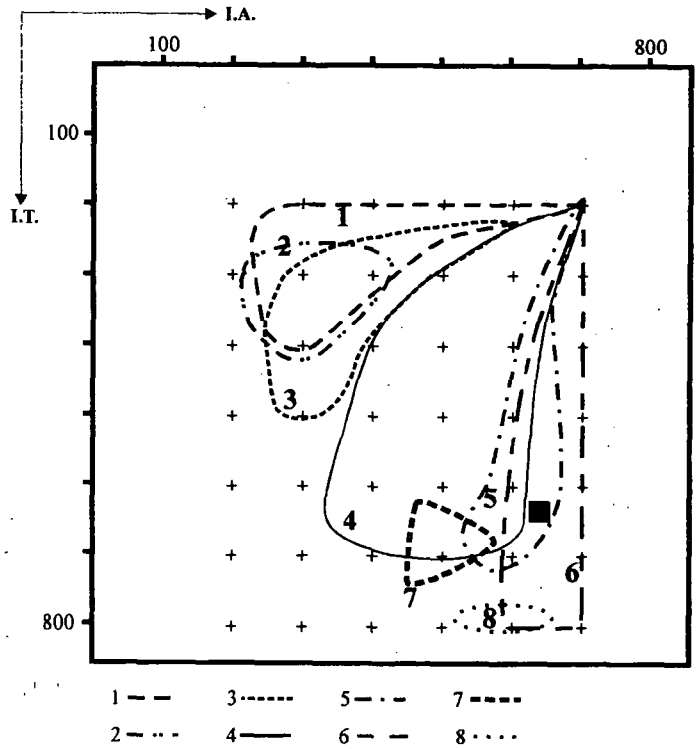

Fig. 5: Distribution of granitic rocks in the typologic diagram (PUPIN, 1980, 1985 slightly modified): aluminous leucogranites (1), (sub)autochtonous monzogranites-granodiorites (2), intrusive aluminous monzogranites-granodiorites (3), calc-alkaline and K-calc-alkaline series granites (4), subalkaline series granites (5), alkaline series granites (6), continental tholeiitic granites (7), oceanic tholeiitic series granites (8), sample ÁGK-6839 (■).

fication scheme (1985) it means that it is either a granite of hybrid (mantle+crust) origin, or represents mantle-derived granitoid rocks. Comparing typological distribution diagrams of the zircon population with that of the studied granite (*fig.* 6.), it can be experienced that it is similar to the alkaline series type (h type).

On the basis of the frequency of the zircon types, it can be stated that the rock studied belongs to the group of alkaline granites of mantle origin. Possibly, it is a differentiation product of mantle ultramafic rocks. This statement is in good agreement with the model given by PÁL MOLNÁR (1998).

Considering the rock-forming minerals of the studied samples, some of them contain hornblende. Therefore, in the *fig.* 3. they fall into the section of the fields of crust+mantle (i.e. hybrid origin) and alkaline rocks. However, origin based on the characteristic minerals is only informative, so the mantle origin of the studied sample based on the zircon typology is acceptable.

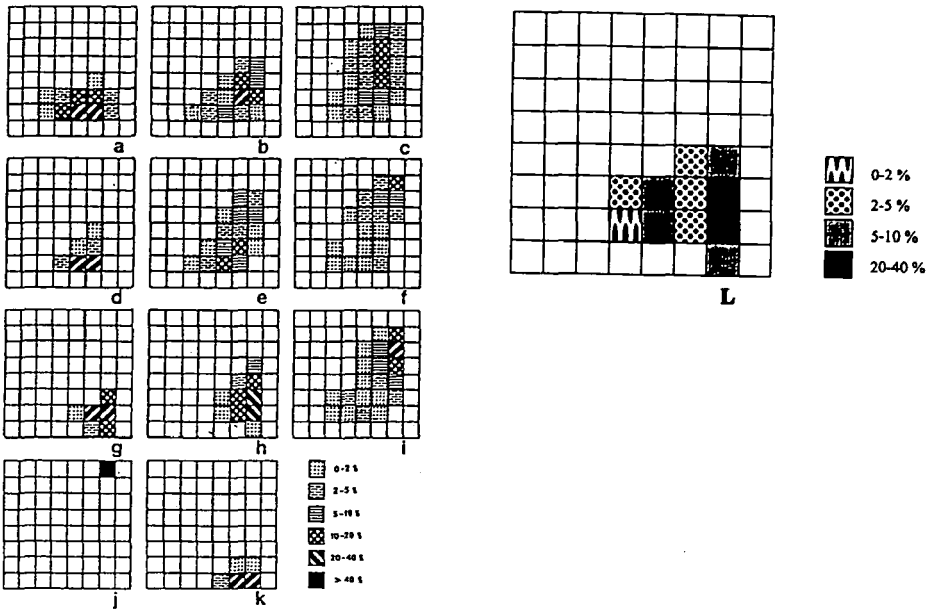

Fig. 6: Zircon crystals from granitic rocks with their subtypes. Typologic classifications from granites (Pupin, 1980): calc-alkaline series (a, b, c); subalkaline series (d, e, f); alkaline series: hypersolvus (g), transsolvus (h), subsolvus (i) granites; hyperalkaline albitized granite (j); tholeiitic series (k); sample ÁGK-6839 (L).

CONCLUSIONS

Zircon morphological studies of granitoid rocks from the Ditró Massif presented here are the first analyses of this kind. The most frequent zircon types of the monzogranite (ÁGK-6839) and syenogranite (ÁGK-6853) samples are P_4, P_5, P_3, P_{19}, P_{24}, and D. This fact suggests that the zircon crystals were formed in a hyperalkaline environment at 800-850 °C. On the basis of the calculated I.A. and I.T. values, the studied granite belongs to the field of the subalkaline hybrid (crust+mantle) granites or that of mantle-derived alkaline granites. Based on the zircon morphological studies, we prefer the mantle origin. Since the studied sample represents a characteristic type of the Ditró Massif, we regard these results as generally acceptable for the origin of the granitoid rocks from the Ditró Massif.

ACKNOWLEDGEMENT

The authors thank Prof. Tibor Szederkényi for making the analytical measurements financially possible, and Lívia Rudnyánszky for her helpful advises on the zircon preparations.

REFERENCES

ANASTASIU, N., CONSTANTINESCU, E. (1977): Feldspaţii potasici din Masivul alcalin de la Ditrău. (Potash Feldspars of the Ditrău Alkaline Massif). Dări de Seamă ale Şedinţelor Inst. Geol. Geofiz., LXIV, 13-36, Bucureşti.

ANASTASIU, N., CONSTANTINESCU, E. (1981): Feldspaţii plagioclazi din Masivul alcalin de la Ditrău. (Plagioclase feldspars from the Alkaline Massif of Ditrau). Stud. Cerc. Geol. Geofiz. Geogr. Ser. Geol., 26/1, 83-95, Bucureşti.

JAKAB, GY. (1982): Studiul mineralogic şi geochimic al mineralizaţiilor metalifere dintre Voşlobeni şi Corbu. Tez. doct. Univ. I. Cuza, Iaşi, Manuscript.

KLÖTZLI, U.S., PARRISH, R.R. (1996): Zircon U/Pb and Pb/Pb geochronology of the Rastenberg granodiorit, South Bohemian Massif, Austria. Mineralogy and Petrology, 58, 1997-214.

KOVÁCS, G., PÁL MOLNÁR, E. (1998): Petrographical characteristics of Ditró (Orotva) granites, Eastern Carphatians, Transylvania, Romania: A preliminary description. Acta Min. Pertr., Szeged, XXXIX, 35-48.

PÁL MOLNÁR, E. (1994): Adalékok a Ditrói szienitmasszívum szerkezeti és kőzettani ismeretéhez (Contributions on structural and petrological knowledge of Ditró Syenite Massif.), MTA SZAB Competition, Manuscript, 2-45.

PÁL MOLNÁR, E. (1998): .A Ditrói szienitmasszívum földtani felépítése és petrológiája különös tekintettel a hornblenditek és dioritok kialakulására (Structure and Petrology of Ditró Syenite Massif with Special Sense the Development of Hornbelndites and Diorites.) (In Hungarian with English resume) PhD thesys, Szeged.

PÁL MOLNÁR, E., ÁRVA-SÓS, E. (1995): K/Ar radiometric dating on rocks from the northern part of the Ditró Syenite Massif and its petrogenetic implications. Acta Min. Petr., Szeged, 34, 101-116.

PUPIN, J.P. (1980): Zircon and Granite Petrology. Contr. Mineral. and Petrol. 73, 207-220.

PUPIN, J.P. (1985): Magmatic zoning of Hercynian Granitoids in France based on Zircon Typology. Schweizerische Minereraloghische und Petrographische Mitteilungen, 65, 28-55.

PUPIN, J.P. (1988): Granites as indicators in paleogeodynamics. Rendiconti della Societa Ital. di Miner. e Petr., 43-2, 237-262.

SHAND, S.J. (1947): Eruptive Rocks. Their Genesis, Composition, Classification, and their Relation to Ore-Deposits, 3rd edition, J. Wiley and Sons, New York, 488 pp.

STRECKEISEN, A. (1935): Zur Differentiation in Nephelinsyenit–Massif von Ditro (Rumänien). Bul. Lab. Mineral. Univ. Bucareşti, I, 65-71.

STRECKEISEN, A. (1938): Das Nephelinsyenit Massif von Ditro in Rumänien als Beispiel einer kombinierten Differentiation und Assimilation. Verh. Schweiz. Naturf. Ges., 159-161.

STRECKEISEN, A. (1952): Das Nephelinsyenit Massif von Ditro (Siebenbütrgen). I. Teil. Schweiz, Min. Petr. Mitt., 32, 251-309.

Manuscript received: 16. Oct. 1999.

Acta Mineralogica-Petrographica, Szeged, XL, 55–70, 1999

PETROGRAPHIC AND MINERALOGIC STUDIES OF THE LAYERED INTRUSIONS AT JABAL EL-EKEIM, SAUDI ARABIA

M. O. ZUBEIR, T. M. QADHI

Faculty of Earth Sciences, King Abdul Aziz University*

ABSTRACT

Jabal El-Ekeim consists of two differently sized coalescing mafic-ultramafic layered intrusions. The large intrusion is divided into sixteen units, while the smaller one is divided into fourteen units. This classification depends on their cumulus crystals and post-cumulus material. Both intrusions consist of concentric layers dipping radially inwards and have a higher dip at the periphery. The large intrusion has a boat like shape elongated in a NW-SE direction, while the small one has a subcircular shape and is elongated in a NE-SW direction perpendicular to the elongation of the large one. It could be concluded that the elongations of the two intrusions are parallel to main structural trends in the investigated area.

Slump structure, igneous lamination, knobby texture and micro and macrorhythmic layering are the main internal structures distinguish the rocks of the area under inspection. Their formations could be attributed to the combination of different mechanisms of density gravitational stratification and crystal sorting by magnetic concvection currents.

El-Ekeim intrusions include seven rock types: olivine gabbro, troctolite, hornblende-olivine gabbro, olivine gabbronorite, gabbro, anorthosite and peridotite. The essential minerals of El-Ekeim rocks are: plagioclase, olivine, clinopyroxene, orthopyroxene and hornblende. These minerals occur as cumulus and intercumulus phases. The accessory minerals are: biotite, apatite and opaques. The latters consist principally of iron-titanium oxides as magnetite, chromomagnetite, ilmenite, hematite, spinel and hemoilmenite. Sulphides as chalcopyrite, pyrrhotite, pyrite and pentlandite are also present.

The mineral composition of both intrusions indicates that their parent magmas were similar and had a tholeiitic nature. The economic potential of these two intrusions at El-Ekeim is very poor with no signs for concentrations of ore minerals.

Keywords: El-Ekeim two mafic ultramafic layered intrusions. Cumulus and intercumulus, seven rock types, tholeiitic nature, poor economic potentials.

INTRODUCTION

Jabal El Ekeim is located in the Asir mountains in the SE part of the Arabian Shield. It is bounded by latitudes, 19°05' and 19°09' N, and longitudes 43°41' and 43°50' E (*Fig. 1*).

Jabal El Ekeim is a dark colored body enveloped by lighter colored rocks, displaying a notable contrast in color and shape. It actually consists of two coalescing mafic-ultramafic layered intrusions. Both intrusions and their enclosing rocks are included in the Hamdah Quadrangale sheet 19/43D, at the scale of 1:100.000 (ZUBEIR 1989).

Few authors were dealt with the geology of Jabal El Ekeim at reconnaissance level. BROWN and JACKSON (1959) mapped the area as layered gabbro with other ultramafic rocks. In the geological map of the Arabian Peninsula at scale 1:2.000.000, produced by USGS, ARAMCO and DGMR (1963) in ZUBEIR (1989), the area was mapped as layered

* Jeddah, KSA (Kingdom of Saudi Arabia)

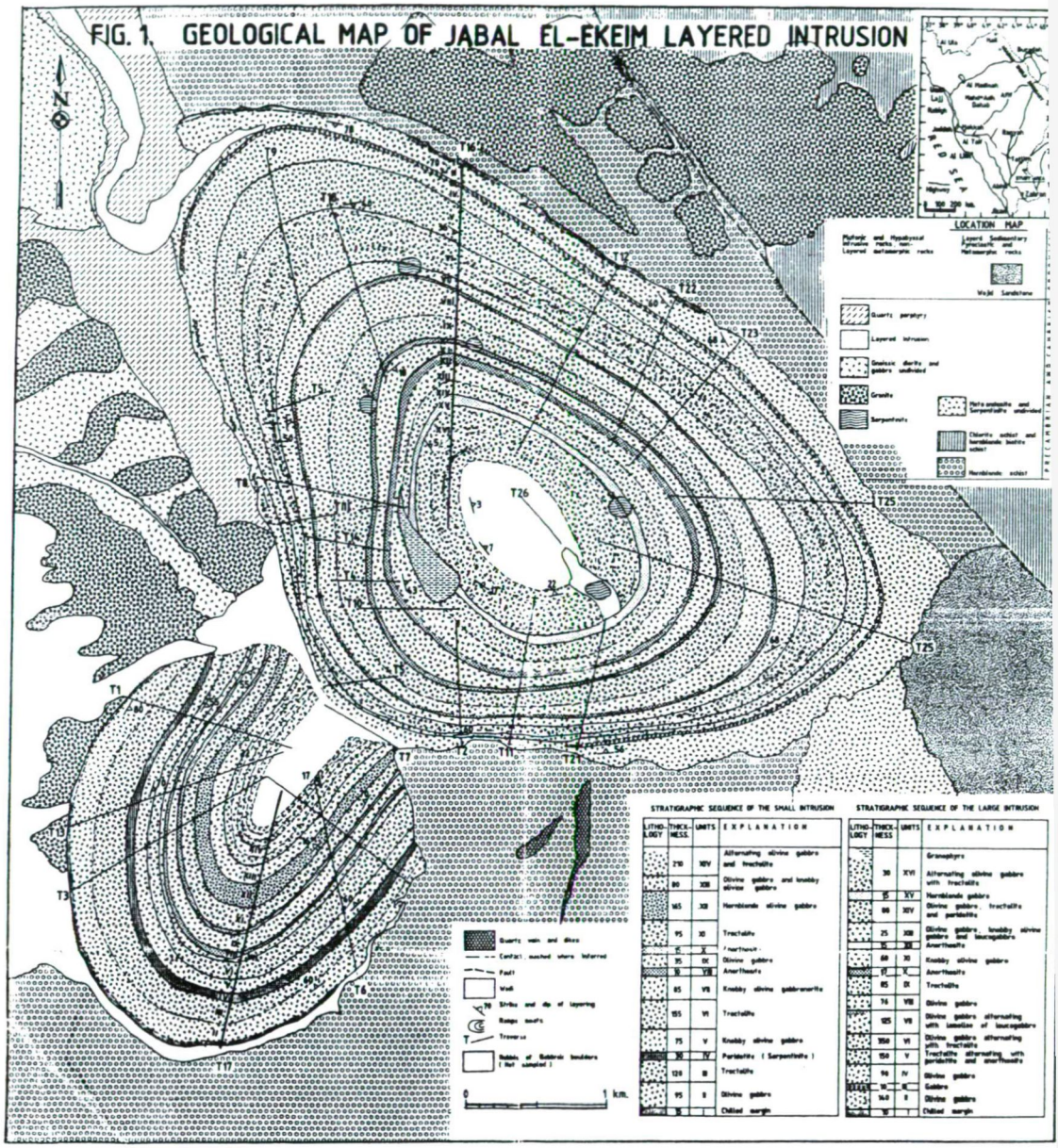

Fig. 1. Geological map of Jabal El-Ekeim layered intrusion

gabbro and basic flow rocks. COLEMAN et al. (1972) briefly identified Jabal El Ekeim along with six other layered gabbro intrusions. OVERSTREET (1978) described El Ekeim as layered gabbro and norite complex forming two ring-shaped bodies. LOWRENCE et al. (1978) explained Jabal El Ekeim as a mass of mafic rocks consisting mostly of gabbro. However, WHITE (1984) attributed El Ekeim to post-tectonic layered gabbroic pluton with three lobes, resulting from coalescence of two separate intrusions.

The objectives of the present work are:

1. To determine the configuration and geological setting of Jabal El Ekeim intrusions as well as their relationships with the country rocks.

2. To determine the petrographic and mineralogic characteristics and reveal any concentration of economic minerals.

3. To investigate the nature of their internal layering with the aim of understandig their mode of formation.

To fulfil the purpose of this study, field work of an area of about 14x20 km^2 including Jabal El Ekeim intrusions and its surroundings has been done by traversing the intrusions along 26 traverses (*Fig. 1*). Samples of four traverses are selected for petrographic and mineralogic investigations. In addition, the petrographic and mineralogic study is performed through about 200 thin and polished sections. Further publications will be produced by the same authors concerning the chemistry of the rocks of the two intrusions, as well as, the microprobe study of some mineral phases.

GEOLOGY OF JABAL EL EKEIM LAYERED INTRUSIONS

Jabal El Ekeim is composed of two coalescing mafic-ultramafic layered intrusions. The southwestern intrusion is smaller than the northeastern one.

A. Geology of the southwestern intrusion (small intrusion)

It has an elliptical shape, with plan dimensions of 2.6x2.4 km^2. The central part of the intrusion forms a high plateau, rising about 320 m above the surrounding wadis. This intrusion consists of layers of different composition and texture, expressed by ramp-moat topography (COLEMAN 1973). At the norheastern part of the intrusion, the layers are not continous due to truncation by the large intrusion. The ramps at the central plateu are generally low, ranging from 10-20 meters high. The concentric, elliptical layers have produced an extraordinary ramp-moat topography. Layers are very steeply dipping (80°-85°) inward at the periphery of the intrusion, and decrease in dip towards the centre to about 10° and less (*Fig. 1*). This disposition of layers is regular throughout the intrusion. The strike of layering swings around to give the general shape of the intrusion (*Fig. 1*).

A discontinous chilled margin with varying thickness against the country rocks was observed in many places. However, xenoliths of the country rocks within the intrusion were not observed. Several dikes of a dark colored basic rock crosscut the country rocks of the small intrusion at the mutual contact, particularly at Wadi Al-Ghabah. These dikes are believed to be offshoots from the intrusion into the country rocks, since they are very similar in many respects to the rock of the chilled margin.

Other dikes and sills occur within both the small intrusion and the country rocks. Three of them are regarded to represent progressively differentiated parts of the main gabbroic magma. They are composed of:

a. Fine-grained gabbroic dikes and sills,

b. Few trondhjemite sills,

c. Two pegmatite and several aplite dikes,

d. A fourth type of dikes is believed to be derived from later dioritic intrusions. These dikes are coarse-grained pegmatite dikes of dioritic composition.

According to the major relationship of the layered sequence, it was possible to divide this mass into fourteen units (I to XIV, *Fig. 1*). They have a total thickness of 1185 m from the margin to the centre of the intrusion.

B. Geology of the northeastern intrusion (large intrusion)

It is elongated and oval in plain view, with the major axis trending NW-SE for 8.3 km (*Fig. 1*). This intrusion is made up of uniformly alternating layers, except at the coalescing part with the small intrusion and at the northernmost part where it is cut by dikes. Dips are generally steep inwardly, 70°-50°at the borders, while at the central parts the dip decreases to few degrees, where the layers are nearly horizontal and the surface is covered by thick rubble of gabbroic boulders. Differential weathering of the concentric layers of this intrusion produced an extra-ordinary ramp-moat topography (*Fig. 2*).

In the northern and southern parts, the intrusion has sharp contacts with hornblende schist and gneiss. Off-shoots and dikes of fine grained gabbro are present and cut both country rocks and the layers of the intrusion. Few pegmatite and quartz veins cut across the layers perpendicularly at the northern and eastern edges of the intrusion.

Few isolated lenticular masses of various sizes of sheared and fractured ultramafic rocks crop out nearly at the central part of the large intrusion (*Fig. 1*). These masses are extensively serpentinized and slightly carbonatized. A large porphyritic granophyric body occurs at the southwestern side of the central part of the large intrusion. It is light in color and mostly fractured and jointed (*Fig. 3*). The layered sequence of the large intrusion is divided into sixteen units (*Fig. 1*). Total thickness of this sequence is 1778 m from the margin to the centre of the intrusion.

Characteristic structural features in both intrusions are recorded during the field work, they are the following:

a. Slumping folds which dominate in Unit III of the small intrusion, usually accompanied by rhythmic layering of thin laminae of anorthosite alternating with troctolite (*Fig. 4*).

b. Knobby olivine gabbro of Unit V of small intrusion exhibits a characteristic outrcop appearance due to spheroidal weathering and differential weathering of the knobs. (*Fig. 5*).

c. Fractures and joints dissect the porphyritic granophyric body at the central part of the large intrusion (*Fig. 3*).

d. Macrorhythmic layering of normal gabbro of Unit III of the large intrusion shows in few cases microrhythmic layering of troctolite and anorthosite. The exposed surface of this unit shows large angular boulders with very well developed igneous lamination and spheroidal weathering (*Fig. 6*).

e. Coarse-grained troctolite of Unit V in the large intrusion contains rthythmic layers of olivine-rich gabbro and peredotite (*Fig. 7*).

The layered sequences in the two intrusions do not show a definite upward pattern in the mineral composition of the layers, except the hornblende gabbro becomes more abundant towards the topmost parts. This may be suggest that the cumulate layering process was continuously interrupted by frequent introduction of fresh surges of magma.

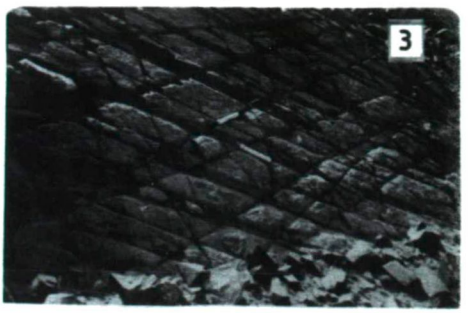

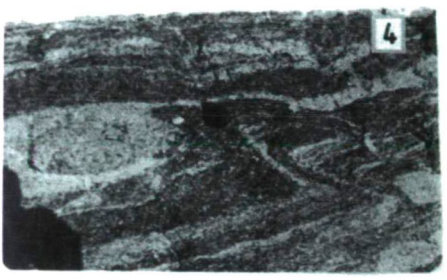

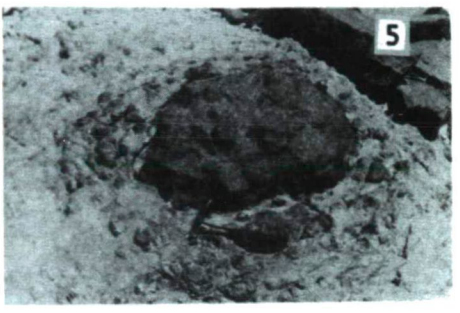

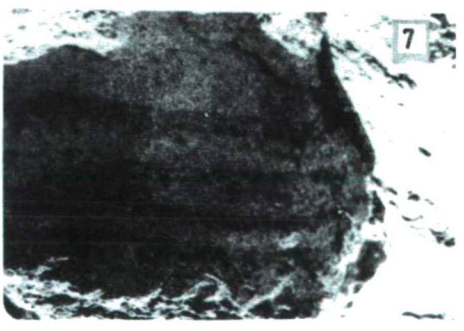

Fig. 2. Ramp-moat topography near the centre of the large intrusion.

Fig. 3. Fractured and jointed outcrop of granophyre at the central part of the large intrusion.

Fig. 4. Rhythmic layering of thin laminae of anorthosite alternating with troctolite slumping features are also observed (small intrusion).

Fig. 5. A large spheroidal boulder from unit V of the small intrusion, showing uniform distribution of large size knobs.

Fig. 6. A typical exposure of Unit III showing boulders with igneous lamination and spheroidal weathering.

Fig. 7. Rhythmic layers of olivine-rich gabbro and peridotite in the coarse-grained troctolite of Unit V in the large intrusion.

From the study of the outcrop pattern and attitude and compositon of layers of the two intrusions, it seems that they are most probably funnel shaped in three dimensions, which is a very common feature for the small layered intrusion, such as Rhum (WAGER and BROWN 1968); Muskox (IRVINE and SMITH 1967); Insizwa (LIGHTFOOT and NALDRETT 1984); Jabal Shayi (COLEMAN 1973) and Timberlana (CAMPBELL 1977). However, the large intrusion is much more elliptical than the small one. This suggests that the large intrusion could have a boat-like shape rather than a circular funnel shape. The small intrusion is slightly elongated in a NE-SW direction perpendicular to the elongation of the large one. It seems that the formation of the two intrusions was controlled by two major regional deep seated fracture zones. Layering of the small intrusion is truncated by the large one indicating that the large intrusion is the younger.

PETROGRAPHY OF THE PRINCIPAL CUMULATE ROCKS TYPES

The petrographic studies on about 150 thin sections showed that both intrusions are composed of the same rock types. Five essential cumulus minerals constitute the major part of these rocks. The minerals are, in decreasing abundance: plagioclase, olivine, clinopyroxene, orthopyroxene and hornblende. Accessory minerals are: biotite, apatite and opaques. Conventional petrographic terminology for the cumulus minerals which tackled by CAMPBELL (1987), IRVINE (1982), STRECKEISEN (1973) and WAGER et al. (1960), are also applied on the description of El Ekeim rocks. Determination of the modal composition of selected samples was carried out by a swift point-counter. The identified rock types of the present study are listed and briefly described below.

1. Cumulate rock types

a. Plagioclase – clinopyroxene – olivine cumulate (olivine gabbro).

b. Plagioclase – olivine cumulate (troctolite).

c. Plagioclase – clinopyroxene – olivine – hornblende cululate (hornblende – olivine gabbro).

d. Plagioclase – orthopyroxene – clinopyroxene – olivine cululate (olivine gabbronorite).

e. Plagioclase – clinopyroxene cumulate (gabbro).

f. Plagioclase cumulate (anorthosite).

g. Olivine – pyroxene cumulate (peridotite).

2. Non-cumulate rock types

h. Hornblende – olivine gabbro (chilled margin)

i. Granophyre.

a. Olivine gabbro

It is the most abundant rock type in both intrusions, and constitutes about 60% of the exposed rocks in the small intrusion, and about 75% in the large intrusion.

In the sections, the rock is medium-coarse grained, roughly equigranular, and consists of fresh plagioclase, pyroxene and olivine. The plagioclase makes up to 45-58% which are mostly labradorite. Pyroxene is the second most abundant cumulus mineral averaging from 52 to 35%. Subhedral olivine is the third most abundant cumulus mineral and froms 15-25%. The orthopyroxene and hornblende form less than 2%. The olivine gabbro of the lower and middle units is characterized by dissiminated opaques which

constitute up to 5%. Orthocumulate to mesocumulate textures are dominant in the upper and middle units, while mesocumulate to adcumulate textures are more dominant in the lower unit.

b. Troctolite

It is the second most dominant rock type in both intrusions. It constitutes about 30% of the small intrusion and about 12% of the large intrusion. Microscopically, the rocks consist mainly of plagioclase and olivine, with subordinate amount of pyroxene, opaques, biotite and apatite as cumulus and intercumulus material. The plagioclase constitutes approximately 50-60% and is usually tabular. Euhedral to subhedral olivine crystals form 20-45% of the rock. In some samples, the olivine crystals are rimmed by a very thin veneer of orthopyrexene that occurs as an intercumulus phase. Serpentinization is so advanced in some thin sections. Mesh texture and igneous lamination are well developed. Troctolite is poor in cumulus opaques, but some intercumulus opaques were observed.

c. Hornblende – olivine gabbro

It makes about 15% of the exposed rocks in the small intrusion and about 5% of the large one. The main cumulus minerals are plagioclase, hornblende and olivine. The plagioclase and olivine crystals are moderately altered.

d. Olivine gabbronorite

It represents about 8% of the exposed rocks of the small intrusion. It is composed mainly of fine – medium grained cumulus plagioclase, orthopyroxene, clinopyroxene and olivine. Opaques and biotite occur as intercumulus phases.

e. Gabbro

It is less abundant than the previous types. The rocks consists mainly of plagioclase and clinopyroxene with minor olivine and hornblende as cumulus minerals. The intercumulus minerals are represented by minor amounts of hornblende and opaques.

f. Anorthosite

It consistutes the whole of Units VIII and X of the small intrusion, with thickness of 10 and 15 m respectively. It also constitutes Unit X with 17 m thickness of the large intrusion. Some thin layers of olivine gabbro and troctolite occasionally forming rhythmic layering in the anorthosite. The plagioclase cumulate crystals represent more than 90% of the whole rock. The rest is represented by intercumulus pyroxene and opaques. The intercumulus material is mostly less than 5%, therefore the rock is an adcumulate. Igneous lamination is well developed in this rock type due to the parallel alignment of plagioclase crystals.

g. Peridotite

It occurs as thick continous layer near the bottom of the small intrusion, and as three discontinous layers at the southern part of the large intrusion. Alternations of thin layers of olivine gabbro and troctolite are prevailed with peridotites. The microscopic study revealed that the main cumulus minerals are olivine (70-85%). Pyroxene, plagioclase and accessories form the rest of the rock.

h. Chilled margin

It forms a single discontinous layer at the outer border of the intrusions at the contact with the country rocks. It is characteristic that the most of the minerals are fine-grained, with non-cumulate texture. Plagioclase, hornblende, pyroxene and olivine are the dominant constituents. However, few opaques, biotite and apatite are also recorded.

i. Granophyre

It occurs as a large elongated body, with a small off-shoot at the top towards the centre of the large intrusion. It is composed of fine-grained potash feldspar, plagioclase, quartz, orthopyroxene, apatite, biotite, ilmenite and magnetite. Olivine crystals are found near the contact. Granophyre represents the late stage of crystallisation of the layered series of the large intrusion, such as Insizwa complex (LIGHTFOOT and NALDRETT 1984) and Jimberlana intrusion (CAMPBELL 1978).

MINERALOGY OF EL EKEIM INTRUSIONS

The essential cumulus minerals of the investigated rock types, in order of abundance are: plagioclase, clinopyroxene, olivine, orthopyroxene and hornblende. However, the main accessory minerals are biotite, apatite and opaques. Some 70 polished sections are performed for the opaque mineral identification. The mineral constituents were examined microscopically in samples collected from four traverses, while two of them were examined by microprobe for further publication by the same authors.

a. Plagioclase

It is the most abundant cumulus mineral in most rocks of the two intrusions. It represents 50-60% by volume of the whole total composition of most rocks. However, some layers contain little or no plagioclase. The dominant plagioclase crystals are euhedral to subhedral, platy or lath-shaped. Their size variable is ranging from 0.2 to 1.8 mm in width and vary from 0.5 to more than 5 mm in length. Some of these crystals are slightly bent (*Fig. 8*) possibly due to accumulation of other crystals on their tops. Orientation or alignment of plagioclase crystals are clearly exhibited in some layers, which causes the prominent igneous lamination (*Fig. 9*). Primary normal zoning is well developed in some plagioclase crystals where some of them show three or more zones (*Fig. 10*). The boundary between the zones is always gradational indicating the gradual slow change of liquid composition and/or temperatures. Reverse and oscillatory zoning in plagioclase are also present indicating fluctuations in temperatures and liquid composition (SMITH and LOFGREN 1983).

Plagioclase also occurs as an intercumulus phase, that is lath-shaped or wedge shaped between the cumulus phases. It was crystallized from intersitial liquid in pores between crystal boundaries. Most plagioclase crystals are fresh, nevertheless some highly calcic plagioclases are altered to saussurite (zoisite, epidote and calcite). Some plagioclase crystals show radiating fractures due to the extensively alteration of the associated olivine (*Fig. 11*).

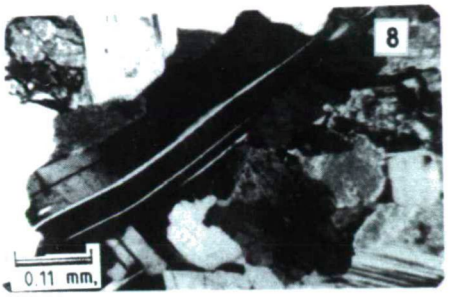
8
0.11 mm.

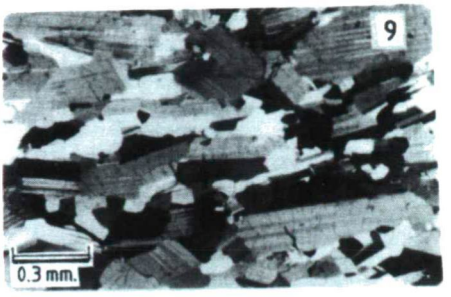
9
0.3 mm.

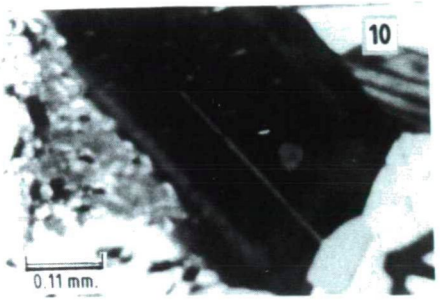
10
0.11 mm.

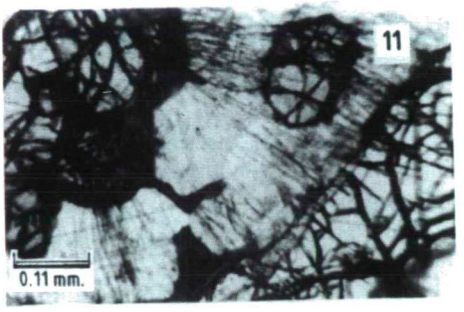
11
0.11 mm.

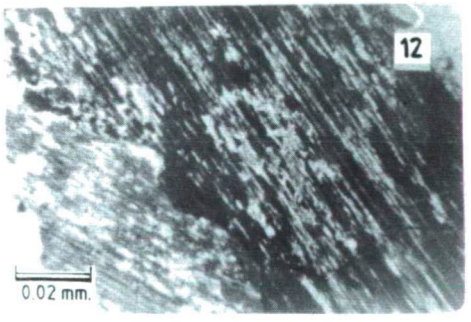
12
0.02 mm.

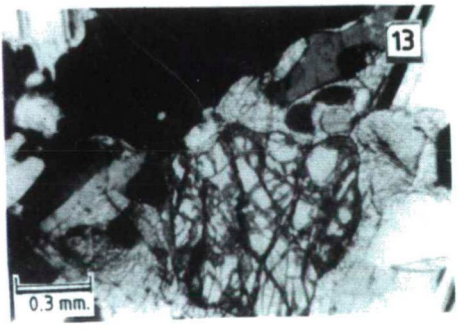
13
0.3 mm.

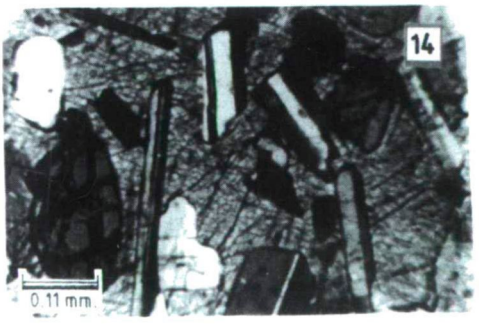
14
0.11 mm.

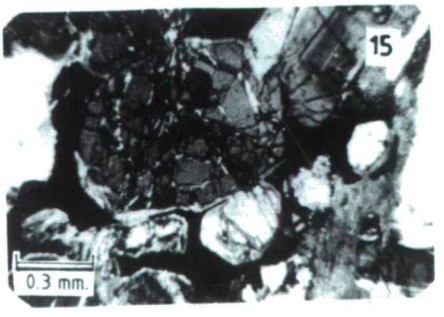
15
0.3 mm.

Fig. 8. Elongated and bent adcumulate plagioclase crystal showing wavy extinction and without zoning. (Transmitted light, C. P.)

Fig. 9. Adcumulate plagioclase showing well development igneous lamination. (Transmitted light, C. P.)

Fig. 10. Zoned Plagioclase crystal exhibiting post-cumulus growth in olivine gabbro. (Transmitted light, C. P.)

Fig. 11. Radiating fractures in plagioclase due to the expansion of extensively altered olivine. (Transmitted light, P. L.)

Fig. 12. Exsolved lamellae of orthopyroxene in clinopyroxene. (Transmitted light, C. P.)

Fig. 13. An olivine crystal rimmed by intercumulus clinopyroxene, which also encloses intercumulus hornblende (dark brown) (Transmitted light, C. P.)

Fig. 14. Knobby olivine gabbro, showing olivine and plagioclase chadacrysts embedded in large anhedral plate of clino-pyroxene. (Transmitted light, C. P.)

Fig. 15. Large subhedral olivine crystal rimmed by thin veneer of clinopyroxene and biotite (corona texture). It is also poikilitically enclose some opaque minerals (Transmitted light, C. P.)

b. Clinopyroxene

It occurs as the second major cumulus mineral in both intrusions. Generally it represents about 20-30% of the whole mineral composition. It is an augite variety. It occurs as cumulus crystals aligned parallel to tabular plagioclase and clustered olivine grains. It is mostly fresh and apperas in euhedral to subhedral prismatic shape. The dimension varies from 0.8 to 1.4 mm in width and 1.2 mm to more than 2 mm in length. Some clinopyroxene crystals are extensively schillerized by tiny small inclusion of opaques. Some augites contain exsolved lamellae of orthopyroxene parallel to {100} plane (*Fig. 12*). These were interpretted as inverted pigeonites (WAGER and BROWN 1967) which is a common feature in differentiated gabbroic intrusions.

Clinopyroxene also occurs as an intercumulus phase in the form of wedge-shaped grains and partial thin rims, in places pseudomorphed by hornblende around olivine and plagioclase crystals (*Fig. 13*). Occasionally, the intercumulus clinopyroxene forms large poiklitic plates enclosing numerous grains of differently sized plagioclase and olivine (*Fig. 14*). This texture is only observed in knobby olivine gabbro.

c. Olivine

It occurs as an essential cumulus constituent in most rock types. It forms about 10-47% of the whole cumulus minerals. The olivine crystals are mostly medium to coarse grained, ranging from 0.7-3 mm in diameter. Most of them are clustered to form elongated thin laminae. The shape is usually subhedral and rarely euhedral. Some olivine crystals poikilitically enclose few grains of plagioclase and/or opaque minerals. Corona texture is common where olivine is uniformly rimmed by reaction rims of pyroxene and biotite (*Fig. 15*).

Olivine also occurs as intercumulus phase, filling the interstitial spaces between plagioclase (*Fig. 16*). Most crystals are fresh. However, some are slightly to extensively altered to serpentine iddingsite or bowlingite. During this alteration, mesh texture is well developed, in which iron is released, filling the fractures (*Fig. 17*).

d. Orthopyroxene

Hypersthene occurs as a cumulus phase in few layers of both intrusions. It mostly represents less than 15% of the whole mineral composition. It commonly forms thin rims surrounding olivine or plagioclase crystals (*Fig. 18*). In some cases, it occurs as a narrow zone between olivine and plagioclase. Occasionally, these zones or rims pass into intercumulus orthopyroxene. They could be interpreted as corona structure, which are

mostly developed around the cores of olivine minerals, where the orthopyroxene shows a sharp boundary against an outer rim of amphibole.

e. Hornblende

It occurs as cumulus and intercumulus phases. The primary cumulus type is brownish in colour, and medium grained, ranging from 0.8 to 1.2 mm across. It mostly occurs in the olivine gabbro. The secondary hornblende is more common and mostly occurs as pseudomorphs after clinopyroxene. It represents less than 5% of the whole mineral composition.

f. Accessory and alteration minerals

They include; biotite, apatite, chlorite and actinolite, and zoisite. Biotite is persistently present as an accessory mineral especially in the olivine gabbro. It occurs as small ragged tabular flakes around the olivine and pyroxene crystals (*Fig. 15*). Possibly both cumulus and intercumulus biotite is present. It was formed after the bulk of the magma had solidified. Apatite is the most common accessory cumulate and intercumulate mineral throughout the intrusions. The large euhedral apatite crystals are inferred to have crystallized late in the magmatic history of the gabbroic rocks, probably from liquid trapped between plagioclase-ferromagnesian precipitates (COLEMAN et al. 1977). Apatite is a common minor orthocumulate phase in iron rich olivine gabbro as in Skaergaard and Bushveld intrusions (WAGER and BROWN 1967).

Chlorite and actinolite are rarely observed along fractures and rims. Zoisite is detected in very few thin sections, it is believed to be derived from alteration of the Ca-rich plagioclase.

g. Opaque Minerals

Opaque sulphide and oxide minerals constitute between 0.2 and 5% by the volume of the mafic-ultramafic rocks of El Ekeim intrusions. These minerals occur either as cumulus or intercumulus phases similar to Duluth Complex (TYSON and CHANGE 1984).

Ore microscopic examination for some 70 polished sections of the various rock types was carried out. The cumulus opaques occur as euhedral-subhedral grains between the cumulus silicates, or enclosed by polikilitic plates of them. However, intercumulus opaques occur as irregular interstitial grains between the silicate minerals. In order of abundance; the sulphide minerals are: pyrrhotite, chalcopyrite, pyrite, pentlandite and covellite. Whilst, the oxides are: magnetite, titano-magnetite, ilmenite, rutile, hematite, ulvospinel and hemo-ilmenite, together with little chromite, goethite and spinel.

The most abundant sulphide mineral is the pyrrhotite which forms 70-80% of the whole opaques. It usually occurs as a cumulus mineral and also as intercumulus as interstitial anhedral grains filling the spaces between the silicate minerals (*Fig. 19*). It is also commonly present as composite grains in association with magnetite, chalcopyrite and pyrite (*Fig. 20*). Pentlandite is present in a relatively minor amount, mostly associated with pyrrhotite forming exsolution texture (*Fig. 21*). The exsolved pentlandite tends to diffuse rapidly to the grain boundaries and along the {0001} planes of pyrrhotite and precipitate as rims around these grains.

Chalcopyrite is the second most common sulphide mineral. It occurs as single anhedral intercumulus grains or as clustered cumulus composite grains of chalcopyrite, pyrite and magnetite. Pyrite occurs in very small amounts, always in association with one or more of pyrrhotite, chalcopyrite and magnetite forming cumulus composite grains. Covellite is rarely observed, it is secondary mineral being formed by alteration of chalcopyrite.

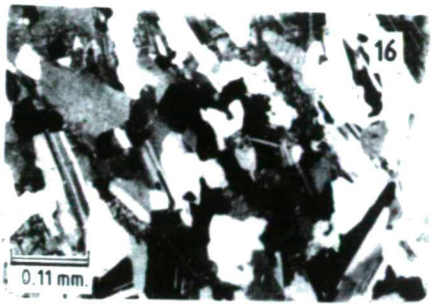
16
0.11 mm.

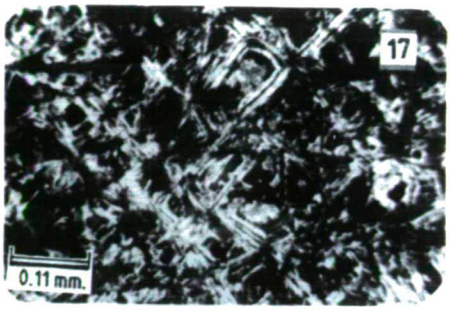
17
0.11 mm.

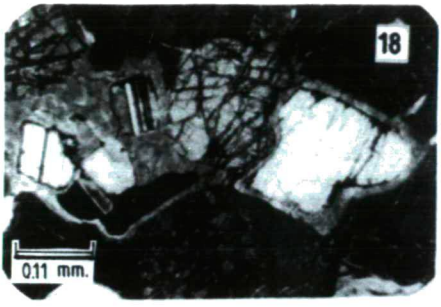
18
0.11 mm.


19
0.06 mm.

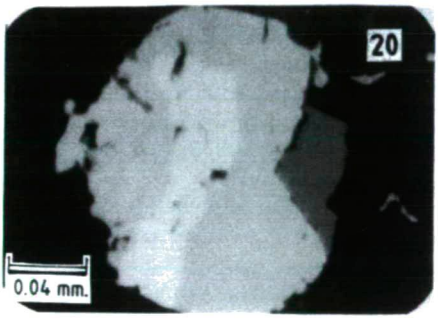
20
0.04 mm.

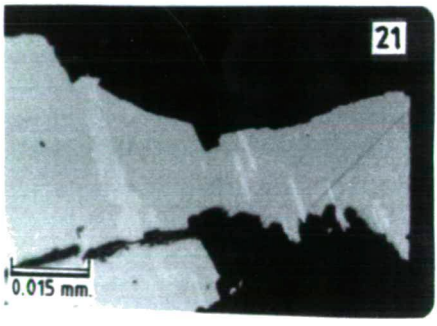
21
0.015 mm.

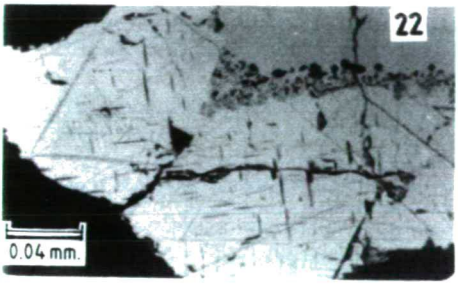
22
0.04 mm.

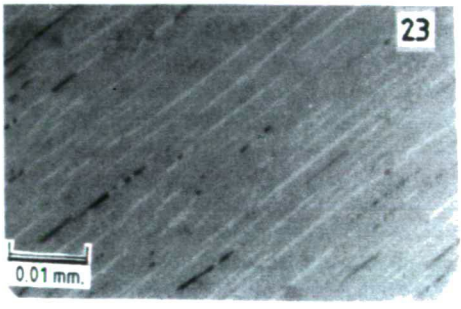
23
0.01 mm.

Fig. 16. Intercumulus olivine crystals occupying spaces between cumulus plagioclase (Transmitted light, C. P.)

Fig. 17. Serpentinized olivine in peridotite showing well developed mesh texture with some preserved relics (Transmitted light, C. P.)

Fig. 18. Thin rim of orthopyroxene surrounded by the olivine and plagioclase crystals. Some plagioclase crystals are embedded in clinopyroxene (Transmitted light, C. P.)

Fig. 19. Composite andhedral pyrrhotite – pentlandite and chalcopyrite filling the spaces between the silicate grains (Reflected light, oil imm.)

Fig. 20. Cumulus composite grains of magnetite, pyrrhotite and pyrite embedded in olivine (Reflected light, oil imm.)

Fig. 21. Pyyrhotite – pentlandite exsolution (Reflected light, oil imm.)

Fig. 22. A composite grain of ilmenite and magnetite. Magnetite contains spinel exsolution. Lamellae of ilmenite are oriented along the magnetite octahedral planes (Reflected light, oil. Imm.)

Fig. 23. Exsolution lamellae of hematite in ilmenite (hemo-ilmenite) (Reflected light, oil imm.)

Oxide minerals are less abundant than the sulphides. Their amount decreases gradually from the bottom to the top of the layered sequences. Magnetite occurs either as small intercumulus anhedral interstitial grains or as a cumulus phase with euhedral to subhedral shape. It forms frequently composite grains with ilmenite. The contact between magnetite and ilmenite grains is either rectilinear or highly curved, with the convexity towards the magnetite, and is often marked by specks fo translucent spinel. Magnetite commonly contains exsolution of ilmenite in various types of intergrowth, among which the fine ilmenite lamellae are oriented along the octahedral magnetite planes to form triangular networks (*Fig. 22*). Magnetite also shows common replacement by hematite as a result of martitization (RAMDOHR 1980). Hematite also occurs as exsolutions (hemo-ilmenite) representing by thin linear or thread-like lamellae in ilmenite (*Fig. 23*).

Chromite was observed in the peridotite, troctolite and olivine-rich layers of the present intrusions. Same results were recorded by (CAMERON 1980 and 1982). It is generally present in the form of rounded to oval shaped idiomorphic homogenous single grains or as clustered grains. Some are highly fractured and filled with either serpentinite or martitized magnetite.

Modal Analysis

Modal analysis was carried out on 59 samples representing the main rock types along the two main traverses in the two intrusions (T 17 in the small intrusion, and T 16 in the large one). The results are represented diagramatically in *Figures 24* and *25*. The obtained data indicate the following:

1. The two chilled margins of both intrusions are very similar in their modal compositon.
2. Both intrusions have the same mineral constituents, with slight difference in relative proportions.
3. Plagioclase seems to be slightly more abundant in T 16 than in T 17. On the other hand, olivine is clearly more abundant in T 17 than in T 16.
4. Orthopyroxene is more persistant with a greater proportion in T 16 than in T 17.
5. The variation in the content of the clinopyroxene in T 16 is clearly less than its variation in T 17, where it shows increase on the expense of olivine in the upper part of the traverse.

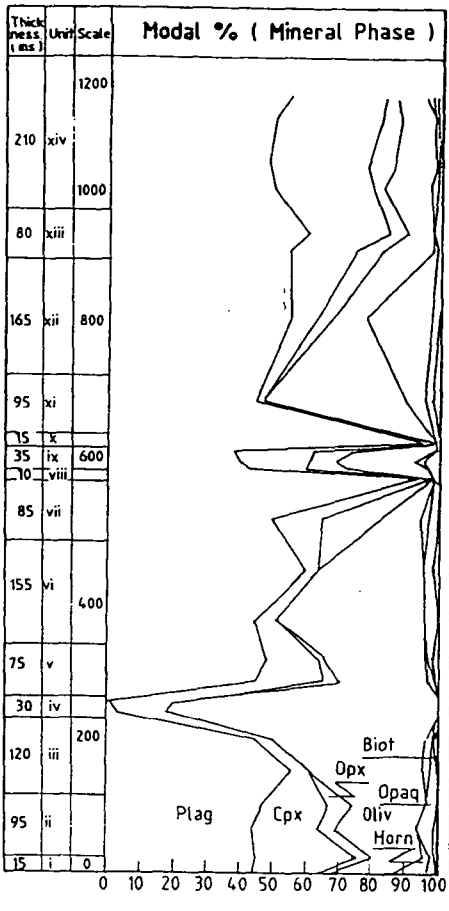

Fig. 24. Modal analysis along T17, small El Ekeim.

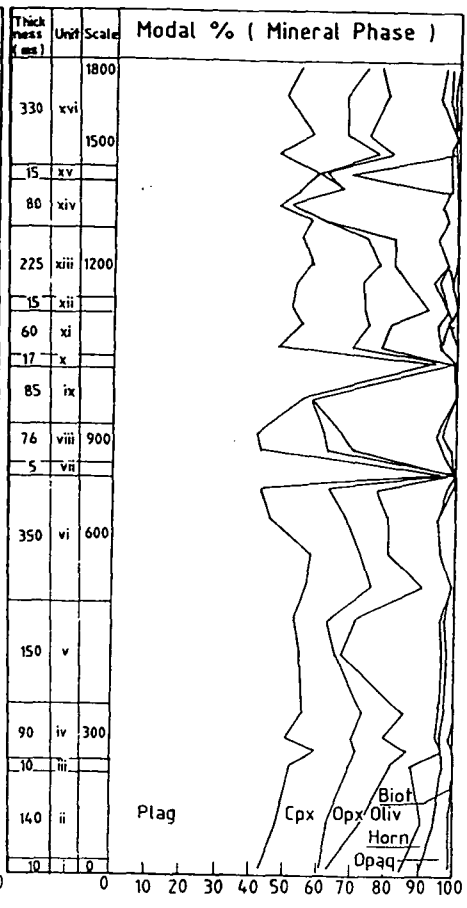

Fig. 25. Modal analysis along T16, large El Ekeim.

CONCLUSIONS

The overall conclusion of the petrographic and mineralogic study can be put in two main points to recognize the parental magma of the two intrusions:

1. The mineral composition of both intrusions indicates that their parent magma is the same and it had a tholeiitic nature.
2. Although the two intrusions are very close in their composition, the parent magma of the large intrusion seems to be slightly more evolved than that of the small intrusion.

Based on the current studies, some other conclusions are reached, they are following:

1. The presence of some internal structures characterizing the units and layers of the two intrusions as slump structures, igneous lamination, knobby texture and rhythmic layering could lead that they were formed by a combination of different mechanisms of density gravitational stratification and crystal sorting by magmatic convection currents.
2. The crystal sorting due to recurrent burts of nucleation, crystallization and gravitational settling (GOODE 1975) seems to have had a major role in the formation of layering of the two intrusions.
3. The layered sequences in the two intrusions do not show a definite upward pattern in the mineral composition of the layers, except the hornblende gabbro becomes more abundant towards the topmost parts. This may suggest that the cumulate layering process was continuously interrupted by frequent introduction of fresh patches of magma.
4. From the outcrop pattern, attitude and composition of layers of the two intrusions. It seems that the formation of the two intrusions was controlled by two major regional deep-seated fracture zone. Layering of the small intrusion are truncated by the large one indicating that the large intrusion is the younger.
5. Zoning in plagioclase is common, with oscillatory zoning more prevalent than normal and reverse zoning. The oscillations of anorthite content are primary, which indicate that minor pulses of fresh magma introduction was common. This feature may equally be due to minor variations in water vapour pressure causing undercooling at the same horizons (AL SHANTI 1974).

REFERENCES

AL-SHANTI, A. M. (1974): Al-Jilani Layered basic intrusion, Ad Dawadimi District Saudi Arabia, DGMR Res, Bull. 12, 1-45.

CAMERON, E. N. (1980): Evolution of the lower critical zone of Bushveld complex and its chromite deposits. Econ. Geol. 77, 845-871.

CAMERON, E. N. (1982): The upper zone of eastern Bushveld complex precursor of the Merensky Reef. Econ. Geol. 77, 1307-1327.

CAMPBELL, I. H. (1977): A study of macro-rhythmic layering and cumulate processes in teh Jimberlana intrusion Western Australia. Part I: Upper Layer Series. Jour. Petrol. 18, 183-215.

CAMPBELL, I. H. (1978): Some problems with cumulus theory. Lithos, 11, 311-323.

CAMPBELL, I. H. (1987): Distribution of orthrocumulate textures in the Jimberlana intrusion. Jour. Geol. 95, 35-54.

COLEMAN, R. G., BROWN, G. F. and KEITH, T. E. (1972): Layered gabbro in Southwest Saudi Arabia. USGS, Saudi Arabian Proj., Rept. K54, D143-D150.

COLEMAN, R. G., FLECK, R. J., HEDGE, C. E. and GHENT, E. D. (1977): The volcanic rocks of Southwest Saudi Arabia and the opening of the Red Sea. DGMR. Bull. 22, 1-30.

COLEMAN, R. G., GHENT, E. D. and FLECK, R. J. (1973): Jabal Shayi gabbro in southwestern Saudi Arabia. DGMR. Bull. 17.

GOODE, A. D. (1975): Small scale primary cumulus igneous layering in the Kalka layered intrusion, Gilex complex, Central Australia. Jour. Petrol. 17, 379-397.

IRVINE, T. N. (1982): Terminology of layered intrusions. Jour. Petrol. 23, 127-162.

IRVINE, T. N. and SMITH, C. H. (1967): The ultramafic rocks of the Muskox intrusion Northwest Territories, Canada, in WYLLIE, P. J. editor. Ultramafic and related rocks 38-49. John Wiley and Sons Inc.

LIGHTFOOT, P. C. and NALDRETT, A. J. (1984): Chemical variation in the Insizwa complex, Transkei, and the nature of the parent magma. Can. Min. 22, 111-123.

LOWRENCE et. al. (1978): Asbestos occurrences in serpentinites of the Hamdah area. Saudi Arabian Proj. Rept. 239, 1-22.

OVERSTREET, W. C. (1978): A geological and geochemical reconnaissance of the TATHLITH one-degree Quadrangle Sheet 19/43: USGS, Saudi Arabian Proj. Rept. 230.

RAMDOHR, P. (1980): The Ore Minerals and Their Intergrowths. English translation of the 3rd edition. Pergamon Press, Oxford.

SMITH, R. K. and LOFGREN, G. E. (1983): An analytical and experimental study of zoning in plagioclase. Lithos. 16, 153-168.

STRECKEISEN, A. L. (1973): Plutonic rocks, classification and nomenclature recommended by IUGS Subcommission on Systematics of Igneous Rocks. Geotimes 18, 26-30.

TYSON, R. M. and CHANG, L. Y. (1984): Petrology and sulfide mineralization of the Partridge River Troctolite, Duluth Complex, Minnesota. Cand. Min. 22, 23-38.

WAGER, L. R. and BROWN, G. M. (1967): Layered Igneous Rocks. Oliver and Boyd, Edinburgh and London. 588 p.

WAGER, L. R., BROWN, G. M. and WARDSWORTH, W. J. (1960): Types of igneous cumulate. Jour. Petrol. 1, 73-85.

WHITE, D. L. (1984): Mineral resource potential of mafic and ultramafic rocks, Hamdah area (19/43 D). Kingdom of Saudi Arabia, Open-File Rept. DGMR-OF-04-27.

ZUBEIR, M. O. (1989): Geology of the layered mafic-ultramafic intrusions at Jabel El-Ekeim, Southeast Saudi Arabia. Ph.D. thesis, 186 p., Faculty of Earth Sciences, King Abdulaziz University, Jeddah, Saudi Arabia.

Manuscript received 4. March 1999.

Acta Mineralogica-Petrographica, Szeged, XL, 71–76, 1999

UPPER CRETACEOUS TRACHYDACITES SOUTH OF BELGRADE - A CONTRIBUTION FOR THE KNOWLEDGE OF THE ANDESITIC VOLCANISM IN THE NORTHERN PART OF THE VARDAR ZONE COMPOSITE TERRANE

STEVAN KARAMATA[1], VERA KNEZEVIC[1] VLADICA CVETKOVIC [1], DANICA SRECKOVIC [1], TATJANA MARCENKO[2]

[1]Faculty of Mining and Geology, University of Belgrade
[2] IGEM RAN, Moscow, Russia

ABSTRACT

Volcanic rocks are abundant as clasts in Senonian sediments south of Belgrade, as well as at the north in the Karadjordjevo formation in Southeastern Bačka and in the Central Banat. These rocks are known in the literature as andesites, but because of the size of grains and mostly high alteration they were not studied yet. An outcrop of andesitic debris-flow deposit interlayered into these sediments was found south of Belgrade and studied. The field and petrographic study reveal a submarine slump of the volcani(epi)clastic debris predominately composed of holo- to hypocrystalline porphyritic volcanic fragments within the fine-grained volcanogenic and marly matrix. Volcanic rocks display a high sodic alkaline character corresponding to trachydacites, respectively to benmoreites and sodic trachytes while their trace element ratios indicate VA (volcanic arc) affinity. These rocks represent members of the Senonian volcanic activity in the central part of the Vardar zone, i.e. in its northernmost exposed part of the Kopaonik block and ridge unit. Given the abundant occurrences of andesitic clasts in the Senonian Karadjordjevo formation in the base of the Neogene of the Pannonian basin further at north, the existence of a Senonian volcanism related to the subduction and the closure of the western branch of the Vardar ocean became more evident.

Keywords: debris-flow, trachydacite, pebbles, volcanic arc, Vardar zone, subduction, suture zone, Upper Cretaceous, Belgrade, Backa-Banat, Northern Serbia

INTRODUCTION AND GEOLOGICAL SETTING

The Vardar zone composite terrane is considered here in the sense of KARAMATA et al. (1994, 1996/1997, 1998), without the later introduced Jadar block (as a different terrane), embracing relics of the Main oceanic basin at the East (VZM) and the Western belt (WB), with the Kopaonik block and ridge unit (KBR) between. The Western belt of the Vardar zone composite terrane represents the relic of an oceanic back-arc basin originated in the Upper Triassic, between the detached Kopaonik block and ridge unit, at the East, and the main part of the Drina–Ivanjica terrane, at the West (*Fig.1*). The remnants of this belt are represented by an olistostrome deposited in the trench and now occurring over the area of collision. The olistostrome contains fragments of greywackes and basaltic rocks (of MORB and IAB type), lens-shaped bodies of Triassic and Jurassic limestones and cherts, as well as fragments of Upper Cretaceous limestones. Campanian limestones were found also as inclusions in the basalts (near Krupanj) or as interlayers

[1] Djusina 7, 11000 Belgrade, Yugoslavia, e-mail: cvladica@eunet.yu
[2] Staromonetny per. 35, 109107 Moscow, Russia

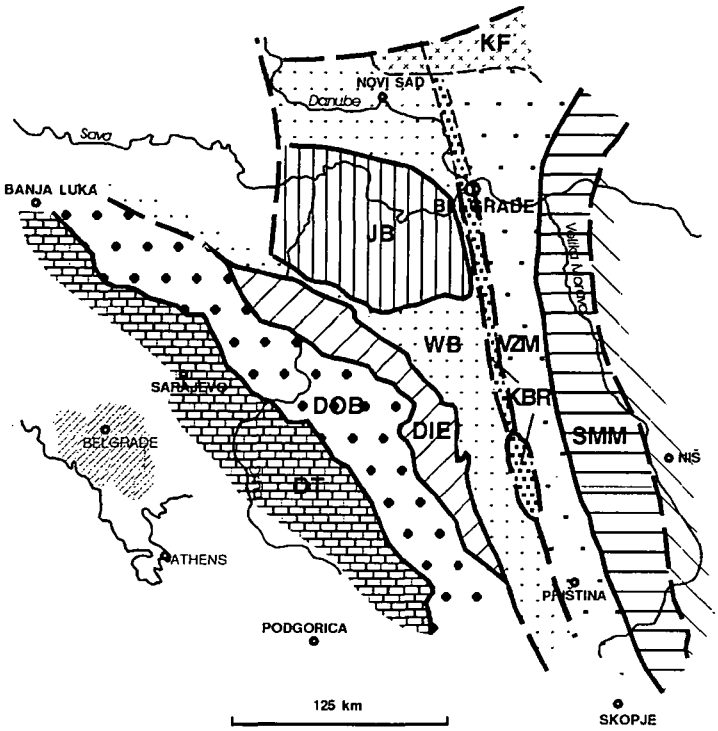

Fig. 1. – The Vardar zone composite terrane and the position of the studied volcaniclastic rocks (after KARAMATA, et al., 1996/97, 1998).
EXPLANATIONS: VZM – Main oceanic belt of the Vardar zone composite terrane, WB – Western belt of the Vardar zone composite terrane; KBR – Kopaonik block and ridge, KF – Karadjordjevo formation, extension beneath the Neogene cover, SMM – Serbian-Macedonian mass composite terrane, DIE – Drina-Ivanjica element/terrane, JB – Jadar block, DOB – Dinaridic ophiolite belt, DT – Dinaridic trunck.

between the pillow lava flows (northern flanks of Kozara Mt.). At the East of the Western belt, south of Belgrade, in the northern continuation of the Kopaonik block and ridge unit, Turonian-Senonian sandy-marly-clayish sediments occur. Within their highest levels abundant clasts of volcanic rocks (fine to middle grains) have been observed (MARKOVIC et al., 1984/85). Similar sediments of the same age, which contain frequent volcanic clasts, locally up to 80 % of the well core, have been reported as members of the Upper Senonian Karadjordjevo formation in the northernmost continuation of the Kopaonik block and ridge unit in the Pre-Neogene basement of the Pannonian basin (CANOVIC and KEMENCI, 1988). These grains are small and mosty altered, thus unconvenient for study, and according to their mineral composition they were named »andesites«. Some years ago, in the uppermost levels of those Turonian-Senonian sediments, situated south of Belgrade, a section with such »andesitic« fragments (up to 30 cm in diameter) was found. Being unaltered or only stightly altered these rocks were suitable for detailed determination of their character and for providing additional data on the evolution of the Western oceanic belt of the Vardar zone during Upper Cretaceous.

PETROGRAPHY OF THE VOLCANOCLASTICS

Volcanic conglomerates of andesitic appearance were found south of Belgrade (10–15 km) and briefly described about 15 years ago (MARKOVIC, et al., 1984/85, TERZIC and KARAMATA, 1968 – unpublished report). They are situated within a Turonian (?)–Senonian sedimentary series composed predominantly of greywackes, shales and marls, more precisely within its highest, andesitic clasts bearing levels, probabaly of Campanian age. These rocks are exposed in a new outcrop (oriented WNW-ESE), in a mainly covered area, as a 20 m long and up to 7 m high unit. This unit can be divided into three levels – the lowermost and the uppermost levels built of marls and sandstones, and the middle level predominantly composed of conglomerates with abundant volcanogenic fragments. The contact in the base of the conglomeratic level with underlying sedimentary rocks is sharp.

The middle level is an about 3 m thick section of volcaniclastic deposits, built of well rounded (in lower parts) to subrounded (in higher parts) andesite-like and rare sedimentary rock fragments enclosed by a fine-grained volcanic to mixed volcanic + marly matrix. Fragments of volcanic origin make from almost total mass to 60-80 % (vol) of all clasts. Coarse detrital material is moderately sorted, it highly predominates giving rise to pronounced closed framework of the deposit. Within some levels of the middle unit appear to be thin (up to 80 cm long) sandstone lenses. This level probably represents a submarine slump from an andesitic high.

The volcanic pebbles (up to 30 cm in diameter) are porphyritic rocks of various colour (pink, red, grey to black or green). The phenocrysts are represented by andesine (32-41% an), biotite and hornblende (chloritized), and in some samples rare augite. The hypo– to holocrystalline groundmass consists of plagioclase, K-feldspar and quartz microlites. Apatite, magnetite (?) and very rare zircon are the main accessories. Secondary chlorite, calcite, sericite and clay minerals are ubiquitous and often very abundant. Some volcanic fragments have a completely calcitized groundmass with almost invisible plagioclase microlites.

TABLE 1

Trace element contents of the studied trachydacites

Sample No	Zr (ppm)	Nb (ppm)	Y (ppm)	Sr (ppm)	Rb (ppm)	Ba (ppm)
1. BR2/8	217	14	19	332	13	2696
2. BR2/9	229	17	22	473	17	4763
3. BR2/10	238	15	30	520	30	969
4. BR2/11	242	17	22	558	29	4218
5. BR2/12	229	15	28	379	26	2169
6. BR2/13	242	19	28	605	31	4042
7. BR2/14	282	19	25	296	9	540
8. BR2/15	318	16	26	407	24	3082
9. BR2/16	253	17	23	461	19	1330
10. BR2/17	265	15	21	375	16	928
11. BR2/18	238	18	23	501	20	1420
12. BR2/19	300	17	21	318	20	1047
13. BR2/20	228	18	21	467	17	2356
14. BR2/21	241	15	23	472	21	3240
15. BR2/22	141	11	22	521	26	1334
16. BR2/23	215	15	21	433	17	2167
17. BR2/24	237	17	24	294	28	5232
18. BR2/25	300	16	22	291	23	1161

ROCK CHEMISTRY

The studied volcanic rocks are characterized by SiO_2 content ranging from 55 to 64%, mostly between 61 and 63% and with relatively high Na_2O (6.00 to 8.50 %) and low to medium K_2O (1.30 to 2.90. %) content. Only some highly altered rocks are poorer in-silica. According to LE BAS et al., (1986) these rocks correspond to sodic types and belong to trachydacites/benmoreites and sodic trachytes (*Fig.2*).

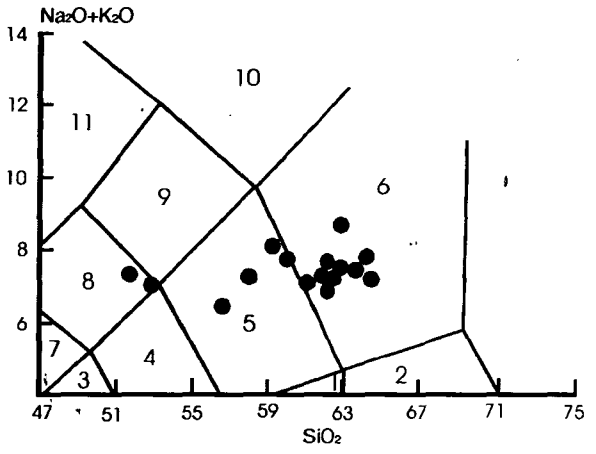

Fig. 2. – Total Alkali vs Silica diagram (after LE BAS et al., 1986): dots represent the trachydacitic rocks from the surrounding of Belgrade. EXPLANATIONS: 1 – andesite; 2 – dacite; 3 – trachybasalt; 4 – basaltic trachyandesite; 5 – trachyandesite; 6 – trachyte (q<20%) or trachydacite (q>20%); 7 – tephrite (ol<10%) or basanite (ol>10%); 8 – phonotephrite; 9 – tephriphonolite; 10 – phonolite; 11 – foidite

The contents of some characteristic trace elements (analyzed by XRF in the Laboratory of the IGEM of the Russian Academy of Sciences, Moscow, anal. T. MARCHENKO), presented in table 1, are without any significant variance. Even the rock alteration does not influence their contents, not only of the elements which are believed to behave immobile (Nb, Y and Zr), but of Sr and Rb, as well. However, Ba contents show considerable variations that could be measured by tens order of magnitude (540-5232 ppm)

In order to define the geological setting of origin of these rocks the discrimination diagrams for granitic rocks elaborated by PEARCE et al. (1984) were used. These diagrams consider the granitic rocks of the "Volcanic arc" belts, as well as those of the "Within plate" and "Collision" granites, comprising the rocks with more than 56 % SiO_2, and can be used for the determination of the geological setting of their volcanic equivalents, too. The studied volcanic rocks of the surrounding of Belgrade do meet the required criteria. According to the Nb/Y and Rb/Y+Nb (*Fig. 3 a,b*) discrimintion diagrams the studied rocks display volcanic arc affinity, while the Rb/SiO_2 (*Fig. 3 c*) ratios plot into the VAG+ WPG field and the Y/SiO_2 ratios (*Fig. 3 d*) into the VAG + COLG + ORG field. Since these trachydacites are situated within the Vardar zone, i.e. in a suture zone, the WPG character is excluded, and the COLG and ORG affinities are not likely because of the Rb/Y+Nb and Nb/Y ratios. According to the presented chemical characteristics these rocks belong to a volcanic arc granitic association, i.e. they are

related to subduction processes. Somewhat lower Rb contents than could be expected for the subduction related rocks might have been the consequence of biotite fractionation.

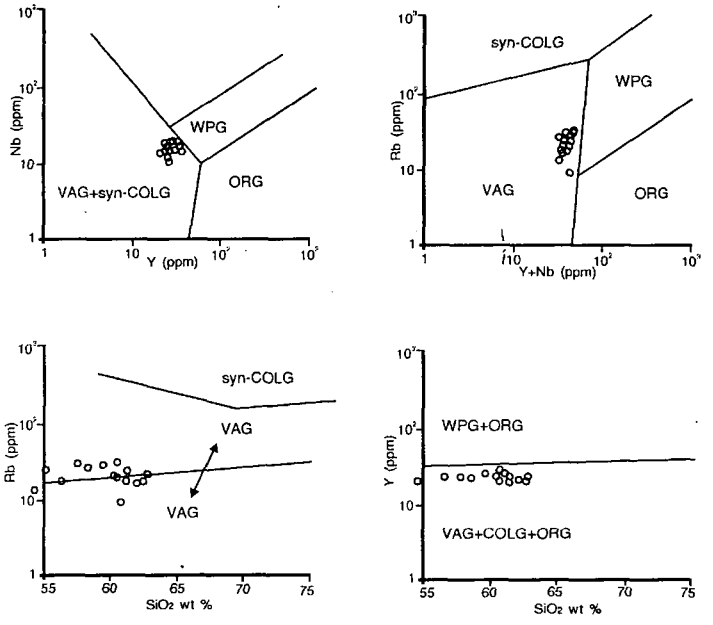

Fig. 3. – Nb – Y (a), Rb – Nb+Y (b), Rb – SiO2 (c) and Y – SiO2 (d) discrimination diagrams (after PEARCE et al., 1984).
EXPLANATIONS: Dots represent the trachydacitic rocks of the surrounding of Belgrade: VAG – Volcanic arc granites; WPG – Within plate granites; ORG – Ocean ridge granites; COLG – Collision granites; syn-COLG – Syn–collision granites.

CONCLUSION

The trachydacitic volcano(epi)clastic debris-flow of submarine slump features, close to the southern suburb of Belgrade, indicates the existence of a subduction related volcanism in this area during Senonian. The presence of small volcanic (andesitic, after MARKOVIC et al., 1984/85 or trachydacitic) clasts within (probably Upper) Senonian graywackes in the vicinity of Belgrade and of andesite and trachyte clasts (after CANOVIC and KEMENCI, 1988) in the Senonian, Campanian to Pre-Late Maastrichtian, Karadjordjevo formation in Central Banat and southern Backa in the basement of the Neogene deposits of the Pannonian basin, as the northernmost continuation of the Kopaonik block and ridge unit, represent further evidence for the existence of a significant volcanism in this area during Upper Cretaceous. The area of the volcanism was situated at the East of the Western belt (formerly an oceanic basin) of the Vardar zone. That fact further illuminates the problem of closure of the western branch of the Vardar zone. The age of oceanic basalts which include Campanian limestones near Krupanj and contain Campanian sandy limestone interlayers at the northern flanks of

Kozara Mt. in western Bosnia, together with the volcanic-arc geochemical features of the trachydacitic rocks near Belgrade, as well as the position of the subduction related volcanism, indicate that the Western (oceanic) basin of the Vardar ocean terminated by an eastward oriented subduction during Senonian. The overstep sequence is (Late) Maastrichtian flysch. By the subduction and collision processes, as well as by the later horizontal movements of the blocks, a primarily distal trench melange and a volcanic arc, related to subduction, approached to each other.

These new results date the closure of the western branch, i.e. the last existing of the northern parts of the Vardar zone in the Senonian, most probably in Upper Campanian or Early Maastrichtian .

ACKNOWLEDGEMENT

The very useful suggestions of Prof. A.G.H. Mitchell (Oxford) are acknowledged. The paper was enabled by the financial support of Serbian Academy of Sciences and Arts, Belgrade – Geodynamic Project.

REFERENCES

CANOVIC, M., KEMENCI, R. (1988): The Mesozioc of the Pannonian Basin in Vojvodina (Yugoslavia). Stratigraphy and facies, magmatism, paleogeography (In Serbian with English summary). Monography, Matica Srpska..352. Novi Sad.

KARAMATA, S., KNEZEVIC, V., MEMOVIC E., POPEVIC A. (1994): The evolution of the northern part of the Vardar zone in Mesozoic. 7th Cong. of the Geol. Soc. of Greece 25-27. May, Thessaloniki, Abstracts, 56-57.

KARAMATA, S., KRSTIC, B., DIMITRIJEVIC, D.M., DIMITRIJEVIC, N.M., KNEZEVIC, V., STOJANOV, I., FILIPOVIC, I. (1996/1997): Terranes between the Moesian plate and the Adriatic sea. In: IGCP Project No 276: Terrane maps and terrane descriptions. Annales Geolog. des Pays Hellen., 37, 429-477, Athens.

KARAMATA, S., DIMITRIJEVIC, N.M., DIMITRIJEVIC, D.M. (1998): Okeanski prostori u sredisnjem delu Balkanskog poluostrva tokom mezozoika (Oceanic realms in the Central part of the Balkan peninsula). XIII Kong. Geol. Jug., Herceg Novi. II, 119-123.

LE BAS, M.J., LE MAITRE, R.W., STRECKEISEN, A., ZANETTIN, B. (1986): A Chemical Classification of Volcanic Roks Based on the Total Alkali–Silica Diagram. Journal of Petrology, 27, 745 – 750.

MARKOVIC, B., OBRADINOVIC, Z., VESELINOVIC, M., ANDJELKOVIC, J., STEVANOVIC, P., RAKIC, M., 1984/85: Geology and explanatory text for the Sheet Beograd. Savezni Geoloski Zavod, 52. Belgrade.

PEARCE, J.A., HARRIS, N.B.W., TINDLE, A.G. (1984): Trace Element Discrimination for Tetctonic Interpretation of Granitic Rocks. Jour. Petrol., 25/ 4, 956 –983.

TERZIC, M., KARAMATA, S. (1968): Kredne andezitske stene Avale. Faculty of Mining and Geology. 12, Beograd

Manuscript received 18. May 1999.

Acta Mineralogica-Petrographica, Szeged, XL, 77-96, 1999

GEOCHEMISTRY, MINERAL CHEMISTRY AND TECTONIC SETTING OF THE OLDER GRANITOIDS FROM EAST OF EL-TOR, SW-SINAI, EGYPT

A. M. ABDEL-KARIM[1], I. KUBOVICS[2] and ZS. MOLNÁR[3]

[1] Geology Department, Faculty of Science, Zagazig University
[2] Department of Petrology and Geochemistry, Eötvös University
[3] Study-Reactor, Technical University

ABSTRACT

The older granitoids of Wadi Hibran-Wadi Mear, East of El-Tor constitute the westernmost outcrops of the granitic intrusion of Sinai massif of Egypt. They intrude small masses of gneisses and are, in turn, invaded by huge masses of younger granites and crosscut by mafic and felsic dyke swarms.

They consist of trondjemite-granodiorite (TR-GD) suite and belong to the low- to medium K calc-alkaline series. The TR suite comprises quartz-diorite, quartz monzodiorite and tonalite, meanwhile the GD suite includes proper granodiorite.

Amphiboles are calcic-type and vary in composition from magnesio-hornblende in TR to ferroedenitic hornblende in GD. Amphiboles from more evolved rock-types contain higher values of mg [Mg/(Mg+Fe) ratio] than those of the coexisting biotites. Biotite mg-values decrease with increase Si from TR to GD rocks. Chemical parameters of amphiboles, biotites and plagioclases indicate a pressure less than 5 Kb. and temperature of about 700-850 °C for the host TR-GD suite.

Based on REE geochemistry, the older granitoids show two different types of REE patterns; A) less differentiated type represented by TR suite and B) differentiated type related to GD suite. The less differentiated type has REE distribution patterns marked by positive Eu anomaly, whereas the differentiated type has wide range of total REE abundance and displays negative Eu anomaly. Both of them have smooth concave REE distribution patterns. These patterns are fairly similar to the models involving partial melting of eclogite/quartz eclogite parents.

Tectomagmatic setting reveals that the present granitoids belong to two calc-alkaline mafic magmas emplaced through a pre-plate collision to post-collision regime. They are highly comparable with the volcanic arc granites of active continental margin.

INTRODUCTION

The Wadi Hibran-Wadi Mear area lies at the western sector of the basement rocks of the Sinai massif. It is occupied by old granitoid rocks. Old granitoids previously referred to as „Old", „Shaitian", „Grey" or „Syn-tectonic". HUSSEIN et al. (1982) believe that the majority of the older granitoid plutons are subduction related granodiorite and closely associated island arc andesites. NOWEIR et al. (1990) subdivided the Egyptian Older Granites into three types namely, normal-, gneissic-, and Shaitian type older granites and closely associated with mature island arc. On the basis of the age dating the Egyptian Older Granitoids are subdivided into three events of igneous activity (HASSAN and HASHAD, 1990). These are Shaitian (800 and 850 Ma), Hafafit (670 and 710 Ma) and Meatiq event (630 and 610 Ma).

[1] Zagazig, Egypt
[2] H-1088 Budapest, Múzeum krt. 4/a, Hungary
[3] H-1111 Budapest, Műegyetem rakpart 9, Hungary

The granitoid rocks of the present area correspond to grey/older granites of EL-RAMLY and AKAAD (1960), syn-orogenic granites of EL-GABY (1975), G 1 granites of HUSSEIN et al. (1982), and calc-alkaline, autochthonous and para-autochthonous granites of EL-GABY et al. (1988). The studied granitoids were described by El-Mezayen et al. (1994) as calc-alkaline, metaluminous, post collisional uplifting older granitoids.

Petrography are concerned with 45 samples; modal analyses were carried out on 16 selected samples (average point counts c = 4500). Chemical analyses for major elements (13 samples) were determined by standard wet chemical technique method. Twenty seven chemical analyses of plagioclases (6), amphiboles (9) and biotites (12) have been carried out using standard Amray-1830 I electron microprobe under operating condition of 20 Kv and 1-2 nA. In most cases core and rim composition were determined for mineral grains. The chemical analyses for the minerals and rocks were done at the Department of Petrology and Geochemistry, Eötvös University of Budapest. Also, six of these samples were analysed for the trace as well as the rare-earth elements using the standard INAA at Atomic Reactor of Technical University, Budapest, Hungary.

GENERAL GEOLOGY

The older granitoids east of El-Tor constitute the extremely western outcrops of granitic intrusion of the Sinai massif. They occupy about 55 square Km area extending from Wadi Hibran in the north to Wadi Mear in the south (*Fig. 1*). The older granitoids are medium to coarse grained equigranular to porphyritic textures. The plutons cover a compositional spectum ranges from tonalite, trondhjemite to granodiorite. The tonalite is passing locally into trondhjemitic and granodioritic equivalents with gradational contacts. The rocks are sometimes foliated and greissose. In certain area, specially near the batholith borders, the granitoids form ragged terrains and high relief. They contain abundant xenoliths, rafts and bands of the country rocks of more mafic composition. These inclusions are variable in sizes and stages of digestion and decrease in their abundance away from the hill borders.

The older granitoid rocks intrude a small masses of gneiss with sharp and mylonitized contacts. The composition of gneiss ranges from diorite to granodiorite. The present granitoids are, in turn, intruded by huge masses of younger granites and cut by various dyke swarms ranging from basic to acidic in composition. These dykes strike NNE-SSW, NE-SW and ENE-WSW trends. The present plutons are jointed in different directions, mostly NE-SW and NW-SE trends. The main faults traversing the plutons have NNE-SSW and NNW-SSE trends.

CLASSIFICATION AND MINERAL CHEMISTRY

The trondhjemite-granodiorite suite exhibit a wide range of mineralogical and textural variations. The modal mineral percentage of 16 selected samples are given in Table 1. In STRECKEISEN's (1976) AQP diagram (*Fig. 2*) the studied rock-types are given by tonalite, quartz-diorite, granodiorite and quartz-monzodiorite. According to the evolutionary trends proposed by LAMEYER and BOWDEN (1982) the studied granitoids are calc-alkaline type and belong to (1). The trondhjemite (TR) suite (low-K): quartz diorite and tonalite and (2). The granodiorite (GD) suite (medium-K): granodiorite and quartz monzodiorite (*Fig. 2*).

TABLE 1

Modal analyses of the studied granitoids

	Samp. no.	Plag.	Hornb.	Biot.	Quartz	K-feld.	Access.
Trondhjemite suite	1	54.6	1.7	14.9	26.7	2.0	0.1
	2	61.5	2.1	16.2	17.9	1.9	0.3
	3	65.0	12.6	10.1	11.7	0.1	0.6
	4	67.5	2.3	10.7	19.2	0.3	0.2
	5	73.2	2.0	10.3	14.0	0.2	0.4
	6	74.5	13.9	4.3	4.7	1.7	0.8
Granodiorite suite	7	50.0	14.2	10.8	13.3	13.0	0.7
	8	52.8	17.0	8.0	10.0	11.9	1.3
	9	52.9	5.5	8.7	15.5	15.7	1.7
	10	53.6	13.4	5.5	11.0	14.5	2.0
	11	54.5	5.3	15.2	12.5	12.0	0.5
	12	55.2	7.6	9.7	15.4	11.6	0.5
	13	55.5	2.0	4.2	23.5	13.5	1.3
	14	55.6	12.3	7.3	11.6	12.2	1.5
	15	56.5	2.5	9.0	18.0	13.0	1.0
	16	59.5	17.0	6.3	4.2	12.7	0.3

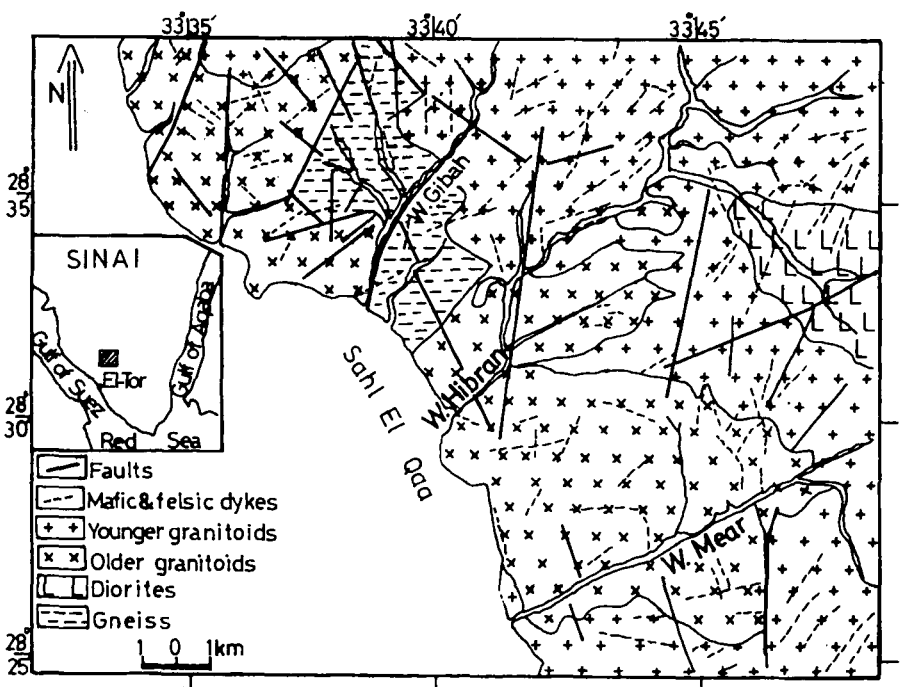

Fig. 1. Geological map of the Wadi Hibran-Wadi Mear area, East of El-Tor, Southern Sinai (modified after EL MEZYEN et al., 1994)

On the chemical classification diagram (*Fig. 3*) of DEBON and LA FORT (1983), the TR suite correspond to quartz diorite, quartz monzodiorite and tonalite while GD suite fall within the granodiorite field. Moreover, on the normative classification diagram (*Fig. 4*) of BARKER (1979), the TR suite fall in the trondhjemite and tonalite fields whereas the GD suite fall within the granodiorite field.

The TR suite is characterized by gneissic and poikilitic textures, whereas the GD is marked by perthitic, poikilitic and myrmekitic textures. Mafic mineral contents are about 22.4 vol. % and 17.3 vol. % in the TR and GD suite relatively. Accessory minerals are zircon, titanite, apatite and iron oxide minerals. Secondary minerals are chlorite and prehnite.

Plagioclase is an early-crystallized phase. It is represented by prismatic subhedral to euhedral crystals up to 3.3x4.7 mm belonging to polyphase generation as evidence by the wide difference in crystal sizes, their degree of alteration and the reaction rims between the adjacent plagioclase crystals.

The averages of microprobe analyses of 2 plagioclase grains are given in Table 2. Their composition ranges between oligoclase ($Or_{3.9}$ $Ab_{66.5}$ $An_{29.6}$) in TR suite and andesine ($Or_{2.5}$ $Ab_{65.5}$ An_{32}) in GD member respectively (Table 2). Plagioclase reveals both primary and secondary zonation. It is slightly sericitized probably due to hydrothermal alteration, and alkali metasomatic processes belonged to the intrusion of the adjacent younger granites.

Amphibole occur as subhedral crystals up to 0.6x1.5 mm, mostly pleochroic from yellow green to green or from greenish brown to green colour. Amphibole percentage decreases from GD to TR member. Occasionally amphibole crystals are present in cluster form and corrode the older plagioclase. The cluster in TR suite is morphologically elongated parallel to the gneissosity plains. Hydrothermal fluids partly affected amphibole. The alteration of amphibole into chlorite and epidote results in libration of iron oxide seen scattered in amphibole. Quartz is poikilitically enclosed in amphibole crystals indicating that most amphibole crystallized under silica-saturated condition.

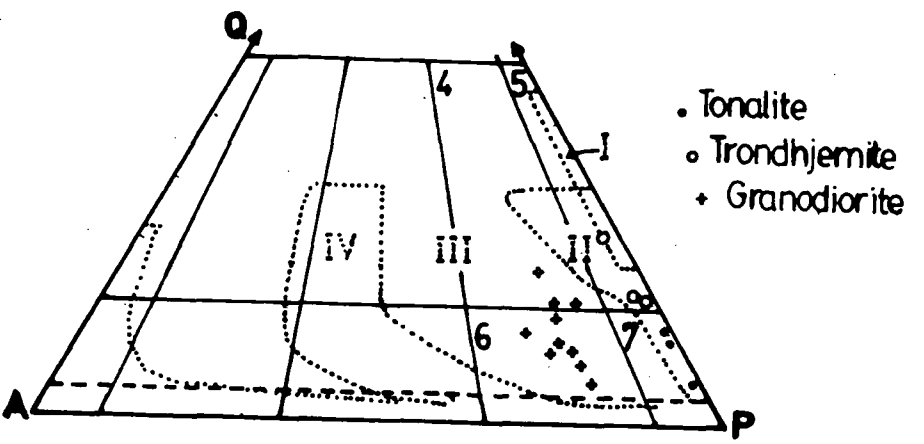

Fig. 2. Modal AQP diagram showing the classification of the studied older granitoids (after STRECKEISEN, 1976). 4 = granodiorite, 5 = tonalite, trondhjemite, 6 = quartz-monzodiorite and 7 = quartz-diorite. Fields of various granitoid suites: I = tholeiitic, II = calc-alkaline trondhjemitic (low-K), III = calc-alkaline granodioritic (medium-K) and IV = calc-alkaline monzonitic (high-K) after LAMEYER and BOWDEN (1985).

TABLE 2

Averages of microprobe analyses of the studied granitoids

Plagioclases			Amphiboles				Biotites				
Samp. no.	2 (Av. 3) TR	3 (Av. 3) GD		1 (Av. 3) TO	2 (Av. 3) TR	3 (Av. 3) GD		4 (Av. 3) TO	1 (Av. 3) TO	2 (Av. 3) TR	3 (Av. 3) GD
Si_2O	61.91	59.38	SiO_2	49.10	46.10	44.26	SiO_2	35.36	36.12	35.77	36.37
Al_2O_3	22.98	27.34	TiO_2	0.53	0.59	1.53	TiO_2	3.83	3.80	3.92	3.62
CaO	6.13	5.85	Al_2O_3	4.57	7.42	7.89	Al_2O_3	13.66	13.25	13.68	14.32
Na_2O	7.43	6.60	FeO[t]	18.59	20.02	20.72	FeO[t]	21.32	21.70	23.30	23.16
K_2O	0.68	0.39	MnO	0.80	0.47	0.54	MnO	0.26	0.29	0.25	0.21
Total	99.23	99.56	CaO	12.53	11.66	11.34	CaO	0.00	0.00	0.05	0.00
			MgO	11.72	10.39	8.90	MgO	10.05	10.66	8.92	8.91
Si	2.772	2.637	Na_2O	0.00	1.17	1.94	Na_2O	0.00	0.00	0.47	0.38
Al	0.228	0.363	K_2O	0.34	0.51	0.79	K_2O	9.50	9.31	9.76	9.11
Al	0.980	1.074	Total	98.18	98.33	97.91	Total	95.28	95.13	96.12	96.39
Ca	0.294	0.279									
Na	0.661	0.570	Si	7.204	6.818	6.710	Si	5.544	5.568	5.567	5.637
K	0.039	0.022	Al^{iv}	0.785	1.182	1.290	Al^{iv}	2.453	2.445	2.443	2.363
			Al^{vi}	0.006	0.112	0.118	Al^{vi}	0.027	0.000	0.077	0.231
Or	3.89	2.53	Ti	0.060	0.065	0.175	Ti	0.443	0.442	0.458	0.418
Ab	66.53	65.51	Fe^{3+}	0.670	0.769	0.506	Fe^{3+}	2.831	2.923	3.034	2.644
An	29.58	31.96	Fe^{2+}	1.612	1.679	2.120	Fe^{2+}	0.003	0.010	0.000	0.000
			Mn	0.100	0.057	0.071	Mn	0.034	0.039	0.032	0.028
			Ca	1.970	1.849	1.796	Ca	0.000	0.000	0.008	0.000
			Mg	2.564	2.291	2.011	Mg	2.538	2.453	2.070	2.044
			Na	0.000	0.336	0.569	Na	0.000	0.000	0.140	0.112
			K	0.064	0.151	0.153	K	1.801	1.835	1.939	1.785
			Mg	0.529	0.514	0.434	Mg	0.449	0.456	0.409	0.406

1, 2, 3, etc. = Sample numbers, TO = Tonalite, TR = Trondhjemete, GD = Granodiorite.
Plagioclase ion number on the basis of 8 oxygens.
Amphibole ion number on the basis of 23 oxygens.
Biotite ion number on the basis of 22 oxygens.

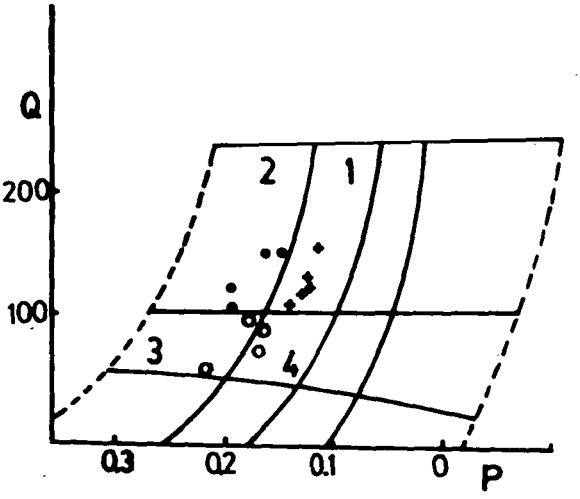

Fig. 3. Q (Si/3*[K+Na+2Ca/3])-P (K*[K+Na]) chemical variation diagram (after DEBON and LA FORT, 1983) for the studied granitoids. 1 = granodiorite, 2 = tonalite, 3 = qz-diorite, 4 = qz-monzodiorite.

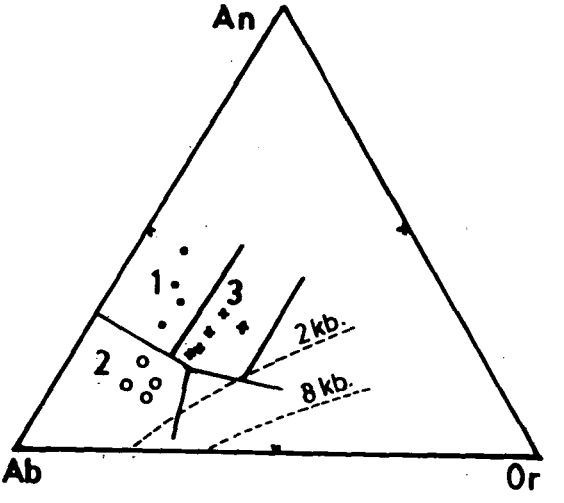

Fig. 4. O'Connor Ab-An-Or classificaton diagram (after BARKER, 1979). 1 = tonalite, 2 = trondhjemite, 3 = granodiorite. Water saturated peritectic compositions at 2 and 8 Kb are after WHITNEY (1975).

The averages of microprobe analyses of 3 amphibole grains are given in Table 2. The studied amphibole is classified according to the content of $(Na+K)_A$, Ti, Fe^{3+}, Al^{vi} of LEAKE (1978) diagram (*Fig. 5*) into calcic amphibole. It is corresponded to magnesio-hornblende in TR suite (*Fig. 5a*) and ferro-edenitic hornblende in GD suite (*Fig. 5b*). The occurrence of magnesio- and edenitic hornblende possibly indicate that this amphibole was formed at about 700-750 °C (HENDERSON et al., 1989). On the Al^{vi}-Si and Ti-Al variation diagrams of RAASE (1974) and HYNES (1982), this hornblende corresponds to low-pressure amphibole (*Fig. 6a* and *b*) suggesting that it is slightly overprinted by greenschist-lower amphibolite facies. The present calcic amphibole is

probably crystallized under pressure lower than 5 Kb (RAASE, 1974). Moreover, the variation of Al^{vi} relative to Si of Ca-amphibole (*Fig. 6a*) revealed a negative correlation in amphibole from TR to GD suite. While a positive relation is deduced from the plot of Ti versus Al of this amphibole (*Fig. 6b*). The partitioning of mg-values between amphibole and biotite reveals that amphibole contains higher proportion of Mg-content than the biotite (*Fig. 7*). Amphibole from tonalite and trondhjemite rock types have high mg-values relative to the granodiorite rocks probably consistent with the classic progressive differentiation trend from tonalite to granodiorite.

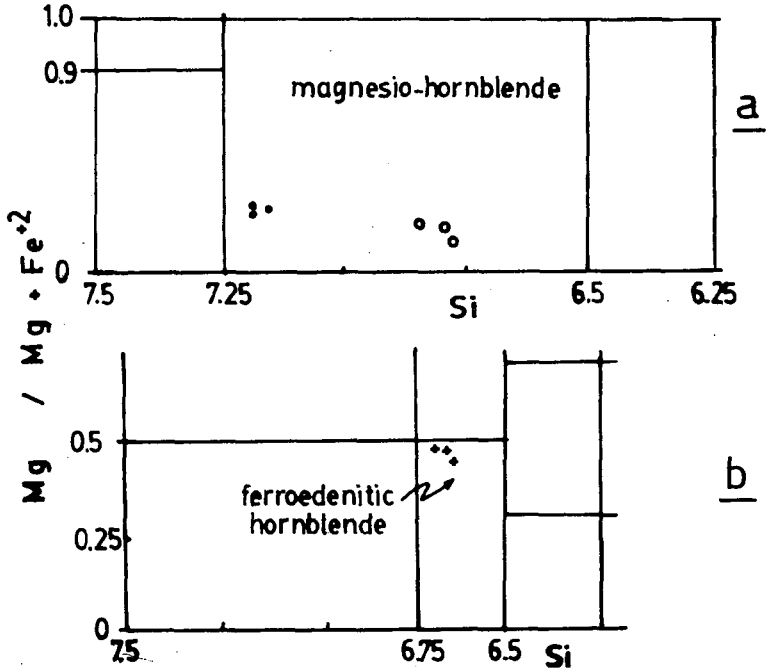

Fig. 5. Classification of the studied calcic amphiboles (after LEAKE, 1978): a) $(Na+K)_A > 0.5$, $Ti < 0.5$, $Fe^{3+} < Al^{vi}$ and b) $(Na+K)_A < 0.5$, $Ti < 0.5$.

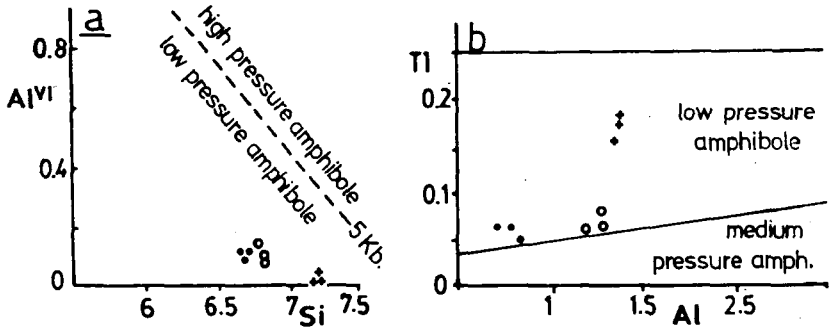

Fig. 6. Plots of hornblendes from studied granitoids in a) Al^{vi}-Si diagram (after RAASE 1974) and b) Ti-Al diagram (after HYNES, 1982) for comparison

Biotite forms fine flakes up to 2.2x1.2 mm, intergrews with amphibole and quartz, and is usually associated with apatite, iron oxide and zircon. Some biotite flakes are fresh, while others are intensively altered and interleaved by chlorite. Biotite is sometimes arranged with their long axes showing marked parallelism imparting the rock a gneissose texture as in TR suite.

The averages of microprobe analyses of 4 biotite grains are given in Table 2. The chemical data are plotted in FeO^t-MgO-Al_2O_3 diagram (*Fig. 8*). On this diagram, the biotite samples correspond to the metamorphic-metasomatic type (NOCKOLDS, 1947; GOKHALE, 1968) and belong to biotite coexisting with hornblende (NOCKOLDS, 1947). The Gd suite has higher contents of the coexisting biotite relative to that from TR suite suggest a more differentiation of the granodiorite. The plot of the mg [Mg/(Mg+Fe)] versus Si (*Fig. 9*) reveals two separate plots for the present granitoids. The mg-values of the coexisting biotite decrease with increase of Si for the tonalite in one hand, and constant with increase of Si for TR to GD rocks, on the other hand. Moreover, the biotite of the tonalite have enriched in mg values and depleted in Si relative to those of the granodiorite member (*Fig. 9*) indicate again the more differentiation trend of the granodiorite.

Figure 10 shows the plot of 100 x Fe/(Fe+Mg) ratio on the biotites stability diagram of WONES and EUGSTER (1965). It is evident that Fe/(Fe+Mg) ratio of the studied biotites ranges between 52.3 and 59.8 which corresponds to a range of temperature approximatly between 700 °C–750 °C with the more Fe-rich biotites crystallizing with fall down of temperature. This result is consistent with data given by RAGAB et al. (1977) and KABESH and SHAHIN (1992).

K-feldspar consists of microcline and perthite and appears the last crystallized phase filling the interspaces between plagioclase grains. Perthite occurs as veins of albite in a microcline host.

BULK ROCK CHEMISTRY

Selected 13 rock analyses of the studied TR-GD suite are given in Table 3. The investigated rocks show a wide variation in major and trace element contents. These rocks are poor in ferro-magnesian elements, e. g. TiO_2+Fe_2O_3+MgO ranges in average from 6.5 % in TR to 4.6 % in GD suite. The studied granitoids display a wide range of differentiation index (e.g., D.I. = Qz+Or+Ab+Co) which increases from TR rocks (62 % average) to GD member (70%) (Table 3). The variation of the D.I. values versus the major elements reveals that the GD suite has relatively high D. I. values and is enriched in K_2O and depleted in TiO_2, CaO and MgO, suggest their progressively differentiated trend.

Correlation with other granites

The results of the chemical analysis of the studied granitoids compared with granites of the other localities are given in Table 3. The chemical composition of the investigated granitoids appears to be in good parallelism with that of quartz monzodiorite-granodiorite suite of Fawakhir, Eastern Desert, Egypt (EL-MAHALLAWI, 1989; EL-MAHALLAWI and BÉRCZI, 1989), oceanic volcanic arc granites of Jamaica and volcanic arc granites of active continental margins of Central Chile (PEARCE et al., 1984).

TABLE 3

Averages of microprobe analyses of the studied granitoids

	Tonalite				Trondhjemite				Granodiorite					Averages		
	187	27	206	48	202	96	296	30	131	292	45	I	26	I	II	III
SiO_2	59.18	59.61	59.90	64.86	57.72	58.59	61.17	62.20	62.60	63.30	63.80	64.50	67.50	62.85	68.43	74.50
TiO_2	1.30	0.50	0.95	1.25	1.87	1.16	0.85	0.78	0.72	0.70	0.84	0.73	0.60	0.91	0.33	0.16
Al_2O_3	16.14	13.80	16.90	15.18	14.31	17.11	14.12	13.11	17.02	16.60	16.02	16.10	15.02	16.27	14.44	12.52
Fe_2O_3	2.84	4.21	2.85	1.10	4.11	4.44	3.28	3.31	3.23	2.08	1.40	1.26	1.30	1.91	3.35	1.00
FeO	4.68	3.90	4.02	3.62	3.92	3.38	3.66	3.35	1.61	3.22	3.55	3.89	2.30	3.32	–	–
MnO	0.09	0.09	0.10	0.05	0.11	0.11	0.11	0.12	0.08	0.10	0.09	0.11	0.07	0.09	0.06	0.01
CaO	6.17	5.95	4.04	4.50	5.55	3.42	4.37	4.70	3.18	3.46	3.99	3.47	3.60	3.78	2.36	0.29
MgO	3.13	4.11	3.35	2.33	3.21	3.08	2.10	3.21	2.37	2.38	2.41	1.87	1.83	1.68	1.35	0.07
Na_2O	3.34	3.81	3.38	3.79	4.91	4.88	4.60	4.39	4.10	3.75	3.72	4.50	3.59	4.32	3.70	3.56
K_2O	1.20	1.62	1.38	1.77	1.89	2.03	2.30	2.21	2.58	2.51	2.76	2.81	2.90	2.90	3.13	5.31
H_2O+	1.26	1.21	1.51	0.55	1.50	1.26	1.89	0.55	1.35	1.19	1.04	0.22	0.44	1.71	3.21	0.94
H_2O-	0.37	0.42	0.52	0.37	0.40	0.10	0.49	0.37	0.42	0.12	0.11	0.11	0.07	–	–	–
P_2O_5	0.19	0.20	0.84	0.20	0.23	0.38	0.12	0.20	0.23	0.25	0.23	0.20	0.17	0.35	0.12	0.01
Sum.	99.89	99.40	99.47	99.57	99.73	99.94	99.87	99.57	99.48	99.66	99.96	99.77	99.39	100.10	100.48	98.57
D. I.	52	56	60.3	65	61.4	66.1	67	66	71.5	68.7	66.2	70.4	72.1			

I = Qz-diorite-granodiorite suite of Fawakhir, Eastern Desert, Egypt (EL-MAHALLAWI, 1989; EL-MAHALLAWI & BERCZI, 1989)
II = Oceanic volcanic arc granites, mainly calc-alkaline arcs, Jamaica, (PEARCE et al., 1984)
III = Volcanic arc granites of active continental margins, Central Chile (PEARCE et al., 1984)

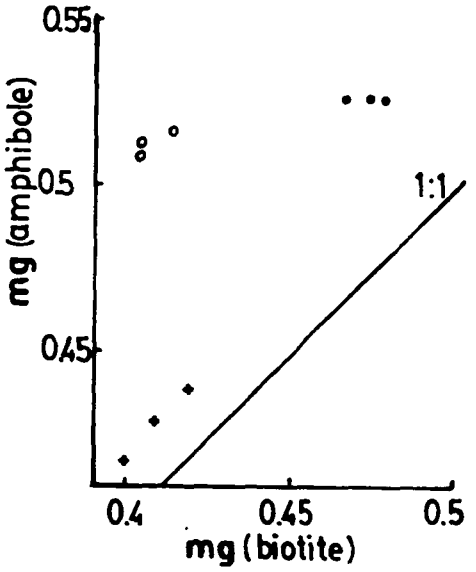

Fig. 7. Distribution of Mg and Fe between coexisting amphiboles and biotites

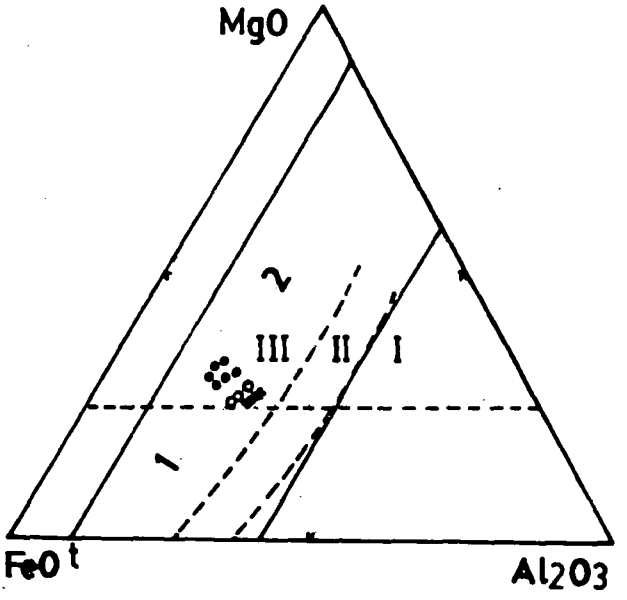

Fig. 8. Plot of FeO^t, MgO and Al_2O_3 of biotites from studied older granitoids. // zone demarked for biotites of igneous rocks and II zone separated the biotites unaccompanied with other mafic minerals (II) from those associated with muscovite (I), and hornblende (III) after NOCKOLDS (1947). --- line drawn by GOHKALE (1968) separating biotites of magmatic rocks (1) from those of metamorphic-metasomatic rocks (2).

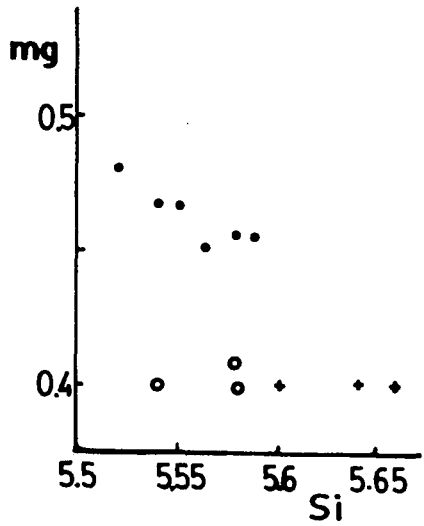

Fig. 9. mg [Mg/(Mg+Fe)] versus Si plot of biotites from the older granitoids.

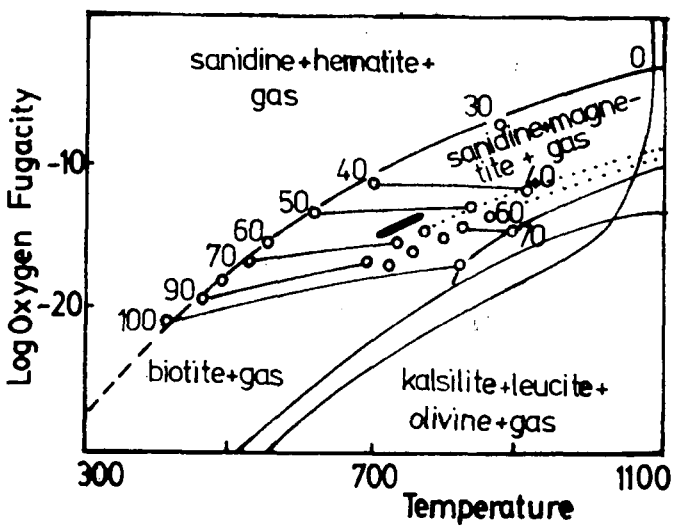

Fig. 10. Biotite stability diagram of specific Fe/(Fe+Mg) values as a function of oxygen fugacity (after WONES and EUGSTER, 1965). Heavily shaded area presents the studied biotites.

Magma type

Two generalized igneous rock trends are observed in granitic terrains (CONDIE, 1981; RAMSAY et al., 1986) (*Fig. 11a*). The widespread is the tonalite-trondhjemite trend which exhibits a rather constant K/Na ratio with decreasing Ca. The other, a more calc-alkaline trend, exhibits an increasing K/Na with decreasing Ca. In this figure the TO-TR samples follow the trondhjemite trend and plot in the field of typical non-ophiolitic

trondhjemites. The other samples follow early stage of the calc-alkaline trend and fall within the field of granodiorite (CONDIE, 1981; RAMSAY et al. 1986). Moreover, the trondhjemite affinities of the present rocks are redemonstrated using Na-Ca-K diagram (*Fig. 11b*). On this diagram, the samples follow the trondhjemitic trend and fall in field of I-type granitic magma (BARKER and ARTH, 1976). The calc-alkaline magma nature is revealed again on the AFM-diagram (*Fig. 12*). Plotting of the normative Ab-Qz-Or values on the water saturated liquidus field boundaries of TUTTLE and BOWEN (1958) and LUTH et al. (1964, *Fig. 13*). The TR-GD suite fall at moderate to high water vapour pressure and temperature mostly higher than 700°, suggesting that they were probably emplaced at deep levels in the crust. The same results have been proved before on the Ab-An-Or diagram (*Fig. 4*) which showed that the present rocks have been formed at a pressure of more than 8 kb. Further information may be drawn from Ab-Q-Or diagram (*Fig. 13*) leading to a distinction between the classic calc-alkaline differentiation and the trondhjemitic series (BARKER and ARTH, 1976). On this diagram the TR suite follows a trondhjemitic trend, whereas the GD rocks mostly parallel to the calc-alkaline trend. These results support the conclusions withdrawn from modal and normative analyses (*Fig. 2* and *4*), pointing out to the depletion to fair K_2O content calc-alkaline character of these rocks.

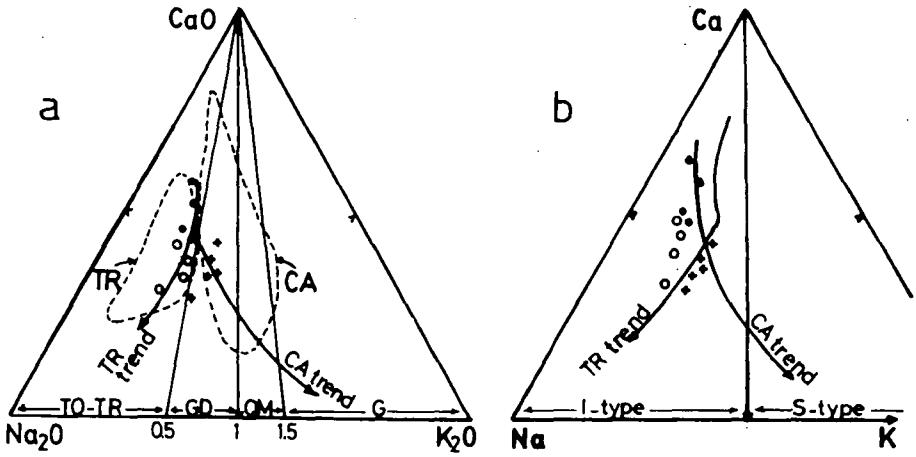

Fig. 11. Plots of studied granitoids in a) Na_2O-CaO-K_2O diagram (after CONDIE, 1981), TO-TR = tonalite-trondhjemite, GD = granodiorite, QM = qz-monzonite, G = granite; b) Na-Ca-K diagram (after BARKER and ARTH, 1976), TR = trondhjemite, CA = calc-alkaline. Dashed line field of TR and CA after RAMSAY et al. (1986).

Tectonic setting

Using the AFM (*Fig. 12*) from the tectonic aspect, the present rocks fall on the compressional suite trend of PETRO et al. (1979). Moreover, these granitoids fall in the volcanic arc field as appear in Rb versus Y+Nb diagram after PEARCE et al. (1984), and Rb-Hf-Ta diagram after HARRIS et al. (1986) (*Fig. 14a* and *b*). In the tectonomagmatic discriminate diagram (*Fig. 15*) after BATCHLOR and BOWDEN (1985) the studied TR-GD suite plot in the field of granitoids, particularly during the pre-plate collision to post-collision environment. Whatever preferred model (i. e. melting, fractional crystallization

or mixing) the existence of two distinctive suite in the older granitoids suggest the probability of two parental mafic magma materials with different compositions. This magma probably originated from a subduction of oceanic crust and intruded in a volcanic arc environment. Later on post-magmatic albitization processes affected on the magma before solidification.

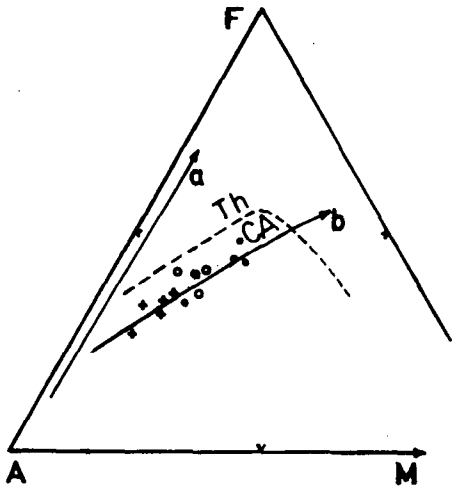

Fig. 12. AFM variation diagram. Solid lines represent the trends of extentional suite (a), and compressional suite (b) after PETRO et al. (1969).

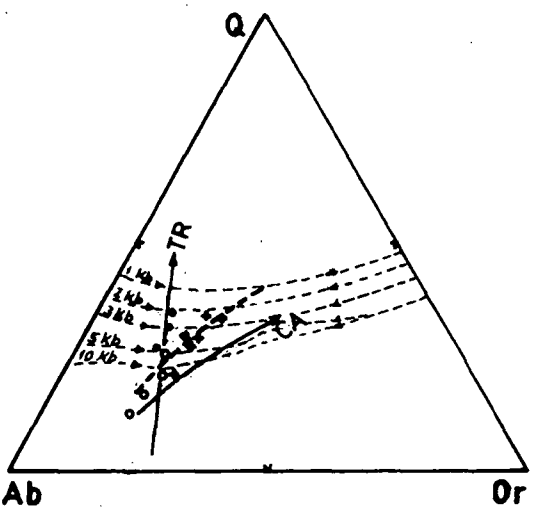

Fig. 13. Ab-Q-Or variation diagram. Dashed lines represent the H_2O saturated liquidus field boundaries in the system Ab-Q-Or-H_2O for water pressures 1, 2, 3, 5, 10 K bar (temperature of minimum eutectic: 1 Kb. = 720°, 2 Kb. = 685°, 3 Kb. = 665°, 5 Kb. = 650°, 10 Kb. = 630°) after TUTTLE and BOWEN (1958) and LUTH et al. (1964). Trends, TR = trondhjemitic, CA = calc-alkaline (b) after BARKER and ARTH (1976).

Magma source

In order to verify the nature of the source magma, a few spiderdiagrams are constructed based on the relative variations in the trace elements (Table 4).

On the ocean ridge granite (ORG)-normalized spiderdiagram (*Fig. 16*) adapted by PEARCE et al. (1984), the studied granitoids clearly display a pattern characteristic more skin to the volcanic arc suite. This pattern is characterized by enrichments in K, Rb, Ba and Th relative to Ta, Na, Hf, Zr, Sm, Y and Yb. A further significant feature is their high values of Ce and Sm and Y relative to the neighbouring elements as in volcanic arc calc-alkaline and shoshonite series. All these characteristics are highly comparable with the volcanic arc granites of active continental margins from Jamaica and Central Chile (PEARCE et al, 1984) (*Fig. 16*). Moreover, this pattern is relatively compared with that of the Fawakhir granitoids, Eastern Desert of Egypt (EL-MAHALLAWI, 1989).

TABLE 4

Chemical analysis of trace and rare earth elements of the studied granitoids

	Tonalite		Trondhjemite		Granodiorite		Averages		
	237	97	187	206	26	48	I	II	III
Sc	35.5	19.2	15.7	17.3	6.7	13.0	n. a.	n. a.	n. a.
Cr	420.0	\225.0	175.0	213.0	100.0	81.0	n. a.	n. a.	n. a.
Co	38.3	25.5	22.5	23.4	8.7	12.0	n. a.	n. a.	n. a.
Zn	76.0	80.0	70.0	75.0	47.0	76.0	n. a.	n. a.	n. a.
Rb	< 10.0	25.0	< 10.0	59.0	67.0	62.0	87.0	63.0	169.0
Mo	6.0	5.0	5.4	5.2	6.0	4.2	n. a.	n. a.	n. a.
Ba	360.0	290.0	450.0	359.0	590.0	560.0	000.0	750.0	331.0
Cs	2.1	1.2	1.2	1.1	2.3	3.8	n. a.	n. a.	n. a.
Hf	1.6	3.1	3.3	3.2	3.8	5.8	6.9	2.9	5.7
Ta	0.2	0.4	0.3	0.3	0.5	0.7	1.6	0.8	1.8
Th	0.5	1.7	2.1	2.0	3.9	8.5	8.8	4.3	20.3
U	–	–	–	1.0	1.4	1.5	n. a.	n. a.	n. a.
Sr	240.0	–	595.0	–	–	430.0		210.0	93.0
Nb	9.0	8.5	6.0	9.0	6.0	13.0	10.6	9.0	17.0
Y	21.0	20.0	14.0	18.0	7.4	27.0	22.0	10.0	30.0
Zr	73.0	88.0	94.0	95.0	100.0	134.0	154.0	104.0	184.0
La	5.7	10.5	17.5	19.8	24.0	39.0	38.2	17.7	40.1
Ce	14.0	30.0	34.0	37.0	44.0	74.0	80.4	31.6	85.8
Nd	12.0	13.0	16.0	15.0	18.0	44.0	20.3	15.4	36.2
Sm	2.1	3.2	3.2	4.2	3.0	6.1	6.0	2.2	8.4
Eu	0.9	1.5	1.3	1.5	0.8	1.4	1.8	0.7	0.8
Tb	0.4	0.5	0.6	0.7	0.4	0.7	1.0	0.3	1.2
Yb	1.8	1.9	1.4	1.6	1.0	2.5	2.6	1.4	3.1
Lu	0.3	0.3	0.2	0.3	0.1	0.4	0.4	n. a.	n. a.
Sum	37.2	60.9	74.2	80.1	91.3	168.1	150.7	–	–

I = Qz-diorite-granodiorite suite of Fawakhir, Eastern Desert, Egypt (EL-MAHALLAWI, 1989; EL-MAHALLAWI and BÉRCZI, 1989)

II = Oceanic volcanic arc granites, mainly calc-alkaline arcs, Jamaica (PEARCE et al., 1984)

III = Volcanic arc granites of active continental margins, Central Chile (PEARCE et al, 1984)

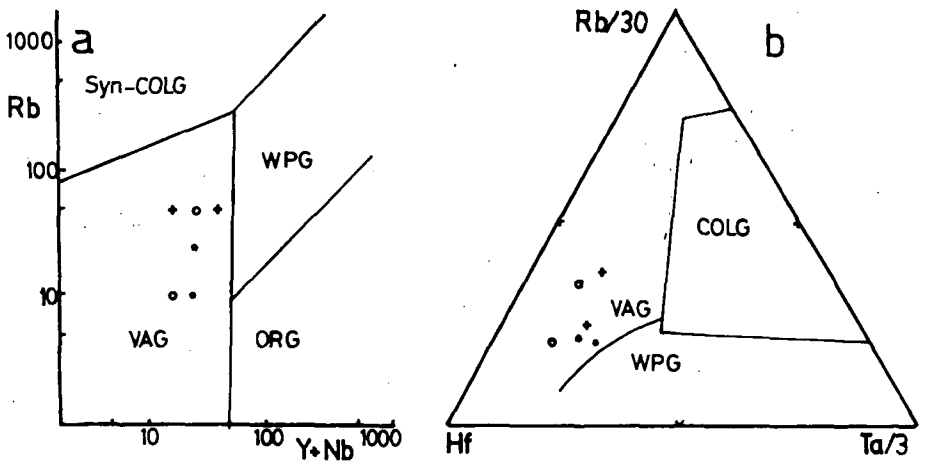

Fig. 14. Plot of the studied granitoids in a) Rb-(Y+Nb) diagram (after PEARCE et al., 1984) and b) Hf-Rb-Ta diagram (after HARRIS et al., 1986). COLG = collision, VAG = volcanic arc, WPG = within plate and ORG = oceanic ridge granites.

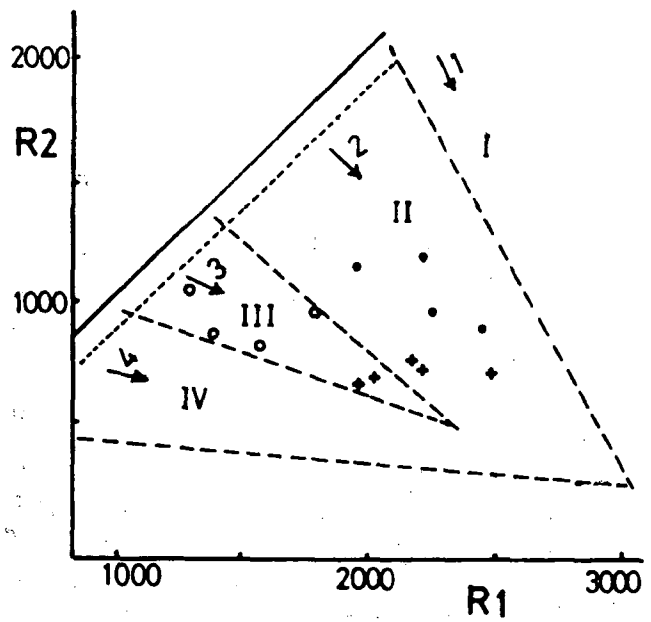

Fig. 15. DE LA ROCHE's plot and the petrographic equivalents are after LAMEYER and BOWDEN (1982): Group 1 = tholeiitic, Group 2 = calc-alkaline and trondhjemitic, Group 3 = high-K calc-alkaline, Group 4 = subalkaline monzonitic. Discrimination fields are after BATCHLOR and BOWDEN (1985): I = mantle fractionates, II = Pre-plate collision, III = Post collision uplift, IV = Late-orogenic environment.

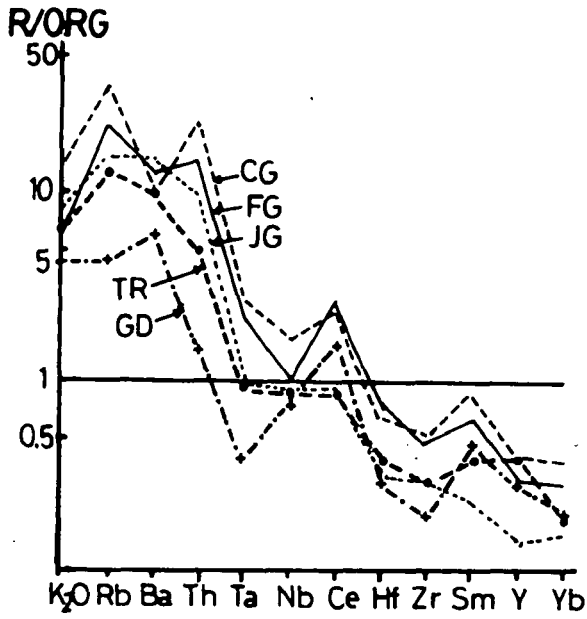

Fig. 16. Oceanic ridge granite (ORG) normalized geochemical patterns for studied trondhjemite (TR) granodiorite (GD) suite compared with Fawakhir granites (FG), Eastern Desert, Egypt (EL-MAHALLAWI, 1989); volcanic arc granites from Jamaica (JG) and from Chile (CG) (PEARCE et al., 1984). ORG values after PEARCE et al. (1984).

The REE data of the TR-GD suite (Table 4) have been normalized to the chondritic values of NAKAMURA (1974) and their patterns are illustrated in *Fig. 17a* and *b*. It is clear from this figure that the TR suite have tight REE patterns marked by positive Eu anomaly where Eu/Eu* ratio varies from 3.5 to 4.7 and relative slight light-REE enrichment (Fig. 17a). The TR rocks are slightly fractionated and the Ce_n/Yb_n ratio gradually varies from 1.96 to 6.1. The present REE patterns of the TR rocks are quite comparable with the range of the Archean high-Al_2O_3 tonalite-trondhjemite (CONDIE, 1981) and the average of the quartz monzodiorite of Fawakhir, Eastern Desert, Egypt (EL-MAHALLAWI and BÉRCZI, 1989). Moreover, the tonalite rocks are depleted in light-REE abundance as well as the total REE, and enriched in the positively value of the Eu anomaly compared with the TD (Table 4) suggest their less fractionation trend. On the other hand, GD suite have a well tight REE pattern (*Fig. 17b*) characterized by negative Eu anomaly (Eu/Eu* ratio fall from 3.18 to 2.58) and relative enrichment of light and depletion of heavy REE abundance compared with that of the TR suite. A feature indicates the more differentiation rocks (Ce_n/Yb_n = 7.46–11.24) of the GD suite. The present REE pattern of the GD suite is in a good parallelism with that of the Archean granodiorites given by CONDIE (1981) and Fawakhi granodiorite, Eastern Desert, Egypt (EL-MAHALLAWI and BÉRCZI, 1989)

DISCUSSION

The relationship of the mineral constituents and the major chemistry or the REE has been studied before. HASKIN et al. (1968) assumed that the increase of sum REE is associated with the increase in silica content of igneous rocks. Moreover the degree of heavy REE depletion and an increasingly positive Eu anomaly appears to accompany increasing SiO_2 (HUNTER et al., 1978). MCCARTHY and KABLE (1978) mentioned that the behaviour of REE in granitic system may be variable, as accessory minerals evidently play major part in controlling their behaviour in granitic rocks.

The studied rocks show a good relationship between sum REE and their relative age of intrusion and silica enrichment. The sum REE increase from 37 to 80 in TO-TR suite and 91 to 168 in GD suite in accordance with their pre-plate collision to post-collision uplift and with increase silica content from 57.7 to 62 in TO-TR suite and from 62.6 to 67.5 % in GD suite.

The decrease of the mg-values from amphibole to biotite and from TO-TR to GD rocks is probably consistent with increase of silica and sum REE which suggest the progressive differentiation trend from tonalite to granodiorite.

The present granitoids are probably produced by sinking of simatic lithosphere slabs and the diapiric upwelling of a succession of granitoids that commenced with early Na-rich phases but which later changed to K-rich magma types during the final stages of the crustal cratonization (ANHAEUSSER, 1981).

Two important geochemical processes in the development of magmatic granitic rocks are involved the source of the parent magma, and its differentiation between source and region of emplacement. The REE modelling is now accepted as a useful tool in evaluating the possible source and differentiation processes for granitoid rocks.

Many models have been proposed for the generation of the andesitic-dacitic melts. WILSON (1989) proposed a model for the acidic rocks by partial melting of lower crustal basic rocks of gabbro or granulite (pyroxene-garnet-plagioclase fractionation). Models involving partial melting of quartz-eclogite under hydrous conditions (e. g., 27 Kbar) produces andesitic-alkalic melts as a source granites. These models involving eclogite-quartz eclogite parents gave REE patterns with a smooth concave distribution motifs and general decrease in concentration from La to Lu, but uniformly slightly low in calculated heavy REE (LONGSTAFFE et al., 1983). STERN et al. (1975) gave non-modal melting models for eclogite/quartz eclogite parents (85 % clinopyroxene and 15 % garnet) using mantle phases equilibria with garnet and clinopyroxene entring the melt in equal contents. The equilibrium models shown in figure (18a and b) reasonably describe the REE patterns of investigated TO-TR and GD suite for 5 % and 15 % partial melting respectively. The latter model, however, still exhibits low contents of light-REE comparable with the GD suite. The light-REE abundances predicated by this model are largely controlled by garnet/clinopyroxene ratio allowed to enter the melt. Moreover, the REE pattern of the TO-TR is quite analogous to that of the andesitic granulite parent (LEAKE, 1990) (*Fig. 18a*).

A small positive Eu anomaly occur in some of these rocks (*Fig. 18a*) a feature which may reflect plagioclase accumulation (GLIKSON, 1976). The GD suite have a small negative Eu-anomaly indicating their degree of fractionation, a feature may be partly due to the feldspar fractionation or may also result from its depletion in the parent from the beginning due to fractional melting, where plagioclase is left as residual minerals. (EMMERMANN et al., 1975). Minor amounts of residual garnet are necessary to explain moderate depletion in heavy REE of the GD suite.

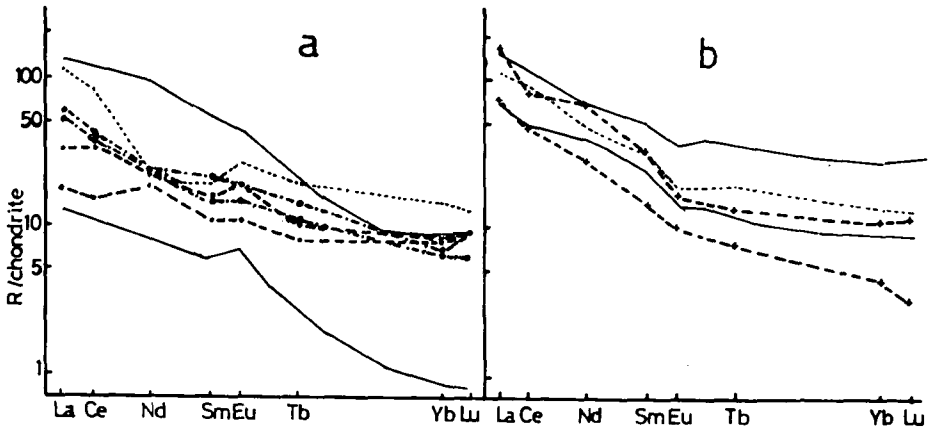

Fig. 17. Chondrite-normalized REE patterns of a) the studied trondhjemite suite (dashed lines) compared with Fawakhir qz-monzodiorite (EL-MAHALLAWI and BÉRCZI, 1989) (dotted line) and Post Archean trondhjemite-tonalite (CONDIE 1981) (solid line), b) the granodiorite suite (dashed lines) compared with Fawakhir granodiorites (EL-MAHALLAWI and BÉRCZI, 1989) (dotted line) and Post-Archean granodiorites (CONDIE 1981) (solid lines). Chondrite values after NAKAMURA.

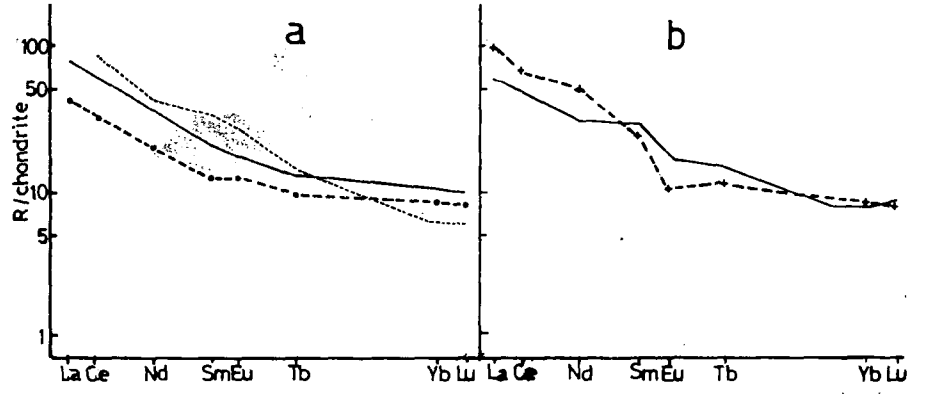

Fig. 18. Chondrite-normalized REE patterns of the averages of a) the studied trondhjemite suite. Solid line represents andesitic granulite parent (LEAKE, 1990) and dotted line represents equilibrium of non-modal melting (5 %) eclogite (85 % clinopyroxene, 15 % garnet) (LONGSTAFFE et al. (1982) b) the studied granodiorite suite. Solid line represents equilibrium of non-modal melting (15 %) eclogite (85 % clinopyroxene, 15 % garnet).

CONCLUSION

The pluton cover the compositional spectrum of tonalite, trondhjemite and granodiorite. They have a wide variation from basic to silicic varieties (57.7–67.5 % SiO_2).

The petrology, mineral chemistry and geochemistry of the studied older granites reveal the existence of two distinctive suites: 1) low-K calc-alkaline trondjemitic suite, and 2) medium-K calc-alkaline granodioritic suite.

Chemical data of amphiboles and biotites suggest that the older granites a probably during their emplacement into the volcanic arc. The existence of magnesio- and edenitic-hornblende and oligoclase-andesine suggest a temperature of about 700–850 °C and a pressure mostly <5 Kb. for the host rocks. Moreover, the proposed temperature for crystallzation of biotites is about 700–770 °C.

The TR suite contains higher mg-values of hornblende and biotite compared with the GD suite suggesting a progressive crystallization trend of the evolved rocks from TR to GD. However, a more sodic plagioclase ($An_{29.6}$) is coexisted with TR suite relative to An_{32} plagioclase GD suite probably indicate a late albitization effect on the TR suite.

Tectomagmatic evolution of these suites indicates that they are related to two calc-alkaline mafic magmas originated through a pre-plate collisional to post-collisional tectonic regime. They are highly comparable with the volcanic arc granites of active continental margin.

Based on REE geochemistry, the older granitoids show two different types of REE patterns; A) less differentiated type represented by tonalite-trondhjemite suite and B) differentiated type related to granodiorite. The less differentiated type has REE distribution patterns marked by positive Eu anomaly. The differentiated type has wide range of total REE abundance and displays negative Eu anomaly. Both of them have smooth concave REE distribution pattern. These patterns are fairly similar to the models involving partial melting of eclogite/quartz eclogite.

REFERENCES

ANHAEUSSER, C. R. (1981): Geotectonic evolution of the Archean successions in the Barberton Mountain land, South Africa. In A. KRONER (ed): Precambrian Tectonics. Elsevier Sci. Pub. Comp., Amsterdam. 137-156.

BARKER, F. (1979): Trondhjemite-definition, environmental and hypothesis of origin. In F. Barker (ed.): Trondhjemites, dacites and related rocks. p. 1-12. Elsevier, Amsterdam.

BARKER, F. and ARTH, J. G. (1976): Generation of trondhjemitic tonalitic liquids and Archean bimodal trondhjemitic-basalt suites. Geology, 4, 596-600.

BATCHELOR, R. A. and BOWDEN, P. (1985): Petrogenetic interpretation of granitoid rock series using multicationic parameters. Chem. Geol., 48, 43-55.

CONDIE, K. (1981): Archean Greenstone Belts. Elsevier Sci. Pub. Comp., Amsterdam, 434 p.

DEBON, F. and LE FORT, P. (1983): A chemical-mineralogical classification of common plutonic rocks and associations. Transaction of Roy. Soc. of Edinb. Earth Sci., 73, p. 135-149.

EL-GABY, S. (1975): Petrochemistry and geochemistry of some granites from Egypt. Neu. Jb. Miner. Abh., 124, 147-189.

EL-GABY, S., LIST, F. K. and TAHRANI, R. (1988): Geology, evolution and metallogenesis of the Pan-African Belt in Egypt. In S. EL-GABY and R. O. GREILLING (eds.): Pan-African Belt of Northeast Africa and Adjacent Areas. 17-68. Freiedr. Vieweg & Sohn Braun./Weis.

EL-MAHALLAWI, M. M. (1989): Tectonic interpretation of some granitic rocks from the central Eastern Desert of Egypt. Sci. Bull. Minia Univ., 2, 1, 279-305.

EL-MAHALLAWI, M. M. and BÉRCZI, J. (1989): Geochemistry of rare earth elements and petrogenesis of some Egyptian granites. Sci. Bull. Minia Univ. 2, 1, 155-176.

EL MEZAYEN, A. M., ABDEL-MAGUID, A. A. and SHAHIN, H. (1994): Petrology, geochemistry and tectonic evolution of older and younger granitoid rocks, southwest Sinai, Egypt. Al-Azhar Bull. Sci. 5, 2, 835-857.

EL-RAMLY, M. F. AND AKAAD, M. K. (1960): The basement complex in the central Eastern Desert of Egypt between Lat. 24°30' and 25°40'. Geol. Surv. Egypt, Pap. 8.

GILKSON, A. Y. (1976): Trace element geochemistry and origin of early Precambrian acid igneous series. Barberton Mountain Land, Transvaal. Geochim. Cosmochim. Acta, 40, 1261-1280.

GOKHALE, N. W. (1968): Chemical composition of biotites as a guide to ascertain the origin of granites. Bull. Com., Geol. Finland, 40, 107-111.

EMMERMANN, R., DAIEVA, L. AND SCHNEIDER, J. (1975): Petrologic significance of rare earth distribution in granites. Contrib. Mineral. Petrol., 52: 267-283.

HARRIS, N. B. W., PEARCE, J. A. and TINDLE, A. G. (1986): Geochemical characteristics of collision-zone magmatism. In COWARD, M. P. and RIES, A. C. (eds.): Collision Tectonics. Geol. Soc. Special Publ. 19: 67-81.

HASKIAN, L. A., HASKIAN, M. A., FREY, F. A. and WILDMAN, T. R. (1968): Relative and absolute terrestrial abundances of the rare earths. In AHRENS, L. H. (ed.): Origin and Distribution of the Elements. Intern. Ser. Monograph Earth Sci., 30, 889-912.

HASSAN, M. A. and HASHAD, A. H. (1990): Precambrian of Egypt. In: R. SAID (ed.): The Geology of Egypt. Balkema Publ., Netherland.

HENDERSON, C. B., PENDLEBURY, K. and FOLAND, K. A. (1989): Mineralogy and petrology of the Red Hill alkaline igneous complex, New Hampshire, U.S.A. J. Petrol., 30, 3, 627-666.

HUNTER, D. R., BARKER, F. and MILLARD, Jr., H. T. (1978): The geochemical nature of the Archean ancient gneiss complex and granodiorite suite, Swaziland: a preliminary study. Precambrian Res., 7, 105-127.

HUSSEIN, A. A., ALI, M. M. and EL-RAMLY, M. F. (1982): A proposed new classification of granites of Egypt. J. Volcan. Geoth. Res., 14, 187-198.

HYNES, A. (1982): A comparison of amphiboles from medium and low pressure metabasites. Contr. Mineral. Petrol., 81, 119-125.

LAMEYER, J. and BOWDEN, P. (1982): Plutonic rock types series. Discrimination of various granitoid series and related rocks. J. Volcan. Geoth. Res., 14, 169-186.

LEAKE, B. E. (1978): Nomenclature of amphiboles. Mineral. Mag., 42, 533-563.

LEAKE, B. E. (1990): J. Geol. Soc., London, 147, 579-589.

LONGTAFFE, F. J., MCNUTT, R. H. and CROCKET, J. H. (1982): Rare earth elements modelling of Archean meta-igneous and igneous rocks, Lake Daspair area, Northwestern Ontario. Precambrian Res., 17, 257-296.

LUTH, W. C., JANNS, R. H. and LUTH, O. F. (1964): The granite system at pressure of 4 to 10 Kb. J. Geophys. Res., 69, p. 759-773.

KABESH, M. L. and SHAHIN, A. N. (1992): Petrochemistry and petrogenesis Gabal Hieranu granitic rocks, Arbaat District, Red Sea Hills, Sudan. Egypt. J. Geol. 36, 1-2, 33-61.

MCCARTHY, T. S. and KABLE, E. J. D. (1979): On behaviour of rare earth elements during partial melting of granitic rocks. Chem. Geol, 22, 21-29.

NAKAMURA, N. (1974): Determination of REE, Ba, Fe, Mg, Na and K in carbonaceous and ordinary chondrites. Geochim. Cosmochim. Acta, 38: 757-775.

NOCKOLDS, S. R. (1947): The relation between chemical composition and paragenesis in the biotite micas of igneous rocks. Am J. Sci., 245, 401-420.

NOWEIR, A. M., SEWIFI, B. M. and ABU EL-ELA, A. M. (1989): Geology, Petrography and petrogenesis of the Egyptian younger granites. Qatar Univ. Sci. Bull., 10: 363-393.

PEARCE, J. A., HARRIS, N. B. M. and TINDLE, A. G. (1984): Trace element discrimination diagrams for the tectonic interpretation of granitic rocks. Jour. Petrol., 25: 956-983.

PETRO, W. L., VOGEL, T. A. and WILBAND, J. T. (1979): Major element chemistry of plutonic rock suites from compressional and extensional plate boundaries. Chem. Geol., 26, 217-253.

RAASE, P. (1974): Al and Ti contents of hornblende, indicator of pressure and temperature of regional metamorphism. Contri. Mineral. Petrol. 45, 231-236.

RAGAB, A. I., KABESH, M. L., HILMY, M. E. and YEHHIA, M. T. (1977): On the petrochemistry and petrogenesis of Mograt granitic rocks, Northern Sudan. Chem. Erde, 36, 238-247.

RAMSAY, C. R., DRYSDAL, A. R. and CLARK, M. D. (1986): Felsic plutonic rocks of the Medyan region, Kingdom Saudia Arabia: Distribution, classification and resource potential. J. Afr. Earth Sci. 4, 63-77.

STERN, C. R., HUANG, W. R. and WYLLIE, P. J. (1975): Basalt-andesite-rhyolite-H_2O: crystallization intervals with excess H_2O and H_2O-undersaturated liquid surfaces to 35 kilobars with implications for magma genesis. Earth Planet. Sci. Lett., 28, 189-196.

STRECKEISEN, A. (1976): To each plutonic rock its proper name. Earth Sci. Rev., 12, 1-33.

TUTTLE, O. F. and BOWEN, N. L. (1958): Origin of granite in the light of experimental studies in the system $NaAlSi_3O_8$-$KAlSi_3O_8$-SiO_2-H_2O. Geol. Soc. Am. Mem., 74, 153 p.

WHITNEY, J. A. (1975): The effect of pressure, temperature, and XH_2O on phase assemblages in four synthetic rock compositions. J. Geol., 83, 1-81.

WILSON, M. (1989): Igneous Petrogenesis. Unwin Hyman, London, Boston.

WONES, D. R. and EUGSTER, H. P. (1965): Stability of biotites, experimental, theory and application. Amer. Miner., 50, 1228-1272.

Manuscript received: 2. September 1999.

Acta Mineralogica-Petrographica, Szeged, XL, 97–104, 1999

MANTLE XENOLITH IN THE MAFIC DYKE AT BEREMEND, VILLÁNY MTS., SW HUNGARY

NÉDLI, Zs.[1], M TÓTH, T.[1]

Department of Mineralogy, Geochemistry and Petrology,
Attila József University, Szeged

ABSTRACT

Spinel lherzolite nodules of an U. Cretaceous mafic dyke in the Villány Mts. were studied. The xenolith consists of olivine, enstatite, Cr-diopside and Cr-Fe spinel as primary phases. No garnet or plagioclase is present. Alteration of the rock resulted in breakdown of olivine and formation of calcite, limonite and clay minerals. These processes can geochemically be followed by a significant loss of Mg and Ni as well as a gain of Ca relative to an average spinel lherzolite.

Key words: spinel lherzolite, alteration, Villány Mts.

INTRODUCTION

Although, igneous rocks play only a suservient role in the Villány Mts., those crosscut the Aptian limestone at several places over the area may include fundamental information about the early Alpine evolution of the Tisia. There are two localities, where mafic dykes have been studied intensely, and partly reinterpreted in the last years, Beremend and Máriagyűd. Firstly, MOLNÁR and SZEDERKÉNYI (1996) reported essential petrographical as well as geochemical results about these rocks. They concluded that the subvolcanic bodies consist of altered basalt of unknown age. Further studies (NÉDLI, 1999, NÉDLI, M TÓTH, 1999/A) confirmed the mafic composition of the original igneous material and infer an alkaline character. Based on geochemical investigations they also suggest that the rocks developed on a mature island arc and are probably in relation with the U. Cretaceous ancient arc of the Vocin, Pozega region (Croatia). Recent microscopic observations resulted in textures similar to those characteristic of lamprophyres (NÉDLI, M TÓTH, 1999/B).

The basaltic material of both dykes studied contains xenolithes of different composition. In this study we present some early petrographical and geochemical results of the ultramafic xenoliths and xenochrysts.

PETROGRAPHY

Both dykes studied crosscut Aptian and Albian carbonate rocks (Nagyharsány limestone - Urgon facies). Petrologically, the dykes are altered basalts and consist essentially of secondary phases, calcite and clay minerals (smectite, nontronite). In

[1] H-6701 Szeged; P. O. Box 651.

relatively fresh specimens two generations of *cpx*, as well as *ol, ap, ilm, mgt, amph, bio* and *pl* can be recognized as primary phases. Small, euhedral crystals of *ol* are usually present as pseudomorphs (Plate 1/1.). At places also well-developed mesh texture suggests previous *ol*. *Cpx1* forms large (250-500 μ) euhedral grains, which at places contains also a xenocrystal core of *cpx* or *opx* (Plate 1/2.). *Ap* forms tiny laths in the matrix. While these grains represent the early stage of the crystallisation process, *cpx2* together with *amph, bio* and *ilm* should have crystallised subsequently. The latter three minerals usually occur in separated drops and possibly form ocelli.

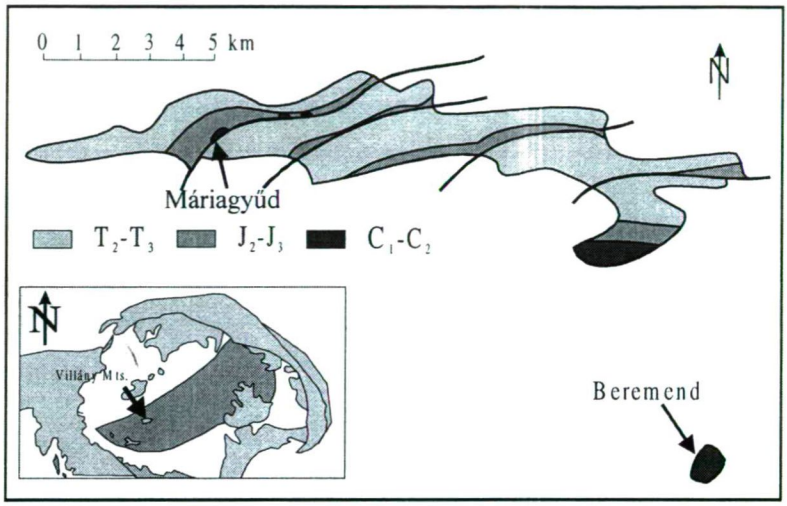

Fig. 1. Geological sketch map of the studied dyke

In addition to the *cpx, opx* and *ol* xenocrystals, highly altered xenoliths also occur in the two dykes (Plate II/1.). Based on microscopy as well as XRD and XRF data, these pale green, rounded, 2-8 cm large nodules consist of *opx* (enstatite), *cpx* (Cr-diopside), *Cr-spn* and minor *ol* as primary phases. No *ol* was able to be detected by XRD, its previous presence as a significant primary phase is suggested by the general mesh texture of the rock. No trace of previous *plag, gar* or *amph* can be recognized, the only Al-phase in each sample is *spn*. As secondary minerals, the nodules also contain a significant amount of *cc* and clay minerals. The xenoliths are spinel lherzolites petrographically.

GEOCHEMISTRY

Major element composition, as well as Cr and Ni of two xenolith samples were measured by the standard wet chemical (MÁFI) and PIXE (ATOMKI) methods, respectively. Because of the significant amount of the CO_2 and H_2O-bearing phases, composition was recalculated on a volatile-free basis. Data are collected and compared to the average composition of spinel lherzolites according to MAALOE, AOKI (1977) in Table 1. Although, both xenolith samples studied fall close the range of a typical spinel

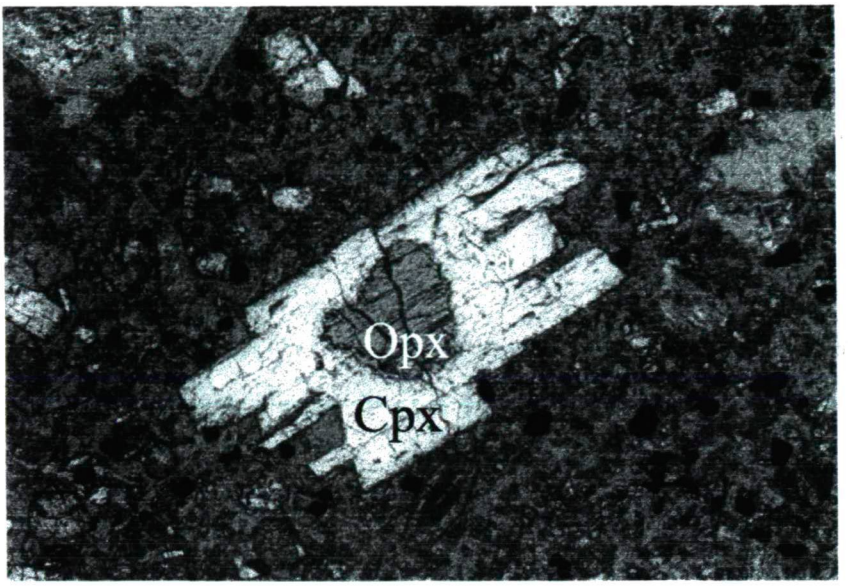

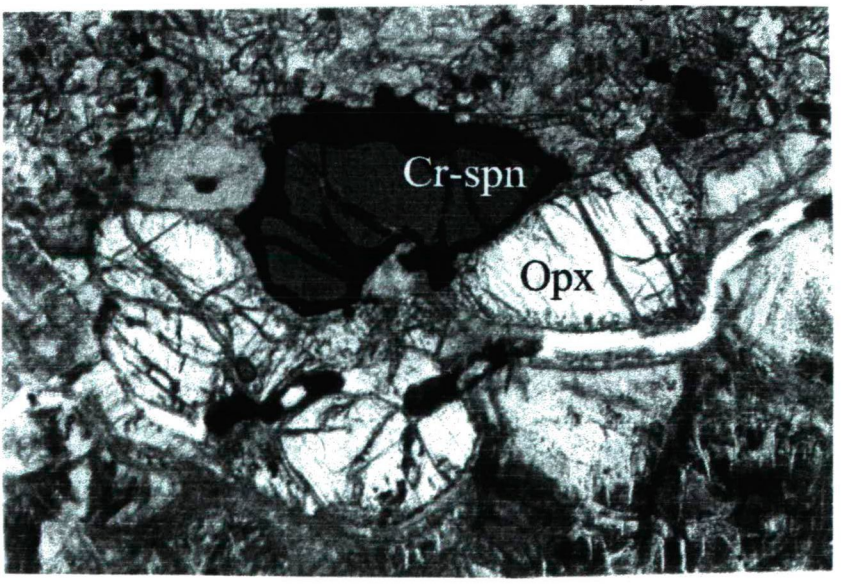

Plate I/1. Opx xenocrystal core of cpx1 in the host rock. N+, 36x
Plate I/2. Typical texture of the xenolith with spn and opx. N , 72x

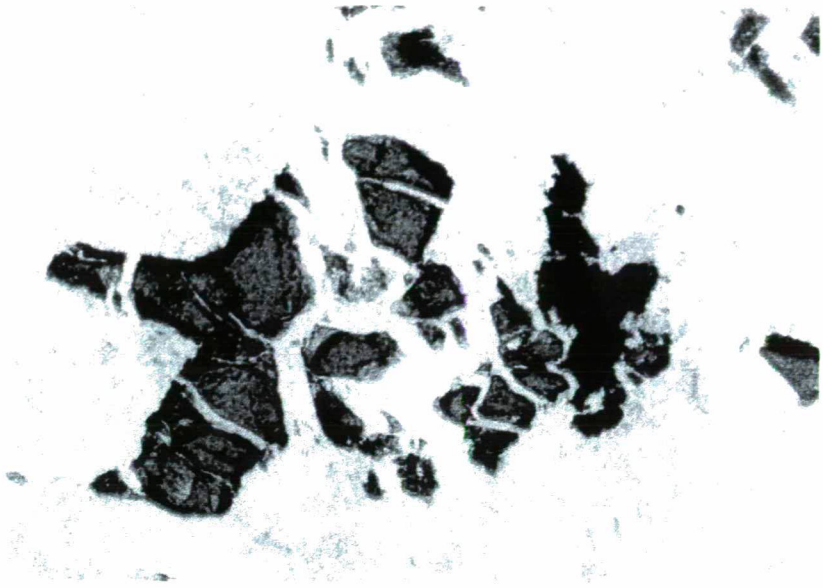

Plate II/1. Spn in an altered ol matrix. N , 72x
Plate II/2. Mesh structure of the xenolith reminds the previous ol. N+, 36x

lherzolite concerning most elements, a significant gain in Si, Al, Fe, Cr and Ca, while lost in Mg and Ni can be recognized. Proportion of Fe_2O_3 and FeO (8.78, 1.19 for sample 6817/a, 8.66, 1.44 for sample 6817/b) shows the role of oxidation in addition to other alteration reactions.

TABLE 1.

Composition of the two xenolith samples, the average spinel lherzolite and the typical range for spinel lherzolite (MAALOE, AOKI, 1977), respectively

Oxide (%) Element (ppm)	6817/a	6817/b	spinel lherzolite[1]	Range for spinel lherzolite[2]
SiO_2	60.90	61.31	44.20	41 - 48
TiO_2	0.08	0.25	0.13	0.0 - 0.2
Al_2O_3	4.22	6.92	2.10	0.5 - 4.5
FeO^{tot}	10.48	10.30	8.30	7 -10
MgO	14.97	13.38	42.20	39 - 47
CaO	8.97	7.47	1.90	0.5 - 4.5
Na_2O	0.10	0.20	0.27	0.05 - 0.40
K_2O	0.16	0.16	0.06	0.0 - 0.2
Total	99.88	99.99	99.16	
Cr	2360	1922	1505	680 - 2050
Ni	1348	1340	2200	1570 - 3140

DISCUSSION AND CONCLUSIONS

The mafic dyke at Beremend contains a large amount of ultramafic nodules which were examined. Although no xenolith has been found in the dyke at Máriagyűd yet, based on the presence of *opx* and *ol* xenocrystals as well as the common *opx* core of basaltic *cpx1* crystals, a similar origin of the two subvolcanic bodies can be assumed. An analogous evolution was previously stated also by NÉDLI (1999) when studying the two mafic rocks petrographically and geochemically.

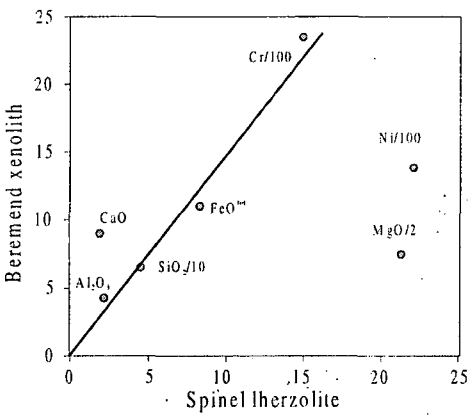

Fig. 2. Comparison of the composition of sample 6817/a to the average spinel lherzolite (MAALOE, AOKI, 1977) on an isocon plot

When comparing chemical data of the two samples studied with those typical for the average spinel lherzolite (MAALOE, AOKI, 1977, see Table 1.) on a diagram suggested by GRESENS (1967) and GRANT (1986), one can follow the behaviour of the elements plotted during the alteration processes. On this plot (*Fig. 2.*) Si, Al, Fe and Cr lie along a straight line approximately, suggesting a similar degree of gain related to the original ultramafic rock. Both Ni and Mg decrease significantly, whereas Ca exhibits a considerable increase. This kind of geochemical nature of the elements is consistent with the petrographical observations. Alteration of *ol*, which is the main Mg and Ni phase in the rock resulted in formation of the typical mesh texture and subsequently the loss of Mg and Ni. XRF data show that both *spn* and *cpx* contain a large amount of Cr. These minerals show no (*spn*), or only partial alteration in good agreement with the immobile behaviour of Cr. Although, Fe had to escape from *ol* as Fe^{2+}, it could form Fe^{3+} minerals (limonite) under the oxidising conditions. Consequently, Fe as FeO^{tot} is immobile. In addition to the Ca-bearing ultramafic phases, also an external Ca-source had to take part in formation of carbonate minerals in the xenolith. The same was stated for the mafic host rock by NÉDLI and M TÓTH (1999/A).

Concluding the geochemical data, one can state that the chemical composition of the original xenolith may have been comparable to spinel lherzolite prior to the alteration processes. The composition changed mainly due to the breakdown of the *ol*, and because of *cc* precipitation in part from external Ca-source. The increase of Si, Al, Fe and Cr can be considered to be virtual.

The only Al-phase in each xenolith sample examined is Fe-Cr *spn*. The lack of *amph, gar* and *plag* in the case of the normal lherzolite chemical composition suggests formation in the PT range of 6 - 14 kbar, 850 - 1000 °C (BUCHER, FREY, 1994). This interval may represent the uppermost part of the upper mantle (ARAMUKI, UI, 1982). If it is so, the xenolith presented in this paper is the first direct sample from the mantle in the Hungarian part of the SW Tisia block. Thermobarometry, however, needs more work.

ACKNOWLEDGEMENT

XRD and XRF measurements were provided by BERTALAN Á. at the JATE, Szeged. SZABÓ GY. detected the trace elements at the ATOMKI, Debrecen. PONGRÁCZ, L., PÉRÓ CS., RÁLISCH-FELGENHAUER, E. and KASSAI, M. are thanked for serving hand specimens and thin sections. The DCM Limestone Mines Co. is gratefully acknowledged for making the field work and sampling possible. We have greatly benefited from discussions with SZEDERKÉNYI T.

REFERENCES

ARAMAKI, S., UI, T. (1982): Japan (in Thorpe, R. S. ed.: Andesites). John Wiley and Sons pp. 263-268.

BUCHER, K. FREY, M. (1994): Petrogenesis of metamorphic rocks. Springler-Verlag pp. 160-163.

GRANT, J. A. (1986): The Isocon Diagram – A Simple Solution to Gresens' Eqation for Metasomatic Alteration. Econ. Geol. 81, pp. 1976-1982.

GRESENS, R. L. (1967): Composition-volume relationships of metasomatism. Chem. Geol. 2, pp. 47-65.

MOLNÁR, S., SZEDERKÉNYI, T. (1996): Subvolcanic basaltic dyke from Beremend, Southeast Transdanubia, Hungary. Acta Min.-Petr., Szeged, 37, pp. 181-187.

NÉDLI, ZS. (1999): Mezozoós szubvulkáni .kőzettestek vizsgálata a Villányi-hegységben. (Examination of Mesozoic subvolcanic bodies in the Villány Mts.) (in Hungarian) Diplom theses, Szeged, JATE.

NÉDLI, Zs., M. TÓTH, T. (1999A): Igneous records of the Meso-Alpine (Upper Cretaceous) subduction in the Villány Mts. (Tisia block, SW Hungary). In Székely et al. Eds., Tübinger Geowissenschaftliche Arbeiten, Series A, 52, pp. 188-189.

NÉDLI, Zs., M. TÓTH, T. (1999B): Subvolcanic remnants of the Upper Cretaceous volcanic island arcs of the Tethys in the Villány Mts., SW Hungary. J. Couf. Abs. 4, p 69.

MAALOE, S., AOKI, K. (1977): The major element composition of the upper mantle estimated from the composition of lherzolites. Contrib. Mineral. Petrol. 63, pp. 161-173.

Manuscript received: 10. September 1999.

Acta Mineralogica-Petrographica, Szeged, XL, 105–120, 1999

GEOCHEMICAL TYPOLOGY AND ORIGIN OF THE GRANITOID ROCKS OF WADI AKHDAR, CENTRAL-SOUTH SINAI.

*SOLIMAN, F.A. and *HASSEN, I.S.

*Geology Department, Suez Canal University

ABSTRACT

The granitoid rocks of Wadi Akhdar area are represented by comagmatic granodiorite, hornblende and biotite granites and biotite monzogranites. Mafic xenoliths and microxenoliths are relatively more abundant in the mafic granitoids. Variations within the granitoids reflect the degrees of separation of restites from the melt produced during fusion event.

Geochemically; the Akhdar granites show calc-alkaline affinity and they have similar ranges for alumina balance, alkali ratio, alkali/calcium ratio, normative feldspar, and trace elements distribution. They show remarkably similar degrees of differentation and tectonic setting (volcanic arc granites"VAG", and orogenic granites type "OGT").

Geochronologically; in accordance with field relationships, the emplacement of the Akhdar granites has taken place almost simultaneously and at least three phases of granite magmatism are recognized.

The syn-collision granodiorite (older phase of granite magmatism), is deeply eroded, melanocratic and it ranges from mild metaaluminous to peraluminous, and it is poorly to moderately differentiated. In contrast, the younger phase of granite magmatism has been produced strongly differentiated melanocratic biotite-bearing granites.

Based on the obtained petrographic and geochemical data the magmas of the Akhdar pluton have been formed at 700-850 °C temperature and under 6-8 Kb. pressure. Probable petrogenesis of Akhdar granitoids should involve partial melting of meta-igneous rocks and fractional crystallization of the produced melts.

INTRODUCTION

The southern Sinai mapped area comprises rocks formed during the main Late Precambrian events [HASSEN, et al. (in press)]. The metamporphic series of Hebran-Solaf-Feiran belt of Sinai includes in addition to parametamorphic rocks, orthogneisses of granitic and dioritic compositions representing remnants of more or less four plutons. Generally, the plutonic rocks in south Sinai range in composition from gabbro to granite with some considerable occurrences of ultramafic intrusions.

Alkaline to subalkaline magmatic associations are represented by the Catherine ring series which comprises alkali rhyolite, quartz monzonites and quartz syenites (of the Catherine ring dyke) and biotite leucogranite (of the Catherine Pluton). Volcanic rocks of Gabal Abu-Durba (EL BYIALI, 1998), and the alkali granites of the Serbal-Sarabiel plutons, also belong to this magmatic series.

The Akhdar granitoids form a part of the Arabian-Nubian Shield and are characterized by the following associations; a) ortho- and para-gneisses of older shelf sequence, b) island arc assemblages, c) ophiolitic suites, and d) granitoid intrusives. In accordance, the Egyptian granitoid rocks have been calssified in

* Ismailia, Egypt

different ways into; „Grey granites" by EL-RAMLY and AKAAD (1960), the sheared cataclastic granites „Shaitian granites" discribed by SHURMANN (1953), „Synorogenic granites" by EL-SHAZLY (1964), „Older granites" by AKAAD and NUWEIR (1980), „Older and younger granitoids" by GASS (1979) and HASHAD (1980), and „Subduction related granites" by HUSSEIN et al (1982). The emplacement of the older granitoids have been occured about 700-750 Ma (DIXON, 1979), and the younger granites, on the other hand have been emplaced in the restricted age 565-590 Ma (FULLAGAR and GREENBERG 1978).

This paper deals with the chemical and mineralogical variations, genesis, and the classification of the Akhdar granitoid pluton.

FIELD GEOLOGY

The distribution of Akhdar granitoids is shown in *Fig. 1*. The Akhdar granodiorite is well-known rock type of central south Sinai showing many significant geological characters. They are generally elliptical in outline and structurally discordant.

The granodiorite is grey, coarse-grained, porphyritic rock with extensive hornblende--rich dark green xenoliths and black spots of xenocrysts which show all stages of the resorption. The granodiorite locally manifests hybridization features, interpreted as a result of hybridization of Akhadar meta-gabbroid rocks and acidic magma. A gradual change can be observed in the east direction, where they became progressively decreased in the amounts of hornblende and xenoliths. They are enriched in biotite and alkali feldspar, while the porphyritic texture is gradually disappeared. Sometimes the boundaries of the xenoliths become indistinct and their colour becomes increasingly lighter.

The Akhdar granitoids are essentially massive but a weak foliation occures in the more mafic and xenolith-rich types and near their contacts with metagabbro. The foliation results from the alignment of the mafic xenoliths (*Fig. 2*) and, the less commonly, by hornblende crystals. The xenoliths form platy to elliptical macroscopic enclaves of metagabbro-diorite complex varying in colour from grey to black. Their diameters are sometimes half meter but, more commonly, are less than 10 cm ranging down to microscopic dimensions. They frequently have ovoid shape, but sometimes they are angular. The boundaries between xenoliths and their host rocks are commonly sharp, and the xenoliths are surrounded sometimes by a zone of large K-feldspar crystals (up to 3 cm). All stages in xenolith disintegration can be observed.

Country rocks-related xenoliths are restricted to the immediate vicinity of the granitoid contacts. They are relatively medium grained and hornblende-bearing mafic types which relatively are common in the granodiorite exhibiting dark colour. There is a definite correlation between the abundancy of xenoliths and the colour index of the host rock. Thus, they are rare in the more felsic rock types.

Hornblende-bearing mafic xenoliths are considered to be of local country rock origin, whereas, metagabbros and ortho-amphibolites are associated with the granitoids at present level of the exposure. All available field evidences imply that the xenoliths have been assimilated from gabbroid country rocks.

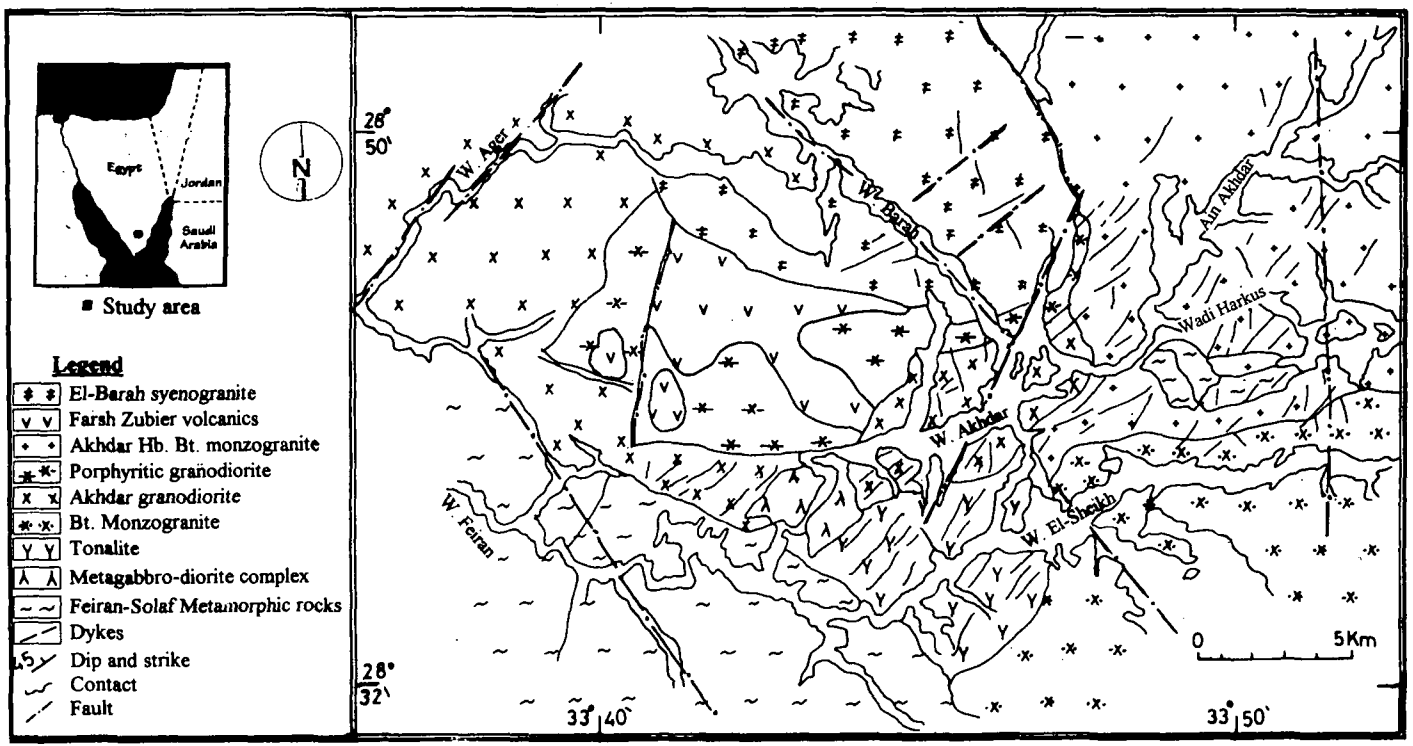

Fig.1. Geological Map of Wadi Akhdar Area

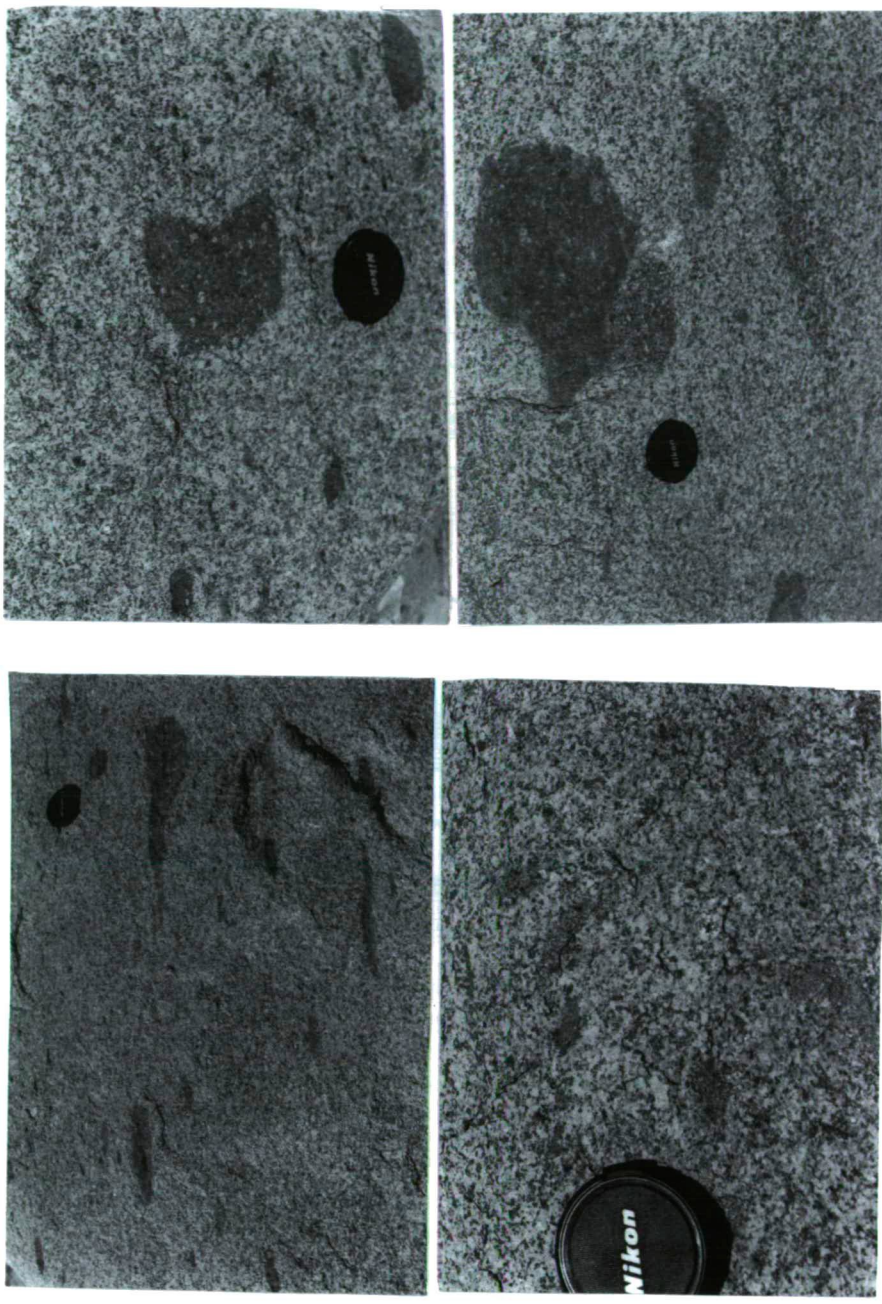

Fig. 2. The various types of magmatic mafic enclaves and xenocryst-rich mafic enclaves of the Akhdar granitoids, see also elongated enclaves and the two types of composite enclaves that are locally enclosed in the granitoid rocks

MODAL ANALYSES

The granitoid modes are plotted in terms quartz, K-feldspar and plagioclase (*Fig. 3*). The granitoids form a series ranging from granodiorite through adamellite and quartz-monzodiorite. Relatively, the younger granitoids are high in the K-feldspar content. Xenoliths usually consist of the same minerals as the host granitoids, with more abundant mafic minerals. Colour indices of the xenoliths range from 58 to 30 as the xenolith compositions merge toward those of the granitoids. The hornblende in the xenoliths from gabbroid country rock generally exceeds biotite in amount, but the relative amounts are related to the K-feldspar content. Sphene content of the xenoliths is related in its occurrence to the host granitoids.

Petrographically, the Akhdar granitoids are coarse- to medium-grained rocks. The K-feldspars form the larges phenocrysts which frequently are pale pink and sometimes white in colour occurring in the granodiorite around the contact with the syenogranite.

The most significant textural feature of the granodiorite is the presence of „mantled" plagioclase crystals. They have a clouded core of relatively uniform composition riddled with alteration products. The core has rounded margins and surrounded by clear plagioclase, often with oscillatory zoning, passing out into normally zoned outer margins.

Rare clinopyroxene cores are found in the hornblende crystals of xenoliths near the contact with metagabbro. There is no other petrographic evidence of disequilibrium among the mafic minerals. In the felsic types; they contain very small amounts of hornblende, which occurs as a part of an equilibrium mineral assemblage. Another prominent textural feature is the occurrence of apatite as minute crystal, concentrated within the mafic minerals.

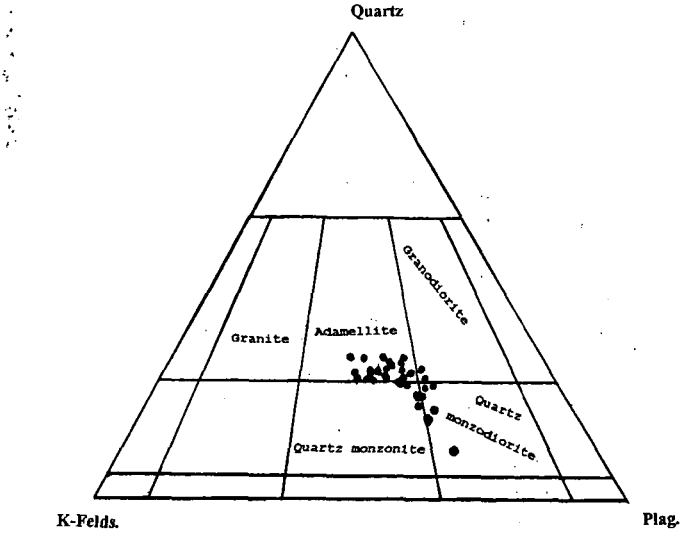

Fig. 3. Modal compositions (quartz, K-feldspar, plagioclase) of granitoid rocks from Wadi Akhdar. The classification used after STRECKEISEN et al. (1973). The upper limit for the quartz content of quartz-monzonite and quartz-monzodiorite is taken as 25% of the total quartz+felsdspar compared with the value of 20% chosen by the IUGS Subcommission.

WHOLE ROCK GEOCHEMISTRY

The present study is based on 90 samples collected mainly from Wadi Akhdar. After a detailed thin sections study, 10 of the characteristic samples of the different rock types were selected for geochemical analysis with respect to the major, trace and rare earth elements (REE) in Budapest, Hungary using the XRF (for the major and trace elements) and the ICP(for REE) analytical techniques.

Granite typology

Several processes have been proposed to explain the geochemical various characters observed in granitoid plutons. WHITE and CHAPPELL (1977, 1983 and 1988) suggested the restite unmixing model as the main process responsible for such variations. WALL et al. (1987) critically examined the restite model and found that the criteria for the recognition of restite components are equivocal.

Nomenclature

According to the MIDDLEMOST (1985) diagram of SiO_2(wt %) versus $Na_2O + K_2O$ (wt. %), the Akhdar granitoids lie in the fields of the granodiorite and granite (*Fig. 4a*). Also, according to DEBON and LE FORT (1983) P-Q schemes (*Fig. 4b*), the Akhdar granitoids could be named either as granodiorite or tonalite rocks.

Petrochemical Trends

The alumina balance is calculated after DEBON and LA FORT (1983) as Al((Na+K+2Ca) and also after DE LA ROCHE (1980) as 2Al-(Fe+Mg+4Ca+2Na-K). Considering these parameters, according to DEBON and LE FORT (1983), the studied Akhdar granitoids are miled metaaluminous to peraluminous affinity (*Fig. 4c*). In general, the alumina balance does not discriminate the granites sharply, however, relatively with differentiation, the granites are less peraluminous than they were in the early phase.

Colour index of granites is mainly controlled by the amount of biotite and is defined as the sum of Fe+Mg+Ti (DEBON and LE FORT, 1983). The Akhdar granitoid plots are illustrated on *Fig. 4c*.

The alkali/calcium ratio is calculated as (Na+K)/Ca. It shows that the Akhdar granodiorites are more calcic than the monzogranitic type. The younger granitic types are not separated from one another by this parameter (Table 1).

The geochemical trends define a systematic changes in particular in the granite types within a given batholith. In this respect several schemes were applied. The plots of the analysed granitic rocks on the (AFM) diagram proposed by IRVINE and BARAGAR (1971), they show calc-alkaline character and compression envitronment (*Fig. 4d).*

Granites may also be considered in terms of their lineage (ATHERTON, 1988), which includes source, intermediate evolution, and emplacement history, which may produce considerable variation at the level of exposure. These can be graphically summarised in terms of their normative components Qz-Ab-Or-An. Plots on the Qz-Ab-Or diagram (*Fig. 5*) compare the normative compositions of simple granite systems as determined by TUTTLE and BOWEN (1958), LUTH (1969) and JAMES and HAMILTON (1969). According to experimental studies, an increase in PH_2O shifts the minimum melting point toward the Ab apex, whereas, an increase in the An content under constant pressure produces the reverse effect, and hence this projection is only strictly applicable to low Ca granites. MANNING (1981, 1982) demonstrated that the presence of fluorine and boron in the Qz-Ab-Or-H_2O system will also cause a shift in the ternary minimum composition toward the Ab apex.

TABLE 1

Major, trace and rare-earth elements composition of Wadi Akhdar granitoid rocks

	1	2	3	4	5	6	7	8	9		
	Akh	*Akh1*	*Akh2*	*Akh3*	*Akh4*	*Akh5*	*Akh6*	*Akh7*	*Akh8*	*mean &*	*std.dev*
SiO2	65.97	68.75	66.95	72.87	66.93	65.39	71.96	70.96	67.96	68.638 ± 2.074	2.698
TiO2	0.74	0.58	0.58	0.42	0.52	0.55	0.35	0.29	0.24	0.474 ± 0.124	0.161
Al_2O_3	15.32	15.22	14.85	14.23	15.98	15.47	14.72	13.78	15.20	14.975 ± 0.512	0.666
Fe_2O_3	2.99	2.95	2.32	1.28	2.13	3.95	1.43	1.84	1.83	2.302 ± 0.659	0.857
FeO	0.97	1.91	1.97	0.65	1.79	1.43	1.24	0.88	1.22	1.340 ± 0.363	0.472
MnO	0.09	0.09	0.09	0.06	0.34	0.07	0.09	0.09	0.12	0.116 ± 0.066	0.086
MgO	1.67	1.39	1.23	0.69	1.28	1.35	0.91	0.89	1.51	1.213 ± 0.246	0.320
CaO	2.82	2.65	2.34	2.33	2.53	2.52	2.44	2.21	2.52	2.473 ± 0.124	0.161
Na_2O	4.42	4.74	4.65	3.79	4.63	3.95	4.45	4.17	4.66	4.384 ± 0.262	0.340
K_2O	3.09	2.19	2.39	3.45	3.19	3.04	3.56	3.22	3.48	3.068 ± 0.367	0.478
P_2O_5	0.21	0.14	0.11	0.22	0.31	0.26	0.03	0.14	0.06	0.164 ± 0.071	0.093
LOI	0.56	0.44	0.40	0.57	0.59	0.96	0.22	0.38	0.76	0.540 ± 0.196	0.235
Cr	22.00	19.00	14.00	9.00	9.00	4.00	2.00	19.00	22.00	13.333 ± 5.879	7.649
Ni	15.00	13.00	13.00	10.00	15.00	29.00	7.00	32.00	33.00	18.556 ± 7.649	9.951
Co	9.00	6.00	8.00	3.00	6.00	20.00	3.00	14.00	18.00	9.667 ± 4.816	6.265
Sc	5.00	1.60	3.90	2.00	1.00	4.00	3.00	3.30	1.00	2.756 ± 1.098	1.428
V	87.00	51.00	49.00	8.00	43.00	39.00	23.00	35.00	33.00	40.889 ± 16.755	21.797
Cu	26.00	9.00	9.00	5.00	5.00	11.00	10.00	6.00	9.00	10.000 ± 4.907	6.384
Pb	30.00	18.00	17.00	22.00	13.00	11.00	19.00	24.00	21.00	19.444 ± 4.401	5.725
Zn	82.00	22.00	48.00	20.00	33.00	26.00	23.00	48.00	16.00	35.333 ± 16.147	21.006
Rb	59.00	78.00	89.00	110.00	99.00	95.00	141.00	82.00	122.00	97.222 ± 18.890	24.575
Cs	1.79	0.91	1.60	3.09	1.32	2.99	2.81	2.75	2.66	2.213 ± 0.624	0.811
Ba	950.00	1000.00	960.00	710.00	876.00	989.00	750.00	791.00	839.00	873.889 ± 82.727	107.624
Sr	611.00	626.00	635.00	422.00	650.00	544.00	246.00	475.00	539.00	527.556 ± 100.51	130.753
Ga	18.00	7.00	16.00	12.00	11.00	16.00	20.00	27.00	18.00	16.111 ± 4.440	5.776
Ta	0.03	0.02	0.04	0.03	0.05	0.03	0.52	0.12	0.06	0.520 ± 0.000	0.000
Nb	8.20	6.00	9.00	7.22	6.00	11.00	9.80	6.80	21.70	9.524 ± 3.747	4.875
Hf	5.30	8.00	4.90	2.61	2.11	3.50	3.80	2.12	4.90	4.138 ± 1.450	1.886
Zr	231.00	40.00	203.00	135.00	210.00	177.00	119.00	179.00	189.00	187.000 ± 31.017	40.352
Y	9.00	11.00	14.00	11.00	13.00	13.00	19.00	17.00	16.00	13.667 ± 2.461	3.202
Th	17.00	11.00	9.51	7.00	11.21	9.86	10.00	14.00	11.88	11.273 ± 2.202	2.865
U	5.00	6.00	5.30	4.00	8.40	2.50	3.10	4.43	2.44	4.574 ± 1.457	1.896
La	22.32	27.80	27.33	42.60	27.35	27.87	18.00	21.32	26.45	26.782 ± 5.298	6.892
Ce	44.00	52.00	57.43	69.87	48.60	53.07	33.96	56.87	57.40	52.578 ± 7.691	10.005
Nd	19.90	28.27	29.69	29.32	27.66	18.30	13.97	15.87	19.50	22.498 ± 4.771	6.207
Sm	3.64	4.88	4.39	3.66	4.33	5.37	3.22	4.43	4.37	4.254 ± 0.509	0.662
Eu	1.06	1.33	1.35	0.88	1.37	1.05	0.84	0.91	1.24	1.114 ± 0.164	0.213
Gd	3.02	4.96	3.59	2.56	3.68	2.22	1.92	1.32	2.41	2.909 ± 0.968	1.157
Tb	0.38	0.42	0.47	0.36	0.42	0.38	0.33	0.47	0.43	0.407 ± 0.037	0.048
Tm	0.25	0.23	0.23	0.25	0.24	0.23	0.22	0.24	0.25	0.238 ± 0.008	0.011
Yb	0.95	1.42	1.48	1.27	1.47	1.04	0.79	1.07	1.09	1.176 ± 0.189	0.246
Lu	0.18	0.24	0.26	0.22	0.26	0.24	0.22	0.21	0.25	0.23 ± 0.020	0.026
ΣREE	95.70	121.55	126.22	150.99	115.38	109.77	73.47	102.71	111.39	111.91 ± 16.46	21.41
La/Yb	23.49	19.58	18.47	3.35	18.61	26.80	22.78	19.92	24.27	22.11 ± 2.34	43.05
Sm/Tb	9.58	11.62	9.34	10.17	10.31	14.13	9.76	9.43	10.16	10.53 ± 1.17	1.52
Tb/Yb	0.4	0.30	0.32	0.28	0.29	0.37	0.42	0.44	0.39	0.35 ± 0.05	0.06
La/sm	6.13	5.70	6.23	11.64	6.32	5.19	5.59	4.81	6.05	6.41 ± 1.56	2.03
La/Lu	124.00	115.83	105.12	193.64	105.19	16.13	81.82	101.52	105.80	116.56 ±24.01	31.24

	1	2	3	4	5	6	7	8	9		
	Akh	*Akh1*	*Akh2*	*Akh3*	*Akh4*	*Akh5*	*Akh6*	*Akh7*	*Akh8*	*mean &*	*std.dev*
Eu/Sm	0.29	0.27	0.31	0.24	0.32	0.20	0.26	0.21	0.28	0.26 ± 0.03	0.04
Ce/Yb	46.32	36.62	38.80	55.02	33.06	51.03	42.99	53.15	52.66	45.52 ± 6.18	8.03
Ba/Cs	530.73	1098.90	600.00	229.77	663.64	330.77	266.90	287.64	315.41	480.42 ±215.38	280.21
Ba/Sr	1.55	1.60	1.51	1.68	1.35	1.82	3.05	1.67	1.56	1.75 ± 0.39	0.50
Ba/Rb	16.10	12.82	10.79	6.45	8.85	10.41	5.32	9.65	6.88	9.70 ± 2.59	3.37
Rb/Sr	0.10	0.12	0.14	0.26	0.15	0.17	0.57	0.17	0.23	0.21 ± 0.11	0.14
Nb/Ta	0.00	0.00	0.00	0.00	0.00	0.00	18.85	0.00	0.00	18.85 ± 0.00	0.00
Th/U	3.40	1.83	1.79	1.75	1.33	3.94	3.23	3.16	4.87	2.81 ± 0.920	1.20
Zr/Hf	43.58	30.00	41.43	51.72	99.53	50.57	31.32	84.43	38.57	52.35 ± 18.41	23.94

TABLE 1 (contin.)

Major Element Composition Data and CIPW of Wadi Akhdar ganitoids.

	1	2	3	4	5	6	7	8	9
	Akh	Akh1	Akh2	Akh3	Akh4	Akh5	Akh6	Akh7	Akh8
SiO2	65.97	68.75	66.95	72.87	66.93	65.39	71.96	70.96	67.96
TiO2	0.74	0.58	0.58	0.42	0.52	0.55	0.35	0.29	0.24
Al2O3	15.32	15.22	14.85	14.23	15.98	15.47	14.72	13.78	15.20
Fe2O3	2.99	2.95	2.32	1.28	2.13	3.95	1.43	1.84	1.83
FeO	0.97	1.91	1.97	0.65	1.79	1.43	1.24	0.88	1.22
MnO	0.09	0.09	0.09	0.06	0.34	0.07	0.09	0.09	0.12
MgO	1.67	1.39	1.23	0.69	1.28	1.35	0.91	0.89	1.51
CaO	2.72	2.65	2.34	2.33	2.53	2.52	2.44	2.21	2.52
Na2O	4.42	4.74	4.65	3.79	4.63	3.95	4.45	4.17	4.66
K2O	3.09	2.19	2.39	3.45	3.19	3.04	3.56	3.22	3.48
P2O5	0.21	0.14	0.11	0.22	0.31	0.26	0.03	0.14	0.06
LOI	0.00	0.44	0.40	0.57	0.59	0.96	0.22	0.38	0.76
Sum	***98.19***	***101.05***	***97.88***	***100.56***	***100.22***	***98.94***	***101.40***	***98.85***	***99.56***
				CIPW norms					
Q	19.94	24.20	23.16	31.89	20.25	22.65	25.85	28.16	19.64
C	0.26	0.57	0.62	0.55	1.05	1.72	-	-	-
Or	18.26	12.94	14.12	20.39	18.85	17.97	21.04	19.03	20.57
Ab	37.40	40.11	39.35	32.07	39.18	33.43	37.66	35.29	39.43
An	12.12	12.23	10.89	10.12	10.53	10.81	9.68	9.37	10.28
Cpx	-	-	-	-	-	-	1.81	0.55	1.48
Di	-	-	-	-	-	-	1.21	0.34	1.05
Hd	-	-	-	-	-	-	0.60	0.21	0.43
Opx	5.86	6.20	5.39	2.46	5.59	6.54	2.67	3.49	4.83
En	4.16	3.46	3.06	1.72	3.19	3.36	1.70	2.06	3.28
Fs	1.70	2.74	2.32	0.74	2.40	3.18	0.96	1.44	1.56
Mt	2.46	2.94	2.60	1.21	2.49	3.22	1.75	1.71	1.98
Il	1.41	1.10	1.10	0.80	0.99	1.04	0.66	0.55	0.46
Ap	0.50	0.33	0.26	0.52	0.73	0.62	0.07	0.33	0.14
Mg#:	56.80	46.65	46.72	52.87	50.88	43.26	52.55	50.71	61.54
DI:	75.60	77.25	76.64	84.35	78.28	74.05	84.55	82.47	79.64
SI:	35.32	42.46	40.42	53.47	35.02	39.19	44.17	48.13	34.78
Alk rat.	2.43	2.27	2.39	2.55	2.46	2.27	2.75	2.72	2.70
Ox. degr.	0.76	0.61	0.54	0.66	0.54	0.73	0.54	0.68	0.60
Al/Alk	1.17	1.21	1.20	1.18	1.20	1.28	1.10	1.12	1.11
Na+K/Ca	2.90	2.83	3.25	2.84	3.04	2.73	3.6	3.65	3.53
Na/K	2.17	3.29	2.96	1.67	2.21	1.98	1.90	1.97	2.04

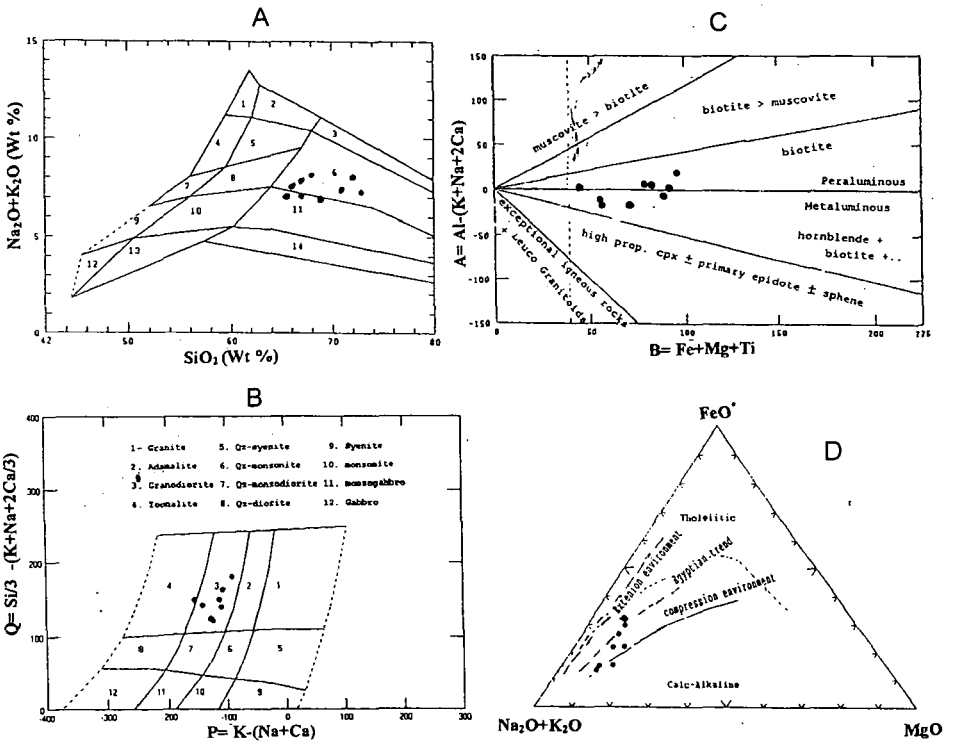

Fig. 4. A: SiO2 Vs. Na2O+K2O diagram of Middlemost 1985. Classifying the Akhdar granitoids: 1. Alkali feldspar Syenite, 2. Alkali feldspar Quartz Syenite, 3. Alkali feldspar Granite, 4. Syenite, 5. Qz-Syenite, 6. Granite, 7. Monzonite, 8. Quartz Monzonite, 9. Monzodiorite, 10. Quartz Monzodiorite, 11. Granodiorite, 12. Diorite and Gabbro, 13. Qz-Diorite, 14. Tonalite.

B: Q-P diagram of DEBON and LE FORT (1983). Molar proportions, where Q=Si/3-(K+Na-2Ca/3), P=K-(Na+Ca).

C: A-B variation plots of DEBON and LE FORT (1983) showing the plots of the Akhdar granitoids where, (A) = alumina saturation index {A= Al-(K+Na+2Ca)} and (B)= color index {B=Fe+Mg+Ti}.

D: AFM diagram of PETRO et al., (1979) Showing the trends for compressional suites and extensional environment. Tholeiitic and calc-alkaline fields after IRVINE and BARAGAR (1971). The Egyptian granites is defined after HUSSEN et al. (1982).

In order to interpret the crystallization feature of the granodioritic magma with experimental data avaliable, if the water pressure at the initial crystallization of the magma is roughly equal to the rock pressure, i.e., the load pressure 5 Kb, the depth of initial crystallization was about 18 Km. However, masses of the magma from a parent body differentiating at depth might have moved up to a higher zone in the crust. Therefore, the crystallization of the magma mostly would have occurred at somewhat higher level with lower pressures than 5 Kb, that is equivalent of 18 Km depth. Accordingly, the normative minerals of Qz-Ab-Or for the granitic rocks are plotted in the tetrahedron Ab-An-Or-Qz (*Fig.5*). This diagram shows that the studied granitic

rocks as a group are distributed along the line m-n in the tetrahedron. The plots are located at the front face at 39% Ab, 58% An and 3% Or, and a point lies at the base of 30% Qz, 20% Or and 50% An. Therefore the crystallization of the granodioritic magma would being to crystallize the basic phase of the granitic rocks at around point m (about 1,100 ° of the H_2O saturated liquids), and continue to consolidate the magma along the m-n trend to the point n (about 600 °C).

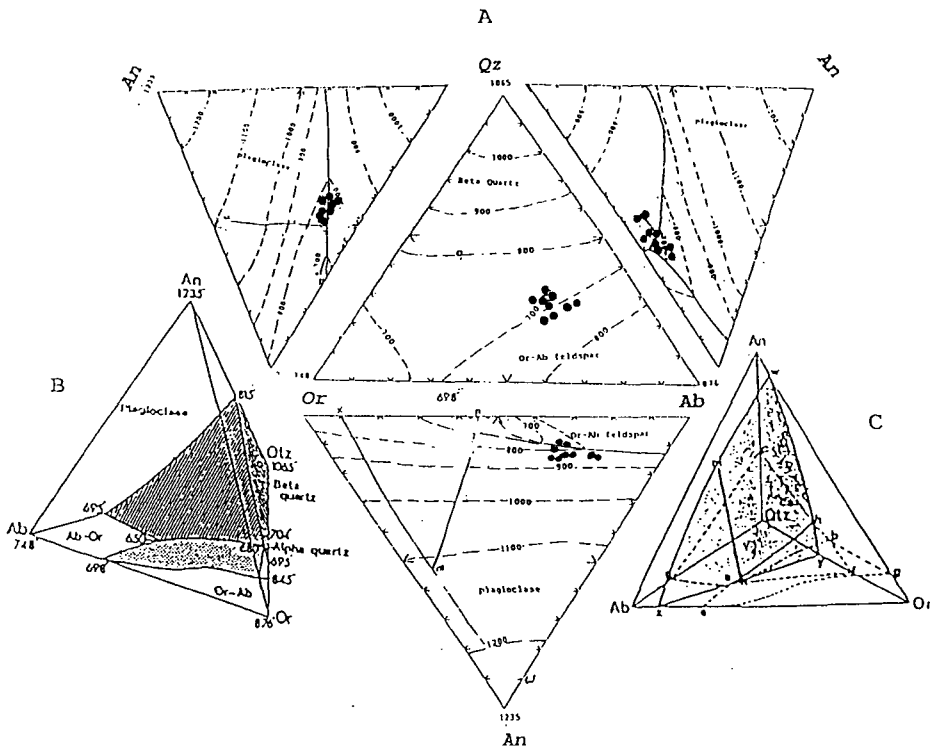

Fig. 5. The tetrahedron showing the liquids relation in the system Or-Ab-An-H2O at 5 Kb H2O pressure. All components are in weight percent.

A: Faces of the tetrahedron showing field boundaries (heavy lines), isotherms (light lines and dashes), and projections of norms of the granitic rocks of Wadi Akhadar area.

B: Three dimensional drawing of tetrahedron showing field boundaries. The minimum lies at 650 °C.

C: Section WXY, bisecting tetrahedron around Ab and An corner and intersecting the Or-Qz join at around midpoint. Projections of norms of the rocks show the generalized crystallization path of the granitic rocks, m-n on the section WXY.

GENETIC CLASSIFICATION

Alkali balance is a useful parameter in the genetic classification of granitoid rocks. This based on that; K and Na tend to show fluctuations both within and between major petrographical grouping, and commonly used as a geochemical discrimination between I- and S-type granitoids (CHAPPELL and WHITE, 1974; CHAPPELL and STEPHENS, 1988 and CHAPPELL and WHITE 1992). Considering HINE et al (1978), LE MAITRE, et.al (1982) and WHITE and CHAPPELL (1983), the plots of K_2O versus Na_2O (*Fig.6a*) are used to show the compositional difference between I- and S-type for the studied granitoids. Notable exceptions to the use of the alkali balance as an I-S discrimination are; potassic calc-alkaline I-types which have an appreciable crustal component, and late stage metasomatic input or exchange such as observed in two phase derivatives of S-type granites (COBBING et al., 1986).

The model proposed by WHALEN et al, (1987), indicates that the Akhdar granitoids are mostly orogenic granite type (OGT) unfractionated granites, close to the line of dividing fractionated granites (FG). On the other hand, some other samples lie in the felsic fractionated granites field (*Fig. 6b*).

Tectonic discrimination of the Akhdar granitoids

The obtained field data indicated that the Akhdar granitoids pluton has been originated during a late kinematic regime. The tectonic setting of the Akhdar granitoids is illustrated on the following diagrams:

The Hf-Rb/30-TaX3 diagram of HARRIS et al. (1986), further separates pre-, syn-, and post-collision granites. On this diagram (*Fig. 6c*), the studied granitoid samples are plotted within the volcanic arc granite field (VAG). Also, on the Rb versus (Y+Nb) diagram (*Fig. 6d*) proposed by PEARCE et al (1984), the Akhdar granitoids plots fall within the volcanic arc granite (VAG) field.

On the multi-element,. MORB-normalized diagram (*Fig.6e*), the Akhder granitoids are characterized by enrichment of the LIL elements (K_2O, Rb, Ba and Th) relative to the HFS-elements (Ta, H, Zr, Y and Yb). A typical feature of most of the granitoid samples as their negative Ta-anomalies.

The chondrite-normalized REE diagrams of the Akhdar granitoids are shown in the *Fig. 6f*) where the Wadi Akhdar granitoid samples show similar patterns. The Sm/Tb_n defined by the MREE (average La/Sm_n= 6.41±1.56 and Tb/Yb_n= 0.35±0.05) and all samples show no negative Eu-anomaly (Table 1). The low REE patterns of the studied granitoid rocks indicate close petrogenetic histories, which will be briefly discussed. Firstly we considered the gabbroid xenoliths-bearing granodiorite rocks which are the representative of melts from which the granitoid rocks might developed by fractional crystallization. The slope of the REE patterns of these rocks without Eu-anomaly reflects the fractionation to yield silic magma which would be dominated by removal of plagioclase, and thus of formed by partial melting of plagioclase-rich rocks, or alternatively have undergone plagioclase accumulation. Those with LREE-enriched patterns, characterized with no negative Eu-anomalies would be compatible with generation by partial melting of mafic source, in which amphibole/or garnet is present as residual phases in the source material (HANSON, 1978).

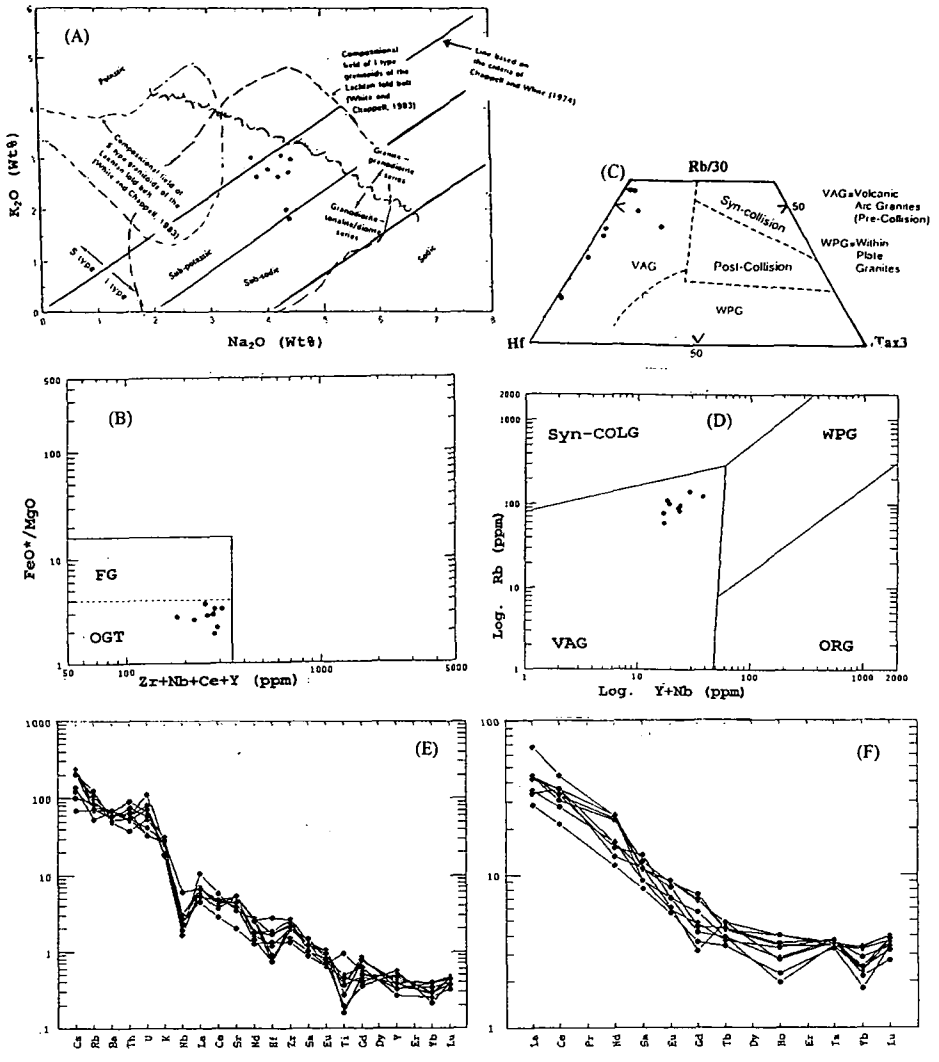

Fig. 6. A: K_2O Vs. Na_2O variation diagram after LE MAITRE, et al. (1982). I-S type after HINE et al., (1978). Compositional field of I- and S-type granitoids after WHITE and CHAPPEL (1983)

B: Zr+Nb+Ce+Y Vs. FeO*/MgO binary diagram of WHALEN et al., (1987). FRAC is the compositional field of the highly fractionated I- and S-types.

C: Ternary diagram of Wadi Akhdar granitoids rocks plotted in Hf-Rb/30-Tax3 after HARRIS et al. (1986).

D: Trace element tectonic discrimination plots of the examined granitoids. Fields are after PEARCE et al. (1984). VAG = Volcanic arc granite; ORG = Ocean ridge granite; WPG = Within plate granite; SCG = Syn-Collision granite

E: Discrimination diagram showing the Akhdar granitoid geochemical patterns. The data was treated due to those proposed by THOMPSON (1982).

F: Chondrite normalized REE distribution patterns of the Wadi Akhdar granitoids, THOMPSON (1982).

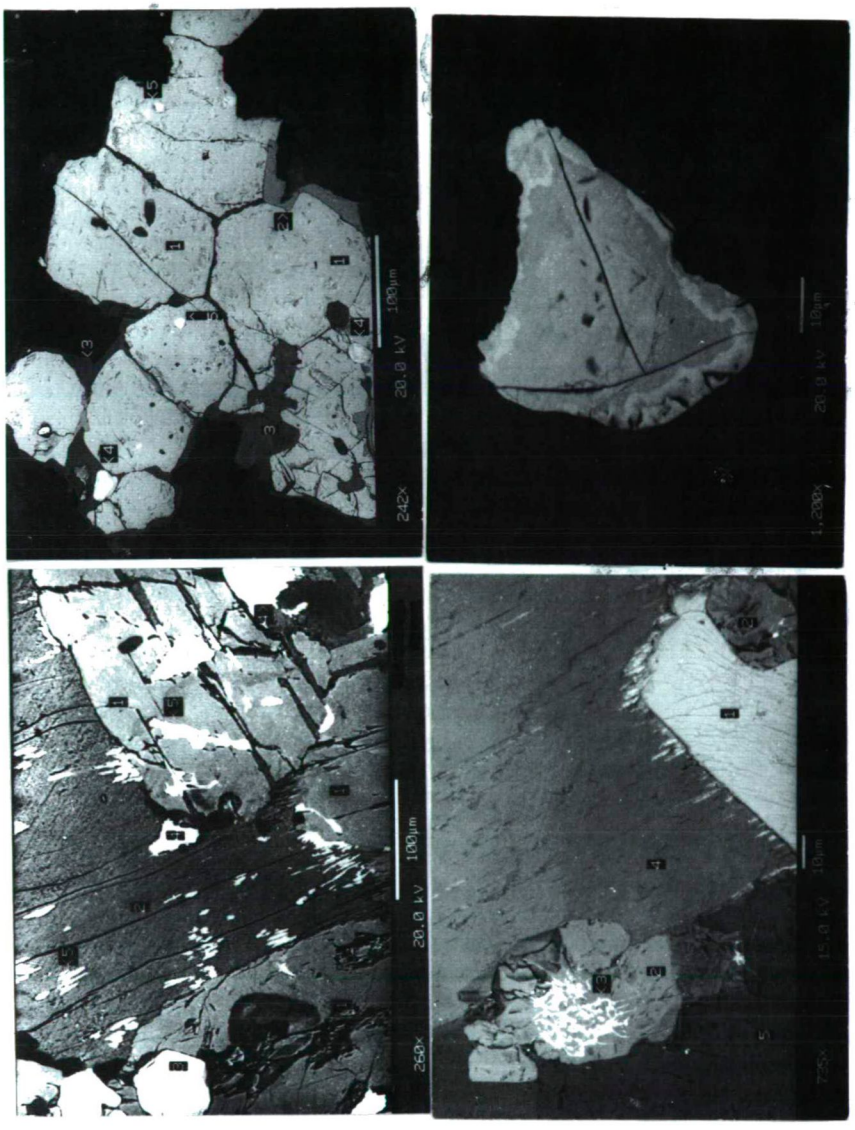

Fig. 7. Microphotographs (SEM): (A) showing 1. Fe-Oxides, 2. ilmenite, 3. titanite, 4. zircon and 5. sphalerite, B (showing) 1. amphibole, 2. albite, 3. apatite, 4. zircon and 5. sphlerite, (C) showing 1. allanite, 2. apatite, 3. Th+REM, 4. biotite and 5. plagioclase, and (D) showing thorite crystals

PETROGENESIS AND ORIGIN

The composition of the Akhdar granitoid rocks suggest that the oxygen fugacity and partial melting favours a define role in the formation of granitoid rocks of Wadi Akhdar. The presence of metagabbro and orthogneiss as a roof pendant and xenolith in the

country rocks (*Fig.2*) and hornblende, biotite, magnetite, Fe-oxides, sphalerite and allanite (*Fig. 7a,b* and *c*) may indicate I-type magma composition for the source rock.

Petrographical and geochemical observations suggest that the initial melt for the considered granites was generated in a water saturated system.

JOHANNES and HOLTZ, (1990 and 1991) found that an initial magma with 50% melt plus 50% quartz and feldspar would occur at 700°C to 900 and 8 Kb pressure, in a closed system. This temperature accords with zircon thermometry, which indicates 800 °C for the initial crystallization of the melt in the older granites (BUDA, et al., 1998). The amount of melt at given P-T conditions would depend upon the availability of water

It seems that in the later stages, an addition of a fluids to the subsolidus granite magma might have occurred, i.e. the second phase of the Akhdar granitoids emplacement as monzogranite type.

The source of suchs fluids can give rise and associated with Fe-oxides, sphalerite Th and rare-earth minerals (REM) mineralization at Ain Akhdar (*Fig. 7C* and *D*).

The intrusion level of the older types can be determined with less confidence than the younger types, because the former is deeply eroded, whereas, the roof zones of the younger granites are still preserved. In general, the roof of the younger types lies nearly parallel to the present surface at many places. The granitic intrusion can be assumed to have been emplaced at depths of between 5 and 8 Km.

CONCLUSIONS

All evidences available from the field observations implied that the xenoliths have been assimilated from gabbroid country rocks. There is no other petrographic evidence of disequilibrium among the mafic minerals. In the felsic types; they contain very small amounts of hornblende which occurs as a part of an equilibrium mineral assemblage. The enclaves are generally hornblende-bearing variety consistant with those of the I-types.

From the major elements geochemistry, the studied granitoid rocks can be classified as granodiorite, tonalite and monzogranite. They are alumino-cafemic magmatic association of mild metaaluminous - peraluminous character and biotite-rich, showing calc-alkaline character and compression envitronment.

The trace element geochemistry encountered pronounced negative Ta and Nb anomalies. similar to that of volcanic arc granites (VAG) (PEARCE et al., 1984 and HARRIS et al., 1986) originated during late kinematic regime. The VAG is probably formed in a late tectonic environment dealing with crustal rather than mantle source.

The light REE patterns of the studied granitoid rocks indicate close petrogenetic histories. The slope of the REE patterns of these rocks without Eu-anomaly reflects the fractionation to yield silicic magma which would be dominated by removal of plagioclase, and thus of formed by partial melting of plagioclase-rich rocks, or alternatively have undergone plagioclase accumulation. Those with LREE-enriched patterns, characterized with no negative Eu-anomalies would be compatible with generation by partial melting of mafic source.

Petrographical and geochemical observations suggest that the later stages, and the addition of fluids to the subsolidous granite magma might have occurred. The source of such a fluid, can give rise and associated with Zn, Th and rare-earth metals (REM) mineralization.

REFERENCES

AKAAD, M. K. and NOWEIR, A. M. (1980): Geology and litho-stratigraphy of the Arabian belt of Egypt between Latitudes 25° 35' and 26° 30': Evolution and mineralization of the Arabian-Nubian Shield. Al Shanti A.M.S. (ed.), King Abdulaziz Univ., Jeddah, Vol.,3:127-135

ATHERTON, M. P. (1988): On the lineage character of evolving granites. Fifth International Symposium on Tin/Tungsten granites in southeast Asia and the western Pacific. Nozawa, T (editor). IGCP project 220, Shimane University, Matsue, Japan:1-5.

BATCHELOR, R. A. and BOWDEN, P. (1985): Petrogenetic interpretation of granitoid rck series using multicationic parameters. Chem. Geol., 48:43-55. Amsterdam.

BUDA, GY., HASSEN, I. and DABBOUR (1998): Typological studies on zircon grains from the granitoids of southern Sinai, Egypt. Fifth Conference on Geology of Sinai for Development. Abstract, October, 1998

CHAPPELL, B. W. and WHITE, A.J.R. (1974): Two contrasting granite types. Pacific Geol. 8:173-174.

CHAPPELL, B. W. and WHITE, A.J.R. (1992): I- and S-type granites in the Lochlan Fold Belt. Trans. Royal Soc. Edinburge, Earth Sci., 83:1-26.

CHAPPELL, B.W. and STEPHENS, W.E. (1988): Origin of infra-crustal (I-type) granite magmas, Trans. Roy. Soc. Edinburgh Earth Sci. 79:71-86.

COBBING, E.J., PITFIELD, P.E.J. and TEOH, L.H. (1986): The granites of the Southeast Asian Tin Belt. J. Geol. Soc. London, 128:421-460.

DE LA ROCHE, H., LETERIER, J. GRANDCLAUDE, P. and MARCHAL, M. (1980): A classification of volcanic and plutonic rocks using R1-R2 diagram and major element analyses- its relationships with current nomenclature. Chem. Geol., 29:183-210.

DEBON, E. and LE FORT, P. (1983): A chemical-mineralogical classification of common plutonic rocks and associations. Trans. Royal Soc. Edinburgh: Earth Sci., Vol. 73:135-149.

EL-BIALY, M. Z. (1998): Geology of the basement rocks of Abu Durba – Abu Haswa area, Southwestern Sinai, Egypt. M. Sc. Thesis, Faculty of Sci. Suez Canal Univ., Ismailia:170p.

EL-RAMLY, M.F. and AKAAD, M.K. (1960): The basement complex in central Eastern Desert of Egypt between Lat. 24° 30' and 25° 40' N. Geol. Surv. Egypt, Paper 8:1-35

EL-SHAZLY, E.M. (1964): On the classification of the Precambrian and other rocks of magmatic affiliation in Egypt. Proc. 22nd Int. Geol. Con. New Delhi 10:88-101.

FULLAGAR, P.D and GREENBERG, J. K. (1978): Egyptian younger granites: a single period of plutonism? Precamb. Res., 6:A-22.

GAS, I. G. (1979): Evolutionary model for the Pan-African basement. In: S.A. TAHOUN (ed.), Evolution and Mineralizaion of the Arabian Nubian Shield. Inst. Appl. Geol. Jeddah, Bull. 3, Pergamon Press 1:11-20.

HANSON, G.N. (1978): The application of trace elements to the petrogenesis of igneous rocks of granitic composition. Earth and Planetary Science Letters. 38:26-43.

HARRIS, N.B.W., PEARCE, J.A. and TANDLE, A.G. (1986): Geochemical Characteristics of collision-zone magmatism. In: COWARD, M.P. and RIES, A.C. (eds): Collision Tectonics. Geological Society, London, Spec. Publ. 19:67-81.

HASHAD, A.H. (1980): Present status of geochronological data on the Egyptian basement complex. Inst. Appl. Geol., Jeddah, Bull. 3:31-46.

HASSEN, I., BUDA, GY. and SZEDERKENYI, T. (1998): The evolution of the Precambrian basement rocks south western Sinai Peninsula (in press)

HINE, R., WILLAMS, L., CHAPPELL, B. and WHITE, A. (1978): "Contrast between I-type and S-type granitoids of the Kosciusko batholith", J. Geol. Soc. Aust, 25:219-234.

HUSSEIN, A.A., ALI, M.M. and EL-RAMLY, M.F. (1982): A proposed new classification of the granites of Egypt. J. Volcan. Geother. Res., 14:187-198.

IRVINE, T.N. and BARAGAR, W.R.A. (1971): A guide to the chemical classification of the common volcanic rocks. Can. J. Earth Sci., 8:523-548. Ottawa.

JAMES, R.S. and HAMILTON, D.L. (1969): Phase relations in the system $NaAlSi_3O_8$ - $KAlSi_3O_8$ - SiO_2 at 1-kilobar water vapour presure. Contrib. Min. Petrol., 21/2:111-141.

JOHANNES, W. and HOLTZ, F.(1990): Formation and composition of H_2O-undersaturated granitic melts. In ASHWORTH, J. and BROWN, M. (eds) High temperature metamorphism and crustal anatexis: 87-104. *London: Unwin Hyman.*

JOHANNES, W. and HOLTZ, F. (1991): Formation and ascent of granitic magma. Geol. Rdsch. 80, 2,225-232.

LUTH, W.C., (1969): The systems $AnAlSi_3O_8$-SiO_2 and $KAlSi_3O_8$ to 20 Kb and the relationship between H_2O content pH_2O and P Total in granitic magmas. Am. J. Sci., 267A:325pp.

MANNING, D.A.C. (1982): An experimential study on the effects of fluorine on the crystallization of granitic melts. 191-203 in: Metallization associated with acid magmatism. Vol. B, EVANS, AM (ed.) London: Wiley.

MANNING, D.A.C. (1981): The effect of fluorine on liquidus relations in the system Qz-Ab-Or with excess water at 1 Kb. Contrib. Min. Petrol., 76:206-215.

MIDDLEMOST, E.A.K. (1985): Magmas and Magmatic Rocks. An Introduction to Igneous Petrology. Harlow, U.K.: Longman.

PEARCE, J.A., HARRIS, N.B.W. and TINDLE, A.G. (1984): Trace element discrimination diagrams for the tectonic interpretation of granitic rocks, J. Petrol., 25:959-983.

PETRO, W.L., VOGEL, T.A. and WILOBAND, J.T. (1979): Major element geochemistry of plutonic rock suites from compressional and extensional plate boundaries: Chem. Geol., 26:217-235.

SCHURMANN, H.M.E. (1953): The Precambrian of the Gulf of Suez area. 19th. Int. Geol. Cong. Algiers, C.R., 1:115-135.

STRECKEISEN, A.L. (1973): Classification and nomenclature of plutonic Rocks. Recommendations of the IUGS Subcommission on the Systematics of Igneous Rocks (private distribution).

TUTTLE, D.F. and BOWEN, N.L. (1958): Origin of granites in the light of experimental studies in the system $NaAlSi_3O_8$-$KAlSi_3O_8$-SiO_2-H_2O.Geol. Soc. Am. Mem., 74:130-142.

WALL, V.J., CLEMENS, J.D. and CLARKE, D.B. (1987): Models for granitoid evolution and source compositions. Journal of Geology, 95:731-749.

WHALEN, J.B: CURRIE, K.I., and CHAPPELL, B.W. (1987): A-type granites: geochemical characteristic, discrimination and petrology. Contrib. Min. Petrol., 95:407-419.

WHITE, A.J.R. and CHAPPELL, B.W. (1977): Ultrametamorphism and granitoid genesis. Tectonophysics., 43:7-22.

WHITE, A.J.R. and CHAPPELL, B.W. (1983): Granitoid types and their distribution in the Lachlan Fold Belt, southeastern Australia. 21-34 in Circum-Pacific Plutonic Terranes. RODDICK, J.A. (ed.) Mmoir of the Geological Society of Am., No. 1159.

WHITE, A.J.R., and CHAPPELL, B.W. (1988): Some supracrustal (S-type) granites of the Lachlan fold Belt, Trans. R. Soc. Edinburgh Earth Sci., 79:169-181.

Manuscript received 15. Sep. 1999.

Acta Mineralogica-Petrographica, Szeged, XL, 121–138, 1999

NATURAL RADIOACTIVE ELEMENT CONTENT OF THE OLD CRYSTALLINE ROCKS IN SOUTHERN TRANSDANUBIA (SW HUNGARY)

E. PÁL MOLNÁR*, I. VADOS**, I. GERZSON**, B. KÓBOR*

*Department of Mineralogy, Geochemistry and Pétrology, Attila József University
**Mecsekérc Environment Protection Co.

ABSTRACT

On the basis of systematisation of several thousand radioactive element content analyses made in laboratories since the 50's, U and Th content of old granitoid rocks of Southern Transdanubia proved to be much higher than the average U and Th content of granitoids in the world. This value of rocks from areas west of Mecsek Mountains as well as near Szalatnak village and Pécs city is twice higher than the world average. Areas west of the Mecsek Mountains show higher U and lower Th contents than areas east of these mountains. Uranium accumulation is higher in aplites and hydrothermal formations than in granites.

The western and eastern granites are less and highly sensitive to leaching, respectively. The intensive U migration resulted in significant U accumulation in young sediments in some places.

INTRODUCTION

Study of natural radioactive element (U /Ra/, Th, K) content of the rocks in Hungary was performed by the Mecseki Ércbányászati Vállalat (Mecsek Ore Mining Company) until 1990, when uranium exploration was stopped in Hungary. Aim of the analyses was to research U sources, therefore, rocks supposed to contain perspective U accumulation were mainly studied.

The aim of this paper is to elaborate many thousands radiological data of granitoid rocks, gneisses and amphibolite-like metamorphic rocks coming from Southern Transdanubia (south of the Szekszárd-Kaposvár-Kutas line to the state boundary, and east of the Kutas-Csokonyavisonta-Barcs line to the Danube).

Data bank of the late Mecseki Ércbányászati Vállalat Kutató Mélyfúró Üzem (Mecsek Ore Mining Company, Research and Drilling Branch) was used as a basis of our study. Now, this data bank is owned by the Magyar Geológiai Szolgálat (Hungarian Geological Survey) and managed by the Mecsekérc Környezetvédelmi Rt. (Mecsekérc Environment Protection Co.).

SUMMARY OF THE APPLIED METHODS AND HISTORY OF RADIOLOGICAL STUDIES ON OLD CRYSTALLINE ROCKS IN SOUTHERN TRANSDANUBIA

Because of the veins containing U ore, radiological research were begun in granite areas all over the world. Similarly, granite was the first rock which was studied by

* H-6701 Szeged, P.O.Box 651, Hungary
** H-7633 Pécs, Esztergár út 19., Hungary

radiological methods in Hungary. Scientific and industrial research began in 1948 and 1953, respectively.

In Southern Transdanubia the first radiometric measurements were performed in the granite area near Mórágy village as the greatest surficial granite occurrence in Hungary. Research of the environment of two small granite outcrops near Nyugotszenterzsébet and Nagyváty village situated in the westernmost part of the Mecsek Mountains was begun as late as the early 60's. Granite outcropping in the city of Pécs town, although it has been known for a long time, can be studied only in a very limited area, and the rock is quite weathered.

Granite is slightly explored even in the Mórágy Mountain, however, aerial and field (by car and on foot) gamma-radiation measurements were performed since the middle of the 50's. Since the significant covering, soil gas-radon method was also used in the beginning of the industrial research work. Detailed study of the radioactive anomalies and areas of higher radioactivity was made by removal of the soil cover (trench or pit) or by drilling. Of course, granite and other crystalline rocks of the basement were also exposed by drilling that were made to expose the Permian sedimentary U accumulations. Moreover, crystalline formations of the basement were also found during coal, petroleum, drinking- and thermal water prospecting. Structure wells, which were deepened for exposure of the basement, provided important information on this topic, too. Outcrops, trenches and wells made direct study, sampling and radiological analysis of the rocks belonging to the crystalline basement possible.

Although, gamma-radiation measurements characterise radiological conditions (e.g. in the case of borehole logging or surficial measurements), but these are characteristic for only sum total of radioactive elements; influence and ratio of the three most important natural radioactive elements (U, Th, K) can not be determined. Gamma spectrometry enables the distinction between them on the basis of the difference between energy spectra of gamma radiation of the given radioactive elements. This kind of measures were also used during the aerial and the field measurements. Aerial measurement can be regarded as a review, the obtained results can hardly be correlated with rock outcrops because of the bad exposure conditions.

As it will be presented, aerial measurements are followed by field controls where radioactive element content of the rock outcrops were also determined by using gamma spectroscopy. That time however, these determination required long time because of the simple apparatus. Moreover, error of the measures was significant because of the low energy resolving power of the detector, thermal sensitivity of the instrument, and variation of geometrical conditions of the measure. Radioactive equilibrium radon exhalation difference resulted in further decrease in accuracy of the measurements.

Taking these facts into consideration, only laboratory analyses of the collected rock samples were regarded suitable for an exact characterisation of radiological condition of the studied formations.

Both radiometric and chemical methods were used for laboratory analyses. Radiometric analyses have been performed by using multichannel analyzer since the middle of the 70's, which made U, Ra (uranium equivalent value), Th detection of some ppm sensitivity and detection of total potassium content (by means of K-40 isotope) of some % sensitivity. U and uranium equivalent of Ra are almost corresponding to each other. In the cases of the surficial samples, there is little difference for Ra. For a comparison of chemical U analyses, uranium values are listed in the tables. Of course, this accuracy can be reached in case of suitable sample quantity and optimal measuring

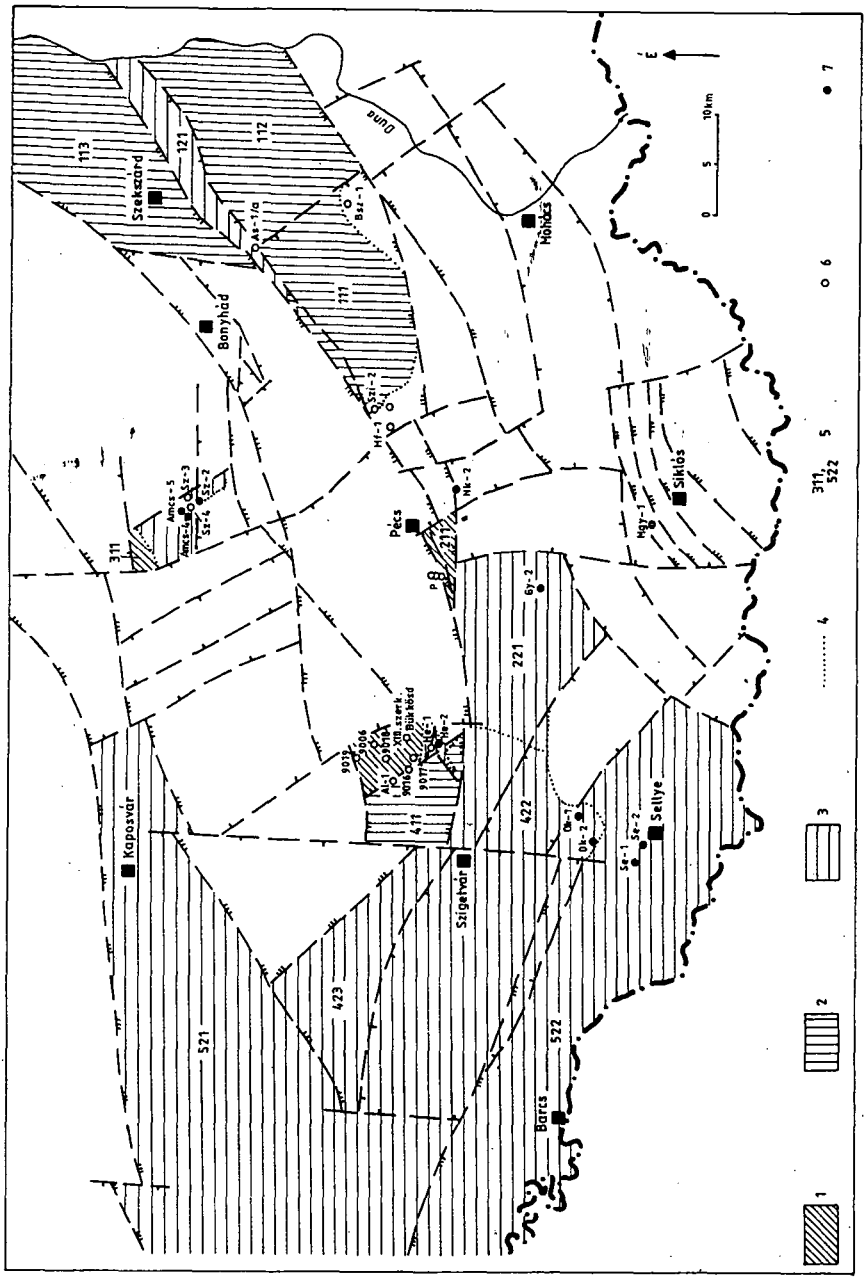

Fig. 1: Uncovered tectonic map of the Southern Transdanubian granitoid and metamorphic basement
1. Granitoid area covered by sedimentary basement formation; 2. Granitoid formations on the surface of the basement; 3. Metamorphic formation on the surface of the basement; 4. Arbitrary division of a crystalline basement block along topographic line; 5. Area code; 6. Borehole reaching granitoid formation under another basement element; 7. Borehole reaching metamorphic formation under another basement element.

time. Unfortunately, the quantity of the samples was often low, and measuring time was also limited because of economic considerations. Hence, detection limit of uranium was as high as 5 ppm in one case.

Theoretically, chemical analyses provide a sensitivity of some ppm, however, uncertainty of chemical digestion could make problem in some cases. Particularly, if major element content of the samples had unexpectedly changed for which chemists were not prepared. In these cases, even high differences occured between chemical and radiometric analyses.

In the beginning, chemical method of Th determination was not suitable, therefore, these results are not listed together with the old chemical analyses.

By developing the methods and the instruments, both chemical and radiometric methods are suitable to product analytical results of the expected accuracy (some ppm and some tenths %). Available data were used by considering the above mentioned facts.

Tectonic units of the rocks of the crystalline basement indicated in the geological map on the scale of 1:200000 are discussed according to figure 1.

It must be noted that, in some cases, great continuous crystalline basement areas were divided (mainly along tectonic lines) because of practical reasons (e.g. 1.1.1., 1.1.2. areas), but some parts were geographically separated from each other (e.g. 2.2.1. and 4.2.2. areas).

RADIOLOGICAL CONDITIONS OF CRYSTALLINE FORMATIONS OF THE MÓRÁGY MOUNTAIN

The crystalline basement is studied the most here, since this is the greatest surficial occurrence of granitoid formation in the Southern Transdanubia.

Radiometric survey were performed three times (1956, 1965, 1986) which were followed by control measures in the field using by gamma and radon methods. During the field measures, samples were also collected; radiological condition of the area are revealed by their U and Th analyses.

Because of the above mentioned facts, only chemical U analyses (table 1) can be considered from samples collected after the report J-0053 of the gamma survey performed by car in 1961 (VINCZE, 1961).

In 1974, during the following research of the area, samples listed in the former table and other samples collected in 1961 were re-analysed by using the more modern radiometric method. The results are listed in table 2 (VINCZE, 1975 - J-0667). There are Th and K analyses too since spectral analysis made them possible.

In 1974 field study followed the aerial measurements, its aim was to check the detected radiometric anomalies on the field. Most of the anomalies can be detected in the cases of crystalline rocks cropping out from loess of lower radioactivity. The analyses are summarised by table 3 (VINCZE, 1975).

On the basis of all samples collected from the area, the author stated that areas north and south of the Pécs-Bátaszék railway line have significantly different radiological mean values (table 4).

Another phase of field control of the aerial radiometric survey in 1965 was limited only to some important points of anomaly, and it had rather focused on petrographic identification. Author of the report J-0130 (SZEDERKÉNYI) studied the rocks by several

TABLE 1

Chemical U analysis of rock-samples in the year 1961 (Vincze, 1961)

Rock type	Chemical U average value 10^{-4}% (ppm)	Min - Max (ppm)	Sample (pcs)
Granite	12	1 - 138	74
Acidic dyke rocks (pegmatite, aplite), clay gouge	16	5 - 69	25
Basic dyke rocks (lamprophyre, biotitite)	7	3 - 17	13
Metamorphic granite and hydrothermal dyke	25	5 - 41	9

TABLE 2

Results of complex radiological study on analyses in the 1961 (Vincze, 1975)

Rock type	U (ppm)	Th (ppm)	K (%)	Sample (pcs)
Amphibolite	1,4	5,8	0,9	10
Granite	5,8	41,3	4,3	101
Metasomatic granite	10,0	35,0	2,3	7
Pegmatite	5,0	17,5	2,5	10
Kersantite	2,6	29,0	4,0	5
Aplite	7,7	41,0	3,8	24
Bostonite	4,9	42,0	5,0	12
Alkaline basalte (diabase)	6,1	35,0	5,7	7

TABLE 3

Results of radiological studies in the year 1974 (Vincze, 1975)

Rock type	U average (ppm)	Th average (ppm)	K average (%)	Samples (db)
Aplogranit, aplite	4,8	59	4,7	31
Microgranite	4,0	56	4,8	11
Medium-grained granite	5,0	52	4,6	25
Coarse-grained granite	5,5	77	4,5	34
Migmatite	5,7	54	5,2	16
Kersantite	4,5	34	5,0	2
Alkaline basalte (diabase)	2,6	19	2,7	5

TABLE 4

Radiological mean values south and north of Pécs-Bátaszék railway line (Vincze, 1975)

Area	U (ppm)	Ra (U equ.) (ppm)	Th (ppm)	K (%)	Samples (pcs)
North of Pécs-Bátaszék railway line	3,8	4,7	34	4,0	250
South of Pécs-Bátaszék railway line	6,0	6,5	55	4,8	144
Whole area	4,6	5,6	42	4,3	394

classifications according to phases of the granitization process. The following rock types were distinguished on the aerial anomaly no. 90 which is situated in 5-700 km from Geresdlak village in NNE direction: a. Agmatites; b. Granite; c. Arterites, venites (monomineralic differentiated melt between the crystals); d. Aplogranite (light red granite without mafic mineral constituents); e. Alkaline basalt ("alkaline diabase").

Mean values were not calculated for the given rock types, only the list of samples are published.

In the case of anomaly no. 89 belonging to the quarry near the railway station of Kismórágy village, mean values (based on estimation) and maximum values were given for rock types listed in table 5.

In his studies no. J-0401 and J-0491, L. KÓSA (1977) studied U-Th content in fresh and weathered granites from the Mórágy Mountains. His results are listed in table 6. Unfortunately, sample number serving as a base for calculation was not published, but his manuscripts no. F-1612 and F-1611 contain several radiometric analyses. Undoubtedly, these analyses refer to this area, therefore, the values were calculated from numerous samples, this way, his results can be regarded as reliable.

The latest aerial (helicopter) survey was made in 1986, and field identification of several detected anomalies was performed by KARDOS et al. (1987 - J-1239).

On the basis of aerial spectrometry measurements they published mean values of the element concentration given in the "content channel" of the aerial apparatus; these values refer to the whole area:

U mean value = 2,18 ppm; Th mean value = 10,00 ppm; K mean value = 1,53 %.

Of course, it must be considered that these otherwise correct mean values refer to the cover areas, too.

During the field control work, rock samples were collected from the studied anomalies that might be correlated with real geological formations. Unfortunately, these samples were analysed by using rapid radiometric method (i.e., method of lower accuracy), and U concentration could generally be detected over 5 ppm.

A relative comprehensive study on samples from outcrops in the Mórágy Mountains were performed in 1974 (NAGY, 1974 - J-0656). Granitoids and metamorphites were divided in a detailed way. Faciology and phases of granitization was also applied for classification.

Elaboration of rock samples from the surface is represented in table 7. Uranium contents of the western and the eastern areas are different, therefore, separated U mean values were calculated. Z. Nagy stated that U content of granites (first phase) is less than that of microaplites (second phase). At the same time, Th an K tends to decrease. From the east to the west U content increases in both granites and microgranites. U and Th content of basic dyke rock is relatively high which is attributed by the author to lateral transportation along the faults.

On the basis of analysis of all surficial samples (including sedimentary rocks, metamorphic schists, limestones, Triassic, Miocene and Pleistocene formations), the author suggested the following mean values for the area:

U: 8,6 pp Th: 30,5 ppm K: 3,7 %

Report J-0656 (NAGY, 1974) deals with granitoid formation found in boreholes out of the strictly speaking Mórágy Mountain but in its vicinity. This author evaluates boreholes Martonfa-1, Szilágy-1 and 2 as well as Báta-1, Bátaszék-1 and Alsónána-1.

TABLE 5

Mean and maximum U and Th values of rocks of the aerial anomaly 89 (Szederkényi, 1965)

Rock type	U average (ppm)	Th max (ppm)	Samples (pcs)
Granite	2-4 (max. 10)	36	19
Aplogranite	10	17	4
Venite	10	24	1
Bostonite dykes	10	56	3
Alkaline basalte („diabase") dyke	2-4	43	7
Dyke (friction breccia, cementated by carbonates)	10	40	5

TABLE 6

Mean U-Th contents of fresh and weathered granites of Mórágy (Kósa, 1977)

Rock type	U (ppm)	Th (ppm)	K (%)
Granite (fresh)	7	33	4,3
Granite (weathered)	5	33	4,1

TABLE 7

Radiometric study on rocks of the Mórágy Mountain in the year 1974 (Nagy, 1974)

Rock type	U (ppm)		Th (ppm)		K (%)		Samples
	aver.	max.	aver.	max.	aver.	max.	(pcs)
Agmatite	10,2	27	27,5	56	2,5	4,4	21
Migmatite	3,5	9	26,6	60	3,9	7,5	13
Pseudopegmatite	6,7	11	20,5	67	2,6	6,4	8
Granite, E	5,3	33	32,0	60	4,3	6,8	69
Granite, W	9,1	70	43,4	320	3,6	7,0	198
Microgranite, E	8,7	15	25,7	45	5,0	6,5	3
Microgranite, W	15,0	21	29,0	60	2,4	5,7	4
Aplogranite	5,5	25	47,8	100	3,9	7,2	33
Aplite	16,8	65	33,3	85	3,8	7,5	51
Bostonite	14,5	32	35,1	75	2,6	4,5	10
Lamprophyre	6,8	18	25,4	42	4,1	7,0	13
Mafic dyke rocks	12,3	31	20,2	21	2,3	2,8	4
Granite (carbonated)	3,0	5	21,4	40	3,1	5,2	5
Hydrothermalithe	18,1	130	18,1	45	2,1	3,7	15
Hornblende-schists	1,4	3	7,8	13	1,9	3,7	18

bored in the western and the eastern margin, respectively (1.1.2. and 1.2.1. areas - figure 1). Mean values of the radioactive elements according to different types of the samples collected from these boreholes are listed in table 8. As it was found in the cases of samples collected from the surface, U contents of these samples tend to increase from the east to the west. (The author noted that borehole Bátaszék-1 does not show this tendency, possibly, because the two samples were obtained from a place of maximum gamma intensity.)

TABLE 8

Mean radioactive element content of granitoid formations from the boreholes in the immediate vicinity of the Mórágy Mountain (Nagy, 1974)

Rock type	Borehole	U (ppm)		Th (ppm)		K (%)		Sample (pcs.)
		aver.	max.	aver.	max.	aver.	max.	
Pseudopegmatite	Bátaszék-1	4,5	5	40,0	42	3,1	3,3	2
	Szilágy-1	5,5	6	42,0	45	4,5	5,1	2
Granite	Bátaszék-1	7,5	11	47,7	72	3,4	5,2	39
	Alsónána-1	4,5	9	25,3	37	4,2	5,2	22
	Báta-1	16,0	16	15,5	16	5,7	5,8	2
	Szilágy-1	5,4	15	26,9	40	4,3	4,9	7
	Martonfa-1	12,1	32	25,8	37	4,7	7,2	25
Aplogranite	Bátaszék-1	21,0	21	24,0	24	5,9	5,9	1
Bostonite	Alsónána-1	4,8	10	22,3	40	4,4	5,2	12
Granite	Alsónána-1	6,7	9	25,0	36	3,8	4,6	13
(cataclastic)	Báta-1	7,5	9	42,5	44	3,3	4,0	4
Granite	Báta-1	6,9	14	49,0	63	3,3	4,4	26
(carbonated)	Alsónána-1	4,0	4	22,0	22	4,1	4,1	1

TABLE 9

Radioactive element conditions of formations in the Mórágy Mountain (Nagy, 1974)

Rock type	U	Th	K	Samples
	accumulation factor			(pcs)
Agmatite	1,2	0,9	1,2	21
Migmatite	0,4	0,9	1,1	13
Granite, E	0,6	1,0	1,2	69
Granite, W	1,1	1,4	1,0	198
Aplogranite	0,6	1,6	1,1	33
Aplite	2,0	1,1	1,1	51
Bostonite	1,7	1,2	0,7	10
Lamprophyre	0,8	0,8	1,1	13
Alkalinebasalt (diabase)	0,5	0,9	1,4	11
Granite (carbonated)	0,3	0,7	0,8	5
Hydrothermalite	2,1	0,6	0,6	15
Hornblende-schists	0,2	0,3	0,5	18
Helvetian sand	0,8	0,4	1,1	75
Cainozoic clay	1,6	0,5	0,9	17

In this report, Z. Nagy attempted to calculate radioactive element factors of the given rock types, i.e. to demonstrate how the formations of the Mórágy Mountains relate to each other according to their radioactive element contents (table 9) (accumulation factor = mean value for the formation/mean value for the area). Here, there is also an obvious tendency of increasing accumulation from the east to the west: 0,6→1,1. Higher U accumulation of hydrothermal formation is evident. Aplite and bostonite are relatively more accumulated. The well-known fact that young formations may fix U in higher quantity can also be observed. There is a characteristic difference between distribution diagram of U contents of the western and eastern granites.

TABLE 10

Radiometric analyses of weathered granite samples from boreholes in the Mórágy Mountain and its environment (Kósa, 1985)

Borehole	Depth (m)	Sample 12-K-	U (ppm)	Th (ppm)	K (%)
Martonfa-1	780,0	1218	30	27	2,8
	784,0	978	2	37	5,8
	784,7	978	5	28	6,3
Szilágy-1	498,7	970	3	19	4,5
	501,6	971	4	28	3,7
Szilágy-2	630,0	999	15	23	3,6
Fazekasboda-1	54,3	557	12	10	3,0
	55,0	558	5	29	6,1
	61,1	563	12	10	1,0
	62,9	566	11	10	1,1
	69,0	1000	8	25	4,6
Fazekasboda-2	78,0	653	12	11	4,7
	87,4	1017	5	28	4,1
	93,4	1018	5	24	2,7
Alsónána-1	156,2	938	3	21	4,3

TABLE 11

Radiometric analyses of rocks from the borehole Szalatnak 3 (Várszegi, 1971)

Sample	Rock type	Radiometric			Chemical	
		U (ppm)	Th (ppm)	K (%)	U (ppm)	Th (ppm)
8563	Diorite-syienite, (quartzic)	12	45	5,8	5	35
8562	Diorite-syienite (quartzic)	16	46	6,1	12	43
8561	Pyroclastics (carbonated)				9	44
8560	Granodiorite (carbonated)	3	20	3,8	3	15
8559	Diorite	12	39	5,0	8	42
8558	Diorite	9	33	5,3	4	36
8534	Dyke rock (essexit typ)	3	11		2	7
8533	Andesite				4	14
8532	Syenite	4	37	5,4	3	32
8530/a	Syenite				2	25

It must be noted that T. Szederkényi made a summary report on boreholes in Szilágy and Bátaszék area (SZEDERKÉNYI, 1962 - J-0062). Unfortunately, sensitivity of analytical methods of that time did not allow the correlation of the detailed petrographic evaluation with radiological data.

Radiometric analyses of weathered granites exposed by boreholes in the Mórágy Mountains and its vicinity were collected by L. KÓSA (F-1602). These are listed in table 10. Moreover, KÓSA send 14 samples for chemical U and Th analysis. These samples coming from the boreholes Feked-1, -2, -4, -5, -6, and are described in manuscript no. F-1504 (KÓSA, 1985). The analyses were surely done, however, results have not been available. It is expected to come to light during the further arrangement of the data bank.

RADIOLOGICAL CONDITIONS OF CRYSTALLINE FORMATIONS IN THE MÁGOCS-ALSÓMOCSOLÁD-SZALATNAK AREA

There have been some boreholes in the area, however, only few analytical data have been found. Research work performed in this area was reported by K. VÁRSZEGI (1971 - J-0142).

Beside a detailed petrographic and tectonic study, only the samples from crystalline basement exposed by borehole Szalatnak-3 from 510-580 m were published. Even analyses of these samples are not complete. Description of the rocks and the analytical result are listed in table 11.

On the basis of the chemical analyses, mean concentrations of the samples listed in this table are 5,2 and 29,3 ppm for U and Th, respectively. Disregarding essexite-type (basic) dyke rocks, mean concentrations increase: U = 5,6 ppm, Th = 31,8 ppm. Mean values of the radiometric analyses (U = 8,4ppm; Th = 33 ppm) are similar to those of samples from boreholes of the Mórágy Mountain (U = 8,1; Th =35,1).

RADIOLOGICAL CONDITIONS OF CRYSTALLINE BASEMENT ROCKS IN PÉCS AND ITS ENVIRONMENT

As it is mentioned above, granitoid rocks in Pécs are weathered and difficult to get at. Granitoid formations were exposed by the U exploration well no. 4716. Luckily, it was continued to clear tectonic conditions, and exposed formations of the crystalline basement. More than 300 samples were petrographically studied by L. Kósa, and these samples were analysed for determination of U and Th content (KÓSA, 1980 -J-0917).

Tables 12 and 13 show radioactive element content of the rocks grouped in detailed and comprehensive ways.

It must be noted that three samples qualified as metaarkose coming from the point of maximum radiation intensity in the section 1110-1113 m had much higher mean values than the mean value above:

U = 17,5 - 20 ppm Th = 32 - 53 ppm.

Comparing layered migmatites to diatexites, there is remarkable difference between their Th contents. While Th/U = 6 for layered migmatites, this value is 11 for diatexites.

The crystalline basement (mainly metamorphic rocks) was found by several boreholes south of Pécs. A petrographic evaluation of three of them was made by K. TÖRÖK Jr. (TÖRÖK, 1986 - J-1140 in his diploma work). Two-mica gneiss ranging from 1124,8 to 1172 m was intersected by structure well XII near Szentlőrinc village. Chlorite gneiss, muscovite gneiss and two-mica gneiss ranging from 1533,6 to 1701 m was intersected by borehole Máriagyűd-1. Borehole Nagykozár-2 exposed two-mica schist and milonite between 1953,1 and 1964,2 m as well as pink gneiss and cataclasite originated from orthoclase gneiss was intersected between 1964,2 and 1992,4 m. Unfortunately, the petrographically evaluated cores were not radiologically analysed in the frame of this work, and analytical results concerning these samples have not been found.

TABLE 12

Radiometric analyses of granitoid formations of the borehole 4716 (Kósa, 1980)

	Rock type	U (ppm)	Th (ppm)	Mintasz.(db)
Migmatite	Biotite migmatite	4,0	23	30
	Migmatite (layered)	3,4	23	32
	Migmatite (porphyroblastic)	4,1	25	28
	Migmatite (leucosome)	5,0	23	20
Diatexite	Diatexite (biotitic)	2,7	36	49
	Diatexite	3,0	34	41
	Aplitoid	4,0	40	14
	Microgranite	3,8	38	5
	Skialith	3,4	32	12

TABLE 13

Radiometric analyses of formations of the borehole 4716 (Kósa, 1980)

Rock type	U (ppm)	Th (ppm)	Samles (pcs)
Phyllite, metasandstone, metaarkose, sericiteschist	2,2	15	99
Layered migmatite	4,1	23	110
Diatexites	3,0	34	121
Fault zone (clay minerals)	2,8	20	21
Gneiss	2,2	22	3

TABLE 14

Radioactive element content of granitoids in the Mórágy Mountain and the W Mecsek Mountains (Kósa, 1977)

Area	Rock type	U (ppm)	Th (ppm)	K (%)
Mórágy Mountain	Granite (fresh)	7	33	4,3
	Granite (leached)	5	33	4,1
W Mecsek	Granite (fresh)	23	26	3,3
	Granite (leached)	8	24	2,9

TABLE 15

Uranium and thorium content of granitoid rocks in the W Mecsek Mountains (Buda, 1984)

Rock type	U		Th		Abundance
	ppm	σ	ppm	σ	(%)
I. Diorite, tonalite	2,6	± 1,3	28,3		11
II. Granodiorite, quartzmonzonite	15,5	± 13,5	40,8	± 25,2	32
III. Monzogranite	5,5	± 3,5	22,4	± 15,4	53

Note: uranium concentration of type II ranges from 3,5 to 4,5, variation of thorium is lower than that of uranium.

ENVIRONMENT OF GRANITE OUTCROPS NEAR NYUGOTSZENTERZSÉBET-NAGYVÁTY, RADIOLOGICAL CONDITIONS OF CRYSTALLINE BASEMENT IN THE AREA WEST OF THE MECSEK MOUNTAINS

Metarhyolite near Gyűrűfű village (west margin of the Mecsek Mountains) was begun to study as early as the first decade of the uranium exploration; later, research of the granite outcrops near Nyugotszenterzsébet and Nagyváty villages started. Possibility of a study on the surface is very limited because of the small extension of the exposed rocks. During the drilling research of U accumulation near Kővágószőlős in the area west of the village some boreholes exposed granitic rocks under Permian beds in the environment of Korpád village.

Development in analytical sensitivity made correct detection of low concentration differences of radioactive elements possible. This way, it could correctly be stated that U content of granite from western part of the Mecsek Mountains is higher than that of granite from the eastern part of the mountains as well as weathering resulted in a significant decrease in U concentration of the western granite. It was interesting, since it was questionable whether origin of U ore in Mecsek Mountains can be explained by dissolved uranium of significant quantity, and whether usable U accumulation is possible in other younger sediments.

L. KÓSA dealt with this problem in his report J-0491 and J-0401 (KÓSA, 1977). He compared radioactive element contents of the western and the eastern granites, and studied their fresh or weathered state (table 14).

In a later report, GY. BUDA (BUDA, 1984 - J-1088) studied granitoid rocks of the W Mecsek mountains from a mineralogical-petrological point of view, and published chemical U and Th analyses, too. He distinguished three types of rock (table 15).

Examples for these types together with the sampling places is listed in table 16. Variety of rocks belonging to type II is obvious.

Samples from crystalline basement situated in the western margin of the Mecsek Mountains, west of Bükkösd fault line, were analysed by L. KÓSA (KÓSA, 1985 - F-1533).

Mean values of the analyses of formations from boreholes exposed granitoids are listed in table 17. Besides the mean values, σ-values (standard deviation) are also given.

Data published in report F-1533 suggest that analyses of samples from several boreholes in the western granite area were preliminary elaborated. It is supposed that L. KÓSA used these data for his reports J-0401 (1977) and J-0491 (1977). Since these are direct connection with given boreholes, these data are listed in table 18.

There are several hundreds analytical results in reports F-1603 and 1606. However, these data can not be identified, only the fact that these come from samples collected from the Western Mecsek Mountains, and that most of them are in connection with the crystalline basement. Probably, these data were used for calculation of mean values published in other reports.

TABLE 16

Uranium, thorium and potassium content of the W Mecsek Mountains (Buda, 1984)

	Borehole	Depth (m)	U (ppm)	Th (ppm)	K (%)
I.	Dinnyeberki-19	77	1,7	4,0	-
	Nyugotszenterzsébet-6	52	3,3	58,3	4,3
	XIII. struct. (Bükkösd)	761	6,4	6,2	-
	Nagyváty-101	77	4,1	38,2	4,5
	Nagyváty-101	70	1,3	12,5	5,3
II.	9016 (Dinnyeberki)	261	7,9	9,4	4,2
	9016 (Dinnyeberki)	265	3,6	4,4	-
	9017 (Dinnyeberki)	452	11,5	77,0	-
	9017 (Dinnyeberki)	495	16,9	60,5	3,2
	Dinnyeberki-203	53	6,5	24,0	3,0
	Almáskeresztúr-5	283	18,6	28,3	-
	Nagyváty 2/1	131	43,5	61,4	5,6
	Nagyváty-104	67	3,5	24,8	-
III.	Nyugotszenterzsébet-5	35	6,5	8,7	-
	Nyugotszenterzsébet-5	38	4,0	17,5	-
	Nyugotszenterzsébet-6	29	2,8	13,6	3,5
	Nyugotszenterzsébet-6	61	3,6	52,8	3,9
	Almáskeresztúr-5	239	7,3	22,5	-
	XIII. struct. (Bükkösd)	703	13,1	40,7	-
	Nagyváty-104	66	3,0	17,4	-

TABLE 17

Means of analysed samples of boreholes exposing granitoids of the W Mecsek Mountains for the every formation (Kósa, 1985)

Sample	Subsurface sampling (m)	Rock type	Means of chem. analisys (ppm)		Sample (pcs.)
			U (±σ)	Th (±σ)	
	Db-44 46,7-87,3	GRANITOIDS	2,5 (1,3)	30 (8,7)	36
		granite-gruss	3,5 (0,8)	30 (8,1)	10
		granite	1,6 (0,5)	34 (6,7)	21
		granite (with feldspar)	4,7 (0,9)	17 (1,8)	5
9-K--26464--26480	Db-28 71,0-96,6	GRANITOIDS microgranite (fresh nad weathered)	5,0 (1,9)	23 (3,4)	14
	Db-45 65,6-102,5	granite-gruss	2,6 (0,9)	31 (9,5)	14
	Nyszterzs.-4 96,5-125,3	GRANITOIDS	8,0 (5,5)	23 (8,6)	32
		granite (yellow)	4,6	17	4
		granite (pink, leached)	2,9	27 max. 76	
		granite (pink, fresh)	11,8	27 max. 42	11
		feldspar dyke	18,0	35	3
		granite (green)	10,0	18	9

Sample	Subsurface sampling (m)	Rock type	Means of chem. analisys (ppm)		Sample (pcs.)
			U (±σ)	Th (±σ)	
		granite (weathered)	7.7	20	5
	Nagyváty-103	GRANITOIDS	10,0 (8,0)	27 (9,0)	45
	75,1-120,7	granite-gruss	9,7 (9,9)	27 (10,0)	12
		granite (red)	11,3	30	14
		granite (porphyroblastic)	8.8	26	10
		fault clay	6.6	24	7
	Nagyváty-102	GRANITOIDS	8,3 (5,3)	36 (10,0)	28
	79,3-102,0	granite (weathered)	4,4 (1,9)	27 (4,1)	7
		microgranite	6.9	43 (6,6)	4
		fault clay	4.1	34 (11,0)	4
		microgranite	13,0 (4,1)	40 (9,8)	10
	9018 (Korpád)	GRANITOIDS	10,0 (6,8)	29 (3,6)	52
	425,4-539,4	granite-gruss	2,5 (0,8)	27 (3,5)	16
		granite (green)	13,0 (5,1)	30 (3,3)	31
		granite (red)	17,0 (5,5)	28 (2,1)	5
	Nagyváty-4	GRANITOIDS			
	153,7-471,1	feldspar dyke	16,0 (4,4)	17 (4,5)	23
		granite (red)	12,0 (4,7)	28 (7,3)	69
		granite (grey)	13,0 (2,8)	25 (5,2)	64
		granite (carbonate-bearing)	10,0 (2,5)	23 (3,7)	11
		granite dyke	12,0 (3,1)	33 (6,4)	7
	Almáskeresztúr-5	GRANITOIDS			
	127,6-536,0	granite (pink)	6,5 (1,8)	29 (3,8)	26
		microgranite	8,9 (2,0)	30 (3,8)	11
		granite	13,8 (5,0)	32 (4,7)	20
		granite (grey)	5,4 (1,4)	29 (1,8)	5
		granite (amphibole-bearing)	6,7 (1,3)	28 (2,1)	12
		granite (bright grey)	6,0 (2,0)	27 (4,5)	25
		microgranite (pink)	8,5 (2,1)	32 (2,6)	22
		microgranite, anomalistic tract	16,5 (4,7)	64 (29,0)	5
		microgranite (carbonate-bearing)	17,0 (13)	32 (3,5)	1
		microgranite (weathered)	8,6 (3,0)	30 (3,9)	4
		microgranite (grey)	7,1 (1,8)	23 (5,3)	9
	127-159	feldspar dyke	4,7 (2,3)	14 (8,6)	7
	287-300	feldspar dyke (pink)	13,5 (3,7)	16 (3,2)	18

TABLE 18

Analytical data connecting to some boreholes in the W Mecsek Mountains (Kósa, 1985)

Sample	Rock type	Means of chemical analisys					
		U (ppm)	pcs.	Th (ppm)	pcs.	K (%)	pcs.
9006 (Korpád)	Granite (fresh)	24,8	10	25,0	1	1,5	2
	Granite (weathered)	8,8	6	16,5	2	4,4	2
9008 (Korpád)	Granite (fresh)	26,0	1	30,0	1	-	
	Granite (weathered)	6,5	2	-		-	
9010 (Korpád)	Granite (fresh)	-		-		-	
	Granite (weathered)	5,2	5	38,6	5	6,2	5
9011 (Korpád)	Granite (fresh)	-		-		-	
	Granite (weathered)	4,0	6	37,3	6	5,8	6
9012 (Korpád)	Granite (fresh)	25,5	4	31,3	3	-	
	Granite (weathered)	-		-		-	
9013 (Korpád)	Granite (fresh)	-		-		-	
	Granite (weathered)	3,0	1	-		-	
9014 (Korpád)	Granite (fresh)	30,0	1	20,0	1	3,0	1
	Granite (weathered)	6,5	2	-		-	
9015 (Korpád)	Granite (fresh)	20,6	29	27,2	29	3,8	28
	Granite (weathered)	5,5	2	39,0	2	2,8	2
Nyugotszenterzsébet-1	Granite (fresh)	36,0	1	20,0	1	1,0	1
	Granite (weathered)	-		-		-	
Nyugotszenterzsébet-2	Granite (fresh)	31,0	3	19,3	3	2,5	3
	Granite (weathered)	-		-		-	
Nyugotszenterzsébet-3	Granite (fresh)	22,5	2	23,0	2	4,1	2
	Granite (weathered)	6,0	3	17,6	3	3,9	3
Almáskeresztúr-1	Granite (fresh)	34,5	2	33,5	2	4,6	2
	Granite	-		-		-	

Sample	Rock type	Means of chemical analisys					
		U (ppm)	pcs.	Th (ppm)	pcs.	K (%)	pcs.
	(weathered)						
Helesfa-2	Granite (fresh)	12,5	2	33,5	2	5,1	2
	Granite (weathered)	3,3	3	30.0	2	4,4	2
Nagyváty-1	Granite (fresh)	46,0	1	21,0	1	1,4	1
	Granite (weathered)	-		-		-	

CONCLUSIONS

1, On the basis of U, Th and K analyses of rock samples from the Mórágy Mountains and the area east of the Mecsek Mountains, the following conclusions can be drawn:

a. Mean values of U = 2,2 ppm and Th = 10,1 ppm are detected by aerial measurements over granitoid rocks covered by loess more than 90 %.

b. Mean values of granitoid samples for the whole area are: U = 8,6 ppm and Th = 30,5 ppm,

c. Mean values of samples qualified as granite are: U = 8,2 ppm and Th = 40,1 ppm.

d. U content ratio for fresh and weathered granites is 7:5 (1,4); Th content ratio for fresh and weathered granites is 33:33 (1,0).

e. U content ratio for western and eastern part of the Mórágy Mountains is 1,5-1,6 (regarding both surface and boreholes). Th content ratio for western and eastern part of these mountains is 1,3 and 0,7 for samples from surface and boreholes, respectively.

f. Accumulation factors (=mean value for formation/mean value for the area) are: Aplite = 2,0; Bostonite = 1,7; Hydrothermal formations = 2,1; Granite = 1,0; "Western" granite = 1,1; "Eastern" granite = 0,6.

g. Granite from the Mórágy Mountain has higher (approximately twice) U and Th content than the world average for granite.

2, Mean values of U and Th content of crystalline basement in the Mágocs-Alsómocsolád-Szalatnak area (U = 8,1 ppm; Th = 35,1 ppm) are similar to those of samples from boreholes in the Mórágy Mountain.

3, Radiological conditions of granitoids of the western area can be summarised as it follows:

a. Granites west of the Mecsek Mountains have higher U and lower Th contents than granites east of these mountains.

b. "Western" granites are highly sensitive to leaching. A fresh granite may loose 60 % of its U content even in covered borehole. Loss of Th is only about 15 %.

c. Dissolved U re-precipitated in young sediments as important accumulation, therefore, an intensive migration of U solution can be regarded to be proved.

d. Uranium content of granodiorite-quartz monzonite type of the granitoid rocks is 3-5 times higher than that of diorite or monzogranite; its Th content is 1,5 times higher. Variety of the U content is the highest in the case of this type (3,5-43,5 ppm).

ACKNOWLEDGEMENT

This work has been supported by the National Science Research Foundation (OTKA) No. F 017369.

REFERENCES

BUDA, GY. (1984): Vizsgálati jelentés a Nyugati-Mecsek területén mélyfúrásokkal feltárt granitoidok ásvány-kőzettani vizsgálatáról. J-1088, Doc. Dept. of Mecsekérc Enviroment Protection Co., Manuscript.

KARDOS, I. et al. (1987): Jelentés az 1986. Évi légi gammaspektrometriai mérések terepi ellenőrzéséről a Mórágyi-hegység területén. J-1239, Doc. Dept. of Mecsekérc Enviroment Protection Co., Manuscript.

KÓSA, L. (1977): Irányelvek a Nyugati-Mecseki terület nyomdetektoros kutatásához. J-0401, Doc. Dept. of Mecsekérc Enviroment Protection Co., Manuscript.

KÓSA, L. (1977): Hazai gránitok urántartalma. J-0491, Doc. Dept. of Mecsekérc Enviroment Protection Co., Manuscript.

KÓSA, L. (1980): Pécs-Bárányteto 4716/1 sz. fúrásban feltárt metamorf és granitoid kőzetek radiokémiai vizsgálatának vázlata. J-0917, Doc. Dept. of Mecsekérc Enviroment Protection Co., Manuscript.

KÓSA, L. (1985): A DK-Dunántúli gránitokat feltáró fúrások (főleg Ny-Mecseki) mintaelemzései és azok feldolgozásának mukafüzete. F-1504, Doc. Dept. of Mecsekérc Enviroment Protection Co., Manuscript.

KÓSA, L. (1985): Ny-Mecsek, Mórágyi-hegység és Velencei-hegység gránitmintáinak elemzési adatai. F-1533, Doc. Dept. of Mecsekérc Enviroment Protection Co., Manuscript.

KÓSA, L. (***): A Mórágyi-hegység és környékéről származó fúrások gránitmintáinak U, Th és K tartalma. F-1602, Doc. Dept. of Mecsekérc Enviroment Protection Co., Manuscript.

KÓSA, L. (***): A Mecsek és Villányi hegység közötti terület felszíni magmás kőzetmintáinak U, Th, K tartalma. F-1611, Doc. Dept. of Mecsekérc Enviroment Protection Co., Manuscript.

KÓSA, L. (***): A Mecsek és Villányi hegység közötti területen mélyült fúrások magmás kőzetmintáinak U, Th, K tartalma. F-1612, Doc. Dept. of Mecsekérc Enviroment Protection Co., Manuscript.

NAGY, Z. (1974): Mórágyi-hegység kőzeteinek sugárzó anyag eloszlása a négykomponenses elemzések alapján. J-0656, Doc. Dept. of Mecsekérc Enviroment Protection Co., Manuscript.

SZEDERKÉNYI, T. (1962): A II. sz. kutatócsoport összefoglaló jelentése a Szilágy-Bátaszék kutatási területen 1961. évben végzett kutatásokról. J-0062, Doc. Dept. of Mecsekérc Enviroment Protection Co., Manuscript.

SZEDERKÉNYI, T. (1965): Földtani jelentés a Mórágyi-hegységi légigamma anomáliák földi ellenőrzéséről. J-0130, Doc. Dept. of Mecsekérc Enviroment Protection Co., Manuscript.

TÖRÖK, K. (1986): Adatok a Dél-Dunántúl kristályos aljzatának felépítéséhez. J-1140, Doc. Dept. of Mecsekérc Enviroment Protection Co., Manuscript.

VÁRSZEGI, K. (1971): Összefoglaló jelentés a szalatnaki területen végzett kutatásokról. J-0142, Doc. Dept. of Mecsekérc Enviroment Protection Co., Manuscript.

VINCZE, V. (1961): A II. sz. kutatócsoport 1960. Évi jelentése a Mórágyi gránitterületen végzett komplex autós-gamma felvételről. J-0053, Doc. Dept. of Mecsekérc Enviroment Protection Co., Manuscript.

Vincze, V. (1975): Jelentés az 1974-ben végzett komplex radiológiai anomália ellenőrző vizsgálatokról, Mecsek és Mórágyi gránitterület. J-0667, Doc. Dept. of Mecsekérc Enviroment Protection Co., Manuscript.

*** (***): Ny-Mecseki fúrások és felszíni minták elemzési eredményei. F-1603, Doc. Dept. of Mecsekérc Enviroment Protection Co., Manuscript.

***(***): Ny-Mecsek, Zselic és Hegyhát területéről származó felszíni és fúrásbeli minták elemzése. F-1606 Doc. Dept. of Mecsekérc Enviroment Protection Co., Manuscript.

Manuscript received 10. June 1999.

Acta Mineralogica-Petrographica, Szeged, XL, 139–156, 1999

NATURAL RADIOACTIVE ELEMENT CONTENT OF OLD GRANITOID ROCKS IN THE GREAT HUNGARIAN PLAIN

E. PÁL MOLNÁR*, B. KÓBOR*

Department of Mineralogy, Geochemistry and Petrology, Attila József University

ABSTRACT

Mean concentrations of radioactive elements of granitoid areas were determined for lithostratic and geodynamic units on the basis of analyses of natural radioactive element content of borehole samples from old granitoid rocks of crystalline basement of the Great Hungarian Plain.

Granitoids of the basement of the Great Hungarian Plain can be characterised by high U and Th content. Uranium content exceeds mean value for granites in the Earth for almost every granitoid formation of the Great Hungarian Plain; in some places it is three times higher.

Radiological conditions of the given area comparing with that of Hungary as well as local features, accumulations, and leaching are discussed in summaries found at the end of subdivisions.

Accumulation factor for radioactive elements of Codru Terrain is given for units (complex by complex), while that of Kunság Terrain has been determined for subunits, too.

INTRODUCTION

Radiometric analysis of more than 150 granitoid rock samples from the crystalline basement of the Great Hungarian Plain was performed in the Department of Mineralogy, Geochemistry and Petrology, Attila József University, Szeged.

NP-424 P four-channel amplitude analyzer, ND-424 L detector, 7S117068 scintillator, NZ-490 lead castle and NY-424 Marinelli vessels were used for radiological analysis of the samples. The following data were detected by radioactive isotopic measurements:

- energy resolution by NaJ (Tl) scintillator referring to Cs137 661 keV gamma line: 8,4 %,
- base line scale energy linearity in the energy range of 0,02-1,5 MeV: 1,5 %,
- error at 2,7 MeV: 5 %,
- stability: a. peak position change referring to Cs137661 keV gamma line: $\pm$ 5 keV;
  b. impulse number change in peak position: according to statistics.

This laboratory apparatus provides simultaneous determination of four radiological parameters: specific activity, Th, U (Ra) (accepting an equilibrium for these two elements is practically correct, and deviation should be studied by more sensitive and reliable methods) and K concentrations.

Sample vessel filled by inert material (quartz sand) was used for determination of background values.

Detailed description of laboratory methods can be found in a text-book by SZEDERKÉNYI, PÁL MOLNÁR and VADOS (1994).

* H-6701 Szeged, P.O.Box 651, Hungary

Control measurements were performed in the Radiometric Laboratory of Mecsekérc Környezetvédelmi Rt. (Mecsek Ore Environmental Protection Company) (table 1). A multichannel spectrometric system (PCA - 3 Oxford analyzer and GR 2519 CANBERA Hp Ge detector) was used for rock-sample analysis. The obtained spectra were qualitatively and quantitatively evaluated by Gamma Trac Oxford Program.

Effective screening and relative high efficiency (25 %) of the measuring gauge as well as the long measuring time (20-25 thousands sec.) made reliable determination of the low radioactive element content possible, too. The gamma-spectrometry system was calibrated by international standards.

The difference between control samples and our measures was less than 10 % in every case.

Geographic position and petrographic characterisation of the units are also given, though, study on much more sample would need to prove a relationship between petrographic and radiological features.

RADIOLOGICAL CONDITIONS OF GRANITOID FORMATIONS IN CODRU TERRAIN (S-HUNGARIAN NAPPE BELT)

According to the widely accepted theory, continuation of Codru nappe system of the Romanian Apuseni Mountains can be found in the area of the Codru Terrain in the basement of Southern Great Hungarian Plain; regarding the Mesozoic formations, it corresponds to the Békés Zone.

It is supposed that it was formed before the Upper Cretaceous, during the Austrian-Pre Gosau Orogenic Phase. Bigger part of its area is in Vajdaság (Voivodina, Serbia) and in the northern part of Bánát. It is bordered by the Maros Ophiolite Zone in the south, and a half circle major tectonic line extending through Kelebia, Nagyszénás and Sarkadkeresztur villages in the north. On the basis of geodynamical studies and Pre Alpinic formations, further units (sub-terrains?) can be divided (SZEDERKÉNYI, 1998): Kelebia Complex (Unit), Tisza Complex (Unit), Battonya Complex (Unit), Sarkad-keresztúr Complex (Unit).

The eroded crystalline mass of Codru Terrain is characterised by three granitoid ranges divided by young tectonic movements, and by limbs of meso- and katametamorphic rocks joining with granitoid ranges:

1. The Mezőhegyes-Battonya range has a well-developed granite core; its northern limb is formed by crystalline schists of the Pusztaföldvár area, the southern one is in Romania.
2. Only the northern limb of the granitoid range having an axis zone of Deszk-Ferencszállás-Makó is in Hungary (Madaras-Kelebia-Ásotthalom-Üllés-Algyő area). Some narrow epimetamorphic zones of ENE-WSW strike with wide friction breccia belts are wedged into it at Algyő.
3. The Sarkadkeresztúr migmatite range can be found only in a length of 25 km in Hungary, its other part joints with the Codru Mountains in the east.

Battonya Complex (Battonya Unit)

Granite occurs in 48-50 % in drilling cores of metamorphic rocks from the Battonya Unit. This granite is dominantly light red, sometime grey, and porphyroblastic. Migmatite of the marginal zone represents further 15-20 %. In addition, this marginal

zone is formed by kata- and mesometamorphic gneiss and mica-schist alternating each other, aplite and pegmatite veins, and some amphibolite intercalation in some places. This complex is broken through by Lower Permian rhyolite conduits.

Since the nomenclature of metamorphic rocks of the units is quite varied depending on the authors, our classification is based on our own macro- and microscopic observations.

Radiometric analyses of fresh granitoid samples from boreholes in the Battonya Unit are listed in tables 2 and 3.

The following conclusions can be drawn from U, Th, K analyses of granitoid samples from the Mezőhegyes-Battonya granite range of Codru Terrain:

a. Mean U-Th-K content of granitoids of the Battonya Unit in the cases of fresh and weathered rocks:

Rock	Specific activity (Bq/kg)	U (ppm)	Ra (ppm)	Th (ppm)	K (%)
Fresh rock	192	8.8	8.1	13.3	2.7
Weathered rock	159	5.5	4.7	11	2.8

b. Ratio of U and Th content of fresh and weathered granitoids is 8,8:5,5 (1,6) and 13,3:11 (~1,2), respectively.

In the cases of drill cores, considerable conclusions concerning leaching can not be drawn. Metasomatised or hidrothermally altered samples that possibly did not come from surficial weathering crust of the granite bodies were also regarded as weathered rock-type. It is quite frequent that U-Th concentration exceeds values characteristic for the given area. Moreover, local accumulations may occur both in fresh and weathered sections even within one drilling.

c. Comparing the Battonya granitoid samples with the well-known and radiometrically thoroughly analysed granitoids of Southern Transdanubia, it can be stated that

- Mean U content of the granitoid of the Battonya Unit is approximately similar to that of surficial granitoid of Southern Transdanubia, however, the latter has 2,5-3 times higher Th content.

d. Uranium content of granitoids of the Battonya granite area is about twice higher than the world average U content of granites. However, their Th concentration is lower than the world average.

e. Pegmatoid samples from this area are characterised by higher U content than the mean value for the area. This was the only case where provable relation could be found between the radiometric features and the petrographic characters (texture, grain-size, mylonitization, etc.) of the samples.

f. Mean U and Th concentrations of the samples from the western (Mezőhegyes) part of the Battonya granite range are 15 and 20,7 g/t, respectively.

Mean U and Th content of the samples coming from the Battonya-Dombegyháza area decreases (U: 9 g/t; Th: 14,5 g/t). Uranium content ratio of granitoid samples from the western and the eastern part of the Battonya Unit is ~1,6 for the western part; in the cases of Th contents, this ratio is ~1,42 for the western part.

TABLE 1

*Analytical data of the control samples**

Samples	Specific activity Bq/kg	U (g/t)	Ra (U_{equ})	Th (g/t)	K (%)
ÁGK 1663	260 ± 3,5%	14 ± 5%	14 ± 3%	6 ± 5%	4,6 ± 5%
ÁGK 1315	150 ± 4,5%	8 ± 4%	7 ± 1,5%	12 ± 2%	2,3 ± 3%
ÁGK 1447	100 ± 5,0%	6 ± 4%	5 ± 2%	6 ± 2%	0,8 ± 4%
ÁGK 1609	330 ± 2,0%	17 ± 2%	15 ± 1,1%	23 ± 2%	3,1 ± 2,5%
ÁGK 2134	105 ± 6,0%	3 ± 6%	3 ± 3%	10 ± 2%	2,2 ± 3%
ÁGK 1461	450 ± 2%	28 ± 3%	27 ± 1,2%	14 ± 3%	3,4 ± 4%
ÁGK 1657	195 ± 3%	7 ± 4%	6 ± 2%	9 ± 2%	4,1 ± 3%
ÁGK 1508	520 ± 2,5%	29 ± 3%	28 ± 1,2%	25 ± 2%	3,9 ± 4%
ÁGK 1659	1490 ± 2%	120 ± 2%	115 ± 2%	5 ± 15%	3,4 ± 5%
ÁGK 965	240 ± 3%	12 ± 3%	12 ± 1,3%	13 ± 2%	4,3 ± 3%

**Notes* - *specific activity in Ra-226 equivalent*
- *the relative calculating statistical error given in % means a reliability level of 95 %.*

TABLE 2

Radiometric analyses of fresh granitoid samples from the boreholes in the Battonya Unit

Borehole	Rock type	Depth (m)	Specific activity (Bq/kg)	U (g/t)	Ra ($U_{equi.}$)	Th (g/t)	K (%)
Mezőhegyes-1	microcline granite	1148-1150m	305	16	15	20	3.2
Mezőhegyes-1	"	1167-1168m	280	13	13	21	3.0
Mezőhegyes-2	"	1187-1188m	360	18	17	26	2.9
Mezőhegyes-3	"	1163-1166m	385	21	19	28	3.4
Mezőhegyes-5	granodiorite	1203-1204,3m	410	24	23	31	2.9
Mezőhegyes-6	microcline granite	1214-1216m	250	11	11	16	3.1
Mezőhegyes-12	"	1194,5-1195,5m	390	22	21	28	3.7
Mezőhegyes-16	microgranite	1183m	195	8	7	10	3.8
Mezőhegyes-16	"	1193-1195m	170	7	6	15	3.1
Mezőhegyes-17	"	1214-1217m	365	20	19	30	2.7
Mezőhegyes-18	"	1220-1220.8m	330	17	15	23	3.1
Mezőhegyes-19	granite	1200-1201m	185	8	6	10	4.1
Mezőhegyes-20	"	1184-1186m	210	10	10	12	3.6
Dombegyháza-	microcline granite	1436-1440m	140	8	7	11	2.4

Borehole	Rock type	Depth (m)	Specific activity (Bq/kg)	U (g/t)	Ra ($U_{equi.}$)	Th (g/t)	K (%)
DNy-1 Dombegyháza-	migmatite	1465-1469m	190	9	8	13	3.4
DNy-1 Dombegyháza-	microcline granite	1313-1315m	120	4	3	11	2.4
D-1 Dombegyháza-	biotitic migmatite	1350-1352m	150	8	7	12	2.3
DNy-2 Battonya-1	microcline granite	1051-1055m	285	12	12	16	4.1
Battonya-1	"	1067-1067,5m	210	12	11	19	4.0
Battonya-3	granodiorite	1087m	260	10	10	23	3.3
Battonya-5	microcline granite	1033-1036m	225	11	10	14	4.2
Battonya-5	"	1050-1050,5m	170	8	7	13	2.2
Battonya-6	granite	1043m	230	7	6	18	4.6
Battonya-10	granite	1072-1073m	130	7	7	13	2.3
Battonya-13	microcline granite	1042-1047m	185	8	7	15	3.8
Battonya-13	"	1047-1052m	155	6	6	14	3,6
Battonya-14	"	1044-1045,5m	205	9	8	14	4,2
Battonya-15	"	1075-1077m	170	8	8	13	4.0
Battonya-17	"	1031-1036m	155	4	4	15	3.9
Battonya-28	"	1077-1078m	295	12	11	16	4.2
Battonya-36	granodiorite	1024-1026m	240	9	8	19	3.4
Battonya-36	"	1032-1033m	215	8	7	20	3.2
Battonya-37	pegmatitic granite	1043-1045m	445	22	21	23	3.1
Battonya-37	migmatite	1056-1058m	280	13	12	13	4.1
Battonya-41	microcline granite	1073-1075m	190	7	7	9	3,7
Battonya-45	migmatite	1081-1084m	305	14	13	19	3.5
Battonya-47	microcline granite	1108-1109m	205	9	8	8	3.7
Battonya-48	microcline-porphyroblastic granite	1174-1176m	170	7	7	11	2.8
Battonya-64	microcline granite	1024-1025,5m	215	10	8	11	3.6

Borehole	Rock type	Depth (m)	Specific activity (Bq/kg)	U (g/t)	Ra ($U_{equi.}$)	Th (g/t)	K (%)
Battonya-64	microcline granite	1031-1032,5m	245	8	7	14	3.3
Battonya-K-14	biotite granite	1075-1077m	180	7	6	13	2.6
Battonya-K-15	"	1080-1083m-	215	9	8	14	3.1
Battonya-K-16	"	1072-1077m	170	6	6	12	2.6

TABLE 3

Radiometric analyses of weathered granitoid samples from the boreholes in the Battonya Unit

Borehole	Rock type	Depth	Specific activity (Bq/kg)	U (g/t)	Ra (U_{equ})	Th (g/t)	K (%)
Mezőhegyes-7	microcline gran. (weathered)	1198-1199.5m	135	4	3	8	1.5
Mezőhegyes-9	granodiorite (weathered)	1187-1188m	165	7	6	11	2.6
Mezőhegyes-11	pegmatitic microcline gran. (weathered)	1262-1265m	195	7	7	16	2.3
Mezőhegyes-13	microcline gran. (weathered)	1184-1190m	120	4	3	11	2.4
Mezőhegyes-14	muscovite gran. (berezitic)	1191-1195m	145	5	4	10	3.0
Mezőhegyes-14	„	1205-1207m	180	6	5	13	3.3
Mezőhegyes-15	„	1194-1198m	105	3	3	10	2.3
Kunágota-1	biotite granite (kaolinic)	1797-1804m	195	7	6	10	4.2
Kunágota-2	granite (weathered)	1908-1911m	145	5	4	11	3.8
Battonya-49	microcline gran. (weathered)	1046-1049m	120	3	3	8	2.9
Battonya-63	muscovite gran. (berezitic)	1029-1034m	210	6	5	14	4.1
Battonya-75	microcline gran. (weathered)	1065-1071m	110	3	2	6	2.4
Battonya-K-6	microcline gran. (weathered)	1019-1020m	205	7	6	16	3.6
Battonya-K-9	microcline gran. (weathered)	1058-1060m	100	3	2	6	2.1
Battonya-K-13	granite	1069-1071m	190	8	8	13	4.0
Battonya-K-17	muscovite granite	1059-1061m	215	10	9	8	3.4
Battonya-K-18	" (weathered)	1079-1082m	115	4	3	7	3.2

Borehole	Rock type	Depth	Specific activity (Bq/kg)	U (g/t)	Ra (U_{equ})	Th (g/t)	K (%)
Battonya-K-19	granite (kaolinic)	1052-1054m	165	7	7	12	3.0
Végegyháza-K-1	granite (kaolinic)	1287-1290m	215	6	5	19	2.7

Tisza Complex (Tisza Unit)

The Tisza Unit is a rock mass of epi-, meso- and katametamorphic rocks, mainly alternating gneiss–mica-schists with intercalations of some amphibolite and leptinolite (mesometamorphic acidic tuff), marble and dolomitic marble of greater quantity as well as frequent Upper Cretaceous banatite intrusions (Ferencszállás Formation). Migmatite zones and smaller granitic bodies (4x1 km) are known in the Deszk-Ferencszállás-Makó axis zone of the complex. They are formed by pink or light grey porphyroblastic granite (GYALOG, 1996).

These granite bodies are associated with aplite and pegmatite veins. Only the NW limb of the granitoid range can be found in Hungary (Madaras-Kelebia-Ásotthalom-Üllés-Algyő), its southern limb is in Yugoslavia (HAAS, 1996). In the Algyő area belonging to the northern limb some epimetamorphic bands of NE-WSW strike together with wide friction breccia zones are intercalated (Haas, 1996).

Granitoids are subordinated in the Algyő area, they occur in gneiss as 5-30 cm wide veins of aplite and microgranite (SZEDERKÉNYI, 1991).

Granite (dominantly light grey or pink porphyroblastic granite, subordinately micro- and medium-grained granite), occurs only in about 10-12 % of the cores from the Tisza Complex (Unit). Migmatite, aplite and pegmatite veins represent further 5-6 % (BALÁZS et al., 1984).

Radiometric analyses of granitoid samples from boreholes in the Tisza Unit are listed in table 4.

The following conclusions can be drawn from U-Th-K analyses of granitoid samples from Tisza Unit of the Southern Hungarian nappe zone (Codru Terrain):

a. Mean U-Th-K contents of granitoids of the Tisza Unit are 13,8 g/t, 10,9 g/t and 3,95 %, respectively.

b. The tectonically "tortured" cataclastic granite coming from the borehole Ferencszállás-8 has eye-strikingly high specific activity (1490 Bq/kg) resulted by the extreme high U content (120 g/t) of the sample. In all likelihood, it is a local maximum that could be resulted by local accumulation formed by solutions that contain leached uranium in a great quantity, and move in the fracture and collimation systems. Moreover, several km wide contact pneumatolytic and hydrothermal zone of "banatite" is characteristic for the Ferencszállás area.

This was the reason why the U concentration of the above mentioned sample was not taken into consideration in calculation of mean U content of granitoid formations of the Tisza Unit. This sample had increased the mean value for the area as high as 20,5 g/t because of the small number of samples. Otherwise, Th and K concentrations correspond to (or lower than) the mean value for the area (Th: 5 g/t; K: 3,4 %).

c. Mean U and Th contents of the granite of the Deszk-Ferencszállás-Makó axis zone are 12,6 and 10,6 g/t, respectively. There is a higher mean U concentration (15,2 g/t) in

the Algyő area which is supposed to be the northern limb of the above mentioned axis zone. The relatively high U concentration can be explained by the fact that the granitoid samples of this area are often coming from pegmatites or aplite veins, and they were frequently influenced by metasomatic impacts.

There is no relevant difference in the mean Th content (at Algyő: 11,2 g/t; Deszk-Ferencszállás-Makó: 10,6 g/t).

d. Area of granitoids of the Tisza Unit is not lithostratigraphically uniform since products and influences of young magmatism can be found there (SZEDERKÉNYI, 1991). We do not have enough samples to detect these differences. It can be stated, however, that the mean U content of the analysed granites is 3-4 times higher than the world average for granites, while their Th content is about 40-50 % lower than world average.

Sarkadkeresztúr Complex (Sarkadkeresztúr Unit)

Position of the Sarkadkeresztur Major Tectonic Unit has been discussed for a long time. According to the present statement of the Hungarian Stratigraphic Committee, it is a part of the Southern Hungarian Nappe Zone.

The buried basement range was exposed by gravitational measures as early as 1934-35. It begins at Sarkadkeresztúr as a comb of E-W strike, and ends in Romania 18-20 km east of this village.

It is composed of light grey diatexite and some porphyroblastic granite. Its NNW and SSE part join with a katametamorhic gneiss-mica-schist margin intercalated amphibolite (GYALOG, 1996). Tectonically intercalated mesometamorphic rocks also occur in subordinated amount (SZEDERKÉNYI, 1991).

Migmatite coming from two-mica schists and gneiss is the most frequent formation of the area. Most of the samples underwent metasomatism and/or sericitization, chloritization, albitization (BALÁZS et al., 1984), however, geological conditions of this process have been discussed.

Mean U-Th-K contents of granitoid samples from the Sarkadkeresztur Unit are listed in table 5.

The following conclusions can be drawn from U, Th and K analyses of granitoid samples from the range of granitic axis zone of the Sarkadkeresztúr Unit:

a. Mean U-Th-K contents of granitoid from the Sarkadkeresztúr Unit:

U: 9,1 g/t; Th: 13,3 g/t; K: 4-45 %.

b. Mean U-Th-K content of the unambiguously granite samples are:

U: 7,6 g/t; Th: 13,6 g/t; K: 4,36 %.

There is no difference between Th and K contents of migmatite and granite in the studied area, however, mean U content of the migmatite (9,8 g/t) is much higher than that of granite.

c. Conclusions concerning geographical distribution of the analysed elements and leaching differences between fresh and weathered samples cannot be drawn because of small number of samples. In general, it can be stated that the mean U concentration of granitoids of the area is twice higher and the Th content is 40-45 % lower than the world average for granite.

TABLE 4

Radiometric analyses of granitoid samples from the boreholes in the Tisza Unit

Borehole	Rock-type	Depth	Specific activity (Bq/kg)	U (g/t)	Ra (U_{equ})	Th (g/t)	K (%)
Algyő-30	microgranite (hydrothermal weathered)	2723-2725m	240	12	11	11	5.1
Algyő-56	medium-grained microcline granite	2519-2521m	195	8	7	6	4.2
Algyő-57	granite	2660-2663m	275	14	13	6	4.4
Algyő-68	microgranite	2662-2665m	310	21	20	13	4.1
Algyő-82	"	2697-2698,5m	220	12	11	15	3.8
Algyő-94	"	2605-2606m	410	26	26	16	3.2
Algyő-442	granite	2505-2507m	265	14	14	12	4.1
Deszk-1	granite	2580-2582m	190	8	8	9	3.5
Deszk-1/A	microgranite	2382-2385m	270	15	14	18	2.7
Ferencszállás-3	microgranite	2382-2385m	180	7	6	10	3.9
Ferencszállás-3	biotite granite	2390-2393m	235	7	7	12	4.2
Ferencszállás-4	granite	2321-2324m	260	12	11	15	3.8
Ferencszállás-5	migmatite	2422-2423m	195	7	6	9	4.1
Ferencszállás-8	cataclastic granite	2535-2538m	1490	120	115	5	3.4
Ferencszállás-12	granite	2365-2371,5m	260	14	14	6	4.6
Ferencszállás-35	granite	2324,6-2327,7m	470	31	29	12	4.1

TABLE 5

Mean U-Th-K contents of granitoid samples of the Sarkadkeresztur Unit

Borehole	Rock type	Depth (m)	Specific activity (Bq/kg)	U (g/t)	Ra (U_{equ})	Th (g/t)	K (%)
Sarkadkeresztúr-6	microgranite (chloritic)	2860-2863m	240	12	12	13	4.3
Sarkadkeresztúr-9	porphyroblastic migmatite	2700-2703m	205	8	7	10	4.9
Sarkadkeresztúr-19	cataclastic granite	2814-2832m	310	14	14	17	4.8
Sarkadkeresztúr-19	migmatite	2805-2814m	210	8	8	15	4.0
Sarkadkeresztúr-18	microcl.-bearing migmatite	2900-2901m	245	11	10	14	5.1
Sarkadkeresztúr-22	porphyroblastic granite	2762-2770m	190	7	6	11	4.2
Sarkadkeresztúr-22	porphyroblastic granite	2850-2856m	280	9	8	17	4.5
Sarkadkeresztúr-34	porphyroblastic granite	2714-2722m	230	7	7	13	4.4
Sarkadkeresztúr-33	granitoid (chloritic)	2942-2945m	185	6	5	10	3.9

RADIOLOGICAL CONDITIONS OF THE MIDDLE HUNGARIAN "PARAAUTOCHTHON" (KUNSÁG TERRAIN) IN THE BASEMENT OF THE GREAT HUNGARIAN PLAIN

The Middle Hungarian "autochthon" (actually "paraautochthon"), which is recently called as Kunság Terrain on the basis of geodynamical considerations (Szederkényi, 1998), extends from the Middle Hungarian Lineament to the Southern Hungarian Nappe Zone (Codru Terrain). According to our present knowledge, it stretches to Transylvania in the East where it forms the so-called Bihar "autochthonous" part of the Apuseni Mountains and surficial crystalline mass of the area north of these mountains (SZEPESHÁZY, 1978; DIMITRESCU, 1981; SZEDERKÉNYI, 1984, 1991, 1998; BALÁZS et al., 1986).

According to the widely accepted concept, there are two parallel major crystalline schist anticline systems of ENE-WSW strike (which becomes to be E-W at the state-boundary) with granitoid axis zone. In fact, it is a symmetrical rock-complex in which migmatite, kata- and mesometamorphic amphibolite-facies zones (sometime lower metamorphic gneiss and mica-schists belts) occur at both sides of an anatectic granitoid zone. Therefore, this terrain is divided into two geodinamic and lithostratigraphic units (sub-terrains): Mórágy Complex (Unit) and Körös Complex (Unit) (HAAS, 1996).

1. Mórágy Complex is a granite range extending from Szigetvár and can be traced along the line of Western Mecsek - Mórágy Mountain - Soltvadkert - Kecskemét - Cegléd. It is associated by metamorphic limbs affected by younger faults at their sides. There is an intercalation of lower metamorphic range of schists of Ófalu and metasandstones of Nagykőrös at the axis zone (HAAS, 1996).

2. Anticline of granitoid axis zone of the Körös Complex is not a continuous mass; it is formed by three granitoid bodies of 30-70 km length and 15-30 km width connected by a migmatite zone: Baja-Jánoshalma, Jászszentlászló-Pálmonostora and Endrőd ranges.

Granite is the dominant rock of this ranges. Similarly to Ófalu schists of the Mórágy Complex, there is intercalation of Upper Cretaceous metasandstones and carbonate phyllites at the axis zone (HAAS, 1996). Considering the area accumulation factor, mean values of units can be calculated rather than those of formation unless belonging of the part-areas to one formation is beyond debate. The studied areas are divided according to the classification recommended by the Hungarian Stratigraphic Committee in this paper. (Of course, this concerns Codru Terrain, too.)

Mórágy Complex (Mórágy Unit)

This range is of light red, orthoclase- and microcline-rich (and containing many plagioclase crystals in some places), porphyroblastic granodiorite (subordinately granite) with dark grey, biotite- and amphibole-rich xenoliths and a network of aplite and pegmatite veins. Feldspar porphyroblasts of the granite is often oriented (lineated). Size of xenoliths coming from the former basic rocks may reach some meters.

Characteristic rocks of the Mórágy Unit are Mórágy-type granodiorite (from Szigetvár to Miske) and granite (it is a muscovite granite without lineation in Cegléd region) (HAAS, 1996).

The granitoid axis zone is bordered by a zone containing migmatite and alternating low- and high metamorphic rocks (gneiss - amphibolite - mica-schist) from the north-west and the south-east (GYALOG, 1996).

The petrographically varied granite represents 60-65 % of the cores of metamorphic rocks coming from this unit of the basement of the Great Hungarian Plain, and further 15-18 % of the cores is granitoid migmatite coming from mainly the marginal zone.

Radioactive element content of granitoid samples of Mórágy Complex found in boreholes of basement of the Great Hungarian Plain is shown by table 6.

The following conclusions can be drawn from radiological analysis of granitoid cores of the Mórágy Unit coming from the basement of the Great Hungarian Plain:

a. Mean U-Th-K content of the studied samples coming from the unit (sub-terrain):

U: 13,54 g/t Th: 17,9 g/t; K: 3,58 %.

b. Mean U-Th-K content of samples that were unambiguously qualified as granite:

U: 13,3 g/t; Th: 17,8 g/t; K: 3,4 %.

Therefore, there is not any significant difference between radioactive element content of granite and that of migmatite (probably it comes from mainly the marginal zone) of the anticline.

c. Regarding the weathered samples, group of the leached samples from weathering crust (U: 6 g/t; Th: 17 g/t) definitely separates from that of muscovite and sericite containing samples affected by hydrothermal metasomatism, which have a U content not less than the mean value for the area (calculating for the whole unit).

d. Three areas having characteristic radioactive element content can be separated by radiological analysis of granitoids of the region. Rocks of these areas also differ from each other in their petrographical features. Because of these differences, which were also mentioned in the summarised petrological characterisation of the unit, this kind of examination of the samples is reliable:

Samples from the Kecel-Soltvadkert region have higher Th content (20 g/t) than the mean value for the area; their U and K content corresponds to the average of the formation (U: 12,9 g/t; K: 3,5 g/t).

Uranium concentration in the Kecskemét region is higher than that of samples from the other part-areas (17,2 g/t), while Th content (17,6 g/t) corresponds to the mean Th content of the Mórágy Unit.

Concentrations of muscovite granite of the Cegléd region are lower than mean values of the unit (U: 10,2 g/t; Th: 16,3 g/t); the low U content is particularly eye-striking.

Unfortunately, connection between radiological features and petrographical characters can not be proved, however, the authors emphasized importance of further studies.

Körös Complex (Körös Unit)

The Körös Complex shows a petrographical variety: it is formed by alternating meso- and katametamorphic gneiss and mica-schist with some intercalation of leptinolite (mesometamorphic tuff) and amphibolite of considerable quantity in the eastern part of Transtibiscia. In the axis zone of the unit granite bodies wedged by migmatite of great quantity are known (GYALOG, 1996).

The granites are dominantly pink, porphyroblastic, and generally not-oriented, however, differences corresponding to the part-areas can also be found here. Granitoids of the complex underwent strong tectonic movements, and suffered mylonitization, diaphtoresis and cataclasis (e.g., Kömpöc, Kiskunhalas, Jánoshalma).

Granitic bodies do not represent a continuous range within this unit but form three granitic areas of 15-30 x 30-70 km connected by migmatite. These areas are situated in the regions of Baja-Jánoshalma, Jászszentlászló-Pálmonostora and Endrőd. Granitoids or granites *sensu stricto* were also found in boreholes which are relative far from the axis zones characterized by the above mentioned villages; therefore it is discussed whether these granitoid part-units are real ranges or only granitoid areas.

Radiometric analyses of granitoid samples from boreholes of the Körös Unit are listed in table 7.

The following conclusions can be drawn from radiological analyses of granitoid samples from the Körös Complex (Körös Unit):

a. Mean U-Th-K contents of granitoids of the Körös Unit are:

U: 10,56 g/t Th: 17,4 g/t K: 3,2 %.

b. Two groups of weathered granitoid samples are sharply separated on the basis of their radioactive element concentration. Samples from weathering zone of the granite ranges (which come from some meters below reaching the crystalline basement, or suffered strong tectonic, cataclastic effect) are leached comparing them with the average of the area (U: 7 g/t; Th: 12 g/t). In general, the other group is also affected by tectonic movements (mylonitization, diaphthoresis), but was influenced by hydrothermal-metasomatic effects; radioactive elements of samples from this group are not leached, in fact, their radioactive element concentration often exceeds the average of the area. Distribution of these samples does not seem to show geographic pattern, but it would be proved by petrological analysis of more samples.

c. Uranium content of granitoid samples from the Jánoshalma-Kiskunhalas region, which are generally tectonically "tortured", is the lowest one of the whole unit (U: 7,2 g/t); similarly, Th content of the region (Th: 14,2 g/t) is also lower than the average of the area.

TABLE 6

Radioactive element contents of granitoid samples from the boreholes of the Mórágy Complex in the basement of the Great Hungarian Plain.

Borehole	Rock type	Depth (m)	Specific activity (Bq/kg)	U (g/t)	Ra (U_{equ})	Th (g/t)	K (%)
Soltvadkert-1	granite (weathered)	1148-1150m	195	5	4	16	3.8
Soltvadkert-1	"	1230-1239m	280	11	10	21	3.5
Soltvadkert-3	"	1500-1504m	330	14	13	24	3.4
Soltvadkert-3	"	1508-1513m	290	12	11	22	3.2
Soltvadkert-9	" (weathered)	1225-1231m	220	6	5	16	3.7
Soltvadkert-É-4	"	1138-1140m	450	17	15	29	3.3
Soltvadkert-K-1	"	1300-1305m	390	14	13	26	3.5
Soltvadkert-K-2	"	1345-1350m	365	12	11	22	3.6
Solti-3	"	1175-1179m	240	12	12	15	4.0
Kecel-K-2	"	2450-2451m	410	21	20	16	3.4
Kecel-K-1	mylonityc gran.	1995-2000m	285	18	18	13	3.1
Kecskemét-1	migmatite	1137-1140m	440	23	22	18	3.6
Kecskemét-2	microgranite	1081-1091m	460	19	17	21	4.0
Kecskemét-2	"	1152-1154m	390	21	20	16	3.7
Kecskemét-3	"	1092-1105m	320	17	15	19	3.4
Kecskemét-3	"	1145-1150m	290	14	14	15	4.1
Kecskemét-4	" (cataclastic)	1130-1134m	210	7	6	15	3.3
Kecskemét-Ny-2	migmatite	1156-1160m	395	11	10	21	3.8
Kecskemét-Ny-2	"	1180-1183m	325	14	13	17	3.4
Kecskemét-D-4	porphyroblastic migmatite	1614-1616m	450	28	27	14	3.4
Kecskemét-D-6	microgranite	1289-1298m	335	18	17	20	3.3
Nagykőrös-6	microgranite	1272-1273m	220	10	10	12	3.6

Borehole	Rock type	Depth (m)	Specific activity (Bq/kg)	U (g/t)	Ra (U_{equ})	Th (g/t)	K (%)
Nagykörös-6	"	1294-1299m	265	12	11	16	3.4
Nagykőrös-D-1	"	1102-1104m	205	7	6	16	3.8
Nagykőrös-D-1	"	1125-1127m	280	6	5	19	4.3
Cegléd-1	muscovite gran.	1450-1475m	260	9	8	20	4.0
Cegléd-1	"	1478-1506m	275	16	15	16	3.6
Cegléd-1	"	1506-1509m	230	14	14	13	3.5
Cegléd-3	"	1624-1629m	195	7	6	14	3.5
Cegléd-3	"	1745-1748m	210	10	9	11	3.8
Cegléd-4	"	1811-1815m	280	15	14	17	3.5
Cegléd-5	migmatite	1599-1603m	255	9	8	23	3.6
Újszilvás-3	microgranite	2018-2021m	310	18	17	19	3.3

TABLE 7

Radiometric analyses of granitoid samples from the boreholes in the Körös Unit

Borehole	Rock type	Depth	Specific activity (Bq/kg)	U (g/t)	Ra (U_{equ})	Th (g/t)	K (%)
Jánoshalma-1	granite (migmatitic)	613-614m	145	7	6	11	2.5
Jánoshalma-5	"	678-682m	190	6	5	14	3.7
Jánoshalma-6	"	694-695m	210	6	5	16	3.6
Jánoshalma-6	"	712-714m	200	8	8	13	3.3
Jánoshalma-Új-1	"	556-558m	270	9	8	20	3.5
Kiskunhalas-Ny -5	"	1057-1070m	110	3	2	9	1.9
Kiskunhalas-Ny-6	"	763-765m	140	6	4	14	2.1
Kiskunhalas-DNy-1	migmatite	950-951m	220	11	10	16	3.8
Kiskunhalas-DNy-1	migmatite	1050-1051m	185	9	8	15	3.0
Jászszentlászló-1	granite (migmatitic)	2083-2084m	310	15	14	24	3.3

Borehole	Rock type	Depth	Specific activity (Bq/kg)	U (g/t)	Ra (U_{equ})	Th (g/t)	K (%)
Jászszentlászló-1	"	2110-2111m	270	13	12	23	3.1
Jászszentlászló-2	"	2003-2004m	225	12	11	19	3.6
Jászszentlászló-2	"	2004-2007m	205	11	11	17	3.4
Jászszentlászló-4	"	2041-2053m	185	9	8	15	3.6
Jászszentlászló-4	"	2053-2062m	200	11	10	16	3.4
Kömpöc-1	"	3314-3317m	135	7	6	13	2.3
Kömpöc-3	mylonitic gran. (weathered)	2692-2695m	230	9	8	13	3.4
Szank-5	migmatitic gran.	2031-2032m	520	29	28	25	3.9
Szank-15	"	2229-2241m	315	17	16	23	3.2
Szank-31	"	2185-2187m	225	11	10	17	3.9
Szank-33	"	1949-1950m	290	12	12	20	3.6
Szank-50	"	1894-1896m	350	20	18	24	3.1
Szank-51	"	2054-2055m	385	22	21	26	3.4
Szank-63	"	2081-2084m	285	12	12	18	3.7
Szank-63	"	2123-2124m	340	13	12	19	3.9
Szank-79	"	1926-1927m	215	12	11	12	3.6
Szank-88	"	1869-1876m	265	10	10	21	3.4
Szank-103	"	1884-1886m	320	15	14	22	3.3
Szank-124	"	1950-1953m	410	23	22	22	3.3
Biharkeresztes-12	granite	1430-1436m	210	12	11	11	3.4
Dévaványa-2	migmatite	2780-2781m	105	3	3	10	2.2
Dévaványa-8	granite	2432-2438m	190	7	6	13	3.8
Füzesgyarmat-6	granite	2076-2077m	160	8	7	14	3.1
Füzesgyarmat-12	migmatite	2094-2103m	100	6	5	6	0.8
Endrőd-2	migmatite	2380-2394m	190	7	6	19	2.0

Borehole	Rock type	Depth	Specific activity (Bq/kg)	U (g/t)	Ra (U_{eq})	Th (g/t)	K (%)
Endrőd-2	"	2394-2425m	175	6	5	17	2.1
Kismarja-8	migmatitic gran.	925-928m	225	12	10	15	3.4
Kismarja-9	"	1169-1172m	270	11	10	17	3.2
Kismarja-31	"	1190-1191m	190	8	7	13	3.2
Mezősas-2	migmatite	2304-2308m	145	7	5	10	2.8
Mezősas-4	granite	2651-2656m	210	11	11	14	3.3
Mezősas-6	brecciated granite	2890-2891m	105	4	3	10	2.3
Szeghalom-9	granite	2203-2205m	230	12	10	15	3.1
Szeghalom-11	migmatite	2069-2070m	170	8	6	11	2.9
Szeghalom-39	granite	2070-2080m	260	10	10	19	3.6

Uranium concentration in the Jászszentlászló-Pálmonostora-Kömpöc-Szank granitoid region is extremely high: it is 40 % higher than mean value of the Körös Unit, and Th content is 50 % higher than mean value of the Unit (U: 14 g/t; Th: 22,1 g/t; K: 3,59 %).

Radioactive element content of the granitoid "range" near Endrőd is lower than mean concentrations of the Körös Unit (U: 8,25 g/t; Th: 13,38 g/t; K: 2,82 %).

d. On the basis of the radiological analyses of granitoid cores from the Körös Complex, it can be stated that U concentration of granitoids of this unit (in fact, 90 % of this granitoids is granite) is twice higher than the world average for granite. In this respect, these granitoids are similar to the granitoids of Mórágy Complex, which are on the surface in Southern Transdanubia. Their Th content, however, hardly exceeds mean concentration of Th for granitoids in the world.

Radioactive element content is highest in the middle part of the Körös Complex (Szank region), and mean concentrations of the three elements are decreasing both eastward and westward (U concentration is often reduced by half, and Th content is reduced by 40-50 %).

CONCLUSIONS

Mean radioactive element content of the granitoid rocks of the Codru Terrain (Southern Hungarian Nappe Zone) is the following: U: 10 g/t; Th: 8,42 g/t; K: 2,24 %.

Mean U, Th and K concentrations of the Kunság Terrain (Middle Hungarian "autochthon") are: U: 12,53 g/t; Th: 16,42 g/t; K: 3,44 %.

Within this terrain, the Mórágy Unit has higher (U: 13,54 g/t; Th: 17,9 g/t; K: 3,58 %), while the Körös Unit has lower (U: 10,6 g/t; Th: 17,4 g/t; K: 3,2 %) radioactive element contents.

Accumulation factor of radioactive elements of old granitoid rocks in the Great Hungarian Plain based on the analysed samples is listed in tables 8-11.

TABLE 8

U-Th-K accumulation factor of granitoid rocks from the Southern Hungarian Nappe Zone (Codru Terrain) for units (complexes)
(accumulation factor = mean value for unit/mean value for terrain)

	Battonya Unit	Tisza Unit	Sarkadkeresztúr Unit
U	0,88	1,38	0,9
Th	1,04	0,85	1,04
K	0,83	1,22	1,38

TABLE 9

U-Th-K accumulation factor of granitoid rocks from the Middle Hungarian "autochthon" (Kunság Terrain) for units (complexes)
(accumulation factor = mean value for unit/mean value for terrain)

	Mórágy Unit	Körös Unit
U	1,08	0,78
Th	1,09	0,72
K	1,04	0,88

TABLE 10

U-Th-K accumulation factor of granitoid rocks from the Mórágy Unit (Mórágy Complex) for part-areas
(accumulation factor = mean value for the studied part-area/mean value for unit)

	W-Mecsek part-area	Mórágy part-area	Kecel-Soltvadkert part-area	Kecskemét part-area	Cegléd area
U	1,56	0,47	0,87	1,17	0,69
Th	1	1,24	0,75	0,66	0,61
K	0,87	1,14	0,93	10,01	0,95

TABLE 11

U-Th-K accumulation factor of granitoid rocks from the Körös Unit (Körös Complex) for part-areas studied
(accumulation factor = mean value for the studied part-area/mean value for unit)

	Jánoshalma-Kiskunhalas part-area	Jászszentlászló-Pálmonostora-Kömpöc-Szank part-area	Endrőd part-area
U	0,67	1,32	0,77
Th	0,81	1,26	0,76
K	0,95	1,12	0,88

ACKNOWLEDGEMENT

The authors thank István Vados for his help in the control measures. This work has been supported by the National Science Research Foundation (OTKA) No. F017369.

REFERENCES

BALÁZS E., CSEREPESNÉ, M. B., NUSSZER, A., SZILI, GY. (1984): Az Alföld prekambriumi-, paleozóos-, triász-, jura és alsókréta korú képződmények összefoglaló áttekintése a mezozóos és idősebb összletek szénhidrogén prognózisa szempontjainak megfelelően. SZKFI, Szolnok.

BALÁZS E., CSEREPESNÉ, M. B., NUSSZER, A., SZILI, GY. (1986): An attempt to correlate the metamorphic formations of the Great Hungarian Plain and the Transylvanian Central Mountains. Acta Geol., 29, 317-320.

DIMITRESCU, R. (1981): Hypotheses sur la sructure du soubassament du secteur sud-oriental de la Depression Pannonique. Rev. Roum. Geol. Geofiz. Geogr., 25, 31-35.

GYALOG, L. (1996): A földtani térképek jelkulcsa és a rétegtani egységek rövid leírása. MÁFI Alk. Kiadv., Budapest.

HAAS, J. (1996): Magyarázó Magyarország földtani térképe a kainozoikum elhagyásával és Magyarország szerkezetföldtani térképe című térképlapokhoz. MÁFI térképmagyarázói, Budapest.

SZEDERKÉNYI, T. (1984): Az Alföld kristályos aljzata és földtani kapcsolatai. Akadémiai doktori tézisek, MTA, Budapest.

SZEDERKÉNYI, T. (1991): Az Alföld mezozóikum előtti képződményeinek komplex földtani-kőzettani-geokémiai vizsgálata. Kézirat, Szeged.

SZEDERKÉNYI, T. (1998): Pre-mesozoic tectono-stratigraphic terranes of Hungarian part of Tisia Megaunit. KBGA XVI. Cong.

SZEDERKÉNYI, T., PÁL MOLNÁR, E., VADOS, I. (1994): A radioaktivitás környezetvédelmi vonatkozásai. Egyetemi jegyzet, JATE, Szeged.

SZEPESHÁZY, K. (1978): A Tiszántúl és az Erdélyi Középhegység nagyszerkezeti és rétegtani kapcsolatai. Ált. Föld. Szemle, 12, 121-198.

Manuscript received 10. September 1999.

Acta Mineralogica-Petrographica, Szeged, XL, 157–160, 1999

NEW GOLD ORE INDICATION IN FORMATIONS OF THE DEEP-LEVEL ORE MINERALISATION IN RECSK

T. TARNAI[3]

Department of Mineralogy, Geochemistry and Petrology,
Attila József University, Szeged, Hungary

ABSTRACT

In 1997 an analytical study on magnetite skarn formations of the deep ore mineralisation in Recsk was made to reveal new potential gold mineralisation. As a result of 34 gold analyses of 10 boreholes, it can be stated that gold accumulation observed in the studied magnetite skarn formations can be qualified as indication, and further study on gold mineralisation in skarn formations of the deep ore mineralisation can be proposed.

INTRODUCTION

Research and mining of precious metals has always played a significant role in ore mining of several centuries in the Parádfürdõ-Recsk region (KISVARSÁNYI G., 1955). Gold, silver and copper ores occurring in hydrothermal veins and stocks near the surface were mainly mined with varying success. To substitute for the exhausting reserves, a deep level prospecting was started in the late 50's (GAGYI P. A. et al., 1972), and new type porphyritic Cu-Mo, metasomatic displacing Pb-Zn and skarn Cu and Cu-Zn ore mineralisations were explored (FÖLDESSY J., 1984). Since economic and political changes in the last decade, however, exploitation of this relatively deep-seated ore reserve has not been begun. Exploration of accessory or even independent gold mineralisation of relatively high concentration would be favourable to the economic judgement of copper and zinc ores of high quantity.

In the expectation of exploration of a new potential gold ore mineralisation gold content of magnetite skarn formations of the deep level ore mineralisation in Recsk was studied in 1997 (TARNAI T. 1997) based on Spanish (A. MARTIN-IZARD et al., 1997) and American analogies as well as some previous Au analytical data from the deep level of Recsk. Northern part of the ore mineralisation explored by more than 130 boreholes was studied.

DESCRIPTION OF THE ANALYSES

Studies were performed in several steps. Analytical study of dominant part of the so-called Rm boreholes deepened in the northern part of the ore mineralisation (figure 1) represented the first step (table 1). After studying and partly revaluation of documentation of the previous boreholes, boreholes and parts of boreholes were

[3] P. O. Box 651, Szeged, Hungary, H-6701

identified in which magnetite skarns occurred. Then, 25 "long" (samples 1-25; 4-5 m) and 9 "short" (samples 26-34; 0.2-1.0 m) sections of 10 boreholes were pointed out for analyses.

TABLE I

The studied boreholes

Rm-9	Rm-29	Rm-40	Rm-49	Rm-59
Rm-10	Rm-30	Rm-41	Rm-50	Rm-60
Rm-15	Rm-31	Rm-42	Rm-51	Rm-62
Rm-16	Rm-34	Rm-43	Rm-52	Rm-63
Rm-17	Rm-35	Rm-44	Rm-53	Rm-64
Rm-19	Rm-36	Rm-45	Rm-54	Rm-65
Rm-21	Rm-37	Rm-46	Rm-56	Rm-87
Rm-22	Rm-38	Rm-47	Rm-57	
Rm-26	Rm-39	Rm-48	Rm-58	

In the following step, the selected sections were sampled in the sample depot of the Recsk Ore Mining Co. The selected samples were powder ones.

Finally, the prepared and weighed powder samples were analysed. Au concentration of the samples were measured by analytical laboratory of the Analabs Pty. Ltd. in Australia under exact technological requirements and standard deviation. Results of the analyses are listed in table 2.

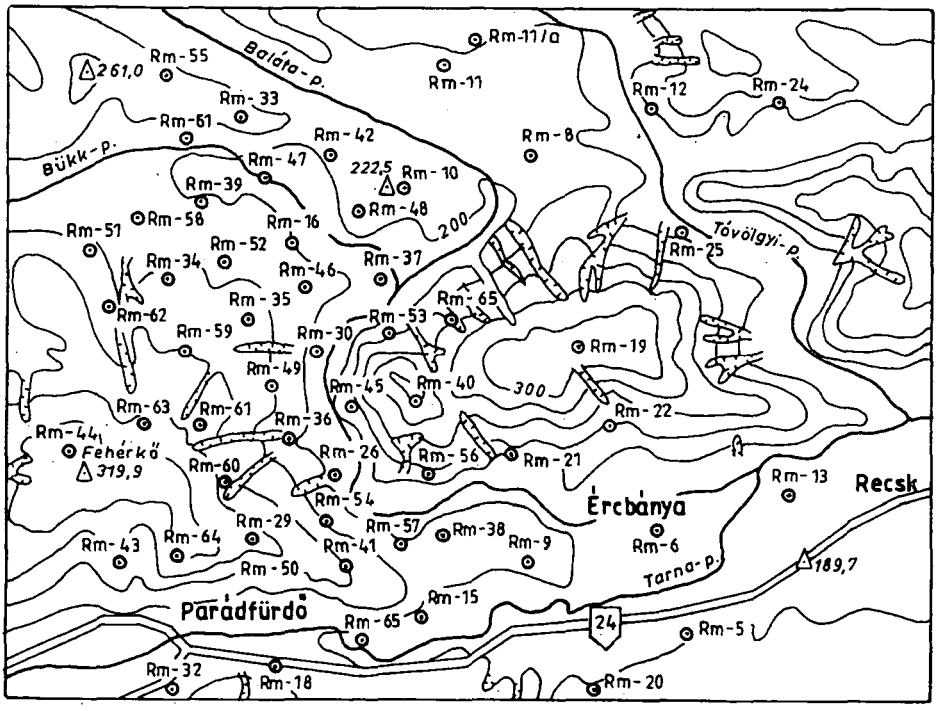

Fig. 1. Sketch map of boreholes deepened in the area of the deep-level ore mineralisation of Recsk.

TABLE 2

Au concentration in the analysed samples

Number of the sample	Symbol of the borehole	Section (m)	Type of the formation	Au (ppm)
1.	Rm-29	1115-1120	? Magnetit skarn ?	0.67
2.	Rm-29	1120-1125	? Magnetit skarn ?	0.25
3.	Rm-29	1125-1130	? Magnetit skarn ?	0.19
4.	Rm-38	790-795	Limestone skarn with magnetite	0.04
5.	Rm-38	795-800	Limestone skarn with magnetite	0.09
6.	Rm-38	800-805	Limestone skarn with magnetite	0.05
7.	Rm-42	900-905	Hematite-magnetite-krokidolite skarn	0.07
8.	Rm-42	905-910	Hematite-magnetite-krokidolite skarn	0.04
9.	Rm-42	910-915	Hematite-magnetite-krokidolite skarn	0.05
10.	Rm-45	825-830	Pyrite deposit with magnetite	0.27
11.	Rm-45	830-835	Pyrite deposit with magnetite	0.13
12.	Rm-45	835-840	Pyrite deposit with magnetite	0.04
13.	Rm-47	1010-1015	Granet-epidote skarn with disseminated magnetite	0.06
14.	Rm-50	1176-1181	Magnetite-krokidolite skarn	0.01
15.	Rm-50	1181-1186	Magnetite-krokidolite skarn	0.01
16.	Rm-52	968-972	Magnetite skarn deposit	0.17
17.	Rm-52	972-976	Magnetite skarn deposit	0.07
18.	Rm-53	570-575	Granet-serpentinite-magnetite exoskarn	0.21
19.	Rm-53	575-580	Granet-serpentinite-magnetite exoskarn	0.25
20.	Rm-53	580-585	Granet-serpentinite-magnetite exoskarn	0.17
21.	Rm-53	585-590	Granet-serpentinite-magnetite exoskarn	0.16
22.	Rm-57	607-612	?	0.04
23.	Rm-59	1105-1110	Serpentine-anhydrite-chlorite-magnetite aposkarn	0.21
24.	Rm-59	1110-1115	Serpentine-anhydrite-chlorite-magnetite aposkarn	0.15
25.	Rm-59	1115-1120	Serpentine-anhydrite-chlorite-magnetite aposkarn	0.18
26.	Rm-59	1113.5-1114.5	Serpentine-anhydrite-chlorite-magnetite aposkarn	0.09
27.	Rm-45	826.0-827.0	Pyrite deposit with magnetite	0.15
28.	Rm-45	827.0-828.0	Pyrite deposit with magnetite (particulary rich ore deposit)	DTF
29.	Rm-29	1123.0-1124.0	? Magnetite skarn ?	0.12
30.	Rm-29	1124.0-1125.0	? Magnetite skarn ?	0.15
31.	Rm-48	935.0-935.5	? Magnetite-hematite skarn ?	0.06
32.	Rm-38	909.7-909.9	? Limestone skarn with magnetite ?	0.14
33.	Rm-56	1108.5-1109.0	Magnetite skarn	0.02
34.	Rm-56	1124.0-1124.5	Magnetite skarn	0.01

CONCLUSIONS

Our study unambiguously proved gold ore indication in skarn zones of the deep level ore mineralisation of Recsk formed in the intrusive series of Recsk Andesite Formation. The highest concentration was 0.67 ppm.

It is interesting that average concentration in samples of the so-called "long" sections was higher (0.14 ppm) than that of the short ones (0.09 ppm). Since short sections came from magnetite or magnetite skarn sections, and the longer ones came from not only or less magnetite skarn sections, it can be concluded that less magnetite and magnetite skarn sections might be more productive. However, a final conclusion can not be drawn because of low amount of the samples. Real facts will only be stated by analysis of more samples, and detailed ore and rock microscopic studies on samples analysed for Au concentration.

Nevertheless, the above analysis suggest that further study of this gold ore indication is reasonable by detailed re-analysis of mining boreholes and revaluation of the geological data.

ACKNOWLEDGEMENT

The author wishes to thank Éva Horváth, János Földessy and Szabolcs Tóth for their human and professional help and example as well as unforgettable experiences received in our common work of one and a half year which will be essential in our future professional career.

REFERENCES

GAGYI PÁLFFY ANDRÁS - CSEH NÉMETH JÓZSEF - ZELENKA TIBOR - IFJ. GAGYI PÁLFFY ANDRÁS - LÁZÁR BÉLA (szerkesztették) NAGY ISTVÁN - CSILLAG JÁNOS - FODOR GYULA - CSONGRÁDI JENŐ - BAKSA CSABA - FÖLDESSY JÁNOS - FÖLDESSY JÁNOSNÉ (1972) A recski mélyszinti színesérc elfordulás összefoglaló jelentése 1971. OÉÁ, Budapest. /ENARGIT Kft adattára/

FÖLDESSY J. (1984) A recski paleogén vulkáni és intruzív képződmények kőzettani és vulkanológiai jellegei. Kandidátusi értekezés. Recsk-Budapest. /ENARGIT Kft adattára/

KISVARSÁNYI GÉZA (1955) Összefoglaló jelentés a Recsk- Parádfürdői ércelőfordulásokról és a Recski Ércbánya ércvagyonbecslése. MÁFI, Budapest. /ENARGIT Kft adattára/

A. MARTIN-IZARD, M. A. CEPEDAL, L. RODRIGUEZ-PEVIDA, E. SPIERING, S. GONZÁLEZ, A. VARELA, C. MALDONANDO (1997) The el Valle deposit: An example of porphyry-related copper-gold skarn mineralization overprinted by Late Epithermal events, Cantabrian Mountains, Spain. Mineral Deposits, Papunen. pp. 659-662

TARNAI T. (1997) A Recsk-mélyszinti ércesedés elemző vizsgálata magnetitszkarnos képződmények feltárására az RM fúrások alapján. Kéziratos jelentés. ENARGIT Ásványhasznosító Kft.

Manuscript received 15. September 1999.

Acta Mineralogica-Petrographica, Szeged, XL. 161–174, 1999

EARLY DIAGENETIC FEATURES OF THE SCLERACTINIANS, PLEISTOCENE CORAL REEF, DAHAB (SINAI, EGYPT)

IBTEHAL FATHI ABDEL RAHMAN

#Geology Department, Faculty of Science, Suez Canal University*

ABSTRACT

Two kms north-east of Dahab, the northernmost remnant of emerged Pleistocene terraces display well preserved coral-reef and associated peri-reefal facies. The Scleractinian corals within the reef sequence display a series of diagenetic features formed by the alteration of the original micro-structures under different diagenetic conditions. Evidence from cement fabrics (aragonite and high-Mg calcite) suggests that the cementation took place exclusively in a phreatic marine environment. Meteoric diagenesis is indicated by traces of minor leaching and sparry calcite cement. Formation of microcrystalline dolomite and halite might take place in a sabkha environment. This suggests under various diagenetic alternation conditions.

Keywords: Sinai, Dahab, Pleistocene, reef terraces, Scleractinian corals, early diagenesis.

INTRODUCTION

The Egyptian coasts of the Gulf of Aqaba are characterized by a series of spectacular Quaternary and recent coral-reef terraces. The emerged Pleistocene coral reefs along the southern Sinai coast occur in two major sequences. They form two morphologically well defined reef terraces. They are situated at altitude ranging from +3 to +30m above the present sea level. The aspects of the diagenesis, geochemistry and carbonate facies of the Pleistocene reefs of the Red Sea and south Sinai coastal plain have been presented by a number of works (FRIEDMAN, 1968; GVIRTZMAN and FRIEDMAN, 1977; GVIRTZMAN et al. 1992; DULLO 1984, 1986, 1990; AL RIFAIY and CHERIF, 1988; YOUSSEF, 1988; STRASSER et al. 1992, 1997; HEISS et al. 1993; FATHY and HAAS, 1994,1997). This publication contributes to the study of the northernmost small remnants of the younger Pleistocene reef sequence, 2 kms north-east of Dahab (*Fig. 1*). The study area is limited to a band of about 10 km in length, starting from Wadi Abu Ma' in the south and stretching northward toward El-Qardud. A corresponding younger reef sequence of south Sinai has been dated by STRASSER et al, 1992 between 140 and 60 ka BP which corresponds to isotope stage 5.

The identification of diagenetic alterations of Scleractinian corals in the emerged sequence which is in the focus of present study may allow the highlighting of sea level fluctuations and climatic changes which prevailed during the formation and diagenesis of the coral-reef system.

---

* Ismailia,EGYPT

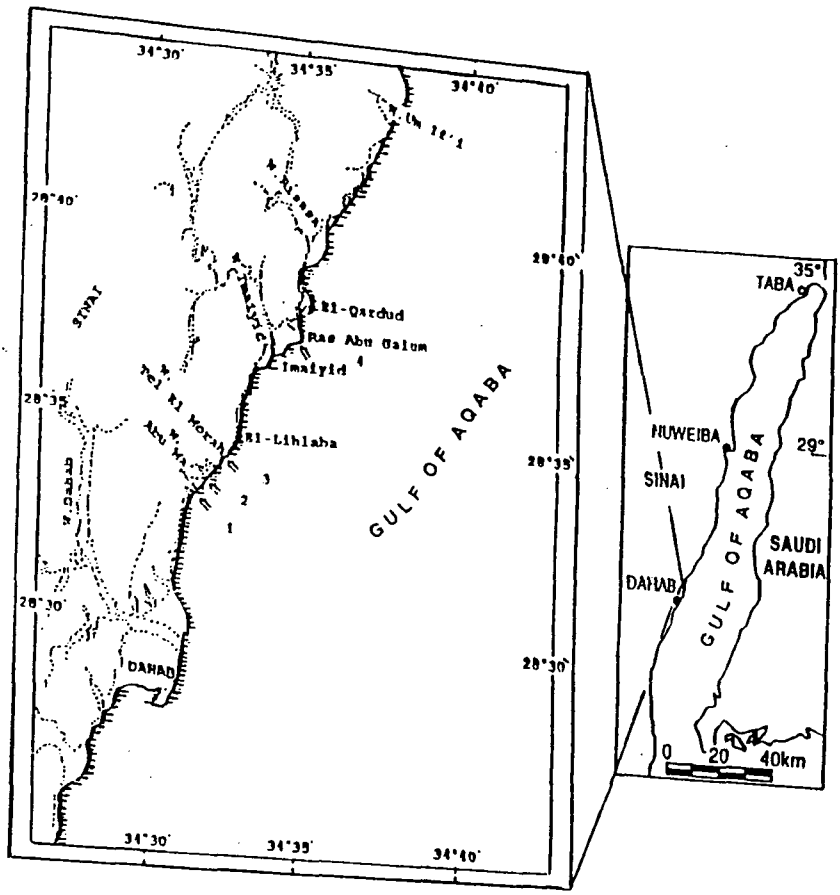

Fig. 1. Location map of the studied cross-sections

STRUCTURAL AND GEOMORPHOLOGICAL SETTINGS

The Red Sea system is generally referred to be a typical rift coast. The rifting has begun in the Late Oligocene. The Gulf of Suez has been started to form by extension and subsidence in the Early Miocene, but the extensional movements slowed down by the Middle Miocene. A left-lateral transform fault was then initiated along the Dead Sea - Gulf of Aqaba fault system (MAKRIS and RIHM, 1991). Some E-W extensional tectonics of Aqaba deformation occurred during the Plio-Quaternary (LYBERIS, 1988). In association with these movements uplift of the graben shoulders and block-faulting occurred and these are still active today (PURSER et al., 1990). GVIRTZMAN (1994) estimated the average uplift rate as 0.085 mm year^{-1}.

DESCRIPTION OF THE STUDIED SITES

The coast is a relatively narrow strip (from 100-600 m wide north of Dahab). At some places the basement relief is located in close vicinity of the shore. The coastal zone is generally covered by unconsolidated pebbles and coarse-grained beach rock. The composition, morphology and elevation of the beach rock indicates clearly its old origin. Locally it is composed of fanglomerates of the nearby crystalline rocks. They could be transported by floods of older wadis (for examples; wadi Abu Ma', wadi Tel El Morah and wadi Imaiyid). The present occurrence of beach rock (at about 50 cm above the present sea level) suggests that the cementation process has been active during the latest period too. Remnants of the beach rock mark the old shore. Beach rock and unconsolidated pebbles cover the Holocene fossil reef flat which is about 50 cm to 1 m above the mean sea level (*Fig. 2* and *Fig.-s 3a* and *b*). By now both the reef flat and the beach rock are strongly eroded and bored by intertidal organisms. The studied coast is of particular importance as a clear indicator of the previously higher sea level or a regional tectonic uplifting in the last few thousand years. Unfortunately, radiometric dating has not been done for the Scleractenian corals.

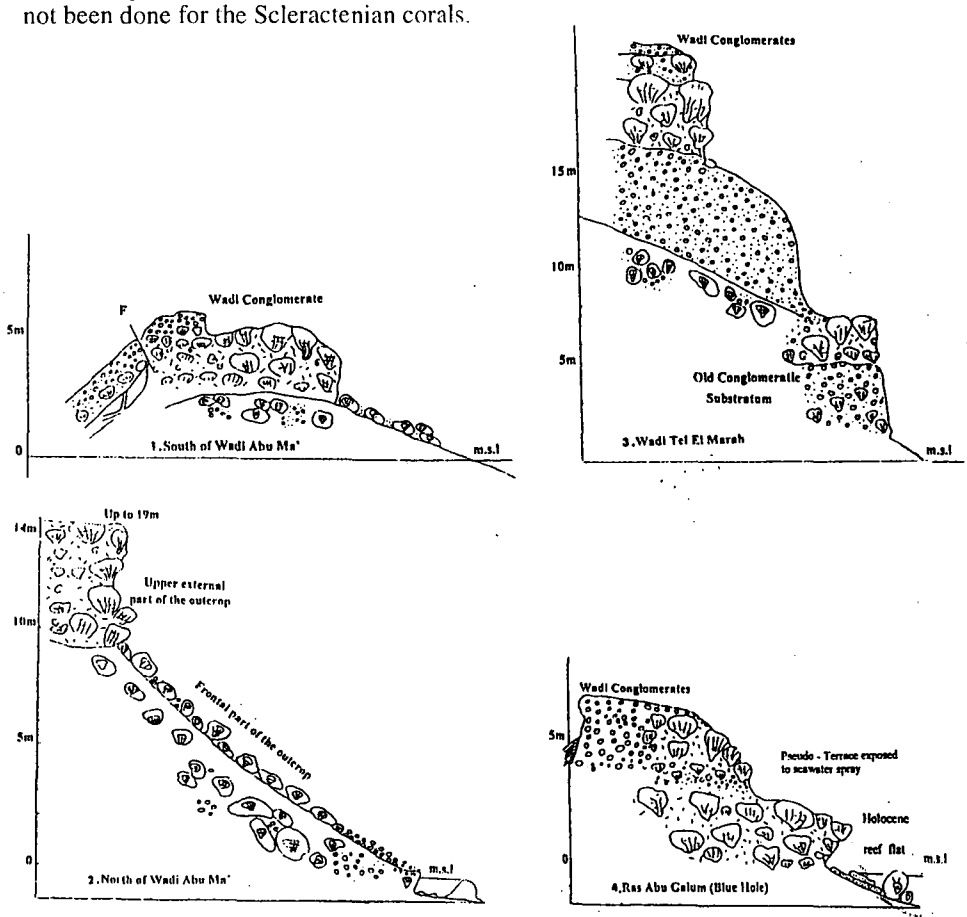

Fig. 2. Sketches of studied cross sections for the last Pleistocene terrace and Holocene reef flat, Dahab, Sinai

Fig. 3a (explanation is on the page)

Fig. 3b (explanation is on the page)

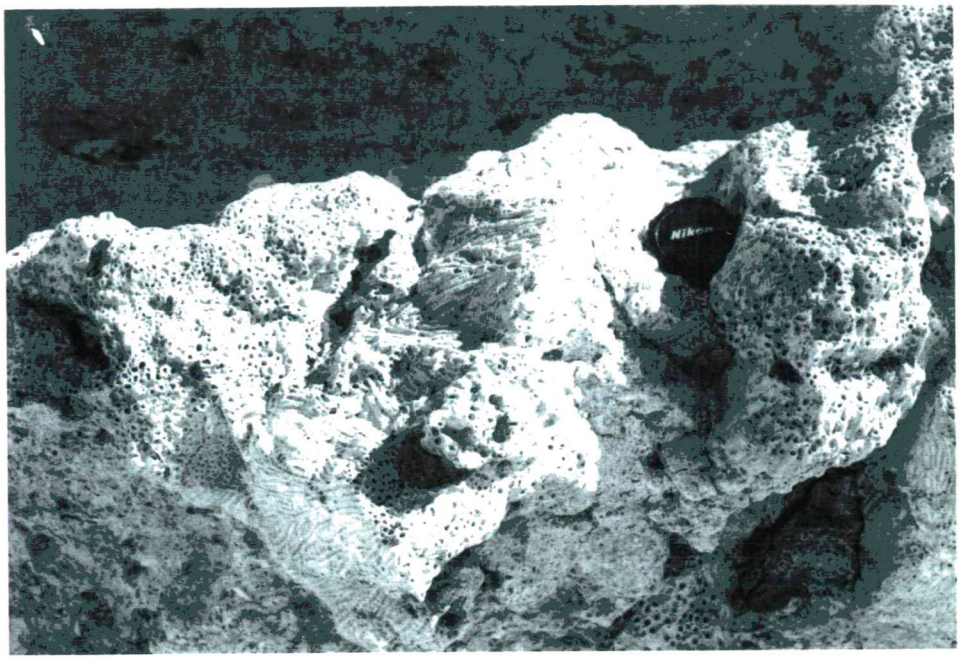

Fig. 3c (explanation is on the page)

Fig. 3d (explanation is on the page)

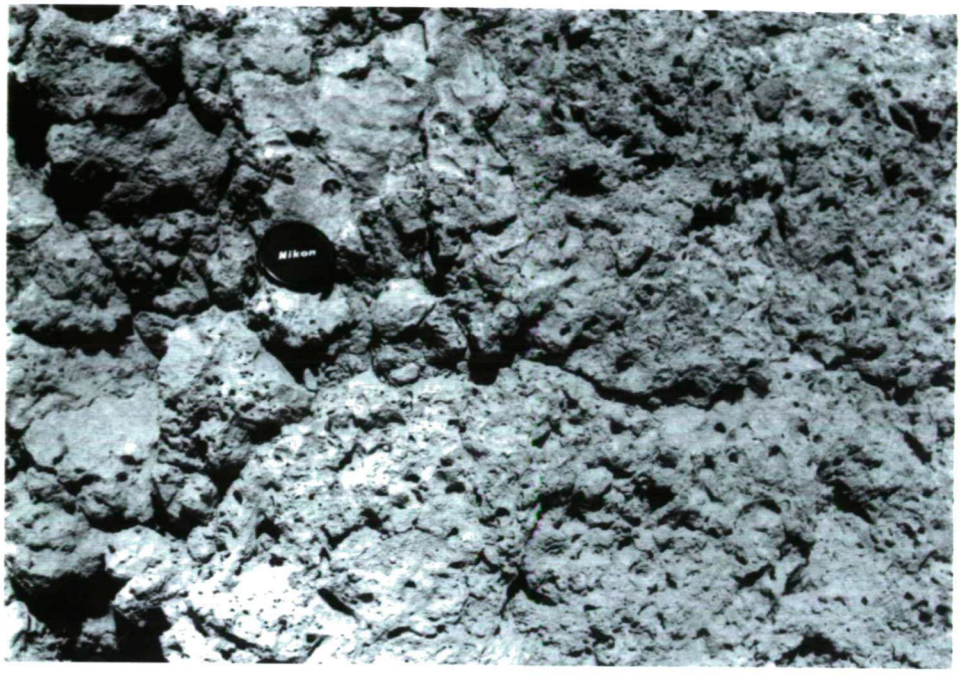

Fig. 3e (explanation is on the page)

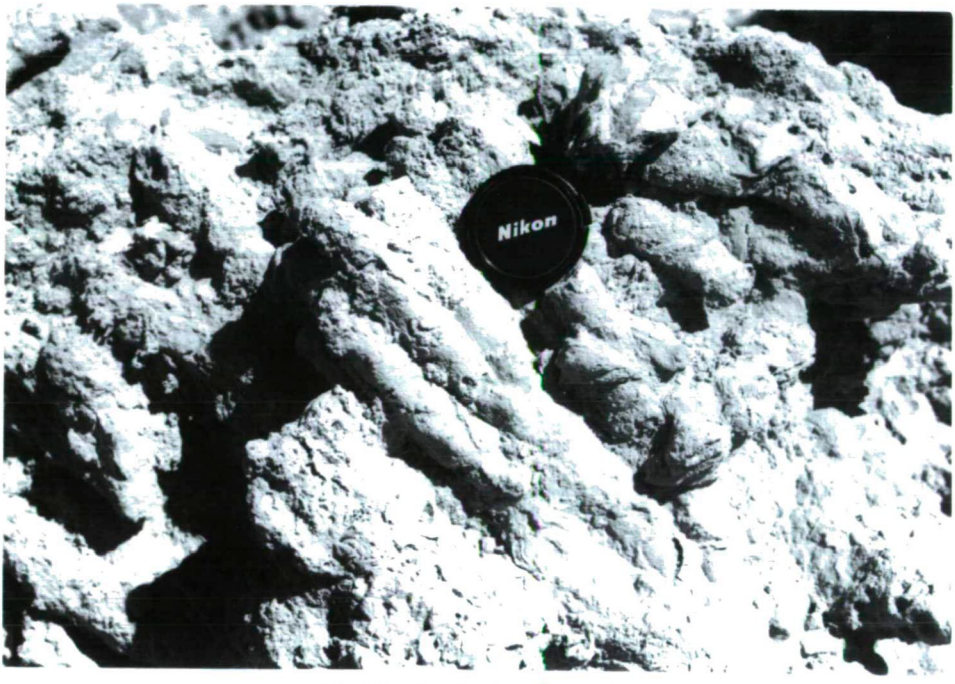

Fig. 3f (explanation is on the page)

Fig. 3. Outcrop Photographs. (a) General view to the south, north of Blue Hole. Holocene fossil reef flat completely emergent at low tide. Rocky beach backed by Late Pleistocene reef. (b) Ras Abu Galuum. The whole outcrop belongs to only one reef but cementation of the lower 2m by sea water spray produced a bench or a pseudo-terrace by differential erosion. (c) Constructed reef facies, with massive coral colonies of Favia Pallida, more or less in-situ., section 3. (d) The giant coral colonies of the upper part of the outcrop indicate the fastest rise of relative sea level and maximum flooding, section 1. (e) Fine grained facies rich in encrusting red algae (arrow) which show white in the outcrop, section 3. (f) Constructed reef facies with corals and vermetid gastropods (arrow) indicate the beginning of the transgression, section 2.

The present study is based on four examined cross-sections from Wadi Abu Ma' to El-Qardud (*Fig. 2*). They belong to one major coral reef sequence which corresponds to the lower (younger) reef sequence in South Sinai and Ras Mohammad area attaining an altitude of 3-15m above the mean sea level (FATHY and HAAS, 1994, 1997). In the studied sections, at Dahab the sequence contains two small, sub-sequences of meter scale: (1) Reefal facies which comprises large coral communities, reflecting the maximum transgression and elevation of sea-level (*Fig. 3c* and *d*) (2) Lagoonal facies with isolated corals, bivalves, gastropods and red algae, indicating sedimentation in a low-energy area, in a lagoon on the reef flat (*Fig 3e* and *f*). Coral rubbles and/or terrigenous beds (gravel- and boulder conglomerates) separate the sub-sequences from each other and their presence indicates a lowering sea-level. Vermetid gastropods typically occur at the transgressive surface.

South of Wadi Abu Ma', the coral terrace is estimated at 6 m above the mean sea level. The top of this terrace is covered with 1 m of terrigenous fanglomerate. The thickness of the siliciclastic input decreases seaward. This section is cut by a recent faulting (N20W/75SE) which caused the drop of the western block (*Fig 2*). To the North the reef terrace attain up to 19 m in altitude above the mean sea level. At Wadi Tel El Marah site the section was uplifted to higher altitudes than elsewhere on the studied coast. It begins with a 3m thick coarse old conglomerate bed which is possibly the substrate of the reef sequence. The terrace is located at about 8 m above the mean sea level at Ras Abu Galum. In all sections (*Fig. 2*), the fanglomerates prograde over the carbonates which are replaced seaward by coral rubbles.

The framework of the reefs usually consists of very large coral colonies in growth position, showing a coarsening trend upwards. Giant coral colonies (0.5-2m in length) are common at the upper external part of the succession. Coraline algae are the dominant frame-building organisms in the sequence, beside a mixture of bioclastic grains, detrital quartz and granitic grains. The most abundant Scleractinians are the following: Porites lutea, P. solida, Goniastrea pectinata, Favia Pallida, F. speciosa, Galaxea ascicularis, Stylophora pistillata, Platygeria dedalae.

LABORATORY METHODS

25 coral samples have been taken from the examined cross-sections. Thin sections were made from all samples and stained with Feigl's solution for distinction between aragonite and calcite and with Alizarine Red-S for separation of calcites and dolomites (FRIEDMAN, 1959). Ten samples of the selected corals were broken, cleaned with distilled water and pressured air and coated with gold for scanning electron microscopy. For SEM investigations AMRAY- 1830I was applied, EDAX detector, PV 9800. The mineralogy of cements was confirmed with the energy dispersive spectrometer (EDS) on samples prepared for SEM.

Bulk X-ray analyses were performed on all samples with X-ray diffractometer Philips PW 1710 Goniometer, employing CuKα radiation at 40 kV/30 mA (scanning speed: 2° min^{-1}).

For the geochemical investigations major and trace element analyses were carried out on 6 samples. The carbonate fraction of the bulk-rock samples was extracted by 1N HCL, following the procedure worked out by ROBINSON (1980). The solutions were analysed for major elements (Ca, Mg) and trace elements (Sr, Na, Fe, and Mn) using JY-70 ICP-OEs spectrometer.

DIAGENETIC FEATURES

The selected Scleractinian corals were collected along the whole sections. Most of them are located directly at the coast, exposed to the sea water spray and storm waves. The studied Scleractinians show no alteration of the primary microstructure. The marine aragonitic fibrous cement has also been preserved. This cement consists of aragonitic needles, which were grown either onto the trabecular structure of the corals or syntaxially, projecting from the micritic envelopes into the primary pore spaces. The high Mg-calcite and aragonite cements strongly suggest that the early cementation took place exclusively in a phreatic marine environment.

The change from the marine depositional environment to the meteoric diagenetic environment was due to subaerial exposure of the reefs, it is indicated by minor leaching of the trabecular centers (*Fig. 4a*). Subsequently, the vugs, that had been formed by leaching, were lined by newly formed sparry calcite and the relics of the primary aragonite microstructure in the periphery of the septa (*Fig.-s 4b,c*). In some interseptal pores, original aragonite needles, peloids and trapped terrigenous grains were preserved. The sediment infilling generally avoided the dissolution, although a few of the particles have been dissolved. The thin micritic envelopes, that form a thin substratum for the micritic cements were resistant against dissolution.

Microcrystalline calcian dolomite crystals appear as small surfacial rhombs, of about 5-10 μm in size. They grow over the earlier Mg calcite and developed in the interstitial voids among the trapped terrigenous grains (*Fig.-s. 4d,e*). The association of aragonite, Mg calcite and microcrystalline dolomite with halite (*Fig.-s 4d,e* and *f*) suggest an evaporative-sabkha origin of these dolomites.

GEOCHEMISTRY OF CORAL SKELETONS

The most significant properties of the Pleistocene Scleractinian corals from Dahab's sequence (IBTEHAL, in press), are:

(1) In the studied fossil corals, carbonates (*Fig. 5*) were represented mainly by aragonite, low and high Mg-calcite, and protodolomite. The amount of protodolomite is relatively low (4-6%). Evaporites (halite and gypsum) were also identified (2-26%).

(2) Sr ranges between 8,000 and 9,500 ppm, 8,575 ppm in average. It falls within the field of values reported for marine aragonite (7700-10,000 ppm, AISSAOUI, 1985). It means that the Sr content in corals was influenced by Sr content of the precursor carbonates.

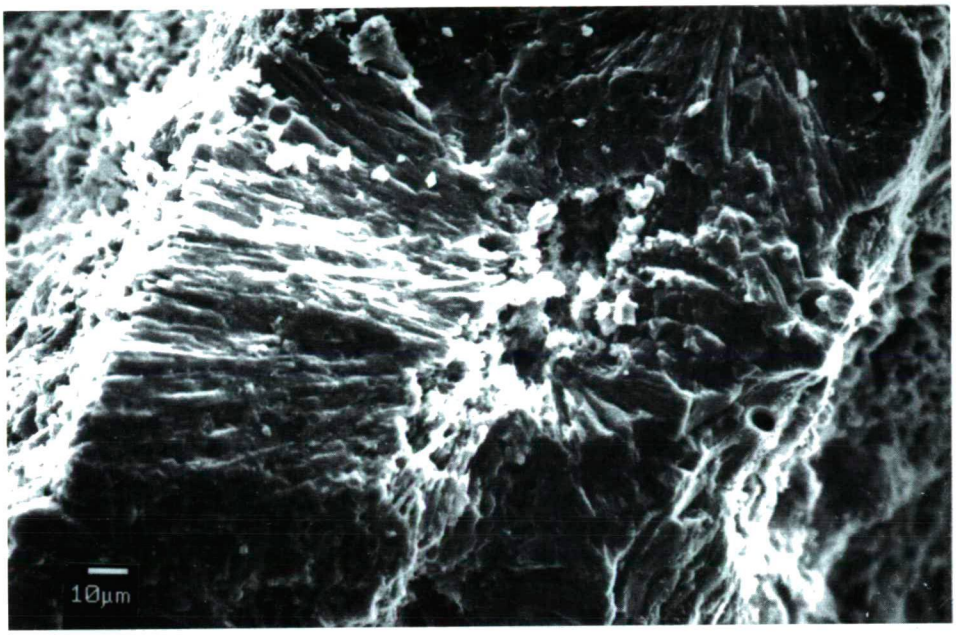

Fig. 4a (explanation is on the page)

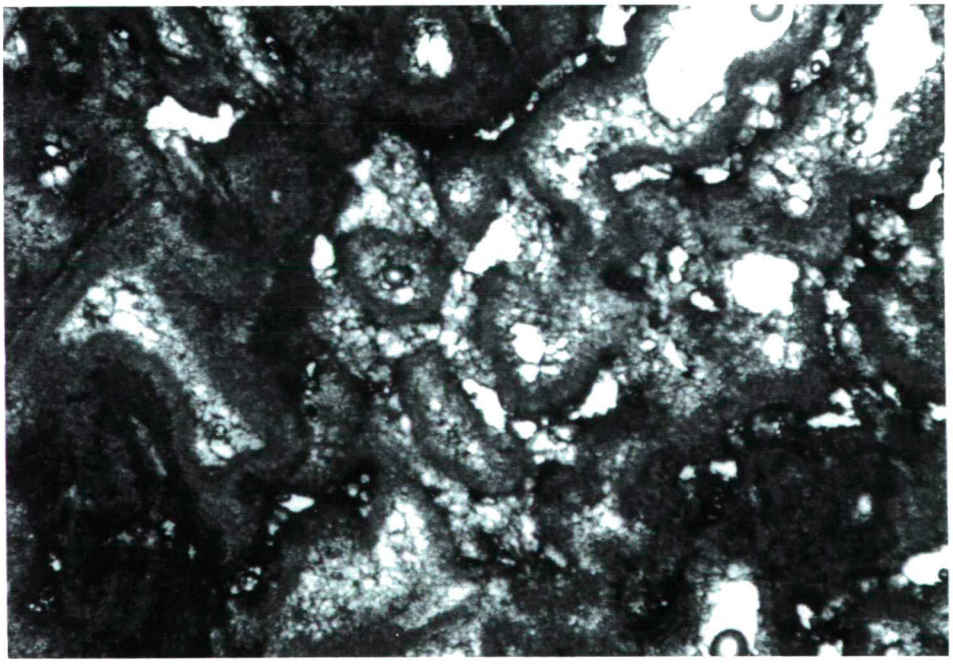

Fig. 4b (explanation is on the page)

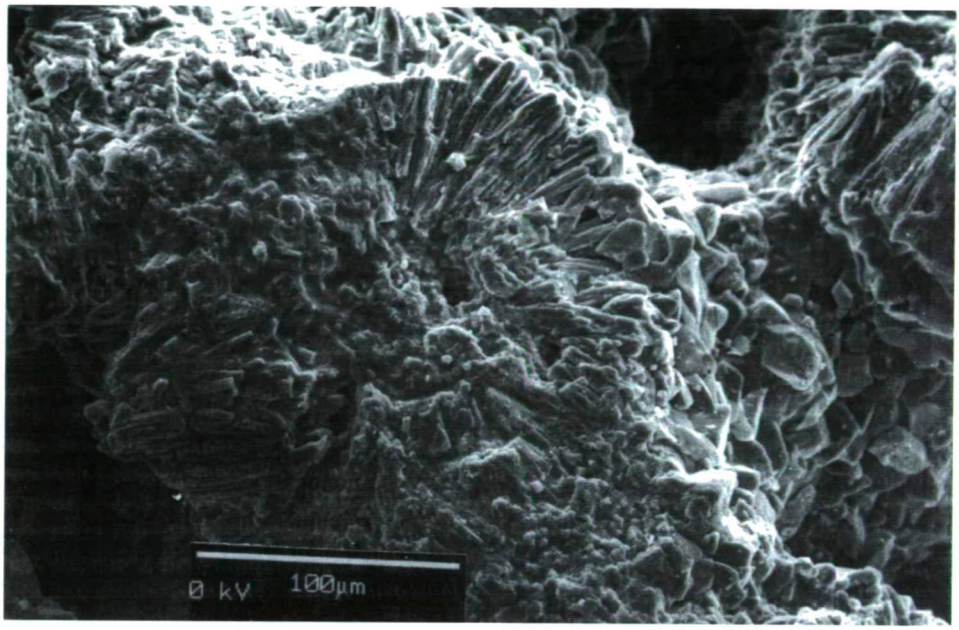

Fig. 4c (explanation is on the page)

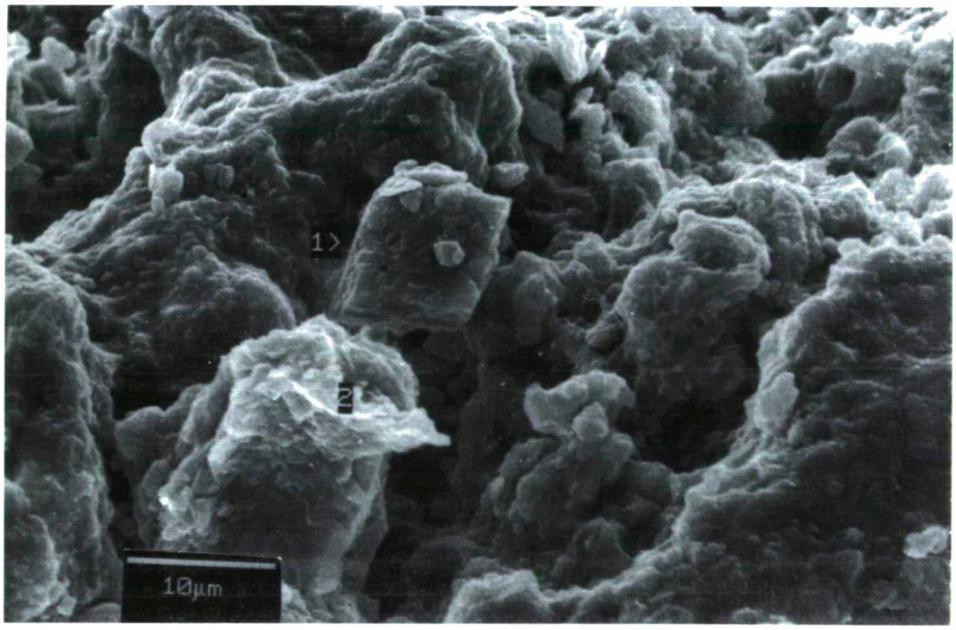

Fig. 4d (explanation is on the page)

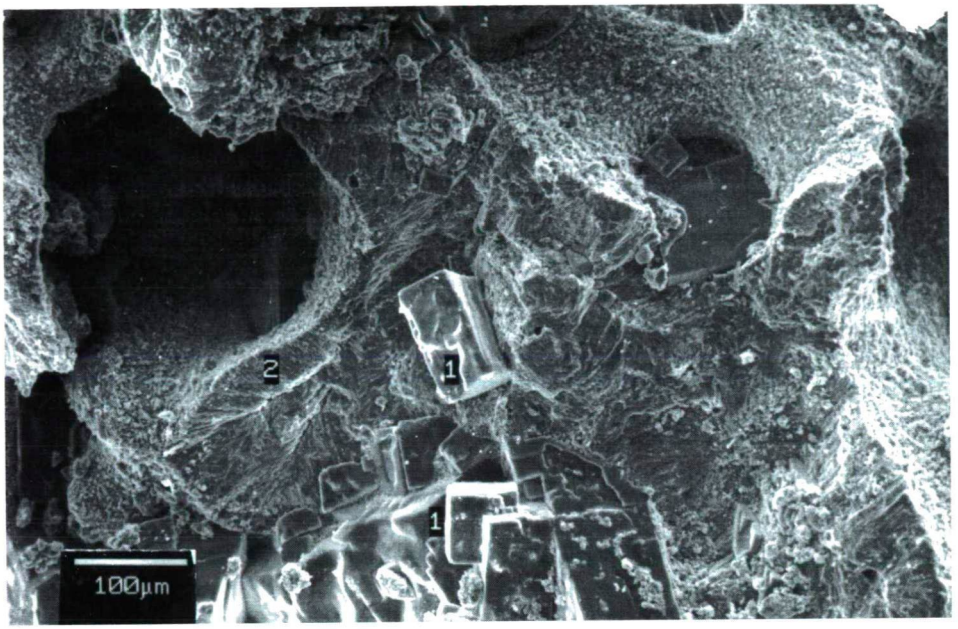

Fig. 4e (explanation is on the page)

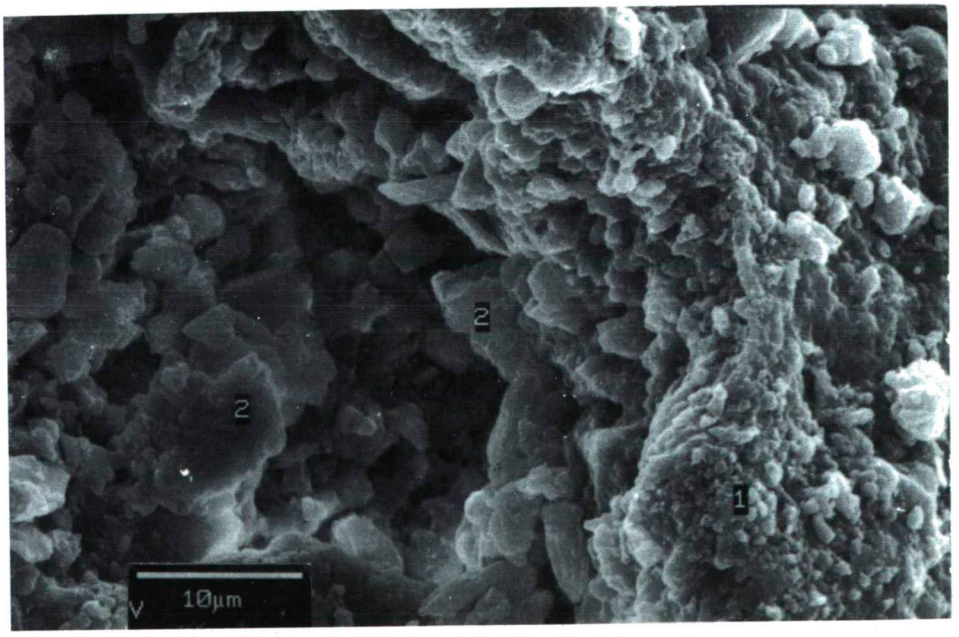

Fig. 4f (explanation is on the page)

Fig. 4. Diagenetic features, stained thin section photomicrographs are taken in non-polarized light. (a) Leached trabecular centers of Porites Lutea, suggesting a meteoric diagenetic environment. (b) The centers of the leached septa were lined by newly formed blocky calcite. The relics of the primary aragonite microstructure occur in the periphery of the septa. Thin section, 25X. (c) Coarse low-Mg calcite cement binds the partial preserved coral sclerodermite. SEM. (d) Microcrystalline dolomite crystals 1 developed in the interstitial voids between the trapped terrigenous grains (2, clay minerals) SEM. (e) Microcrystalline Mg calcite 2 are overgrown by microcrystalline dolomite crystals 1, SEM. (f) The original aragonitic structure of sclerodermite disappeared and has been replaced by large crystals of halite. This is the same sample as in (e), thus showing co-existence of aragonite, dolomite and halite.

(3) Na values are surprisingly high (between 7,000 and 7,900 ppm, with average 7,425 ppm); this was certainly influenced by the precipitation of halite cement, derived from evaporation of marine water during dolomitization.

(4) Ca (with average 46.7 %) and Mg contents (with average 0.38 %) show a negative correlation with each other.

(5) Fe ranges between 140 and 322 ppm, 240 ppm in average. Mn content ranges between 8 and 23 ppm. Fe and Mn values are relatively low at the Dahab fossil corals in accordance with surface dolomitization where Fe and Mn are locked up as oxide/hydroxide compounds.

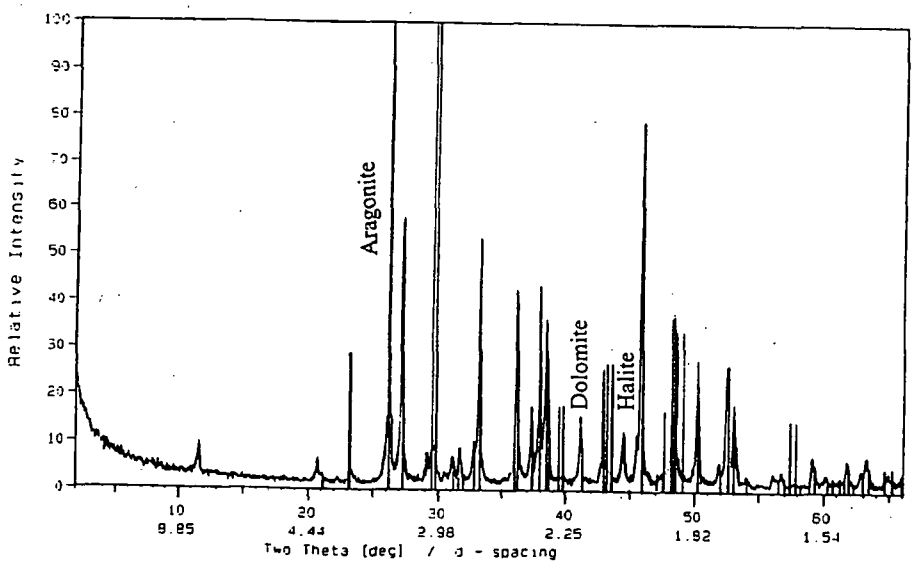

Fig. 5. X-Ray powder diffraction analysis of coral skeleton

CONCLUSIONS

At the Egyptian shoreline of the Gulf of Aqaba, 2 kms NE of Dahab, remnants of Pleistocene coral reefs are preserved. They represent one major depositional sequence corresponding to the lower reef sequence of South Sinai which was formed during the eustatic sea-level high of isotope stage 5 (HAYS et al., 1976 and STRASSER et al., 1992). Tectonic elevation of the Dahab's sequence may also be supported. It exhibits planations at 6 m, 8 m, 15 m, and 19 m, which are traceable all over the studied coast. The latter

two steps were probably formed by tectonic eration (with respect to a reference level of +6 or +8 m). Planation within the contemporaneous lower reef sequence of South Sinai occur at 3 m, 5 m, 8 m, 10 m, 13 m and 15 m above the present sea level (FATHY and HAAS, 1994, 1997). This suggests a slow recent uplift of the Gulf of Aqaba coast.

The Scleractinian corals within the emerged Pleistocene reef sequence reveal a complex pattern of early diagenetic features. The general succession of diagenetic events indicates several short-term sea level oscillations and low-grade climatic changes. Main types of diagenetic evolution are as follows:

a. Precipitation of marine cements (aragonite and high-Mg calcite) occurred contemporaneously or just after the construction of the reefs during the major sea-level highstands.

b. Minor leaching and precipitation of meteoric low-Mg calcite cements took place mainly at a lower sealevel.

c. Poorly ordered and calcium-rich dolomites in association with evaporites (halite and gypsum) formed under the surface of the wide tidal flat. It means that during stillstand or slight fall of sea-level, and under arid climate, intertidal/supratidal evaporative and reflux dolomitization by marine water took place. Such short-term regression with arid climate were favourable for the precipitation of evaporites.

It is likely that the reefs developed during sea level highstands. The diagenesis of coral reefs took place under warm and arid climatic condition which was punctuated by wet periods.

ACKNOWLEDGMENTS

The writer wishes to express her deep appreciation to the Department of Geology, Eötvös Lóránd University, Hungary for use of their analytical equipment particularly the SEM.

REFERENCES

AL-RIFAIY, I. A. and CHERIF, O. H. (1988): The fossil coral reefs of Al-Aqaba, Jordan. Facies. 18, 219-230.

AISSAOUI, DJ. M. (1985): Botryoidal aragonite and its diagenesis. Sedimentol. 32, 345-361.

DULLO, W.C. (1984): Progressive diagenetic sequence of aragonite structures: Pleistocene coral reefs and their modern counterparts on the eastern Red Sea coast, Saudi Arabia. Palaeontographica Americana, 54, 254-260.

DULLO, W.C. (1986): Variation in diagenetic sequences: an example from Pleistocene coral reefs, Red Sea, Saudi Arabia. In: Reef Diagenesis (Ed. by J. H. SCHROEDER and B.H. PURSER), pp. 77-90. Springer, Berlin.

DULLO, W.C. (1990): Facies, fossil record, and age of Pleistocene reefs from the Red Sea (saudi Arabia). Facies 22, 1-46.

FATHY, I. and HAAS, J. (1994): Physiography and Quaternary sedimentation of the coastal zone in the South Sinai, Egypt. Acta Geol. Hung. 37, 311-325.

FATHY, I., HERTELENDI, E. and HAAS, J. (1997): Geochemistry and dolomitization of Pleistocene coral reefs, in the Gulf of Aqaba region, South Sinai, Egypt. Acta Miner. Petr. XXXIII, 73-94.

FRIEDMAN, G.M. (1959): Identification of carbonate minerals by staining methods. J. Sed. Petr. 29, 87-97.

FRIEDMAN, G.M. (1968): Geology and geochemistry of reefs, carbonate sediments, and waters, Gulf of Aqaba, Red sea. J. Sed. Petrol. 38, 895-919.

GVIRTZMAN, G. and FRIEDMAN, G.M. (1977): Sequence of progressive diagenesis in coral reefs. Am. Ass.Petrol. Geol., Stud. Geol. 4, 357-380.

GVIRTZMAN, G., KRONFELD, J. and BUCHBINDER, B. (1992): Dated coral reefs of southern Sinai (Red Sea) and their implication to Late Quaternary sea levels. Mar. Geol. 108, 29-37.

GVIRTZMAN, G. (1994): Fluctuations of sea level during the past 400 000 years: the record of Sinai (northern Red Sea). coral reefs. 13, 203-214.

HEISS, G.A., DULLO, W.C. and REIJMER, J.J. (1993): Short and long term growth history of massive Porites sp from Aqaba (Red Sea). Senckenbergiana Maritima. 23, 135-141.

HAYS, J.D., IMBRIE, J. and SHACKLETON, N.J. (1976): Variations in the Earth's orbit: pacemaker of the ice ages. Science. 194, 1121-1132.

LYBERIS, N. (1988): Tectonic evolution of the Gulf of Suez and the Gulf of Aqaba. Tectonophysics. 153, 209-220.

MAKRIS, J. and RIHM, R. (1991): Shear-controlled evolution of the Red Sea: pull apart model. Tectonophysics. 198, 441-466.

PURSER, B.H., PHILOBBS, E.R. and SOLIMAN, M. (1990): Sedimentation and rifiting in the NW parts of the Red Sea: A review. Bull. Soc. Geol. Fr. 8, 371-384.

ROBINSON, P., (1980): Determination of calcium, magnesium, manganese, strontium, sodium and iron in the carbonate fraction of limestones and dolomite. Chem. Geol. 28, 135-146.

STRASSER, A., STROHMENGER, C., DAVAND, E., and BACH, A. (1992). Sequential evolution and diagenesis of Pleistocene coral reefs (South Sinai, Egypt). Sed. Geol. 78, 59-79.

STRASSER, A. and STROHMENGER, C. (1997): Early diagenesis in Pleistocene coral reefs, Southern Sinai, Egypt: response to tectonics, sea-level and climate. Sedimentology. 44, 537-558.

YOUSSEF, EL SAYED, A.A. (1988): Sedimentological studies of some Quaternary sediments in the Sherm El Sheikh area, Sinai, Egypt. Sediment. Geol. 57, 231243.

Manuscript received: 15. Nov. 1999.

Acta Mineralogica-Petrographica, Szeged, XL, 175–198, 1999

ON THE THERMODYNAMICS OF METEORITES AND PARENT BODIES II: FROM CHONDRITES THROUGH THE PRIMITIVE ACHONDRITE VERIETIES (STAGE A AND STAGE B) TO THE BASALTIC ACHONDRITES

Sz. BÉRCZI[1], K. GÁL-SÓLYMOS[2], Á. HOLBA[3], B. LUKÁCS[3] and K. MARTINÁS[4]

[1] Eötvös University, Cosmic Materials Sp. Res. Gr. Dept. G. Technology
[2] Eötvös University, Dept. Petrology and Geochemistry
[3] CRIP RMKI
[4] Eötvös University, Dept. Atomphysics

ABSTRACT

We study the degrees of thermal evolution over chondritic stages: via primitive achondritic (stage A) stage of acapulcoites, lodranites, winonaites and IAB iron silicate inclusions, through the (stage B) primitive achondrites of ureilites and some lodranites till the basaltic achondrites. We discuss the utility of notion of E, H, L and LL primitive achondrites, too. In this paper we are continuing our previous work of evolutionally arranging the stony meteorites.

INTRODUCTION

Working on meteorite parent body evolution during the last 5 years we made theoretical estimations and statistical comparisons (using NIPR Antarctic Meteorit Dataset, YANAI, KOJIMA & HARAMURA, 1995; NOBUYOSHI & al., 1997) about the role of transitional meteorites between undifferentiated chondritic and well differentiated basaltic achondritic stages. Thus our recent paper is the continuation of BÉRCZI, HOLBA & LUKÁCS (1998) which, consequently, will be cited henceforth as Part I. We are continuing Part II in giving detailed description about the degrees of transitional stages between the (mainly high-temperature) end of chondritic evolution via different primitive achondritic stages which preserved more or less from the original primordial chondritic characteristics till.the final surface products of basaltic achondrites and mantle type residuals of lodranite-ureilite-peridotites.

Thermal metamorphism is an accepted theoretical petrological formalism to define the gradual transition of mineral assemblages (and compositions) between chondritic, primitive achondritic and differentiated basaltic achondritic meteorites. Classification of chondritic metamorphism (VAN SCHMUS, WOOD, 1967) formed standard examples for gradual transitional textures between thermally more and more transformed chondritic stages and made it possible to continue this sequence toward achondritic ones. The continuing of this sequence needs recognition and formulation of textural characteristics

[1] and [4] H-1117 Budapest, Pázmány P. s. 1/a. Hungary
[2] H-1088 Budapest, Múzeum krt. 4/a. Hungary
[3] H-1525 Budapest 114. Pf. 49. Hungary

of further transformations caused by the thermal evolutionary process which affected the parent chondritic body. These studies are in focus of research in the last 20 years. There were important recognitions of the stages following the chondritic stage.

It was important to assert that the first event following chondritic equilibration was the preservation of chondritic chemistry in a primitive achondritic stage. However, this stage seems parallel - at least in the case of some primitive achondrites, - with the partial melting and outflow of iron-sulfide assemblage from the primitive achondritic source. Such kind of transitional meteorites were found for this stage as Rose City, Netschaëvo, Watson, Techado and the latest was the Portales Valley veined H6 chondrite. This last case showed that there were no sharp boundary between stages of chondritic and primitive achondritic stages.

Later studies revealed that thermal evolution of the primitive achondritic assemblage may continue by partial melting of a low melting point basaltic like component which may outflow toward the surface of the asteroidal parent body. Lodranites and ureilites can be considered as representatives of this stage, representatives as residuals of a primitive achondritic station of thermal evolution, although they have less primitive characteristics then that of primitiv achondrites of the original definition (which we call stage A). Therefore we introduced the "primitive achondrite of stage B" expression and name for those achondrites which have lost both their iron and basaltic partial melts, but yet they contain considerable primitive components. Mostly, this component is the carbonaceous vein material in ureilites, but the exhausted (or depleted) peridotitic mineral assemblage also preserves the main chondritic one: olivine, pyroxenes and accessory minerals. This definition made it possible that over well metamorphosed chondrites, primitive achondites of stage A, (explanation later) and further developed primitive achondrites of stage B, (details also will be given later) can be arranged in a sequence, which continues the metamorphic sequence of chondrites. This sequence can be closed finally by the most developed forms of the originally chondritic source: with basaltic achondrites, and different iron meteorites and stony irons which also have place in this more and more complex evolutionary sequence.

Many of our earlier works (our reports on 30th LPSC, No. 1014, 1337) dealt with thermal evolution of chondritic meteorites and characterized this process by projecting Fe-bearing compounds onto the UREY-CRAIG field. On this field the metamorphic types of E, H, L, LL and C groups form thermal evolution paths of their chondritic meteorite parent bodies (BÉRCZI, HOLBA, LUKÁCS, 1995, LUKÁCS, BÉRCZI, 1997b); in the suggested R, G and K groups we still are unable to see evolutionary trends. We found that between E and H groups primitive achondrites occupy a special role. Over this region in E chondrites reduction at petrologic type 4 run toward more reduced stages. For H's more and more reoxidized states follow, see Fig. 12 of Part I. (We described these events by parameters of C/H_2O showing the redox competition of reducing C and oxidising H_2O for Fe, LUKÁCS, BÉRCZI, 1996.) Now we begin the detailed construction of the extended metamorphic chondritic sequence by arranging chondrites and achondrites according to their oxidized iron content and the degree of melting of their iron (primitive achondrite stage A).

THE SEQUENCE OF CHONDRITES: FROM CHONDRITES TO PRIMITIVE ACHONDRITES

The great variety of chondrites probably have some internal structure. A simple relationship is if the *letter* (E, H, L. LL and C) of the chondrite groups shows the *initial condition*, while the *number* (the petrologic type, henceforth PT, from 1 to 7) does the *thermodynamic evolution* from the initial condition. Fig. 16 of BÉRCZI, HOLBA & LUKÁCS (1996) shows the simplest such evolutionary scheme for the 30 samples of the remarkable NIPR Antarctic Thin Section Set. There thermal metamorphism is on the horizontal scale, element contents are on the vertical one, and the idea was that evolution had gone along the increasing petrologic type numbers. This is of course a hypothesis; according to new results it seems oversimplified at least in one point which will be discussed later. However, the most fundamental point of that scheme still seems valid: the "foliated" (i.e. initial condition separated) structure of the "thermodynamic state space" of the meteorites. "Horizontally" there may be genetic connections, but not vertically.

This "foliation" of the thermal evolution tabulation of chondrites can have a strong controll. Initial conditions can be defined by non-volatile element ratios. These were used for the graphs of thermal evolutionary pathways of BÉRCZI, HOLBA & LUKÁCS (1995). Also, some results are displayed in LUKÁCS, HOLBA & BÉRCZI, (1999), and BÉRCZI, HOLBA & LUKÁCS (1999a). In these works we checked the Mg/Si and Fe/Si contents, and also some abundances which do not seem reversible, of which here we mention FeS and C. Hence we think that the following relations are established. (We use abundantly the data of the NIPR Antarctic Meteorite Catalog (YANAI, KOJIMA & HARAMURA, 1995), which is a large, homogeneous body of data. Later reclassifications of individual meteorites occasionally have occurred and may happen in the future, but for definiteness' sake are ignored here. In some points, and definitely for carbon data, we also use Jarosewich's data of JAROSEWICH, 1990).

Among E chondrites PT 3-6 are known so far. Subgroups EH and EL are more or less consequently discriminated in the latest years but the group is rare and so the statistics is not good. For the whole E group Mg/Si is significantly lower than for ordinary chondrites (LUKÁCS, BÉRCZI, 1996), FeS and C is more abundant than in other groups except C. Total Fe is reported to decline from E5 (MASON, 1962), but our opinion is that this is iron loss by dropping out, and so no evidence against genetic connection between early and late E's, we will return to this point later. E achondrites seem direct continuation of the evolution with total metallic (and sulfide) Fe loss. It is worthwhile to repeat MASON's (1962) note that chondrules do not seem in E6's, which is against the VAN SCHMUS-WOOD (1967) convention.

There are the following PT's established so far in the H group: 3, 3-4, 4, 4-5, 5, 5-6, 6. We are now convinced that H3-4's of the NIPR Catalog originated from initial conditions alien from either the H or the E group. Their iron content is significantly higher than in the H group; it would fit into the E group, but H3-4's are poorer in FeS than even E4's. The origin of H3-4's is still obscure. The transitional types 4-5 and 5-6 do not deviate from the H trend (see Fig. 12 of BÉRCZI, HOLBA & LUKÁCS, 1996), and so they can be genuine H's. The H achondrites are not yet known. The H group is characterised by "average" Mg/Si and "high" Fe/Si.

L's are known as 3, 4, 5, 5-6, 6 and 6-7. L5-6's do not deviate from the trend, but the redox processes were simpler without this rare subgroup. If the only L6-7 of the NIPR

Catalog is genuine L, then it shows final Fe° loss (as E5&6, see this later in details). The group has average Mg/Si and low Fe/Si. (Hypersthene achondrite of MASON, 1962 was later named diogenite. But one extraordinary sample: Yamato 790126 was classified to L6, (YANAI, KOJIMA, 1987), however, it did not contain chondrules so may be L7, and this may be the link to L achondrites.)

LL's are found in PT 3, 4, 5, 6 and 7. All of them fit into the trend, with Fe° loss in LL7. LL's are characterised by average Mg/Si and low Fe/Si, just as L's, but their Fe/Si is slightly lower, and Fe°/Si is significantly lower. (Real LL achondrite is unknown. On the basis of FeO/ Fe° ratio chassignite and eucrite was considered as LL achondrite.)

The C group is recently becoming a supergroup, distinguished by second letters as CI (only 1), CM (2, and according to ZOLENSKY & al., 1), CR (mainly 2, but according to ZOLENSKY & al. 1997, in PT 1 too, at least mosaically), CO (only 3), CV (generally 3, but Kaba is maybe 2, and Coolidge 4), CK (4&5?) and so on. The systematics is obviously in change recently. Anyway, the trend seems to be a partial reduction until PT3, and then reoxidation (LUKÁCS, BÉRCZI, 1997a). The C (super)group is characterised by high Mg/Si and high Fe/Si. The ureilites share the high Mg/Si abundance. While their Fe/Si is too low, so they directly cannot be C achondrites, at least they remind us them.

Now, the only possibility for "vertical" transitions is L <-> LL, and even that is not probable, except misclassifications. Between any other 2 groups, as it is shown, conserved ratios differ, so "superselection" rules prohibit transitions. On the other hand, with the above mentioned exception of "H3-4" *within* a group all PT's seem accessible by i) aqueous alteration (see later), ii) by redox processes (for which agents C and H_2O are present, iii) by sulphide loss (details obscure) or iv) by Fe° loss in terminal stages (later).

These genetic chains, then, seem more or less well-founded, and even connect chondrites to ("primitive", i.e. undifferentiated) achondrites. However the two ends of chondritic chains need discussion. In Part I we took the simplest picture when all evolutionary chains started in PT 1, however it seems that the situation is not so simple. Therefore we incorporated here the following 2, short, Sections for completeness' sake, and the problem of parent body initial conditions deserve a more detailed treatment in another paper.

THE PRIMITIVE CHONDRITE STATE FOR E, H, L, LL AND MAYBE FOR C GROUPS

If one wants to read PT's as the direction of Time's Arrow, then the evolution of chondrites start from *no chondrule* (see, with some mental reservation, Part I). The picture is by no means impossible, see e.g. MASON's idea (1962) for olivine & pyroxene chondrules formed from serpentine via heating, H_2O loss &c. In addition, compositions of Orgueil, Ivuna and Y-82162 can be hardly derived from C2's (e.g. because of high FeS). Still, present observations (e.g. ZOLENSKY & al., 1997; MCSWEEN, 1979) seem to prove the inverse route (see below).

For the C chondrites of the NIPR Catalog the "primitive" C seems to be somewhere among C2's. However the general feeling is that the groups E, H, L and LL start in PT 3.

Now, this may be a simple convention. E. g. consider HUTCHISON, ALEXANDER & BARBERS' suggestions (1987) that "LL 3"'s Semarkona and Bishunpur should be reclassified as LL 2.

The problem is twofold. First, a meteorite is an open system, so we do not have such a sure Time's Arrow as specific entropy for closed systems, moreover we must admit that this problem is not finally solved in Thermodynamics. Second, in the VAN SCHMUS-WOOD nomenclature both PT 2 and PT 3 are characterised by "sharp chondrules". The 2 PT's are discriminated via H_2O and C contents, which, however, cannot be used when one compares chondrites of *different initial conditions.*

Still, we can conjecture the evolutionary relations by probability arguments. It is much more probable to almost any process to destroy sharpness of chondrules than produce; loss of volatiles as H_2O and C could be more frequent than gain; and in most meteorites FeS is the only major S source, so FeS cannot grow.

Hence one can say that an LL 2 is something more primitive than LL 3 if its chondrules are sharp too but the H_2O, C and FeS contents are "too high". Now, the suggested LL 2's Semarkona and Bishunpur (HUTCHISON, ALEXANDER & BARBER, 1987) have much higher than average C content, while H_2O and FeS are at least too among the highest (JAROSEWICH, 1990). In BÉRCZI, LUKÁCS, (1999) this suggestion is accepted and the arising carbon trend is quite reasonable. On the same basis we suggest Sharps H3 (JAROSEWICH, 1990) to be reclassified as H2. Fig. 1 shows a three-colour graph for Fe^{tot}, Fe^{ox}, H_2O and C for chondritic types (BÉRCZI, LUKÁCS, 1999) in the spirit of this Chapter.

If so, then the primitive or initial chondritic state is in PT 2 or between PT 2 and 3.

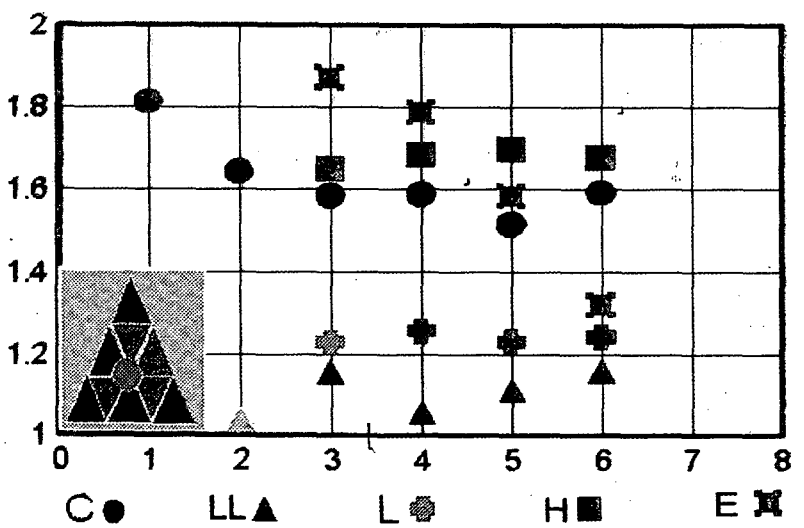

Fig. 1. 5 component color plot of the chondrite type averages of iron-carbon-water content for all chondrite groups (C, LL, L, H and E) of data from the NIPR Catalogue (YANAI, KOJIMA, HARAMURA, 1995). The 5 parameters are: total Fe/Si (y axis), the VAN SCHMUS-WOOD types (x axis) and 3 in colors of iron-carbon-water averages, mixed according to color mixing rules. For colors red is the weight of reduced (metallic) iron, green is carbon, blue is water content. Vertical axis shows the total Fe vs. Si ratio for the chondrites and means different initial conditions for different chondrite groups. Along horizontal axis we can observe trends of parent body evolution. Observe that the data along the thermodynamic evolutionary trend of increasing VAN SCHMUS-WOOD types (texturally and compositionally defined stages by numbers, horizontal axis) points for C and H group chondrites run almost parallel and also this is the observation for the L and LL group chondrites, too. E chondrites may have different origin and along advancing thermal evolution stages their plot crosses the trend of C and H groups.

RETROGRADE (AQUAEOUS) ALTERATIONS: A CASE FOR C-S AND LL-S ONLY?

Now, from the primitive state, according to the circumstances the evolution may go into 2 directions. In dry conditions diffusion starts. This was treated in Part I and will be again detailed in the next Section. However in very wet environment aquaeous processes can start. ZOLENSKY & al. (1997) demonstrated the "retrograde" process CM2->CM1 (and, virtually, CR2->CR1 too), and Kaba is at least an example when it is doubtful if the petrologic class is 2, 3 or 4 (e.g. the chondrules are anomalous).

Here we note only that there are thermodynamic similarities between the "direct" (diffusion) and "retrograde" (aquaeous) evolutions. Preparing an initial stage of sharp chondrules and large gradients in chemical potentials (for ordinaries often regarded as PT 3.0), both processes simultaneously unsharpen the chondrules *and* decrease the gradients of chemical potentials. To see Time's Arrow detailed differences must be observed.

Now we shift our attention to direct evolution and also recapitulate some statements from Part I.

GENERAL TREND FOR CHONDRITES BY: DIFFUSION

Obviously the genesis of parent bodies was complicated and observation is impossible. However diffusion must have been present, and it seems that the main facts of direct chondritic evolution can be interpreted via it.

Assume an initial stage of sharp chondrules and large chemical gradients in a more or less olivine-pyroxene assemblage at the formation of asteroid-sized parent bodies; if it happened just after the primordial crystallization then short-lived nuclei as Al^{26} ($t_{1/2}=7.4*10^5$ y) or Pt^{244} ($t_{1/2}=7.6*10^7$ y) could still produce a high temperature. If one does not believe in this, he may rely on heat from the gravitational accretion.

The simplest model is a constant temperature T_o for a time $t_o \approx t_{1/2}$ and then a negligible equilibrium temperature. Then diffusion establishes homogeneity on a length

$$l_D \approx (D_o t_o)^{1/2} \qquad (1a)$$

$$D_o = D(T_o) \qquad (1b)$$

Let the primordial chondrule size be r_o. This quantity varies from group to group, but now for orientation we take $r_o \approx 0.3$ cm. One can improve the presentation by substituting better values.

Via only diffusion, a chondrule border is **sharp** if $l_o << r_o$ (and then PT is 2 or 3), **clear** if $l_o \sim r_o$ (PT 4&5), **obscure** if $l_o > r_o$ (PT 6) and **not seen** if $l_o >> r_o$ (PT 7 or primitive achondrites). Taking $t_o \sim 10^6$ y (Al^{26}) and the above r_o:

PT 2&3 $D_o << 3*10^{-15}$ cm^2/s
PT 4&5 $D_o \sim 3*10^{-15}$ cm^2/s
PT 6 $D_o > 3*10^{-15}$ cm^2/s
PT 7-∞ $D_o >> 3*10^{-15}$ cm^2/s

Table 1: The values of diffusion coefficients leading to various petrologic types with primordial Al^{26} heating.

Now,

$$D_o \approx A_o \exp(-Q_o/kT) \qquad (2)$$

where Q_o is some energy to form lattice defects to diffuse through, in the order of 1 eV, while for the prefactor A_o, very roughly,

$$A_o \sim a^2\nu \quad (3)$$

where a is the lattice length, and ν is the frequency of the (thermal) oscillations in the lattice.

We would need A_o and Q_o in the temperature range cca. 500 - 1500 K, for all the major olivine, pyroxene (and feldspar) constituents. As will be seen in the next Chapter, there is no problem with olivines, but pyroxenes are more various.

Anyway, one can guess the trends via melting points T_m. Namely, until there is a simple and more or less regular lattice, T_m is determined by the same factors as ν and Q_o, and then

$$Q_o = \alpha k T_m \quad (4)$$

$$\nu = ß(k/h)T_m \quad (5)$$

where k and h are the Boltzmann and Planck constants, respectively, while α and ß are dimensionless and maybe slowly varying factors. Just below T_m we get then

$$D(T_m\text{-}0) \approx a^2 ß(k/h)T_m \exp(-\alpha) \quad (6)$$

and, since for all relevant materials $a \approx 3*10^{-8}$ cm and $T_m \approx 1500$ K, $D(T_m\text{-}0)$ is in the range $0.03ße^{-\alpha}$ cm^2/s.

Now we can see α and ß at least for some metals and simple olivines. For many solid states $\nu \sim 10^{14}$ s^{-1}, whence ß seems 0.3 - 1. For various metals A_o=(0.01-0.1)cm^2/s in accordance with (6). For self-diffusion in metals α is cca. 18, and then a form (4) is told to be good for 10 % (SHEWMON, 1963; LAZARUS, 1960). According to these numerical factors $D(T_m\text{-}0)$ is expected about $1.5*10^{-9}$ cm^2/s. Then from the numbers we gave at the end of the last Chapter it is clear that if a meteorite consisted purely of metals and simple olivines, the diffusion would erase the last traces of chondrules far below melting point. On the other hand, the composition would remain chondritic.

For olivines there is a detailed investigation for San Carlos (Arizona) olivines between 10 and 40 weight % Fe (BUENING & BUSECK, 1973). At higher temperatures, extrapolating to pure forsterite (T_m=2163 K) A_o=0.03 cm^2/s and α=14.21, while for pure fayalite (T_m=1478 K) $A_o=3.4*10^{-4}$ cm^2/s, and α=13.28, so α is slowly varying with composition and not too unsimilar to metals. With these values in an imaginary meteorite of pure forsterite chondrules would be erased by diffusion on 1112 K, while in pure fayalite on 848 K. These temperatures are rather low, pure olivine meteorites are absent, but the numbers show a trend.

We close this Chapter with examples, one from the great variety of pyroxenes, augite, and a Ca-mica, margarite. FECHTIG, GENTNER & ZÄHRINGER (1960) investigated Ar diffusion in them, and, while that coefficient is not just valid for Al, Mg or Fe, it gives an orientation. At 1000 C° D is just below 10^{-10} cm^2/s in margarite, but only about 10^{-13} in augite, showing the variety; Q_o is 1.16 eV for high-temperature augite and 2.31 eV for margarite, while the corresponding A_o's seem to be $8*10^{-9}$ cm^2/s (!) for augite and $7*10^{-2}$ cm^2/s for margarite. The data for the Ca-mica are not unsimilar to those for either metals or olivines; but for the pyroxene augite the diffusion coefficient is order of magnitudes smaller. This suggests that olivines equilibrate much faster than pyroxenes and it is indeed so.

TO THE PETROLOGIC TYPE 4.0 AND BEYOND

According to the previous data we may expect that equilibration happens first in olivines. Also it needs then the highest temperature in forsterite (so E3 chondrites). Taking $t_o \approx 10^6$ y (Al_{26}) and $l_D >> r_O$ *for olivine*, $D(T_o) > 10^{-14}$ cm^2/s is needed. This is 875 K. Well above this temperature diffusion is complete even in the olivine of E's, so our

guess is that the state is beyont E4.0. In the same time $D(T_0)$ is just $3*10^{-15}$ cm^2/s *for augite*, so indeed some structures did not yet diffused away, so the chondrules are still seen, not quite sharp, but clear. Using augite as a model for the beginning of obscure chondrules, PT 6 one would get at least 700-800 C°, and for the beginning of no chondrules at all at least 1000 C°.

In addition observe that chondrules do not seem in E6's (MASON, 1962). If so, then they are really E7's in the present scheme, and then that stage is beyond 1000 C°.

Now let us abandon the augite model and tell simply that measurements would be needed for various pyroxenes relevant in chondrites. In the next Chapter we use scaling laws.

OLIVINES AND PYROXENES ON THE CHONDRITE/ACHONDRITE BORDERLAND

We have seen that, if the silicates do not melt before, a continuous fading of chondrules is expected, and this can be PT 7. Chondrules are no more seen, maybe everything is almost homogeneous, but the bulk composition is still quite chondritic (except maybe for Fe°, see the next Section). Now, according to the rough scaling with T_m, for which we showed examples in the previous Sections, and which is based on the fact that higher melting point means higher interatomic forces, so higher activation energy needed for lattice defects through which diffusion becomes possible, we can guess that if a specific stage has been reached at T_0 in pure Mg-silicate (i.e. extremal forsterite), then in other silicates the same diffusion stage has been got at a temperature lower proportionally with the actual melting points. On Fig. 2 we compare olivine melting points, although E chondrites are rather enstatite, so pyroxenic. For C-s the situation is not so simple, e.g. serpentine may substitute the olivine.

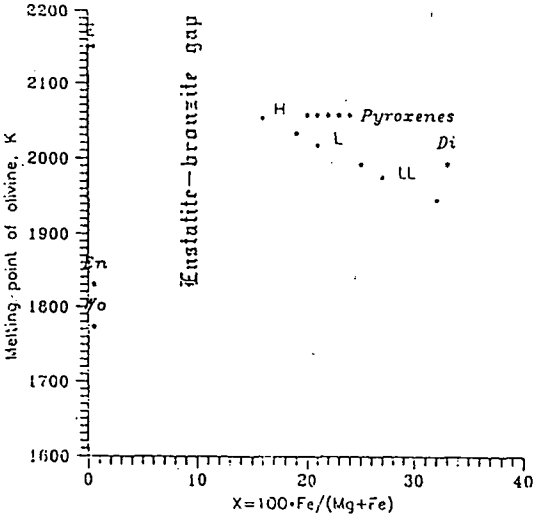

Fig. 2. Melting points of characteristic olivines and some pyroxenes as function of Fe/Mg ratio. This plot may explain partly the enstatite-bronzite gap in the Urey-Craig field, and the point of inflexion between the enstatite chondrites and bronzite chondrites evolutionary paths (LUKÁCS & BÉRCZI, 1997a).

For pyroxenes the melting points are somewhat lower, e.g. T_m is 1830 K for enstatite, 1773 K for wollastonite and 1993 K for diopside.

Now we roughly estimate the important temperatures from Fe loss.

Fe LOSS: VIA C AND FeS TOO

We do see Fe loss in chondrites. MASON (1962) definitely reports a small Fe deficiency in E5 and a serious one in E6 (but, as we saw, it is possible that these states should be called E6 and E7, respectively, from the point of view of diffusion scale). It is possible, of course, that this is not evolution, but different initial condition, and anyways, E's are rare, so the statistics is poor, but still we take the simplest explanation.

Fe° and FeS are not integral parts of the silicate lattice, and Fe specific gravity is much higher than that of the silicate. So the Fe-FeS-C mixture flows out and becomes gravitationally separate if its melting point is reached and some gravity is present. The second condition is fulfilled in parent bodies. As for the first, the exact melting point is hard to calculate, it is well below the silicate melting points. Fe° and FeS melt near to each other. The pure Fe melts at 1535 C°, but already a very small amount of C brings down the melting point below 1500 C°, while pure FeS melts at 1430 C°. The eutectic carbonated Fe melts about 1140 C°, and this needs 4.3 weight % C. Now, since in E's C is cca. 0.4 % and Fe is cca. 25 %, the bulk average of C in Fe is only cca. 1.6 %, but then some 2/5 part of the Fe can flow out at 1140 C°. In addition there is a substantial FeS content, some 1/3 of the Fe° (JAROSEWICH, 1990), decreasing further the eutectic temperature. In the same time the melting point of forsterite is 1890 C° (that of corresponding pyroxenes is somewhat lower), so the E silicates may exist for a wide temperature range after Fe° and FeS leaves molten, for the core of the parent body.

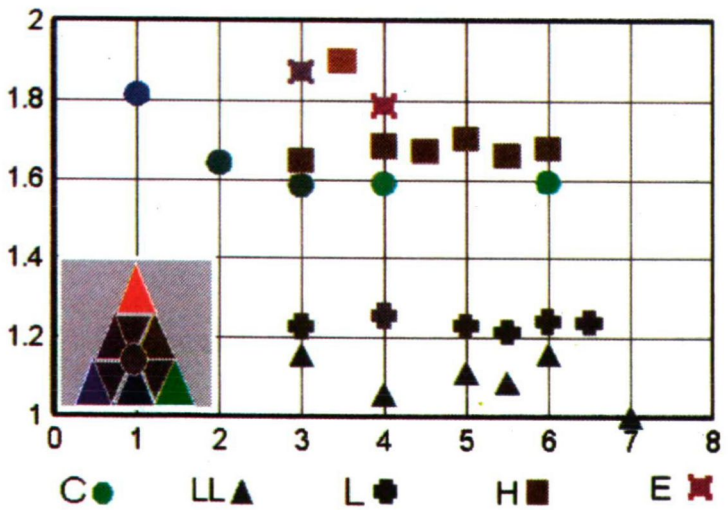

Fig. 3. 5 component color plot of the chondrite type averages of iron-ironoxide-ironsulfide content for all chondrite groups (C, LL, L, H and E) of data from the NIPR Catalogue (YANAI, KOJIMA, HARAMURA, 1995). The 5 parameters are: total Fe/Si (y axis), the VAN SCHMUS-WOOD types (x axis) and 3 in colors of iron-ironoxide-ironsulfide averages, mixed according to color mixing rules. For colors red is the weight of reduced (metallic) iron, green is the weight of oxidized iron, blue is the weight of sulfidized iron content. Vertical axis shows the total Fe vs. Si ratio for the chondrites (means different initial conditions for different chondrite groups). We can observe the parent body evolution trends along the horizontal axis. This shows that now again the points for C and H group chondrites run almost parallel and this is the observation for the L and LL group chondrites, too. This plot also shows that E chondrites may have different origin and also shows that advancing thermal evolution stages their plot begin to cross the trend of C and H groups. The data of H3-4 chondrites may relate these chondrites to the E chondrite group.

Fig. 3 is a three-colour graph using the data of the NIPR Catalog everaged for all combinations of chondritic groups and petrologic types. The vertical position is the total Fe/Si content, the red, green and blue constituents are the metallic, oxidised and sulfidised components. Outflow is directly seen from the vertical position. But also an iron outflow is expected to carry away troilite too, so outflow is more certain if the colour loses a *purple* component.

On the other hand we do not see Fe deficiency in the (average of the) H6's of the NIPR catalog, 23 meteorites, a reliable statistics (LUKÁCS, HOLBA & BÉRCZI, 1999). Now this may have two reasons. First, we saw that the temperature of PT 6 must be lower in H's than in E's, because of the lower Mg content. Second, both C and FeS is less abundant in H's, so melting point decrease is much smaller.

H7 meteorites were unknown till 1997, when Y-75008 was identified as such (YUGAMI & al., 1997; 1998). Since 1987 (YANAI & KOJIMA, 1987) it was known about that sample that it showed a generally chondritic H composition but no chondrules except maybe some relic ones (YANAI & KOJIMA, 1987), and its troilite exhibits a net-like pattern. It, then, percolates, which is a necessary (and sufficient?) condition of flow out. Unfortunately bulk Fe and FeS data are not given in the 1995 NIPR Catalog. However YUGAMI & al. (1998) found a subvolume with 29 volume % FeNi. Since this is much above characteristic Fe° content in H's, it is sure that segregation started. On the other hand, as we saw, it did not start for PT 6.

There are 94 L6's in the NIPR Catalog. In average Fe° and FeS abundances are just the averages of all L's, and very similar to the averages of the 17 L5's. There is one identified L6-7, and it shows a cca. 15 % deficit in both Fe° and in FeS, so it is possible that Fe started to flow out, but one cannot make any statistics with a single sample.

The average of the 18 LL6's of the NIPR Catalog does not show either Fe° or FeS deficit compared to all LL's. However there are two LL7's, and their averages (albeit poor for statistics) show serious deficiency in both ferrous phases. Then the LL6 stage is not hot enough for liquid Fe (we may expect it cooler even than H6), but LL7 is hot enough (TAKEDA & al, 1984).

Finally C's are found only until PT 6, they are even more fayalitic, so they are expected to reach PT 6 at lowest temperature, and we do not see indeed Fe deficit in them.

E, H, L, LL PRIMITIVE ACHONDRITES IN THEIR PARENT BODY EVOLUTION

In the present study we would like to make clear distinction between the usual achondrites, say basaltic meteorites, and the primitive achondrites. Beyond PT 6 chondrules are already absent, but the compositions (with the possible exception of the Fe°-FeS-C triad) are still chondritic. Such an achondrite is clearly not of basaltic, or differentiated composition. Originally the term "primitive achondrite" was used for achondrites with chondritic composition, but *belonging to the E-H gap in the Urey-Craig field.* The accumulation of meteorite samples in the last 30 years mainly by Antarctic samples made it possible to see more transitional meteorites between chondritic and basaltic achondritic stages. Introduction of E, H, L and LL primitive achondritic concepts want to make clear distinction for a stage between chondritic and achondritic (earlier mainly basaltic achondritic) meteorites. In the sequence from chondritic to basaltic achondritic stage the E, H, L, and LL primitive achondritic stages will stand between the metamorphic grade 6 and the basaltic achondritic stages of these

chondritic groups. In *our convention* primitive achondritic state begins roughly with the PT 7 chondritic one (already without chondrules). Then the old primitive achondrites (in the E-H, or enstatite-bronzite, gap), are also primitive achondrites, only of a chondrite group still unknown in its par excellence individuals. The gap still needs its explanation (BÉRCZI & LUKÁCS, 1998).

There are two processes which both distinguishing par excellence chondrites from achondrites: the Fe loss by melt and metamorphism, which go according to different rules. Iron or sulfide melting needs a temperature not more then 1300 K and often much lower for Fe-FeS-C mixtures, and relatively short time. On the other hand metamorphism could be described mostly by diffusion. In the second strip of the borderland, between primitive achondrites (PT 7) and the par excellence (basaltic) achondrites iron loss may or may not still go, but there is a new process, silicate melting (at lower temperatures partial, at higher maybe total). When silicates melt and can macroscopically move and mix, diffusion loses its meaning. After silicate partial melting has started we have already two directions of differentiation. In one direction partial melts are going away and depleted chondritic composition remains. (The extremal remnant of this direction resembles ureilites according to our suspection.) In the other direction the basaltic component is enriched (added to the originally primitive achondritic composition, resembling first Acapulco, later Lodran and so on, MITTLEFEHLDT & al, 1996, MCCOY & al, 1997) and the final product is some kind of basaltic achondrite. Because the silicate melt loss may preserve some components of the primitive achondritic composition (i.e. the carbonaceous material, some "islands" of metal, sulfide and carbon assemblages) we introduce the expression primitive achondrite of stage B for these meteorites. Mainly ureilites and some lodranites are involved in this group.

We may summarize our new definitions: the E, H, L, LL *primitive* achondrite (stage A) is a range which is in between metamorphic diffusion and differentiated endproducts of thermal evolution of chondritic parent body. The *primitive achondritic state is an interval* and it is characterized by the processes of separations: first iron, then silicate-melt. So this range can be divided to two parts: first the range of primitive achondritic **stage A** is characterized by the process of **separation of iron**. Second, the primitive achondritic **stage B** is characterized by the process of **separation of silicate melt**. Both have important role and we note only that this part of parent body thermal evolution is "mixed" with gravitational and rheological effects, too. In one of our earlier works we could show the most crude effects of gravitation if we compared basaltic sequence of the Earth and an asteroid (LUKÁCS, BÉRCZI, 1998). There we found that FeO content of the basaltic sequence is far lower for the terrestrial basalts than basaltic achondrites, and this trend is valid from komatiites to recent tholeiitic basalts, in the same way than from diogenites through howardites to eucrites. Moreover, the counterparts of the high Mg bearing depleted lherzolites could be found in the high Mg bearing ureilites. We cannot assert that all these differentiations (we called it "barometric height formula for silicates", LUKÁCS, BÉRCZI, 1998.) occurred parallel in an asteroid, but we wanted to show that such an effect can be observed in the statistics of the recent dataset (mainly we used the NIPR Catalog, YANAI, KOJIMA & HARAMURA, 1995).

IRON OUTFLOW FROM CHONDRITES: TEXTURE OF THE METAL COLLECTING (VEINED) H6 CHONDRITES AND RELATED II E IRONS WITH SILICATE INCLUSIONS

There are six meteorites in this clan. Three of them were classified to H chondrites, and also three were as primitive II E irons with silicate inclusions (MCCOY, 1995).

Rose City: Fell in 1921, in Michigan State, USA. Its remarkable characteristics was the 36.4 wt.% total iron content. Although brecciated, it was classified as H5 chondrite (its Fa (19) is typical to the H range), which contains larger Fe-Ni inclusions as nodules (WIDOM & al, 1986, RUBIN, 1995, IKEDA & al, 1997). It was shocked and contains portions which are free of metallic Fe-Ni and troilite, like as Chico, too (PINAULT & al, 1999).

Y-791093: Found in 1979 on Antarctica by Japanese Expedition it was classified to H6 (YANAI, KOJIMA & HARAMURA, 1995) but contains equal amounts of metal+sulfide and chondritic portions (in vol.%). If separated, the metal + sulfide portion is texturally similar to IIE irons, the chondritic portion is H6. However, the whole assemblage is similar to Netschaevo and Techado chondrite-like inclusion containing primitive IIE irons (IKEDA & al, 1997).

Portales Valley: Fell in 1998, in New Mexico State, USA. In some protions the metal rich veins penetrate the whole hand-specimen sample with wider and a network of thinner veins. Its metallic Fe-Ni content in some fragments is ca. 35 wt. % (vs. ca. 18 wt. % of average H chondrites, RUBIN & al, 1999). Considered to have been brecciated (KRING & al, 1999, RUBIN & al, 1999), or equilibrium with chondritic portion, melted (PINAULT & al, 1999, RUZICKA & al. 1999). Although descriptions distinguish *adjacent to vein* (finer grained than most of H6 chondrites, enriched in troilite and depleted in Fe-Ni metal) and *away from vein* (normal, Fe-Ni and troilite containing) portions of chondritic parts, both have essentially H6 textural characteristics(PINAULT & al, 1999). The melted metal is typical H-chondrite metal (KRING & al, 1999) and is unlike to veins of Rose City (PINAULT & al, 1999). It resembles to Kernouve veined H6 chondrite (PINAULT & al, 1999). (Kernouve may also be involved to our H6+IIE-clan.)

Netschaëvo: Found in 1846, in Russia. The primitive IIE iron matrix contains angular silicate inclusions, which comprise the 25 vol. % of the meteorite. Silicate portion contains relict chondrules and its refractory element content is in the range of the ordinary chondrites, although the Fa (14) of olivine is outside of the H chondritic range (BILD, WASSON, 1977). Silicate portion has not undergone melting only heating and recrystallization. It has higher Fe/Si ratio, than upper Wiik line chondrites, and this ratio is only the same for Rose City (BILD, WASSON, 1977). Its metallic portion has siderophile element content also higher (cca. 2 times) than H chondritic metal range (BILD, WASSON, 1977). With its characteristics nearer to the E-H point of inflexion Netschaevo can be considered an E-H chondrite related member of our H6+IIE clan.

Techado: Found in 1977, in New Mexico State, USA. This IIE iron meteorite contains a smaller silicate inclusion inside the iron. The mass of silicate is unmelted but exhibits a strongly recrystallized texture. Olivine (Fa 16.4) and pyroxene (Fs 15.3) relates it to H chondrite range. No shock effects have been observed on silicate inclusion, so metallic components may have been locally segregated (CASANOVA & al, 1995).

Watson: Found in 1972, in S. Australia. This IIE iron meteorite contains the larger silicate body ever found inside an iron meteorite. The large mass of silicate, engulfed in

the iron, melted during its including into iron melt, but after recrystallization it preserved its bulk composition similar to H-chondritic one, except metal+sulfide fraction (unlike to Kodaikanal silicate inclusions, which sufferred fractionation after melting, OLSEN & al, 1994). The metal matrix is characteristic to H chondritic metals. It was observed, that metal sufferred shock (OLSEN & al, 1994).

The collected 6 cases of the H+IIE clan meteorites has the following fundamental properties, summarized: (Table 2.)

Name	Silicate	PT (Ch.)	Iron	Shock(Silicate)
Rose City	H	5	IIE	Y(brecciated)
Y-791093	H	6	IIE	Y
Portales Valley	H	6	IIE	olivine mainly in shock st. S1
Netschaëvo	bw. H & E	(Y)	IIE	N
Techado	H	beyond 6	IIE	N
Watson	H in IIE	beyond 6	IIE	?

Table 2: Portales Valley, and some of its possible relatives. Data according to OLSEN & JAROSEWICH (1971); IKEDA ET AL, (1997); OLSEN ET AL, (1994); KRING, HILL & GLEASON (1999); RUBIN & ULFF-MØLLER (1999); RUZICKA, SNYDER, PRINZ & TAYLOR (1999) and PINAULT, SCOTT, BOGARD & KEIL (1999); METEORITE NEWS 1996. Observe that this Table explicitly show Netschaëvo as a "chondrite in the gap": something still with chondrule, and gap composition.

Portales Valley is the only chondrite which has Widmanstätten pattern in its iron portion. Observe that irons of all the 6 clan meteorites are of the same type, conform to iron flowing out of the chondrite matrix. As for cooling times or rates and original and/or transient heating, PINAULT & al. (1999) suggest a rapid heating, metal crystallization in "months or years", Ni cooling rate in taenite cca. 5 K/My, they prefer Al^{26} (or similar) heating. RUBIN & MOLLER (1999) conjecture local shock temperature up to 1635 C° a cooling rate for metal 10 K/My between 700 and 500 C° and doubt about the availability of an Al^{26} heating. Finally KRING & al. (1999) call the exact cooling rate uncertain, as sometimes it is claimed that rapid cooling is also conform with Widmanstätten pattern (RASMUSSEN & AL., 1995) but for the post-impact metal cooling they guess ~10 K/My, and prefer the impact when the parent body was still warm.

STAGE A PRIMITIVE ACHONDRITES FOR H-S: A SELF-CONSISTENT SCHEME

Observe that Table 2 is self-consistent. All iron portions seem to be the same type, and comparing shock and chondrite type, the pattern is not self-contradictory even if, according to Occam's razor, we do not want to postulate outside source for iron.

Namely, we do know that "ordinary" H6's were not hot enough for Fe° outflow; but shock is observed in Portales Valley, Rose City and Y-791093 (and it is worthwhile to note that Y-790126, L6, with a substantial Fe° phase is shocked too; METEORITE NEWS 1998). For Netschaëvo and Techado, where shock is absent, the chondrite is *not* H6. Techado is "beyond H6", i.e. it may have had such a temperature where iron flow started (still far below the melting point of bronzite olivines) and Netschaevo is "between E and H" and we saw at least that there is outflow in E6's. In Watson where we do not show if

shock happened or not, the general composition is H, but the chondrite may be again "beyond H6".

As for "between E and H", we note that regular chondrites are not found in the enstatite-bronzite gap, but such silicates occur in e.g. lodranites. It seems that in the state space there is a repulsive point (BÉRCZI, LUKÁCS, 1998, BÉRCZI, HOLBA, LUKÁCS, 1999a). Fig. 4 shows some "suspected" meteorites, compared to both H6's and E's of the NIPR Catalog. The "anomalous" meteorites are put on the Figure in 2 groups. The first one consists of 7 Yamato meteorites which were found somewhat anomalous for the discoverers and appear in the NIPR Catalog. One (Y-74063) is a G chondrite, denoted such on the Figure, 3 (Y-74357, -75274 and -791493) are lodranites (L), 2 (Y-75097 and -793241) are L6 and here denoted by "6", and one, Y-794046, is H4, denoted by "4". We see that, at least on an FeO-Mg graph, they merge with the H6's, even if at the edge of the strip. The other group is 4 "anomalous" meteorites: ALH-85085 (H), Winona (W), Netschaëvo (N) and Acapulco (A) (JAROSEWICH, 1990). Interestingly enough, on the oxide Fe - Mg plane they form a straight line, but their positions, with the exception of Netschaëvo, project onto the usual chondritic positions. Netschaëvo is clearly "in the gap" (BÉRCZI, HOLBA, LUKÁCS, 1999b).

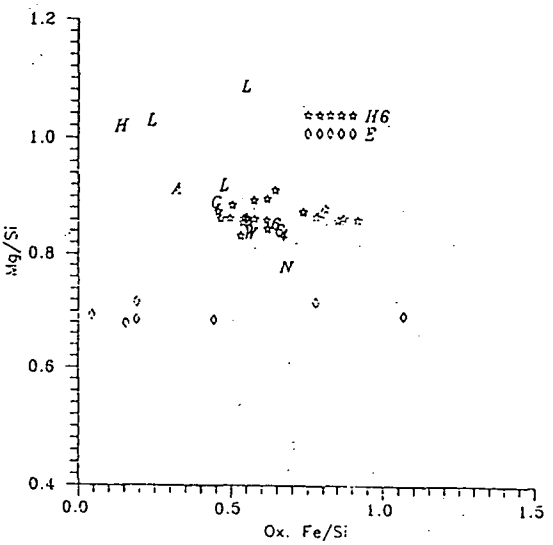

Fig. 4. Mg/Si vs. oxidized-Fe/Si plots for H6 chondrites and E chondrites of the NIPR Catalogue. This plot shows that Mg/Si ratio clearly distinguish E and H chondrites (diamond plot marks and stars) and in the gap we can see a strange meteorite, transitional from chondrites to primitive achondrites stage A: Netschaëvo. Some other strange chondrite meteorite data are also projected (A - Acapulco, L - lodranites).

As for the multiplicity of data about the thermal history there seems no self-contradiction either. It would be dangerous at the present state of art to decide the "Al^{26}, Yes or No" question. We refer only dozens of asteroids down to radii 30-50 km either spherical or differentiated. Something must have melted them maybe just after condensation. If not Al^{26} (or Pu^{244}) then something unkown well mimicking it. We call it for a while "Al^{26}" in the sense of Mark Twain who stated that plays of Shakespeare were written by another person of the same name.

Now in Portales Valley we saw the shock. Then take the normal history of the (H) parent body, the interior at H6 temperature, then a shock sometimes $0<t<t_0$, so in the heydays of "Al^{26}" heating. The shock increased the temperature above Fe (Fe-FeS-C) melting point and the metal solidified back for "periods greater than several weeks" (PINAULT, SCOTT, BOGARD & KEIL, 1999). It seems that the cooling slowed down to 10 K/My only later, at lower temperatures. Now, this slower rate may be the normal (non-shock) cooling rate of a deep interior (KRING, HILL & GLEASON, 1999), but also it is automatic equilibrium cooling if $t_o \sim 100$ My, which is so if the heating went by Pu^{244}.

In this story the shock increased normal H6 temperature beyond H6 and Fe° melting, but this increase was transient. If it lasted much less time than t_o (even if "over months or years"; PINAULT, SCOTT, BOGARD & KEIL, 1999), then there occurred practically no change of the silicate *via diffusion* (so in PT) while permanent change happened in *Fe° and FeS loss*, which went not by diffusion but by flow.

STAGE B PRIMITIVE ACHONDRITES: UREILITES, TEXTURE, MINERALOGY

We studied in details the ALHA77257,77-4 thin section of the NIPR collection, a 4mm X 7mm surface, on loan for studies on the Eötvös University (Pict. 1/a.). The thin section nicely exhibits characteristic features of the ureilitic mineralogy and texture. (YANAI, KOJIMA, 1987) Our carbon distribution map shows that ALHA 77257,77-4 ureilite veins are rich in carbon (Pict. 1/d.). The large olivine and pigeonite grains frequently have triple junctions with 120 degrees. Most inter-grain boundary regions are filled with carbonaceous veins, but many with metal ones. Outer rims of the olivine and clinopyroxene contain reduction-exsolved metal blebs which form transitional semi-opaque boundaries around the minerals. Some veins are alternately filled with carbon and metal. While Ol/px assemblage is more igneous/metamorphic and may be classified together with terrestrial mantle rocks (i.e. lherzolites), the other component, the veins are the remnants of the carbonaceous matrix (JANSSENS & al, 1987): they are last survivors and preservers of chondritic primitive components. Survival of such a primitive component allows us to call ureilites primitive achondrites, although in stage B, because they are very much metamorphosed if compared to acapulcoites and lodranites. (Igneous origin of ureilites was also summarized, e.g. GOODRICH & al, 1986, GOODRICH, 1992)

Microprobe compositional investigations were carried out by an AMRAY 1830I/T6 SEM instrument equipped with an EDAX PV 9800 ED system. Accelerating voltage was 15 keV and we used 1-2 nA beam current. Measurements on olivine and clinopyroxene gave the conventional Fe content range: Fs 15-22.%, Fa 13-25 %. There are 2 kinds of olivine, the darker with 50.54 % MgO, 41.32 % SiO_2, 6.48 % FeO, the lighter with MgO 44.80, SiO_2 40.05, FeO 13, 51 %. Both olivines have Cr_2O_3 bw. 0.69-0.76 %. We found Cr sulfide spherules in olivines; their Cr content varies bw. 9.50 and 24.86 weight %. This high-Cr spherules together with the previously mentioned primary magmatic carbon grains in ureilites (GOODRICH & al., 1986), shows that mafic silicate minerals also contain probably primitive chondritic components (see Pict. 1/b, 1/c and 1/e). If we compare them with other reducing inclusions in chondrules (HANON & al., 1998) we have another probably primordial inclusions in ureilites.

In order to understand ureilite genesis *we placed ureilites into the thermal metamorphic* (thermal evolution) *sequence* from chondrites to different achondrites. Ureilites preserved their main mafic chondritic silicate mineralogy, carbonaceous matrix, but lost most of their iron. Ureilites lost not only main mass of their iron component but

lost their most mobile light silicate components assemblage (TOMEOKA, TAKEDA, 1990), too (although they kept a surprisingly fair amount of water). We defined the place of such meteorites as stage B primitive achondrites. (The known ureilites cover a range of such stage B primitive achondrites, somewhat similar to partly depleted terrestrial mantle rocks.)

TABLE 3

Thermal metamorphic sequence from chodnrites, through primitive achondrites till basaltic achondrites.

Petrolog. type of V Schm-W.	1	2	3	4	5	6	7 Primit. Achondr stage A	Primitiv. Achondr stage B	Basaltic Achond-rites
E			+	+	+	+		Aubrites?	Aubrites?
Between E and H (BEH)			+	+	+	+	Acapulco Lodran Winona	Some of LODRANITES	
H			+	+	+	+	e.g. Port Valley	?	Eucrite, How, Dio
C	+	+	+	+	+	+	?	UREI-LITES	
L			+	+	+	+	+	?	
LL		+	+	+	+	+	+	?	

Although iron loss causes minor changes in the chondritic chemistry and mineralogy, when partial melts of the mobile light silicates move out from the originally chondritic assemblage (TOMEOKA, TAKEDA, 1990) further loss of chondritic character can be observed. Stage B primitive achondrites preserved not only the carbon, but volatiles and oxygene isotopic ratios from the ancient carbonaceous chondritic matrix, too. In bulk chemistry stage B primitive achondrites can be characterized by increased Mg/Si ratios. The outflow of basaltic melts left behind a more mafic silicate content of primitive mantle rocks, then that of chondrites themselves.

PARADOXES FOR UREILITES: RESOLUTIONS AND SOLUTIONS FROM THERMAL HISTORY

There are several paradoxial geochemical and mineralogical composition characteristics of ureilites we intend to reconciliate and explain from the viewpoint of thermodynamics: We note that GOODRICH (1992) when trying to classify ureilites either as metamorphic or as primitive, ran into contradictions, which clearly imply paradoxial features.

1) *Only one type of ureilite exists although we need at least five for the 5 chondrite groups.* This was mentioned in the Table 3. There also aubrites were tentatively mentioned as analogons of ureilies for E condrites (BÉRCZI, HOLBA, LUKÁCS, 1999b). Now, observe Fig. 6, where we displayed the FeO distributions of chondrites, HEDs and ureilites of the NIPR Catalog (YANAI, KOJIMA & HARAMURA, 1995). The Figure demonstrates that after iron loss the remaining Fe content has already a single peak, so it is possible that the different ordinary chondrites would result in similar stage B primitive achondrites (i.e. ureilites, see Fig. 6.).

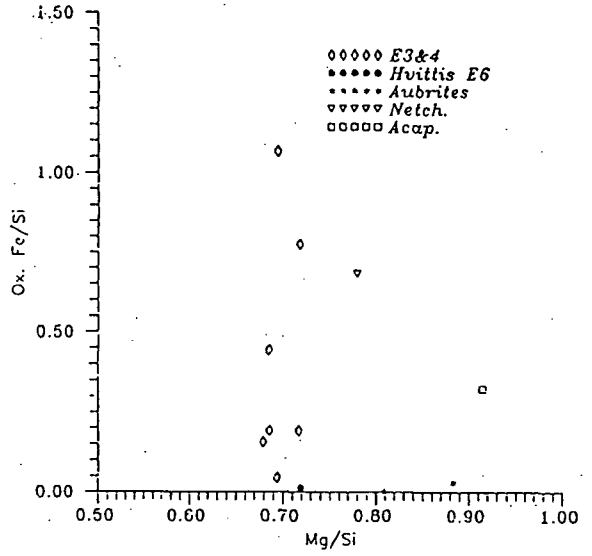

Fig. 5. Enstatite chondrites, their relatives and transitional meteorites from chondrites to primitive achondrites stage A: Acapulco and Netschaëvo on the oxidized-Fe/Si vs. Mg/Si ratio plot.

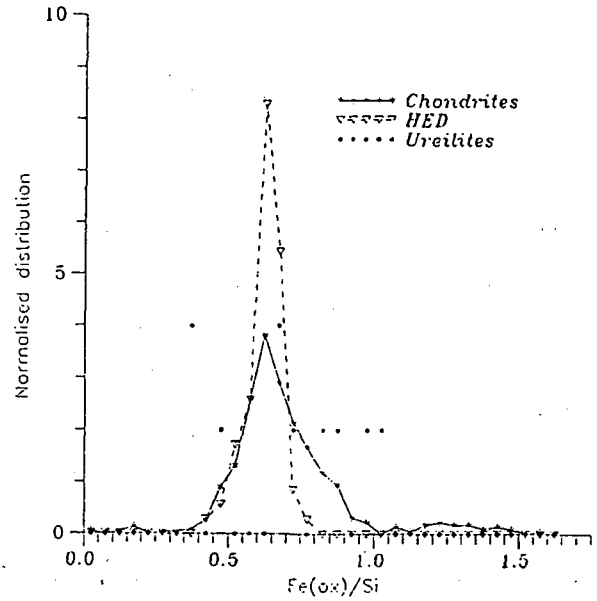

Fig. 6. The place of ureilites as a later evolutionary stage achondrites among the chondrites and the far evolved basaltic achondrites (HED). On the oxidized-Fe/Si vs. distribution (frequency of occurrence) plot the HED basaltic achondrites belong one definite peak of ox-Fe/Si ratio, primitivity of (residual) ureilites is shown their rather uniform distribution along this ratio.

2) *It contains more Mg than the average chondrites.* From statistical data (NIPR dataset, YANAI, KOJIMA, HARAMURA, 1995) it seems that the Mg/Si ratio for ureilites is higher than this ratio for chondrites and even for carbonaceous chondrites. However this property may have a natural explanation. Losing the partial melts can explain this increasing MgO content. Observe the process from the "chair" of the Mg silicates sitting deep in the mantle of the ureilitic parent body asteroid. Originally both olivine and pyroxene might be present in the chondritic mineral assemblage. Partial melting in the peritectic $2MgO.SiO_2$-- SiO_2 system produces first melts of $MgO.SiO_2$ (together with most Na,Ca,Al, silicates) and left more $2MgO.SiO_2$ olivine than $MgO.SiO_2$ pyroxene, so the relative weight of olivine increased. This is a similar process in every planetary mantle chondritic/peridotitic assemblages, and that is why we can observe the parallel trends for peridotite-basalt sequence both for smaller (asteroidal) and larger (the terrestrial) evolutionary sequences (LUKÁCS, BÉRCZI, 1997b, 1998).

The remaining three paradoxes are much more interwoven:

3) *Low Na content is present with rather high water content.* The low Na concentration is no problem, observe that the bulk composition of ALH-77257 is extremely poor also on Al. This simply would mean a deep-mantle residue. However then one would expect water loss too, which is the real problem.

4) *How could it be that water, much carbon and a small amount of metal are in equilibrium.* This clearly implies that under the special circumstances carbon does not dissolve water.

5) *Contrary to their great diffusion-lengths, which means long staying in a hot environment water and carbon is present in considerable amounts.* Contrary to the previous item this means physical properties: both C and H_2O diffuse very easily under familiar circumstances. Note that the fact that carbon has been collected in the inter-grain veins may be explained by diffusion and solid state vacancies transport. The grain boundaries are the zones of weakness in a solid state. Not only diffusion drives incompatible elements (and all other elements not-easily forming crystals) into the veins but the transport effects of vacancies, too. Carbonaceous intergrain regions mean that ureilites were hot for long time. Their presence does not need melting, only long time of hot staying below the melting point. (Between TAMANN temperature = 0.52* T (melting) and T (melting). Because the number of vacancies below melting point is 0.23 %, during a long time heated state diffusion can rearrange texture into a very "igneous"-like metamorphic one.)

We admit that we do not have satisfactory explanations for the last 3 problems. However, we suggest a possibility, which may or may not be true, but with it they are no more paradoxes.

Assume a carbon phase on large pressure and/or high temperature, which is of great molecular weight and almost inert. Then the parts of points 4 & 5 regarding C get explanation: this allotrope of C will not evaporate easily from the lattice and will not dissolve water. We do not know which modifications may be stable or metastable at the ureilite locality (deep mantle?), but an *example* is the buckminsterfullerene C_{60}. It is a large molecule, forming negative ions, so not a concurrent of H for O (HAUFLER & al., (1990); OHSAWA & SAJI (1992)).

Then what would remain would be only something binding water in the lattice more strongly than usual; and we note the enormous Mg in ureilite. Now, silicates of C chondrites are slightly more "mafic" than of ordinary chondrites, and they retain more water at comparable petrologic types, too. We also keep open another possibility for C concentration in ureilites. Deep mantle C may have diffused out of the iron core: C diffuses easily in Fe, and we guess that the diffusion length in a million year may have gone to several km's. We study this possibility in another paper.

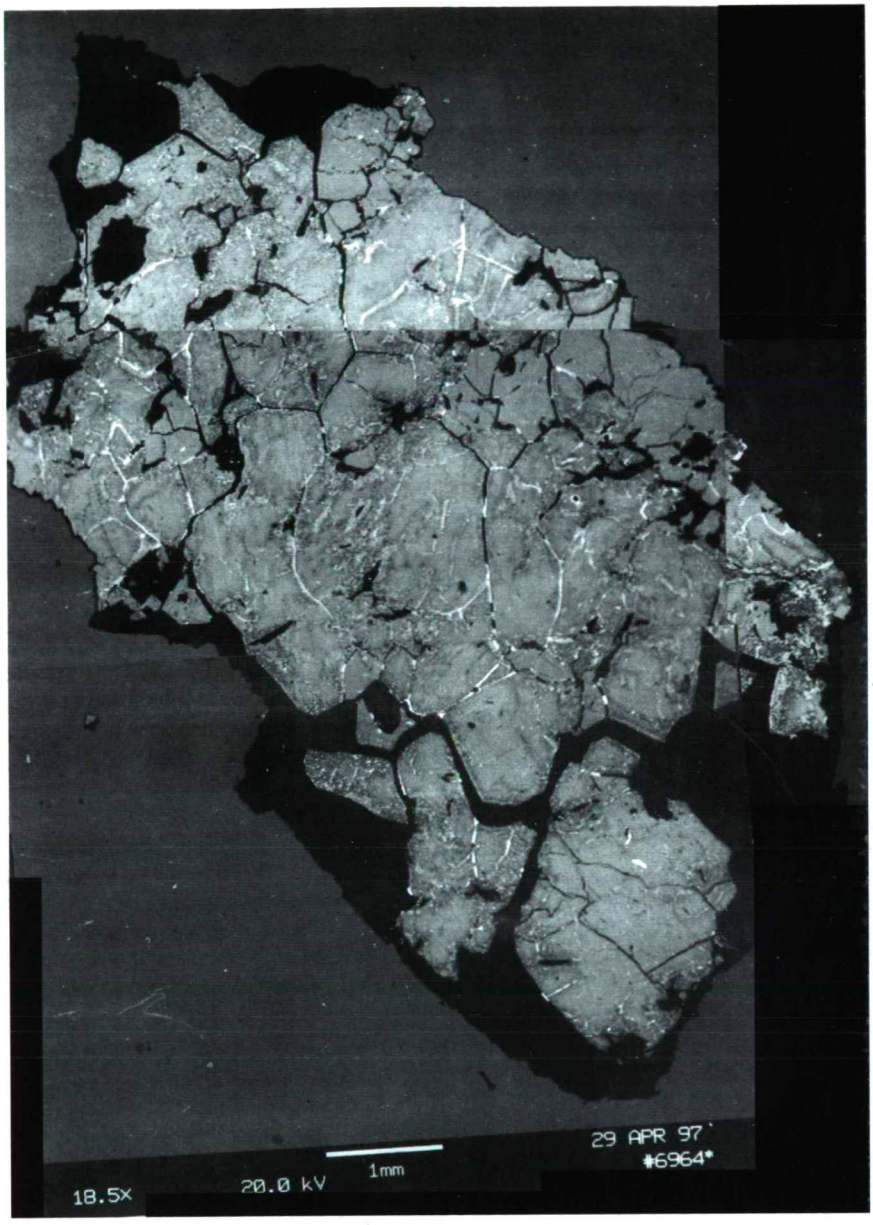

Pict. 1/a. Overview of the ALHA77257,77-4 thin section. (BSE image.)

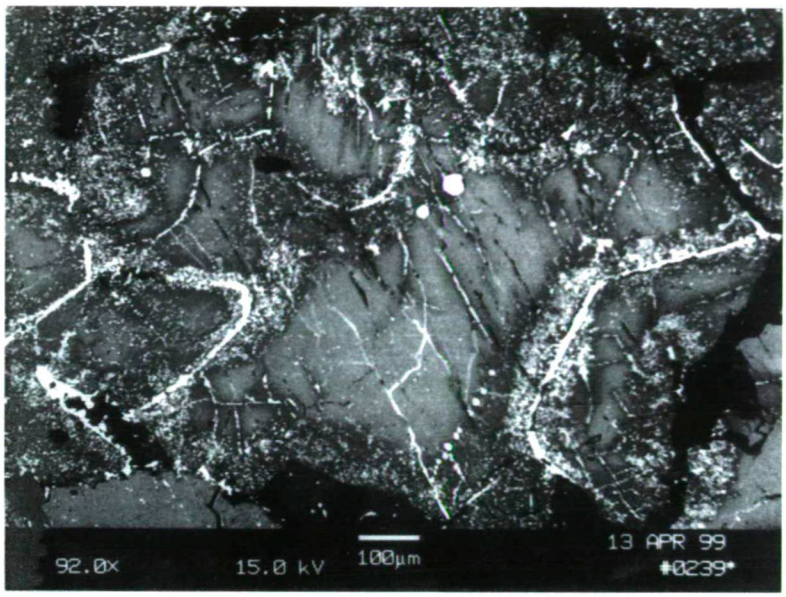

Pict. 1/b. Characteristic ureilite texture. The grain boundary regions are filled with carbonaceous veins, but many of them and intra grain fissures with metal ones. Outer rims of the olivine and clinopyroxene contain reduction-exsolved metal blebs which form transitional semi-opaque boundaries around the minerals. Some veins are alternately filled with carbon and metal. Detail of the ALHA77257,77-4 thin section. (BSE image.)

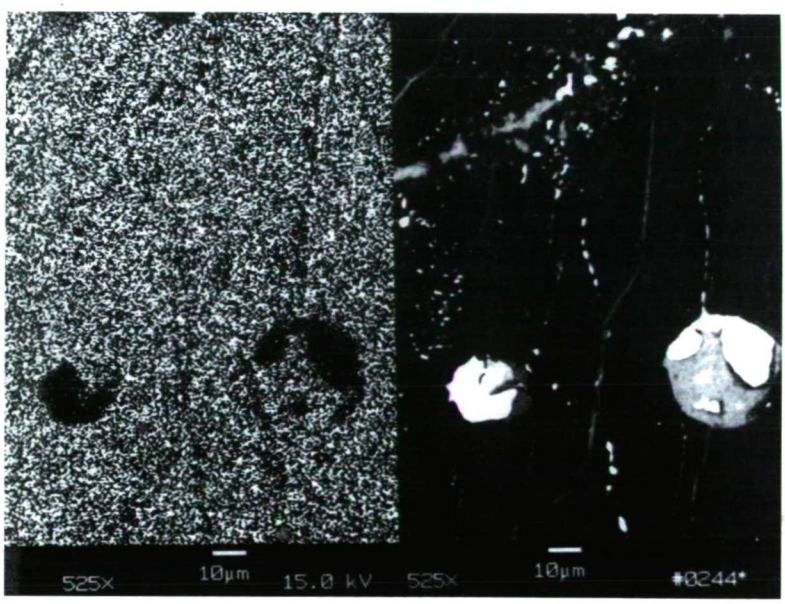

Pict. 1/c. Comparison of the silicon distribution map (left) and the BSE photo of this region (right) about a detail of the ALHA 77257,77-4 ureilite show a mafic silicate mineral which contains a high Cr containing primitive chondritic grain.

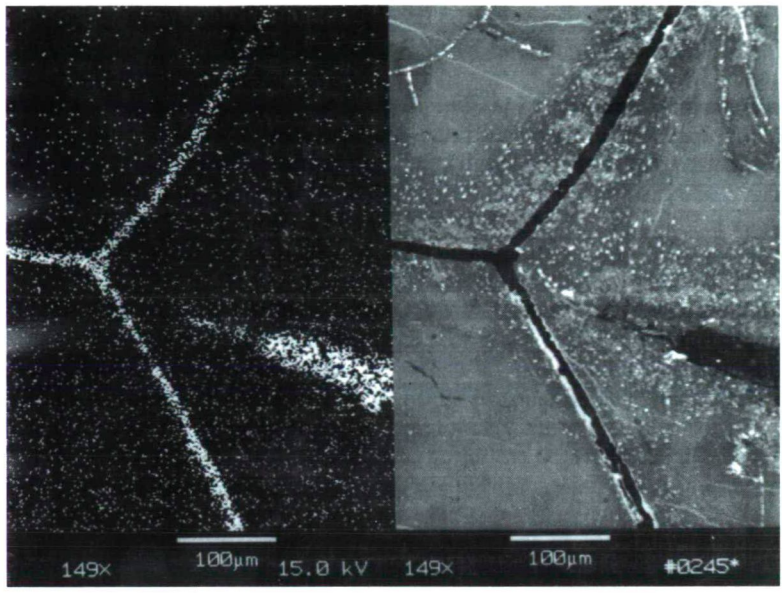

Pict. 1/d. Comparison of the carbon distribution map (left) and the BSE photo of this region (right) about a detail of the ALHA 77257,77-4 ureilite shows that some veins are mainly filled with carbon, others contain metallic iron filling too.

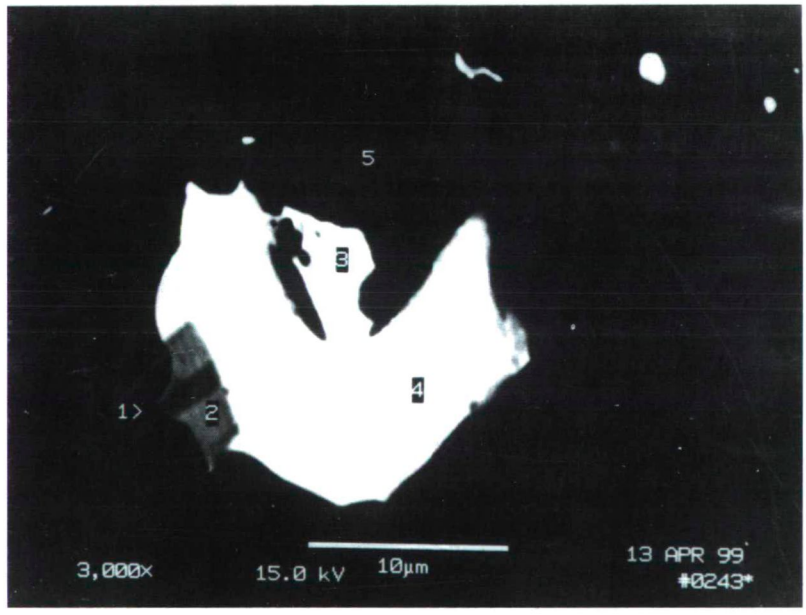

Pict. 1/e. The high-Cr spherule of Pict. 1/c (BSE image). Together with the carbon matrix, primary carbon grains (GOODRICH & al., 1986), these high-Cr spherules represent the primitive chondritic components in the more evolved (partly exhausted) mafic silicate minerals of the primitive achondrite stage B ureilites.

DISCUSSION II: CHONDRITES – PRIMITIVE ACHONDRITES – BASALTIC ACHONDRITES

We studied the difference between *primitive* achondrites (of chondritic composition) and the *par excellence* achondrites (e.g. basaltic achondrites). Of course, the theory tells that primitive achondrites are connected to par excellence chondrites via iron loss, so from the ferrous components we can use only oxidised Fe for composition. Fig. 5 displays Fe^{ox}/Si vs. Mg/Si for the E's of the NIPR Catalog as chondrites, E6 Hvittis to represent primitive achondrites (on the basis of MASON's (1962) remark that E6's have no chondrulae), the aubrites of the NIPR Catalog as E achondrites, Acapulco as something of E-H origin, and Netschaëvo for comparison.

Indeed, the "E primitive achondrite" (?) Hvittis is well among the E3&4's in the metal-free plot. Netschaëvo is not, but it is not expected, "being in the gap". Acapulco is not either; the higher Mg content compared to the almost purely Mg-silicate E's must mean that in Acapulco there is more olivine, so it cannot have direct genetic connection to them. But aubrites are also Mg-richer than E's.

So aubrites are not basalts of the E parent body (say, proto-Hungaria). If they have any close connection to such a parent body, they are rather analogous to ureilites (or in Earth, to lherzolites), and then the E basalt is still unknown. (To the problem of differentiation between primitive and basaltic achondrites we will return in a subsequent paper.)

Portales Valley and the also rather fresh discovery of Yamato 791093 iron-rich chondrites enlarged the circle of those meteorites which help to see more in this complex borderline between chondrites and achondrites, especially in the case of the H group. Their thermal evolutionary process was going deep in the chondritic parent body, that is why so rare the representative transient samples are. In 1995 MCCOY summarized the state of art at that time. His sequence was: Netschaëvo (unmelted, relict chondritic), Techado (unmelted, chondritic recrystallized, but Fe-Ni-S melted), Watson (totally melted, but no silicate differentiation), Miles and Weekeroo Station (opx-cpx-pl partial melted) and Kodaikanal, Colomera, Elga (differentiated silicates). We did not study the differentiated silicate bearing IIE irons, but with the two new discoveries of this H chondrite-to-stage A primitive achondirite clan the new sequence can be given such:

Rose City (only shock melted and brecciated H5),
Yamato-791093 (H6 chondritic, maybe shock induced, but "self-melted" Fe-Ni-S),
Portales Valley (H6 chondritic, maybe shock induced, but "self-melted" Fe-Ni-S),
Netschaëvo (E-H chondritic, "self-melted" Fe-Ni-S),
Techado (unmelted H primitive chondritic, "self-melted" Fe-Ni-S),
Watson (melted but recrystallized H primitive chondritic, melted Fe-Ni-S).

SUMMARY: PRIMITIVE ACHONDRITES OF STAGE A AND STAGE B

We studied different products of the chondritic thermal metamorphism. We extended the metamorphic petrological transformation sequence (VAN SCHMUS, WOOD, 1967) toward basaltic achondrites. We defined the extended gradual transition from chondritic mineral assemblages (and compositions) through different primitive achondritic stages to the most differentiated basaltic achondritic meteorites. This continuing of the metamporphic sequence needed formulation of the main textural characteristics of those transformations which affected the texture after chondritic equilibration. There were two

such processes: one was the partial melting and outflow of iron-sulfide assemblage from the primitive achondritic source, the second was: the partial melting of a low melting point basaltic like component and its outflow toward the surface of the asteroidal parent body. Acapulcoites, lodranites, winonaites represented the first stage A, ureilites and some lodranites represented the second stage B. Those of the second one have less primitive achondritic characteristics then that of primitiv achondrites of the original definition. In order to emphasize the distinction between the two stages we introduced the stage B primitive achondrite expression and name for them, while used the primitive achondrite of stage A for the first group. This division of the chondrite-primitive achondrite range made possible to distinguish different types of primitive achondrites from the traditional or classic achondrites, the basaltic achondrites. Moreover, this refinement of primitive achondrite range helped to genetically relate different iron meteorites and stony irons to these stages in the thermal evolutionary sequence of products on a chondritic-to-achondritic evolved parent body.

The detailed construction of the extended metamorphic chondritic sequence helps arranging the great majority of chondrites and achondrites according to common characteristics which gradually change during the thermal evolution of the chondritc parent bodies.

ACKNOWLEDGEMENTS

The authors would like to thank NIPR for the loan of the ALHA77257,77-4 thin section, to Drs. K. YANAI and H. KOJIMA for illuminating discussions. Partly supported by OTKA T/026660.

REFERENCES

BÉRCZI SZ., HOLBA ÁGNES & LUKÁCS B., 1995: Acta Mineralogica-Petrographica, Szeged, **XXXI**, 53
BÉRCZI SZ., HOLBA ÁGNES & LUKÁCS B., 1996: KFKI-1996-15
BÉRCZI SZ., HOLBA ÁGNES & LUKÁCS B., 1998: Acta Mineralogica-Petrographica, Szeged, **XXXIX**, 87
BÉRCZI SZ., HOLBA ÁGNES & LUKÁCS B., 1999a: LPSC **XXX**, #1014
BÉRCZI SZ., HOLBA ÁGNES & LUKÁCS B., 1999b: KFKI-1999-01
BÉRCZI SZ., & LUKÁCS B., 1998: Antarctic Meteorites **XXIII**, Tokyo, 4
BÉRCZI SZ., & LUKÁCS B., 1999: LPSC **XXX**, #1275
BILD R.W., WASSON J.T., 1977: Science **197**, 58
BUENING D. K. & BUSECK P. R., 1973: J. Geophys. Res. **78**, 6852
CASANOVA I., GRAF T., MARTI K., 1995: Science **268**, 540
FECHTIG H., GENTNER W & ZÄHRINGER J., 1960: Geochim. Cosmochim. Acta **19**, 70
GOODRICH C.A., BERKLEY J.L., 1986: Primary magmatic carbon in ureilites. GCA, **50**, 681-691.
GOODRICH C.A., 1992: Ureilites: A critical review. Meteoritics, **27**, 327-352.
HANON, P., ROBERT, F., CHAUSSIDON, M., 1998: Geochim. Cosmochim. Acta **62**, 903-913.
HAUFLER L. E. & al., 1990: J. Phys. Chem. **94**, 8634
HUTCHINSON R., ALEXANDER C.M.O. & BARBER D.J., 1987: Geochim. Cosmochim. Acta **51**, 1875
IKEDA Y., YAMAMOTO T., KOJIMA H., IMAE N., KONG P., EBIHARA M., PRINZ M., 1997: Antarctic Meteorite Research **10**, 335
JANSSENS M-J., HERTOGEN J., WOLF R., EBIHARA M., ANDERS E., 1987: GCA, **51**, 2275-2283.
JAROSEWICH E., 1990: Meteoritics **25**, 323
KRING D. A., HILL D. H. & GLEASON J. G., 1999: LPSC **XXX**, #1618
LAZARUS D., 1960: Solid State Physics **10**, 71
LUKÁCS B., & BÉRCZI SZ., 1996: 21st Symp. Antarctic Meteorites, Tokyo, 90
LUKÁCS B., & BÉRCZI SZ., 1997a: LPSC **XXVIII**, 853
LUKÁCS B., & BÉRCZI SZ., 1997b: Antarctic Meteorites **XXII**, 94.
LUKÁCS B., & BÉRCZI SZ., 1998: LPSC **XXIX**, #1223

LUKÁCS B., HOLBA ÁGNES & BÉRCZI SZ., 1999: LPSC **XXX**, #1337
MASON B., 1962: Meteorites. J. Wiley & Sons, New York
MCCOY T.J., 1995: Meteoritics **30**, 542
MCCOY T.J., KEIL K., MUENOW D. W., WILSON L., 1997: Geochim. Cosmochim. Acta **61**, 639
MCSWEEN H. Y., 1987: Geochim. Cosmochim. Acta **51**, 2469
METEORITE NEWS 1996: Vol. **6**, No. 1
METEORITE NEWS 1998: Vol. **7**, No. 1
MITTLEFEHLDT D.W., LINDSTROM M. M., BOGARD D. D., GARRISON D. H., FIELD S. W., 1996: Geochim. Cosmochim. Acta **60**, 867
NOBUYOSHI T., HARAMURA H., IKEDA Y., KIMURA M., KOJIMA H., IMAE N., LEE M-S., 1997: Antarctic Meteorite Research **10**, 165
OHSAWA V. & SAJI T., 1992: J. Chem. Soc. Chem. Comm. 781
OLSEN E. & JAROSEWICH E., 1971: Science **174**, 583
OLSEN E. & al. 1994: Meteoritics, **29**, 200
PINAULT L. J., SCOTT E. R. D., BOGARD D. D., & KEIL K., 1999: LPSC **XXX**, #2048
RASMUSSEN K. L. & al., 1995: Geochim. Cosmochim. Acta **59**, 3049
RUBIN A. E. & ULFF-MØLLER F., 1999: LPSC **XXX**, #1125
RUZICKA A., SNYDER G. A., PRINZ M, TAYLOR L. A., 1999: LPSC **XXX**, #1645
VAN SCHMUS W. R. & WOOD J. A., 1967: Geochim. Cosmochim. Acta **31**, 747
SAITO, J., TAKEDA H., 1991: 16th Symposium on Antarctic Meteorites, Tokyo, 1991. 13-1.
SHEWMON P. G., 1963: Diffusion in Solids. McGraw-Hill, N.Y.
TAKEDA H., HUSTON T.J., LIPSCHUTZ M.E., 1984 Earth Planet. Sci. Letters **71**, 329
TAKEDA H., SAITO J., HIROI T., 1991: LPSC **XXII**, 1375.
TOMEOKA K., TAKEDA H., 1990: Geochim. Cosmochim. Acta **54**, 1475-1481.
WASSON J.T., WANG J., 1968: Geochim. Cosmochim. Acta **50**, 725
YANAI K. & KOJIMA H., 1991: Proc. NIPR. Symp. Antarct. Meteorites **4**, 118
YANAI K. & KOJIMA H., 1987: Photographic Catalog of the Antarctic Meteorites. NIPR, Tokyo
YANAI K., KOJIMA H. & HARAMURA H., 1995: Catalog of the Antarctic Meteorites. NIPR, Tokyo
YUGAMI K., TAKEDA H, KOJIMA H. & MIYAMOTO M., 1997: Antarctic Meteorites **XXII**, 220
YUGAMI K., TAKEDA H, KOJIMA H. & MIYAMOTO M., 1998: Antarctic Meteorite Research **11**, 49
ZOLENSKY M. E. & MITTLEFEHLDT D. W., LIPSCHUTZ M. E., WANG M-S., CLAYTON R. N., MAYEDA T. K., GRADY M. M., PILLINGER C. & BARBER D., 1997: Geochim. Cosmochim. Acta **61**, 5099

Manuscript received: 25. June 1999.

Illustrations

Figures should be used only where they are essential to elucidate text.

The illustrations should be numbered according to their sequence in the text, and in the text references should be made to each figure.

All illustrations should be given separately, not stuck on sheets and not folded. The number of the figure and the authors name should be noted on the reverse side of the photographs and on the lower frontside of drawings, indicating at the same time the top of the figure where it necessary.

Captions for all figures should be given typewritten on a separate list at the end of the manuscript. Drawn text in the figures should be kept to a minimum.

Drawings should be made on tracing paper by Indian ink. The thickness of the lines and the size of the lettering should enough to allow a necessary reduction.

Photographs of good contract and intensity on glossy paper are only acceptable. Colour photographs or drawings cannot be accepted.

Use bar scale on all illustrations instead of numerical scales that must be changed if reductions are necessary.

References

All references to publications made in the text should be made by quoting the author's name (without initials) and year of publications in paranthesis.

The list of references at the end of the manuscript should be arranged alphabetically by author's names and chronologically per author.

If the referred publications are written by more than two authors, in the text only the name of the first author should be indicated, the other co-authors are denoted by "et al.", however, in the list of references the names of authors and all co-authors should be mentioned.

In the list of references all references should be written, e. g. Balogh, K., A. Barabás (1972): The Carboniferous and Permian of Hungary. Acta Miner. Petr. Szeged, XX/2, 191–207.

At references to books beside the author's name, year of publicaton, title and the publishing house should also be mentioned.

In the case of references for symposium volumes, special issues or multi-authors books, the following system should be used: Roser, B. P., C. W. Childs, and G. P. Glasby (1980): Manganese in New Zealand. In: I. M. Varentsov and Gy. Grassely (Editors): Geology and Geochemistry of Manganese, Vol. II. Akadémiai Kiadó, Budapest, 199–211.

Manuscripts that are not adequately prepared will be returned to the authors(s).

CONTENTS